

**RISK-INFORMED MULTI-CRITERIA DECISION  
FRAMEWORK FOR RESILIENCE AND SUSTAINABILITY  
ASSESSMENT OF BUILDING STRUCTURES**

**by**

**ESMAEEL ASADI**

Submitted in partial fulfillment of the requirements for the degree of  
Doctor of Philosophy

Department of Civil Engineering

**CASE WESTERN RESERVE UNIVERSITY**

January 2020

**CASE WESTERN RESERVE UNIVERSITY  
SCHOOL OF GRADUATE STUDIES**

We hereby approve the dissertation of  
**Esmael Asadi**  
candidate for the degree of DOCTOR OF PHILOSOPHY IN CIVIL ENGINEERING\*.

Committee Chair

Dr. Yue Li

Committee Member

Dr. Xiong (Bill) Yu

Committee Member

Dr. Wojbor Woyczynski

Committee Member

Dr. Michael Pollino

Date of Defense

November 25<sup>th</sup>, 2019

\*We also certify that written approval has been obtained for any proprietary material  
contained therein.

*This dissertation is dedicated to my parents, Alidad and Koukab, for their endless love and support and to my brother, Ali, for inspiring me to pursue my dreams.*

# Table of Contents

Table of Contents.....	iv
List of Tables .....	viii
List of Figures.....	x
Preface .....	xv
Acknowledgments.....	xvii
Abstract.....	xviii
Chapter 1.....	1
1. Introduction.....	1
1.1 Literature Review and Critical Appraisal .....	5
1.1.1 Resilience Assessment.....	5
1.1.2 Sustainability Assessment.....	15
1.1.3 Sustainability versus Resilience.....	21
1.1.4 Diagrid Structures .....	22
1.1.5 Decision Analysis .....	26
1.2 Critical Appraisal.....	32
1.3 Research Objectives.....	34
1.4 Organization and Outline.....	35
Chapter 2.....	39
2. Seismic Performance Assessment and Loss Estimation of Steel Diagrid Structures.....	39
2.1 Introduction.....	39
2.2 Archetype Diagrid Buildings .....	44
2.3 Seismic Nonlinear Performance of Diagrid Structures.....	51
2.3.1 Static Nonlinear Analysis.....	51
2.3.2 Nonlinear Time-history Analysis.....	55
2.4 Performance Criteria and Damage States .....	60
2.4.1 Collapse Fragility.....	60
2.4.2 Proposed Seismic Performance Levels and Damage States.....	66
2.5 Seismic Loss Estimation.....	73
2.5.1 Methodology .....	73

2.5.2	Criteria for Loss Estimation Analysis.....	74
2.5.3	Expected Loss at a Given Earthquake Intensity.....	77
2.6	Conclusions.....	83
Chapter 3	.....	85
3.	Multi-criteria Decision-making for Seismic Resilience and Sustainability Assessment of Diagrid Buildings.....	85
3.1	Introduction.....	85
3.2	Proposed MCDM Framework.....	91
3.2.1	System Concept and Criteria Module.....	92
3.2.2	Resilience and Sustainability Assessment Module.....	93
3.2.3	Multi-Criteria Decision-Making Module.....	100
3.3	Application to Diagrid Structures.....	106
3.3.1	Archetype Diagrid Buildings.....	106
3.3.2	Fragility Analysis and Uncertainty Modeling.....	108
3.3.3	Time-based Assessment.....	112
3.3.4	Seismic Resilience Assessment.....	113
3.3.5	Sustainability Assessment.....	125
3.3.6	Multi-Criteria Decision Making.....	130
3.4	Conclusions.....	136
Chapter 4	.....	138
4.	Risk-informed Multi-criteria Decision Framework for Resilience, Sustainability, and Energy Analysis of Reinforced Concrete Buildings.....	138
4.1	Introduction.....	138
4.2	Proposed Multi-Criteria Decision-Making Framework.....	142
4.2.1	System Concept and Criteria (SCC) Module.....	143
4.2.2	Resilience, Sustainability, and Energy Analysis (RSEA) Module.....	143
4.2.3	Multi-criteria Decision-making Module.....	148
4.3	Case Studies.....	155
4.3.1	Design and Numerical Modeling of Archetype RC Buildings.....	155
4.3.2	Specifications for Life-cycle Cost Analysis.....	157
4.3.3	Energy Analysis Settings.....	159
4.3.4	Vulnerability Assessment.....	161
4.3.5	Seismic Loss Estimation.....	162

4.3.6	Energy Cost Analysis and CO <sub>2</sub> eq Emissions .....	165
4.3.7	Risk-informed Multi-Criteria Decision Making .....	168
4.4	Conclusions.....	173
Chapter 5	.....	176
5.	Localized Health Monitoring System for Seismic Resilience Quantification and Safety Evaluation of Smart Structures .....	176
5.1	Introduction.....	176
5.2	Trilateral Framework for System Assessment and Decision Analysis .....	181
5.2.1	Life-cycle Functionality Assessment.....	183
5.2.2	Monitoring and Control .....	185
5.2.3	Resilience Assessment .....	191
5.2.4	Post-quake Safety Evaluation and Evacuation Decision-making .....	192
5.3	Van Nuys Instrumented Building .....	194
5.4	Archetype Design, Modeling, and Components .....	198
5.5	Uncertainty Modeling and Fragility Analysis.....	200
5.6	ARX System Identification.....	204
5.6.1	Damage Detection and Damage Location.....	204
5.6.2	Damage Severity and Characterization.....	207
5.7	Resilience Quantification.....	208
5.7.1	Scenario-based Assessment .....	208
5.7.2	Component-based Functionality Curve .....	209
5.7.3	Post-quake Safety Evaluation .....	212
5.8	Conclusions.....	214
5.9	Appendix A.....	216
Chapter 6	.....	219
6.	Multi-dimensional Functional Earthquake Recovery Analysis and Resilience Quantification of Building Facilities.....	219
6.1	Introduction.....	219
6.2	Proposed Framework .....	223
6.2.1	Life-cycle Functionality and Resilience .....	223
6.2.2	Multi-dimensional Functionality Assessment.....	225
6.3	Archetype Building Facilities .....	230
6.3.1	Configuration and Design of Archetypes.....	230

6.4	Scenario-based Assessment .....	233
6.5	Vulnerability Analysis .....	233
6.6	Loss and Downtime Analysis .....	235
6.6.1	Loss and Downtime Functions.....	236
6.6.2	Downtime for Occupancy and Serviceability .....	238
6.7	Multi-dimensional Functionality Analysis.....	240
6.7.1	Functionality Curves.....	240
6.7.2	Functionality Surfaces.....	244
6.7.3	Multi-dimensional Resilience Indices.....	246
6.8	Conclusions.....	248
Chapter 7	.....	250
7.	Summary, Conclusions, and Future Work .....	250
7.1	Summary and Conclusions .....	250
7.2	Future Work.....	256
Appendix I	.....	259
A I.1	Copyright Clearance for parts of Chapter 1 .....	259
A I.2	Copyright Clearance for Chapter 2.....	262
A I.3	Copyright Clearance for Chapter 3.....	263
Bibliography	.....	264

# List of Tables

Table 2.1 Engineering demand parameters under static analysis .....	53
Table 2.2 Response spectrum of all records normalized and scaled to match ASCE7-10 design response spectrum in the site for 4-45 archetype .....	57
Table 2.3 Expected collapse capacity and IDR, the corresponding dispersion and the probability of collapse under DBE and MCE based on logarithmic fragility CDF.....	64
Table 2.4 Damage criteria and illustrative description of damage states for steel diagrid frames.....	69
Table 2.5 Mean and logarithmic dispersion of $S_a(T_1,5\%)$ for each damage state.....	70
Table 2.6 Building specification and assumptions for loss estimation.....	74
Table 2.7 Structural and non-structural fragility and cost specifications .....	75
Table 2.8 Expected loss for different archetypes and intensities.....	79
Table 3.1 Damage and performance criteria for steel diagrid frames (Asadi et al. 2018) .....	109
Table 3.2 Expected collapse capacity and IDR, the corresponding dispersion and the probability of collapse under DBE and MCE based on logarithmic fragility CDF.....	111
Table 3.3 Building specification and assumptions for resilience assessment.....	115
Table 3.4 Total repair time for each component and median repair time for different intensities and models .....	119
Table 3.5 Estimated environmental impacts due to initial construction and annual seismic damage repair .....	128
Table 3.6 Pairwise comparison matrix for Scenario 1- lowest asset loss .....	131
Table 3.7 Pairwise comparison matrix for Scenario 2- lowest time loss.....	132
Table 3.8 Pairwise comparison matrix for Scenario 3- lowest life loss.....	132
Table 3.9 Pairwise comparison matrix for Scenario 4- lowest environmental loss.....	132
Table 3.10 Pairwise comparison matrix for Scenario 5- highest resilience.....	132
Table 3.11 Evaluation matrix obtained from RSA module, total utility ( $U_i$ ) for MAUT method, and relative closeness to ideal solution ( $C^*$ ) for TOPSIS method.....	135
Table 4.1 Pairwise comparison matrix for Scenario 1- minimum asset loss .....	154
Table 4.2 Pairwise comparison matrix for Scenario 2- minimum time loss.....	154
Table 4.3 Pairwise comparison matrix for Scenario 3- minimum life loss .....	154

Table 4.4 Pairwise comparison matrix for Scenario 4- minimum environmental loss...	155
Table 4.5 Pairwise comparison matrix for Scenario 5- maximum resilience .....	155
Table 4.6 Pairwise comparison matrix for Scenario 6- minimum operational energy cost .....	155
Table 4.7 Estimated life-cycle cost of studied archetypes .....	158
Table 4.8 Window glazing properties and costs .....	160
Table 4.9 Expected collapse capacity and collapse IDR and their corresponding logarithmic dispersion.....	162
Table 4.10 Annual energy consumption, cost, and CO2 eq emission due to energy consumption for various archetypes .....	166
Table 4.11 Evaluation matrix obtained from RSEA module and total utility ( $U_i$ ) scores for various scenarios with risk averse (RA), neutral (N), and risk seeking (RS) attitudes for LA archetypes .....	170
Table 4.12 Evaluation matrix obtained from RSEA module and total utility ( $U_i$ ) scores for various scenarios with risk averse (RA), neutral (N), and risk seeking (RS) attitudes for Boston archetypes .....	171
Table 5.1 Variation of steel and concrete member properties randomly sampled using Latin Hypercube Sampling method and normalized by nominal value.....	201
Table 5.2 Expected collapse capacity and collapse IDR and their corresponding logarithmic dispersion.....	202
Table 5.3 Resilience, robustness, and rapidity indices, median monetary loss, and median repair time considering a parallel repair plan for various archetypes for Scenario 1, 2, and 3 earthquakes .....	212
Table 5.4 Probability of minor ( $DS_1$ ), moderate ( $DS_2$ ), or severe ( $DS_3$ ) damage states for critical components .....	214
Table 6.1 Expected collapse capacity and collapse IDR and their corresponding logarithmic dispersion.....	235
Table 6.2 Building specification and assumptions for loss and downtime estimation ...	236
Table 6.3 Resilience index and median loss and downtime based on functionality curve for asset loss (FAL), occupancy loss (FOL), and serviceability loss (FSL) for various archetypes for Scenario 1, 2, and 3 earthquakes .....	247

# List of Figures

Figure 1.2 Schematic of Sutley et al. (2016a; b) proposed coupled framework.....	14
Figure 1.1 Three 3-story diagrid modules and a sample triangular element .....	23
Figure 1.4 Quadrilateral decision criteria .....	28
Figure 1.5 Flowchart for MAUT for the design/retrofit decision-making problem .....	29
Figure 2.1 (a) Main components of a diagrid frame and its triangular base element; and (b) the Hearst Tower, New York City. (Reprinted from ArchDaily (2012), with permission from Chuck Choi).....	40
Figure 2.2 Typical floor plan for (a) 4-, 8-, and 15-story (b) 30-story diagrid archetypes	45
Figure 2.3 Comparison of SAP2000 model having lumped PHs with OpenSees model having fiber elements under pushover analysis for 4-45 archetype.....	48
Figure 2.4 Schematic of diagrid archetype models.....	49
Figure 2.5 Comparison between experimental hysteretic response (Black et al. 1980) and current numerical model results.....	49
Figure 2.6 H-section steel diagrid connections adapted from Kim et al. (2011) .....	51
Figure 2.7 (a) Pushover curves and (b) lateral stiffness versus total drift curves for 8-story models and pushover curves for (c) 4- (d) 15- (e) 30-story archetypes.....	53
Figure 2.8 Pushover curves for 8-45 archetype considering different cases for gravity loads .....	55
Figure 2.9 Response spectrum of all records normalized and scaled to match ASCE7-10 design response spectrum in the site for 4-45 archetype .....	56
Figure 2.10 Elevation of 4-72 model with uppermost incomplete module .....	59
Figure 2.11 Incremental dynamic analysis curves for 4-45 archetype .....	62
Figure 2.12 Empirical CDF of $S_a(T_1, 5\%)$ and fitted lognormal fragility functions for (a) 4-story and (b) 8-story archetypes .....	63
Figure 2.13 Variation of collapse capacity and $IDR_{max}$ for different archetypes .....	65
Figure 2.14 Seismic fragility curves for each damage state for (a) 4-45 (b) 4-63 (c) 4-72 (d) 8-45 (e) 8-63 (f) 8-72 archetype.....	71
Figure 2.15 Expected total loss caused by various components as a percentage of total replacement cost.....	78

Figure 2.16 CDF of total loss for different intensities for (a) 4-story (b) 8-story archetypes .....	83
Figure 3.1 Main components of a diagrid frame and its triangular base element.....	87
Figure 3.2 Main components of the proposed framework .....	92
Figure 3.3 Flowchart for System Concept and Criteria (SCC) Module and its connection with other modules.....	93
Figure 3.4 Flowchart for Resilience and Sustainability Assessment (RSA) Module.....	100
Figure 3.5 Quadrilateral decision-making attributes/criteria .....	102
Figure 3.6 MCDM Flowchart for a design/retrofit decision problem using MAUT and/or TOPSIS methods.....	103
Figure 3.7 Diagrid modules of 4-72A archetype, an alternate configuration for 4-72 archetype.....	107
Figure 3.8 Schematic of diagrid archetype models.....	108
Figure 3.9 Empirical CDF of $S_a(T_1, 5\%)$ and fitted lognormal fragility functions.....	111
Figure 3.10 Adjusted hazard curve for 4-63 archetype obtained from USGS online Hazard Tool divided into 10 intensities .....	113
Figure 3.11 Annual repair cost for (a) 4-45, (b) 4-63 and (c) 4-72 (d) 4-72A archetypes .....	116
Figure 3.12 Repair time for different components and floors as a percentage of total replacement time.....	118
Figure 3.13 Annual downtime assuming parallel planning for (a) 4-45, (b) 4-63 and (c) 4-72 (d) 4-72A archetypes.....	121
Figure 3.14 Cumulative distribution function of injuries for different intensities for 4-63 archetype.....	122
Figure 3.15 Annual rate of injuries for (a) 4-45, (b) 4-63 and (c) 4-72 (d) 4-72A archetypes under seismic hazard.....	124
Figure 3.16 Annual rate of fatalities for (a) 4-45, (b) 4-63 and (c) 4-72 (d) 4-72A archetypes under seismic hazard.....	124
Figure 3.17 Annual probability of total greenhouse gas emission for different archetypes .....	129
Figure 4.1 Main components of the proposed framework.....	142

Figure 4.2 Seismic resilience, sustainability, and energy-consumption analysis (RSEA) Module .....	144
Figure 4.3 Analytic hierarchy model considered for decision analysis and the trilateral sets of criteria/attributes .....	150
Figure 4.4 Utility curves with different attitude towards risk using exponential utility function adapted from (Wood and Khosravianian 2015).....	152
Figure 4.5 Floor plans of archetype RC building with different shear wall ratios, (a) SF archetype with no shear wall, (b) SWs archetype with 2 shear walls, and (c) SWm archetype with one shear wall on each side (dimensions are in meters) .....	156
Figure 4.6 (a) SF archetype 3-dimensional (3D) view built in DesignBuilder and (b) Typical thermal zone designation for all archetypes (dimensions in meters).....	160
Figure 4.7 Empirical CDF of $S_a(T_1,5\%)$ and fitted lognormal fragility functions for (a) LA and (b) Boston archetypes .....	162
Figure 4.8 Cumulative annual repair time for various (a) LA and (b) Boston archetypes .....	163
Figure 4.9 Cumulative annual number of injuries for various (a) LA and (b) Boston archetypes .....	164
Figure 4.10 Annual rate of exceedance of (a) repair cost and (b) fatalities for LA-SF-BG archetype .....	165
Figure 4.11 Annual energy consumptions for various archetype buildings in regions: (a) Los Angeles and (b) Boston.....	166
Figure 4.12 Annual energy costs for various archetype buildings in regions: (a) Los Angeles and (b) Boston.....	167
Figure 4.13 Total utility ( $U_i$ ) scores for various scenarios for (a) LA and (b) Boston buildings with risk aversive (RA), neutral (N), and risk seeking (RS) attitudes .....	172
Figure 5.1 Four different network infrastructure patterns: (a) centralized, (b) distributed, (c) hierarchical, (d) localized infrastructures, adapted from (Ling et al. 2009).....	180
Figure 5.2 Main components of the proposed framework for Assessment and Decision Analysis.....	182
Figure 5.3 Flowchart for System Concept and Criteria (SCC) Module and its connection with other modules.....	183
Figure 5.4 Life-cycle functionality of a system and the effect of evolving conditions on the functionality (not to scale) .....	184

Figure 5.5 Schematic of SHM system for operating in normal stage or during/post-earthquake, Diagrid building in the left is the Hearst Tower in New York City .....	187
Figure 5.6 The flowchart for the Resilience Submodule and its connection with other modules .....	192
Figure 5.7 Lateral displacement from numerical models of Van Nuys Hotel during 1994 Northridge Earthquake compared with recorded displacement from instruments (a) at roof in the longitudinal direction and (b) at various floors in transverse direction, displacement values specified are peak values reported by (Islam 1996) .....	195
Figure 5.8 (a) Repair time for various floors of Van Nuys building and (b) Functionality curve for Van Nuys Building under 1994 Northridge earthquake (numbered arrows show the repair time for various components: (1) structural components, (2) masonry walls of 1 <sup>st</sup> floor, (3) curtain walls, (4) full/partial interior wall partitions, (5) suspended ceilings, (6) independent pendant lighting, (7) elevator, ducting, air handling unit on the roof, and control panel, (8) fire sprinklers.....	197
Figure 5.9 Typical floor plan for (a) steel diagrid framed (SDF) and (b) reinforced concrete framed (RCF) archetypes .....	200
Figure 5.10 Empirical CDF of $S_a(T_1, 5\%)$ and fitted lognormal fragility functions for various archetypes.....	202
Figure 5.11 Sensors located at diagrid nodes and structural members affected by corrosion .....	205
Figure 5.12 Variation of DI for (a) ACC with sensors at diagrid nodes and (b) all EDPs with one sensor at each floor of SDF archetype .....	206
Figure 5.13 Variation of DI for (a) ACC with sensors at beam-column nodes and (b) all EDPs with one sensor at each floor of RCF archetype.....	206
Figure 5.14 Variation of mean DI for (a) Disp, (b) ACC, and (c) IDR for all sensors... ..	208
Figure 5.15 Functionality curve of original SDF archetype under scenario earthquake 2 (numbered arrows show the repair time for various components: (1) structural components including diagonals, beams, and connections, (2) curtain and partition walls, (3) raised access floors and suspended ceilings, (4) independent pendant lighting, (5) hydraulic elevator and chiller on the roof, (6) HVAC ducting, air handling unit, and fire sprinklers.....	210
Figure 5.16 Comparison of functionality curves for (a) SDF and (b) RCF archetypes undamaged and various damaged cases under scenario earthquake 2.....	211
Figure 6.1 Life-cycle functionality of a system (not to scale) .....	224
Figure 6.2 Hearst Tower, New York City, one the first iconic steel diagrid buildings ..	231

Figure 6.3 Typical floor plan for (a) steel diagrid archetypes (SD-45, SD-63, SD-72), (b) RCF, (c) RC-2SW, and (d) RC-1SW archetypes.....	233
Figure 6.4 Empirical CDF of $S_a$ (T1,5%) and fitted lognormal fragility functions for (a) steel and a(b) RC building archetypes .....	234
Figure 6.5 CDF of (a) loss and (b) downtime for SD-63 archetype for Scenario 1, 2, and 3 earthquakes .....	237
Figure 6.6 CDF of (a) loss and (b) downtime for various archetypes for Scenario 2 earthquake .....	238
Figure 6.7 Floor-by-floor repair time for structural and non-structural components affecting occupancy and serviceability for (a) SD-63, (b) RCF, and (c) RC-1SW archetypes .....	240
Figure 6.8 Functionality curve based on asset loss for SD-63 archetype under Scenario 2 earthquake, numbered arrows show the repair time for various components: (1) structural components, (2) concrete tile roof, (3) walls and stair, (4) suspended ceiling and raised access floor, (5) independent pendant lighting, (6) elevator and plumbing, (7) chiller, (8) HVAC, ducting, fire sprinkler, diesel generator, and control panels, (9) furniture .....	241
Figure 6.9 Functionality curve based on occupancy for SD-63 archetype under Scenario 2 earthquake, numbered arrows show the occupancy repair time for various floors .....	243
Figure 6.10 Functionality curve based on serviceability for SD-63 archetype under Scenario 2 earthquake, numbered arrows show the serviceability repair time for various floors .....	244
Figure 6.11 Functionality surfaces based on (a) occupancy and asset losses and (b) serviceability and asset losses for SD-63 archetype under S2 earthquake .....	245

# Preface

A version of Chapter 2 has been published as *Seismic Performance Assessment and Loss Estimation of Steel Diagrid Structures* in the *Journal of Structural Engineering*, 144(10), 04018179. The author developed the framework and performed modeling, data collection, analysis, and writing, with indispensable help from Dr. Yue Li and technical comments from Dr. YeongAe Heo.

A version of Chapter 3 has been published as *Multi-Criteria Decision-Making for Seismic Resilience and Sustainability Assessment of Diagrid Buildings* in the *Engineering Structures*, 191, 229-246. The author developed the decision framework and performed the analyses for case studies and summarized conclusions. Dr. Yue Li and Dr. Abdullahi Salman offered valuable suggestions and guidance throughout the preparation and review.

A version of Chapter 4 is submitted as *Risk-informed Multi-criteria Decision Framework for Resilience, Sustainability, and Energy Analysis of Reinforced Concrete Buildings* to the *Journal of Building Performance Simulation* for possible publication. The author developed the decision framework and numerical models and performed the cost, loss, downtime, and casualty analyses for case studies, wrote the manuscript and summarized the conclusions. Zhenglai Shen helped with whole-building energy simulation and analysis of outputs for energy simulation. Dr. Yue Li, Dr. Abdullahi Salman, and Dr. Hongyu Zhou offered valuable suggestions and guidance throughout the preparation of the manuscript.

A version of Chapter 5 is planned to be submitted as *Localized Health Monitoring System for Resilience Quantification and Safety Evaluation of Smart Structures* to the

*Structural Safety.* The author developed the framework and numerical models and performed the analyses for case studies, wrote the manuscript and summarized the conclusions. Dr. Yue Li, Dr. Abdullahi Salman, and Dr. Bill Yu offered valuable suggestions and guidance throughout the preparation of the manuscript.

# Acknowledgments

I would like to express my deepest appreciation and gratitude to my advisor, Professor Yue Li, who kindly guided me throughout the past three years with his caring attitude and profound knowledge. He continually and openhandedly conveyed a spirit of curiosity, humility, excellence in research, and excitement and devotion in teaching to me. Without his guidance and persistent help this dissertation would not have been possible.

I am also extremely grateful to my committee members, Professor Wojbor Woyczynski, Professor Bill Yu, and Professor Michael Pollino, for their kind support and invaluable insights throughout my study and dissertation preparation. Each of the members of my dissertation committee has provided me extensive technical and professional guidance and I have learned a great deal about both scholarship and professional life from them. I would especially like to thank Professor Bill Yu, the Interim Department Chair, for his devotion to creating a dynamic educational atmosphere in the department and his kind support of me and all students at the Department of Civil and Environmental Engineering.

I am grateful to all my colleagues and classmates and all whom I have had the pleasure to work during this and other related projects. I would like to extend my appreciation to Dr. Abdullahi Salman at The University of Alabama in Huntsville, Dr. Hongyu Zhou at The University of Tennessee, Knoxville, and Ram K. Mazumder with whom I had the pleasure of collaborative research.

Risk-informed Multi-criteria Decision Framework for Resilience and Sustainability  
Assessment of Building Structures

## **Abstract**

By

ESMAEEL ASADI

Seismic risk has increased noticeably in the last decades due to rapid growth of earthquake-prone urban regions and deterioration of aging infrastructure. Meanwhile, mounting evidence of changing climate has reinforced experts' efforts to develop new techniques for sustainable design of structures. Recent studies point to the need for an integrated approach to include both sustainability and resilience criteria in design of building environments.

This dissertation integrates seismic resilience quantification methods with economic input-output life cycle assessment and whole-building energy simulation methods to present a new comprehensive decision model for design of building environments. A new multi-criteria decision framework is introduced to integrate various resilience and sustainability measures including asset loss, downtime, number of casualties, greenhouse gas emissions produced by construction, maintenance, and seismic repair, and annual energy consumption and cost. The risk in decision analysis in addition to vulnerability and loss analyses are included via a combined model using analytic hierarchy process, multi-attribute utility theory, and Technique for order preference by similarity to ideal solution (TOPSIS) methods. Results show that with a multi-criteria approach, the benefits of sustainable design techniques can outweigh possible shortcomings in structural

performance. The proposed framework is implemented on a series of steel diagrid and reinforced concrete buildings. A comprehensive investigation into the nonlinear dynamic performance of steel diagrids is also conducted and new seismic performance criteria are developed for loss estimation. Diagrids are found to have a substantial collapse capacity but, the non-structural loss due to large maximum absolute floor acceleration may increase expected total loss.

Lastly, a new framework is introduced for resilience quantification and rapid safety evaluation of building structures using data obtained from a localized health monitoring system. The framework uses three-dimensional functionality functions based on asset, occupancy, and serviceability losses to quantify a new resilience index. An autoregressive exogenous damage identification model is used to detect, locate, and measure damage in the structure. Minor damages due to corrosion and major damages due to past earthquakes are both studied.

# Chapter 1

## 1. Introduction

Earthquakes cause billions of dollars of economic loss and claim thousands of lives every year around the world. Among 128 significant earthquakes (M7.0 or greater) that occurred worldwide in the last decade, the M9.0 Tohoku, Japan earthquake in 2011 alone caused about 220 billion USD damage (FEMA et al. 2017; NGDC/WDS 2019). Seismic risk has increased noticeably due to significant population growth in earthquake-prone urban regions and the increasing vulnerability of aging buildings and infrastructure (FEMA et al. 2017).

Seismic Resilience refers to the capability of the system to resist an abnormal commonly stochastic disturbance, i.e. earthquake, mitigate the damage, and recover efficiently to the original functionality (Bocchini et al. 2014; Lounis and McAllister 2016; Roostaie et al. 2019). A resilient system need to have four properties (4 R's): (1) robustness is the ability and strength to withstand abnormal demand, (2) redundancy is the ability to provide substitute route to sustain functionality, (3) resourcefulness refers to the ability to identify the problems and priorities, and mobilize the human and material resources

efficiently to repair the damages and restore functionality, and (4) rapidity is the capability to restore functionality and meet the priorities in a timely manner (Alipour and Shafei 2016; Bruneau et al. 2003). Resilience can be assessed for components of a structure/infrastructure system or the entire system. Community resilience represents the ability of the community to withstand an extreme event such as earthquake and/or hurricane, contain and mitigate the disaster impacts once happened, and recover from impacts efficiently. The goal of community resilience is to minimize the social consequences (due to casualty, injury, fatality, post-event depression, etc.) and economic loss (due to damages to structural and non-structural components, reconstruction, closure of business, etc.) caused directly or indirectly by the extreme event. Maintaining the emergency-level functionality state, where emergency services and lifelines are accessible to the entire community, is the primary objective in a resilient community.

In addition, mounting evidence of changing climate and increasing loss due to various natural hazards have reinforced experts' efforts to develop new tools and techniques for sustainable and resilient design and construction of civil structure and infrastructure systems. Global warming driven primarily by increased carbon dioxide concentration in the atmosphere has amplified the frequency and intensity of weather and climate hazards. To reduce the carbon footprint and other environmental impacts, several studies aimed to include sustainability criteria in the design of various structure and infrastructure systems (Kamali et al. 2018; Moussavi Nadoushani et al. 2017; Padgett and Li 2016). Sustainable design of structures can substantially decrease the life-cycle economic and environmental loss whilst improving the resilience of buildings. Seismic environmental consequences can

be significant in seismic regions and need to be an essential part of a comprehensive performance assessment framework (Menna et al. 2013). Using innovative and efficient structural systems such as diagrids can effectively improve the sustainability and resilience of buildings (Asadi and Adeli 2017; Liu et al. 2018; Milana et al. 2015). Due to their aesthetics and structural advantages, diagrid structures have been used for several buildings around the world. However, their seismic performance, collapse fragility, and resilience are yet to be studied.

Resilience and sustainability are both of significant importance in next-generation performance assessment of civil infrastructures and have been increasingly studied in recent decades, but in most cases separately (Bocchini et al. 2014; Phillips et al. 2017). Both topics deal with social and economic impact of structure and infrastructure systems particularly the time-based consequences of inappropriate construction, maintenance, and risk management practices. Yet despite their inherent connection, a few studies have tried to integrate them and produce a uniform multi-purpose performance assessment framework for building environments (Bocchini et al. 2014; Lounis and McAllister 2016; Padgett and Li 2016; Roostaie et al. 2019). To mitigate environmental impacts while addressing the increasing risk due to seismic hazard, recent studies advocate for an integrated approach which includes both sustainability and resilience criteria in design/rehabilitation of structure and infrastructure systems (Belleri and Marini 2016; Bocchini et al. 2014; Phillips et al. 2017; Simonen et al. 2018).

To quantify the total life-cycle cost, a simple approach used in the literature is to convert all losses, including environmental, life, and time loss, into a monetary loss (Han et al. 2016; Mitrani-Reiser 2007). This approach, however, adds to epistemic uncertainty because of regional and case-based assumptions required for such conversion (Chau et al. 2015; Lloyd and Ries 2007). Aiming to study the trade-off between various economic, social, and environmental impacts of earthquakes, multi-criteria decision making (MCDM) methods can integrate various criteria/attributes and quantitatively find the ideal solution (Invidiata et al. 2018; Kumar et al. 2017; Ustinovichius et al. 2007; Wallenius et al. 2008). MCDM provide more flexibility for problems where the objective is not solely minimizing monetary losses, e.g. a problem where the objective is to minimize the number of casualties.

Risk-based decision models need further study as well, given the aleatoric and epistemic uncertainty involved in both resilience and sustainability analyses. Multi-attribute utility theory (MAUT) is recommended for problems involving risk, uncertainty, and subjective probability (Mateo 2012). MAUT is suitable for problems involving subjective criteria and risk and uncertainty in performance (Invidiata et al. 2018; Wallenius et al. 2008; Zavadskas et al. 2007). In MAUT, risk can be included in the decision maker's preference by using different attitudes towards risk while quantifying utility functions. This is a step further than incorporating risk in hazard analysis, vulnerability assessment, and loss estimation.

## **1.1 Literature Review and Critical Appraisal**

### ***1.1.1 Resilience Assessment***

Resilience is the capability of the system to resist, adapt to, and recover from a disruptive event. Resilience can be studied in four phases: anticipation, absorption, adoption, and recovery (Alipour and Shafei 2016). Anticipation refers to the probabilistic state of knowledge about hazard intensity and system performance and may include probabilistic hazard and collapse fragility analyses, hazard and system identification, and vulnerability assessment. Absorption represents the capability of the system to resist the disruptive event and absorb destructive energy. Ductility reflects this capability of the structural systems. Adoption refers to the capability of the system to provide alternative routes to maintain functionality once some routes fail. This capability significantly depends on the redundancy of the system and has been widely studied in terms of progressive collapse resistance of different structural systems (Ellingwood and Leyendecker 1978; Gsa 2003; Izzuddin et al. 2008; Kim and Lee 2010; Pham et al. 2017; Vlassis et al. 2008). The recovery phase discusses the rapidity of regaining the initial functionality and refers to the restorative capacity of the system. Loss/downtime estimation analyses provide a measure for restorative capacity. Thus, resilience assessment integrates several well-established engineering fields of study such as performance-based engineering and risk analysis and management to provide a comprehensive approach for structure and infrastructure system analysis.

Resilience can be achieved by (1) reducing the probability of failure of system and individual components, (2) reducing the consequence and loss due to the disruptive event including the monetary loss, fatality, injuries or any social and/or economic impact, and (3) reducing the downtime, repair and recovery time required to restore the normal/original functionality (Bruneau et al. 2003). Though restoring the original functionality is the typical objective, the original state of the structure and infrastructure system might be insufficient against the required or design functionality or performance considering the continually-updated hazard maps and the impact of climate change. Therefore, the decision-maker may require improved functionality beyond the original state.

#### **1.1.1.1 Seismic Risk Assessment**

Due to uncertainties, risk is a part of any engineering problem. Reliability methods can quantify the potential risk in design processes and find where the code provisions and the potential risk are not balanced (Ang and Tang 2007; Ellingwood 2000). The main sources of uncertainty in structures include ground motion, hazard prediction models, structural response and performance, damage, loss, and consequence, and risk in communication and decision analysis with the ground motion being the most significant (Kinali and Ellingwood 2007; Sakurai et al. 2001). Uncertainty in ground motion is caused by either aleatoric (inherent) randomness of amplitudes, phase angle, and shape of seismic hazard curve or epistemic (modeling) uncertainty in man-made seismic models (Ellingwood and Kinali 2009; Yin and Li 2010). Identification of the aleatoric and epistemic uncertainty is critical since the former is inherent and cannot be reduced but the latter is man-made and can be reduced by improving the accuracy of modeling approaches

(Ang and Tang 2007; Ang and De Leon 2005). Therefore, a comprehensive but practical probabilistic approach is needed for a realistic reliability-based performance assessment (Biondini and Frangopol 2016). Particularly for life-cycle assessment, probabilistic analysis is used to obtain realistic results then represent them in an explicable and detailed manner to decision-maker (ISO 1998, 2007; Lloyd and Ries 2007). The transition from deterministic methods such as allowable stress design (ASD) to semi-probabilistic methods such as load and resistance factor design (LRFD) and the recent FEMA reports (ATC 2009; FEMA 2012) on the practical ways for including uncertainty in performance assessment shows the general consent among engineering body toward probabilistic methods. However, due to complexity of the problem, a numerical method such as Monte Carlo simulation with appropriate sampling techniques such as Latin Hypercube Sampling is needed.

### 1.1.1.2 Loss and Downtime Analysis

The total probability of loss at a given earthquake intensity ( $IM$ ) for mutually exclusive seismic events is defined as follows (Ramirez and Miranda 2012a; Yamin et al. 2017):

$$\begin{aligned}
 & P(L_T > l | IM = z) \\
 &= \int_{EDP} \int_{DS} P(L_T > l | DS = DS_{ij}) P_{DS}(DS | EDP = d) P_{EDP}(EDP | IM = z) dDS dEDP \quad (1.1)
 \end{aligned}$$

where  $P(L_T > l | IM = z)$  is the probability of having a total loss greater than  $l$  given that hazard intensity is equal to  $z$ ,  $P(L_T > l | DS = DS_{ij})$  is the probability of having a total loss greater than  $l$  given that damage state of  $DS_{ij}$  is achieved,  $P_{DS}(DS | EDP = d)$  is the PDF

of achieving a damage state given that the Engineering Demand Parameters (EDPs) reaches a certain value of  $d$ , and  $P_{EDP}(EDP|IM = z)$  is the PDF of the EDP conditioned on a certain hazard intensity  $z$ . The fragility function is used to find the probability that each damageable component reaches a certain damage state as follows.

$$\begin{aligned}
 & P(DS_n = DS_{ij}|EDP = d) \\
 & = \begin{cases} 1 - F_{DS_{ij}|EDP=d_j} & \text{for } j = 0 \text{ (undamaged)} \\ F_{DS_{ij}|EDP=d_j} - F_{DS_{i(j+1)}|EDP=d_j} & \text{for } 1 \leq j < n \\ F_{DS_{ij}|EDP=d_j} & \text{for } j = n \text{ (undamaged)} \end{cases} \quad (1.2)
 \end{aligned}$$

where  $F_{DS_{ij}|EDP=d_j}$  is the fragility function of the  $i$ th component in the  $j$ th damage state given that the EDP is equal to a certain value  $d$ .

The total economic loss ( $L_T$ ) is the summation of direct loss ( $L_D$ ), such as repair or replacement cost of each damaged or collapsed components, and indirect cost ( $L_I$ ), such as downtime cost and cost due to business interruption (Yamin et al. 2017). The direct loss is, in turn, the summation of loss to each damageable component  $i$ .

Another key parameter in seismic resilience assessment, particularly for commercial buildings, is the repair time required to fix the damages caused by earthquakes. This repair time, called downtime, shows the functional recovery and rapidity after an extreme event. Based on the total replacement time, the maximum number of workers per unit area, and the expected repair time required for each structural and nonstructural component, the repair time for each floor can be evaluated. The downtime is usually evaluated for two repairing schemes: (1) parallel schemes where simultaneous repairing on all floors is possible and (2) serial scheme where repair is done for one floor at a time starting from the

first floor to the roof. The actual repair time is between this upper bound, that is the serial repair time, and lower bound, that is the parallel repair time, depending on project planning and scheduling.

### **1.1.1.3 Indirect Losses**

The indirect consequences of an extreme event include the economic loss caused by loss of rental or business income, social consequences due to casualty, fatality, dislocation of residents and property loss, and environmental consequences due to demolition and repair/replacement of the building. The expected loss due to casualty can also be find considering a monetary loss for fatality. For example, fatality is assumed to have an expected monetary loss off 4.16 M USD with a coefficient of variation (COV) of 0.4 (Mitrani-Reiser 2007). The time needed to regain the primary functionality (downtime) is a probabilistic function depending on the damage states and component-dependent repair time as well as the number of workers available per unit floor area per day. Two repair planning schemes: slow-track (serial planning) and fast-track (parallel planning) are considered for downtime analyses. The expected total downtime can be used to estimate the economic loss due to the downtime considering a monetary loss of 960 USD per floor per day (De Iuliis et al. 2019; Dong and Frangopol 2016).

Damage to the main buildings and other components of the community may cause congestion and inaccessibility in some areas of the community. This will increase the travel time and reduce the traffic flow capacity which leads to significant indirect loss, in some cases greater than direct loss due to an extreme event (Alipour and Shafei 2016; Padgett and DesRoches 2007). Also, the inaccessibility will reduce the productivity of industries,

and businesses in the affected region since it affects the delivery time of materials, customer/employee access to store, etc.

#### **1.1.1.4 Casualty Estimation**

A key factor in casualty estimation is the collapse modes of the structure under certain extreme events (Coburn et al. 1992). Based on the number of occupants on each floor, the probability of their hourly, daily, and weekly presence, and the probability of collapse associated with each floor, the PDF of casualty can be evaluated (Nocera and Gardoni 2019; Reinoso et al. 2018). For assessing the number of casualties including injuries and fatality after an earthquake, a population model should be developed for the building, which typically describes the number of people present in the building per 1,000 sq. ft of floor area. A peak population is also defined based on the occupancy of the building, e.g. commercial, residential, and the population during the month of the year, days of the week, and time of day are presented in terms of fractions of the peak population (FEMA 2012).

#### **1.1.1.5 Performance Indicators for Resilience Quantification**

To quantify resilience, a series of performance indicators are commonly considered which can reliably represent the performance and functionality of the system. Performance of the complete structure depends on the damage/health state of its components. Total collapse of a structure starts from local and partial failure of its components. A set of pre-defined damage or limit states, typically two to five states, is used to categorize the step-wise failure of each component and the entire system (Biondini and Frangopol 2016; Burton et al. 2017). Structural performance indicators are used to assess the possible local and global failure in structural system. Ductility, redundancy, robustness, and resilience

are among key structural performance indicators (Ghosn et al. 2016). Ductility is the ratio of collapse lateral displacement to the effective yielding displacement which can be estimated based on nonlinear static analyses (ATC 2009). Ductility represents the structural capacity to dissipate excess energy produced by an extreme event, such as earthquake. Structural redundancy is a measure of alternative load paths in the structure once one fails. The capability of the structural system to redistribute the loads to alternative paths improves system performance under stochastic extreme events such as earthquake (Bertero and Bertero 1999). Robustness is a measure of system capacity to avoid disproportionate response to accidental and abnormal loads (Biondini and Frangopol 2016; Ellingwood 2006). Resilience has been studied not only for the structural systems but also for infrastructure systems and the whole community and as discussed, reflects the systems capability to withstand hazard impacts and regain its original functionality rapidly and efficiently (Cimellaro et al. 2010; Deco et al. 2013; Padgett and DesRoches 2007).

#### **1.1.1.6 Quantifying Resilience**

In most previous studies, resilience is quantified as the rapidity of the system to recover from a damaged state caused by a stochastic hazard to the initial undamaged state and gain its pre-hazard functionality (Venkittaraman and Banerjee 2014). Resilience ( $R$ ) is defined as the integration of functionality ( $Q$ ) over a specific time range ( $T_R$ ) after the event occurs at a specific time  $t_0$  (Cimellaro et al. 2010, 2016).

$$R = 1/T_R \int_{t_0}^{t_0+T_R} Q(t)dt \quad (1.3)$$

After an extreme event such as earthquake, hurricane, or flood, it takes a period of time (downtime) to repair the damages, regain the losses and bring the building back to its primary functionality. The functionality of the building depends on its damaged state after the event. Three to five damage states are to be considered for the building based on damages to primary and secondary structural and non-structural components. The damages are estimated according to damage indicators, EDPs, such as maximum inter-story drift (IDR) and maximum absolute spectral acceleration (ACC). These indicators are evaluated by nonlinear fragility and performance analyses. Considering a five-level criterion per FEMA reports (ATC 2009; FEMA 1997, 2012), the structure falls in undamaged, Immediate Occupancy (IO) or minor damage, Life Safety (LS) or moderate damage, Collapse Prevention (CP) or severe damage, and collapse or fully damaged state after the extreme event.

#### **1.1.1.7 Community Resilience**

The most critical components of the community in terms of the resident's life and community functionality are the power and water distribution systems, emergency health care institutions, and fire and police departments (Bruneau et al. 2003). The serviceability of all these components directly or indirectly depends on critical facilities and buildings which need to be designed for immediate occupancy considering design hazard intensities (Sattar et al. 2018).

Bruneau et al. (2003) proposed a conceptual framework for seismic community resilience assessment. The framework separates the pre- and post-event activities and

includes a decision-making procedure that theoretically leads to a resilient community. The framework, however, lacks quantitative components and has not been evaluated for case studies. Moreover, it does not include sustainability criteria and does not study intelligent structure and infrastructure systems. Nonetheless, their research initiated over a decade of research and discussion on the resilience assessment of systems and communities among engineering communities and academic scholars.

Cimellaro et al. has published a series of analytical studies on resilience assessment various structure and infrastructure systems including buildings, natural gas distribution networks, and urban water distribution networks under natural hazards specifically earthquakes (Cimellaro et al. 2006, 2010, 2016; De Iuliis et al. 2019; Reinhorn and Cimellaro 2014). They propose a dimensionless metric for resilience incorporating the whole-building loss estimation and a simplified recovery time function. Their framework lacks decision-making and sustainability though. Lounis and McAllister (2016) developed a framework for resilience and sustainability assessment of structural systems and used it to assess two sample highway bridges. In their case studies, they consider life-cycle impacts such as concrete degradation, social impacts such as accidents and user time, and environmental impacts such as greenhouse gas emission and waste amount. However, they do not study the casualty, fatality, and other social impacts of the disaster. Sutley et al. (2016a; b) incorporate social impacts on population introducing a coupled framework for seismic community resilience assessment which includes six socioeconomic variables, i.e. age, gender, ethnicity, structure of family, socioeconomic status, and density of the environment. They use the HAZUS database (DHS 2003) and over 33 previous studies to

find the correlation between those variables and three social (morbidity) indicators, which are injury, fatality and posttraumatic stress disorder (PTSD). Figure 1.2 depicts a schematic of their proposed coupled framework incorporating social and engineering models. They illustrate their model through resilience assessment of a residential community in Los Angeles County consist of 100,000 buildings which are based on 37 different wood-framed archetypes. All buildings are assumed to be at the same distance from earthquake epicenter.

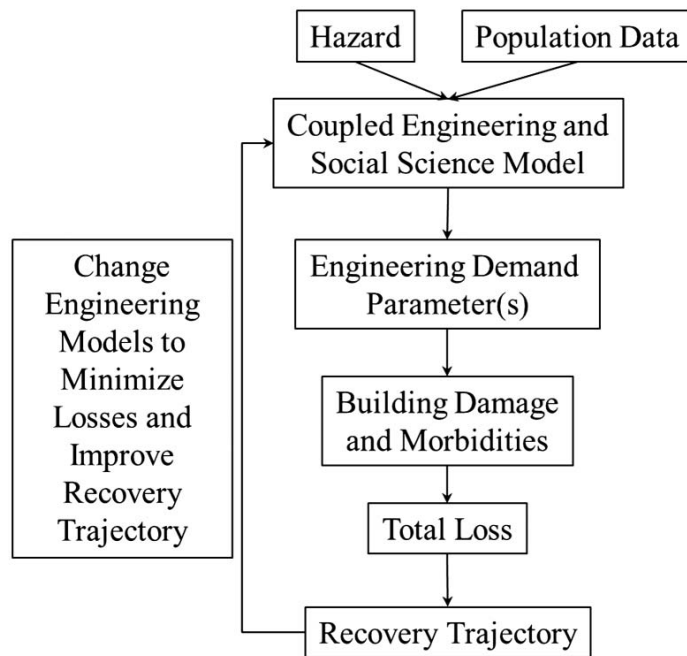


Figure 1.1 Schematic of Sutley et al. (2016a; b) proposed coupled framework

### 1.1.1.8 Structural Health Monitoring for Resilience Assessment

Smart buildings market is a growing industry with a 33.7% annual growth projection in the next five years to a \$31.74 billion market (Singh 2017). Smart buildings can be equipped with a network of sensors for monitoring energy and water consumption and vibration-based response of the structure. The sensor network records the real-time structural performance in normal operation as well as under extreme events like

earthquakes and can provide instant damage reports. The damage reports substantially reduce the time and the cost required for post-event inspection and emergency rescue missions. This will increase the robustness and resourcefulness of the system and reduce the post-event resorting time. A number of researchers in recent years have studied seismic performance and loss of instrumented building structures (Celebi et al. 2004; Cremen and Baker 2018; Hwang and Lignos 2017a, 2018; Porter et al. 2006). Yet, studies on structural health monitoring (SHM) systems are focused on damage identification and as noted by Cremen and Baker (2018), a few applied SHM in loss estimation.

### ***1.1.2 Sustainability Assessment***

Sustainability is a probabilistic function of environmental, economic, and social impacts of construction, maintenance, and demolition. Sustainable design and construction of buildings have been increasingly studied in recent years and it has become one of the main research areas in civil engineering (Alshamrani et al. 2014; Bocchini et al. 2014; ISO 1998; Kaatz et al. 2006). Buildings consume over 40% of energy in US producing substantial amount of greenhouse emission (Horvath 2004). About 30% of all energy consumed in a building during its lifetime is in the form of embodied energy (Ibn-Mohammed et al. 2013). Embodied energy, commonly measured in kg CO<sub>2</sub> equivalent per unit weight material, is the amount of energy needed for the life-cycle of a specific material including energy required for extraction, processing, and transportation. Three ways are proposed for reducing embodied energy: (1) reducing the volume of material required, (2)

using recycled materials, and (3) efficient preparation and erection practice to reduce construction waste (Gallivan et al. 2010; Wei et al. 2015).

The sustainability function ( $M_S$ ) is defined as a summation of consequences (in terms of loss, casualty, carbon dioxide emission, etc.) caused by collapse ( $C$ ) and non-collapse damage ( $NC$ ) under a given hazard intensity ( $IM$ ) (Dong and Frangopol 2016).

$$M_S = C_{Cons|C}P_{C|IM} + C_{Cons|NC}(1 - P_{C|IM}) \quad (1.4)$$

where  $C_{Cons|C}$  and  $C_{Cons|NC}$  are the cumulative distribution function (CDF) of total consequences due to collapse and non-collapse damage, respectively and  $P_{C|IM}$  is the probability of collapse for a given hazard intensity of  $IM$ . Given the probabilistic nature of the analyses, typical Monte Carlo (MC) or Latin Hypercube Sampling (LHS) can be used to evaluate sustainability.

#### **1.1.2.1 Life-Cycle Assessment**

The total life-cycle cost of a building or product includes direct costs due to construction, operation, maintenance, monitoring, repair and replacement in addition to indirect costs due to closure, failure, and defective performance (Biondini and Frangopol 2016; Kamali et al. 2018). The environmental impacts of any product or process can be evaluated using Life-Cycle Assessment (LCA). LCA can be performed with two approaches: (1) non-seismic conventional LCA, e.g. considering the environmental impacts of building construction, maintenance, and daily energy consumption, and (2) LCA of earthquake consequences, e.g. considering the environmental consequence of damage caused by earthquake in addition to economic and social impacts. In high-seismic

regions, the probability of damage due to earthquake is relatively significant throughout the life span of the building making the seismic sustainability assessment a valuable part of decision-making process. Similar to resilience assessment, these impacts will be evaluated with two approaches: intensity-based and time-based approaches.

The environmental consequence of the repair activity is evaluated using the economic input-output (EIO) method and/or bill-of-material (BOM) LCA method. In the EIO method, the cost of the project (here repair project) is used to estimate the environmental impacts. Carnegie Mellon University has developed an EIO-LCA model based on historical economic-environmental data for various industry groups and sectors. The model can estimate the total greenhouse gas emission, energy consumption, toxic release, and water use based on monetary cost of the project (CMU GDI 2018). On the other hand, BOM is a more detailed approach which can produce more accurate result if a reliable database of materials is available. In BOM method, the exact amount of any material used in the project such as steel, concrete, gypsum, glass, etc. needs to be evaluated. These amounts are used to estimate the life-cycle environmental impacts of the project in terms of greenhouse gas emission, energy consumption, etc.

Life cycle assessment (LCA) provides a more comprehensive tool incorporating the life-long environmental, social, and economic impacts of structure and infrastructure in decision analysis (Stewart et al. 2011, 2012). The second-generation performance-based assessment methodology presented in FEMA P-58 (2012) provides a detailed framework for seismic loss analysis of buildings with various structural and non-structural

components. Its 4<sup>th</sup> volume, FEMA P-58-4, expands the methodology to incorporate LCA in seismic performance assessment. LCA is implemented through environmental metrics such as global warming (climate) potential (GWP), primary energy consumption, non-renewable energy, and waste generation to evaluate the lifetime impact of a building (Chhabra et al. 2018; FEMA 2012; ISO 1998). The widely-used GWP metric is a measure of greenhouse gas emission, in terms of kg CO<sub>2</sub> equivalent, which is used to estimate life-cycle environmental footprint of a product or process.

### **1.1.2.2 Recycled Material**

Using recycled material as the primary material for the construction of steel structures will reduce the total embodied energy for the building. The recycled materials come with several benefits. First, producing recycled materials needs less energy than virgin materials. Second, recycled materials are mostly construction waste and otherwise should be discarded hence harmful to the environment. Third, source of recycled material may be closer to the construction site reducing the energy required to transport the material to the site. Even, the material may be acquired from the site itself, e.g. if another building at the site is to be demolished. In addition to mitigating the embodied energy, recycled material may reduce the construction cost as they are cheaper and should be discarded otherwise (Gallivan et al. 2010). However, using recycled materials increase the uncertainty in strength and capacity of the building. This is manifested in the dispersion associated with material yield and/or ultimate strength, section properties of structural members, etc.

### 1.1.2.3 Deterioration and Aging

The aging and deteriorating infrastructure affected by fatigue, chemical attack from polluted air and corrosive soil, physical damage, etc. pose an increasing risk to communities (Ellingwood 2005). The deterioration processes cause unanticipated and unsatisfactory structural performance under service and/or extreme loads. Different agencies have developed their corrosion-damage assessment programs to answer these safety concerns, particularly for bridge and highways infrastructure (Sohanghpurwala 2006). The risk increases considerably once the infrastructure is under excessive loads or seismic, and flood-induced hazards (Guo and Chen 2015; Sanchez-Silva et al. 2011; Zhu and Frangopol 2016). The ASCE (2013) reports that one in nine of the bridges in the US are considered *structurally deficit* and continually deteriorating. Such that annually \$20.5 billion is needed to resolve the backlog for repair by 2028.

Corrosion and fatigue are the main causes of long-time deterioration for steel structures. Corrosion reduces the original thickness causing a decrease in effective cross-sectional area, the moment of inertia or generally the strength of the member. Exposure to salt water and humid atmosphere accelerates the corrosion (Akgül and Frangopol 2004). Fatigue causes initiation and propagation of cracks in the members leading to premature failure below the static design loads (Fisher et al. 1998). For concrete structures, however, several time-variant hazards may cause deterioration including corrosion of reinforcement, carbonation, leaching, chemical attack by acids, salts, sulfate, and chloride, freeze-thaw cycle, alkali-silica or alkali-carbonate reactivity, erosion, abrasion, and thermal stress

(PCA 2002). Biondini and Frangopol (2016) present an exhaustive review of the concepts, methods, and publications regarding life-cycle deterioration assessment of structure.

Since parameters defining the deterioration are usually stochastic, a probabilistic time-variant model needs to be developed to evaluate their impact (Ellingwood 2005). A mathematical description is used to estimate the structural damage caused by progressive deterioration of materials and components. The gradual reduction of cross section can be used to assess damage due to corrosion of steel or abrasion, erosion, crushing, and cracking of concrete component. The damage index  $\gamma$  is defined as follows (Biondini and Frangopol 2014).

$$\gamma = \frac{p}{d_i} \quad (1.5)$$

where  $p$  is damage penetration and  $d_i$  the initial characteristic geometrical parameter. In the absence of accurate mathematical models, empirical data can be used to estimate the deterioration rate using regression analysis (Biondini and Frangopol 2016).

$$\gamma(t) = \alpha(t - t_i)^\beta, \quad \text{for } t > t_i \quad (1.6)$$

where  $\alpha$  and  $\beta$  are regression parameters based on available data and  $t_i$  is the initial time. Also, the uncertainty can be included in the model by considering random variables ( $\varepsilon_1(t)$  and  $\varepsilon_2(t)$ ) representing the error in data or modeling as follows (Melchers 1999, 2003).

$$\gamma(t) = \alpha(t - t_i)^\beta \varepsilon_1(t) + \varepsilon_2(t), \quad \text{for } t > t_i \quad (1.7)$$

### ***1.1.3 Sustainability versus Resilience***

Sustainability and resilience are interrelated objectives; both are centered around mitigating economic and social losses. Improving resilience will mitigate the damage, loss, and downtime if an extreme event such as earthquake or hurricane occurs and improving sustainability will alleviate the life cycle cost and harmful environmental, economic and social impacts of the building environment. The economic, social, and environmental consequences of an extreme event can be respectively evaluated in terms of the repair/replacement costs, the downtime and casualties, and the embodied energy and wasted energy (Asadi et al. 2020; Dong et al. 2013; FEMA 2012; Roostaie et al. 2019).

FEMA P-58 provides a comprehensive fragility specification database and a Performance Assessment Calculation Tool (PACT) which performs Monte Carlo analyses to estimate loss, downtime, and casualty of buildings under seismic hazard. A comprehensive tool to account for sustainability criteria such as greenhouse gas emissions and annual energy consumption needs to be consistent with well-accepted loss analysis frameworks such as FEMA P-58 approach.

### ***1.1.4 Diagrid Structures<sup>1</sup>***

In the past decade, diagrids have become increasingly trendy and several iconic buildings around the globe are built based on diagrid concept including the 36-story Capital Gate, Abu Dhabi, United Arab Emirates and the 41-story Swiss Re Building in London, UK (Ali and Moon 2007; Boake 2014). Their versatile triangulated shape is suitable to create diverse geometrical forms which will enhance the outlook and aesthetical traits of the building.

Diagrid structural system is a variation of tubular structures which employs inclined members instead of conventional vertical columns to carry both gravity and lateral loads. Figure 1.1 shows the components of a conventional diagrid structure. The inclined members, called the diagonals, shape the outer façade of the structure and are connected to each other at diagrid nodes at floor levels. An exterior floor beam, called the ring beams, connects the nodes together at the floor level. In practice, diagrid nodes do not necessarily form in every single floor; in Figure 1.1 for example, they are formed every three floors. The location of nodes is commonly used to define the diagrid modules where the diagrid frame is divided into a number of modules along the height of the structure (3-story

---

<sup>1</sup> The material contained in this Subsection was in part previously published in the journal *The Structural Design of Tall and Special Buildings*. See Appendix I for documentation of permission to republish this material.

Asadi, E., Adeli, H. (2017). Diagrid: An Innovative, Sustainable and Efficient Structural System, *The Structural Design of Tall and Special Buildings*, 26(8):e1358, DOI: 10.1002/tal.1358. See Appendix I for documentation of permission to republish this material.

modules in Figure 1.1). Similar diagonal cross-section may be used for each module. The omission of the columns from the exterior frame provides a more open façade for the light to enter while giving more space to architect to work with. Due to considerable lateral stiffness of the system, there is commonly no need for auxiliary lateral system such as outriggers and the internal structural system mostly carries the gravity loads.

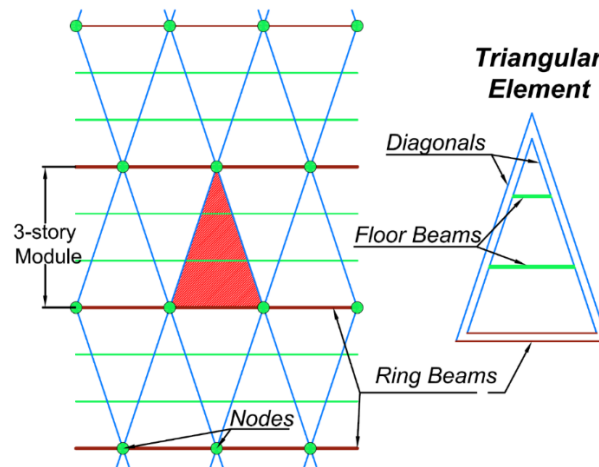


Figure 1.2 Three 3-story diagrid modules and a sample triangular element

A basic element of the diagrid system is the triangulated element consisting of two inclined diagonals and a vertical ring beam (Figure 1.1). One approach to design diagrids is to design them as a set of connected three-edge triangular elements which ignores the shear and bending forces in ring beams (Mele et al. 2014). Another more common approach is to design them as a grid of diagonal members and ignore the effect of ring beams in their behavior (Moon 2008; Moon et al. 2007). A number of preliminary design methods are proposed for diagrid which ignore bending moment and shear forces in diagonal members (Milana et al. 2015; Moon 2011; Moon et al. 2007). Recently, the design and performance of 1diagrid structures have attracted several researchers (Asadi and Adeli 2018a; b;

Heshmati and Aghakouchak 2019; Kim and Lee 2012; Moon et al. 2007; Sadeghi and Rofooei 2018; Tomei et al. 2018; Zhang et al. 2012).

The topology of the diagrid and the angle of the diagonals with the horizontal are the two key factors affecting the lateral stiffness and structural efficiency of diagrids. Moon et al. (2007) study the diagonal angle in the range of  $34^\circ$  to  $82^\circ$  in 20-, 42, and 60-story diagrid building structures with an aspect ratio in the range 2-7. They conclude the best angle for the 42 and 60-story diagrids in terms of maximum lateral stiffness is in the range of  $55^\circ$  to  $65^\circ$  and  $65^\circ$  to  $75^\circ$ , respectively. In a similar study, Kim and Lee (2012) report that for 36-story diagrid structures under seismic lateral loads diagonal angle in the range of  $60^\circ$  to  $70^\circ$  is the most efficient. Zhang et al. (2012) study diagonal arrangements in 30-, 37-, 45-, 60-, and 75- story diagrids with aspect ratio in the 3.6-9 range and propose a varying diagonal angle that decreases from the bottom to the top of the structure. In a similar study, Zhao and Zhang (2015) study diagrids having curved diagonal members and varying angles.

In each diagrid node, at least, four diagonals and two beams are connected to each other making their design, fabrication, and assembly particularly complicated. Because of the diagrid triangulated form, diagonals are mostly under large axial compression or tension loads. Thus, the connections are primarily designed to transfer large axial forces rather than bending moment and/or shear force. Researchers have proposed specific configurations and detailing for diagrid connections based on experimental and analytical

studies on diagrid connections made of steel (Kim et al. 2010, 2011), concrete filled steel tube (CFST) (Huang et al. 2010), and reinforced concrete (Zhou et al. 2013).

To understand the structural behavior of diagrids under extreme loads it is essential to explore the nonlinear characteristics and governing failure mechanisms of the structure. A subject of great interest is the sequence of plastic hinge formation in diagrid members. The governing failure mechanism provides the code developers and designers with a better understanding of diagrid nonlinear behavior. Kim and Lee (2012) study the seismic performance of a number of 36-story diagrid tubular structures with a diagonal angle in the range of  $50.2^\circ$  to  $79.5^\circ$  using static and dynamic nonlinear analyses. They consider two different plan shapes, circular and square, and report that the circular plan yields higher strength than the square plan because of the smaller shear lag effect in the circular case. Using Buckling-Restrained Braces (BRBs) for diagrid members, they claim that they improve the strength and ductility of the structure considerably while providing a slightly smaller stiffness than conventional steel bracings. Milana et al. (2015) consider four 40-story structures: three diagrid structures with a diagonal angle of  $42^\circ$ ,  $60^\circ$ , and  $75^\circ$  and a conventional tubular structure with an outrigger at the 29<sup>th</sup> story. Comparing the weight of the structures they report a weight reduction of up to 33% for the  $75^\circ$  diagrid compared with the conventional tubular structure. They conduct static nonlinear analysis and report that the  $60^\circ$  diagrids have a better overall performance than other cases in terms of strength, stiffness, and ductility.

### ***1.1.5 Decision Analysis***

Decisions on repair/rehabilitation/replacement of a structure, whether for maintenance purpose or to minimize future damages due to extreme events, involve numerous interrelated performance measures, indicators, and criteria called attributes here. In a coupled sustainability and resilience framework, the metrics include economic measures (direct repair cost and time and indirect loss due to downtime), social measures (number of casualties, injuries, and fatalities), and life-cycle environmental measures (greenhouse gas emissions, energy consumption, and waste produced). They include economic, social, and environmental attributes and can be categorized into two major pillars, namely sustainability and resilience. A simple method adopted in a number of studies is to convert various attributes into monetary equivalents to make comparison and decision making possible (Han et al. 2016; Mitrani-Reiser 2007). Yet, this approach may impose unnecessary uncertainties and limitations on the problem since the conversion factors largely depend on the locality and case-by-case properties. To avoid these limitations, multi-criteria decision analysis (MCDA) can be used where all measures are computed in their original unit/space and advanced decision models are used to perform comparison, rank the alternatives, and ultimately find the optimal option.

For multi-attribute decision analysis, loss is categorized into four sets of measures which are asset, time, social, and environmental losses. First set, tangible and intangible asset loss (AL) is quantified in terms of US dollars. It includes repair/replacement cost and may include indirect cost such as rent lost due to closure of the building. Second set, time loss (TL) also referred as downtime, recovery time, or unavailability is quantified in terms

of number of days it takes to restore partial or full functionality of the system. Third loss, social loss (SL) may include casualties (injuries and fatalities) or any other social disruption caused by earthquake such as Post-Traumatic Stress Disorder (PTSD) cases and displaced households. Fourth set, environmental loss (EL) represents the environmental impacts of seismic damage which is quantified in terms of CO<sub>2</sub> equivalent greenhouse gas emissions, energy consumption, or water withdrawal required to repair the damages. Note that environmental loss is the key difference between sustainability and resilience given their overlaps in economic and social consequences. Figure 1.4 depicts these metrics categorized into four sets: asset loss, time loss, life loss, and environmental loss and the effective measures contributing to each of four dimensions. The results of analysis will be sent to a decision-making module where the decision comparison and optimization will be performed. Due to numerous measures involved, multi-criteria decision analysis is the most suitable approach.

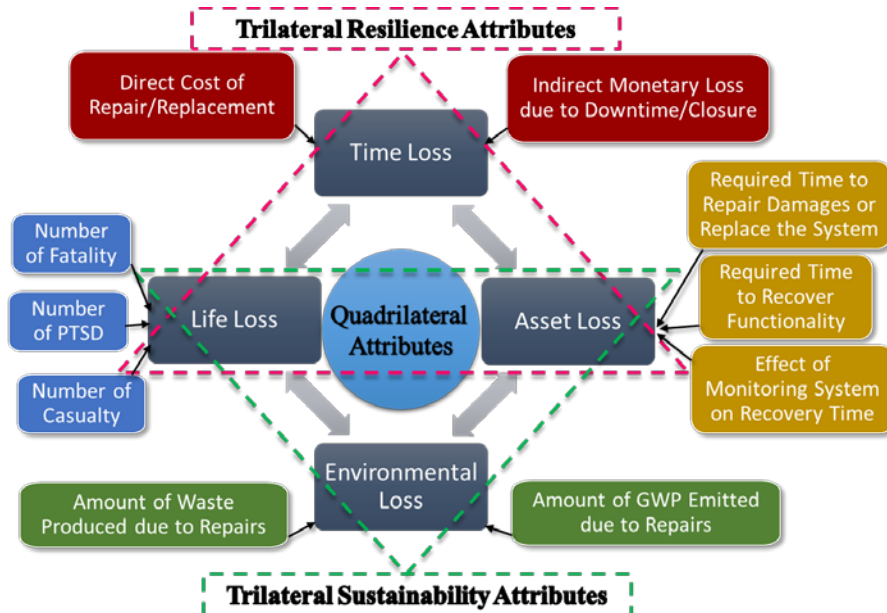


Figure 1.3 Quadrilateral decision criteria

Decision making commonly involves identifying and choosing among different alternatives. In structural engineering, depending on the objectives of the problem, two classes of alternatives may be considered: (1) alternative design choices for new structures, (2) alternative retrofit options for existing structures (Ellingwood and Wen 2005). There are some conflicting and concurring objectives in these problems. For instance, minimizing the time loss will most likely increase the initial construction cost but at the same time, it will reduce the life loss and the repair cost. To address the complexity, a multi-criteria decision-making (MCDM) model is required. The current decision-making problem falls in the category of multiple criteria discrete alternative problems where the sets of alternative options consist of a relatively small number of choices, which are design or retrofit options (Ustinovichius et al. 2007; Wallenius et al. 2008).

Multiple attribute utility theory (MAUT) which considers uncertainty, risk, and subjective probabilities is a suitable approach (Dyer et al. 1992; Govindan and Jepsen 2016; Kumar et al. 2017; Wallenius et al. 2008). Figure 1.5 depicts the main steps for using MAUT to make a decision on the design/retrofit of a structural system.

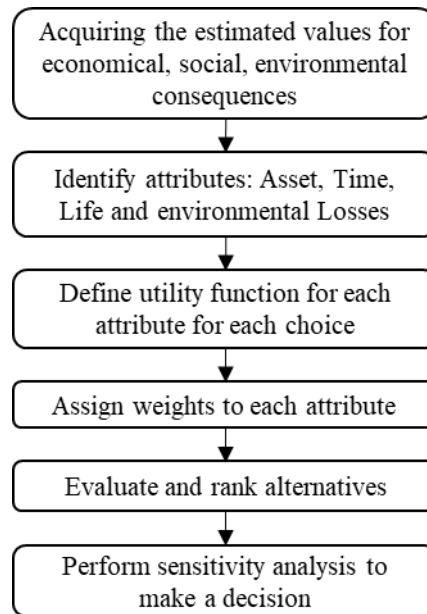


Figure 1.4 Flowchart for MAUT for the design/retrofit decision-making problem

For MAUT, the utility functions defined over a set of attributes are commonly used to quantify the decision maker's preferences (Mateo 2012). The utility functions take a value from zero (for the worst outcome) to one (for the best outcome). They can be defined with three attitudes towards risk, which are risk aversion, risk neutral, and risk seeking. In this study, all four attributes (Asset, Time, Life, and Environmental Loss) need to be minimized as they are all undesirable consequences. Thus, to find the normalized utility values, the best outcome (minimum) of each attribute is assigned a utility value of 1 and the worst outcome (maximum) is assigned a utility of 0.

Then, normalized neutral utility values ( $u_i$ ) are calculated using the following formula for cost criteria (Wallenius et al. 2008):

$$u_i = \frac{A_{max} - A_{ij}}{A_{max} - A_{min}} \quad (1.8)$$

where  $A_{ij}$  is the score (resilience or sustainability metric) evaluated for an attribute  $i$  among  $n$  attributes for a certain alternative  $j$  among  $m$  alternatives, and  $A_{max}$  and  $A_{min}$  are the maximum and minimum scores evaluated for each attribute among all alternatives, respectively. Assuming utility independence, the overall unilateral utility function is formed using the following formula (Ferreira et al. 2009):

$$U_{t,j} = \sum_{i=1}^n w_i u_i(x_i) \quad j = 1, \dots, m; i = 1, \dots, n \quad (1.9)$$

where  $U_{t,j}$  is the overall utility of alternative  $j$ , and  $w_i$ ,  $u_i$ , and  $x_i$  are the importance factor, the utility function (using Equation (6)), and the value of the attribute  $i$ , respectively. The decision-maker need to find the best alternative based on importance factor of each criterion. The importance factor can be evaluated using lotteries between pairs of attributes, e.g. the decision maker compares the importance of cost and downtime and assigns the factors. The importance factor,  $w_k$ , for each attribute can be assigned based on historical data, engineering judgment, and problem objective. Three approaches are suggested for importance factor evaluation, which are ranking based on 1) judgment, 2) summation of weights (reversed rank/sum of ranks), and 3) order centroid weights (sum of reciprocal ranks/no. of ranks).

Another common MCDM method is the Technique for order preference by similarity to ideal solution (TOPSIS) method. For TOPSIS, first the weighted normalized decision matrix needs to be developed using the following equation (Chang et al. 2005; Cheng et al. 2003):

$$v_{ij} = w_i A_{ij} / \sqrt{\sum_{j=1}^m A_{ij}^2} \quad j = 1, \dots, m; i = 1, \dots, n \quad (1.10)$$

where  $v_{kj}$  is an element of the weighted normalized decision matrix. Then, the ideal (most acceptable) and negative-ideal (least acceptable) are found. The ideal solution ( $A^*$ ) and negative-ideal solution ( $A^-$ ) are defined as:

$$A^* = \{v_1^*, \dots, v_n^*\} = \{(\max_j v_{ij} | i \in I'), (\min_j v_{ij} | i \in I'')\} \quad (1.11)$$

$$A^- = \{v_1^-, \dots, v_n^-\} = \{(\min_j v_{ij} | i \in I'), (\max_j v_{ij} | i \in I'')\} \quad (1.12)$$

where  $I'$  and  $I''$  are associated with benefit and cost criteria, respectively. Note that the hazard consequences/losses are considered as the cost criteria. Then, using n-dimensional Euclidean distances, the separation measures from ideal solution ( $D_j^*$ ) and from negative-ideal solution ( $D_j^-$ ) are evaluated:

$$D_j^* = \sqrt{\sum_{i=1}^n (v_{ij} - v_i^*)^2} \quad j = 1, \dots, m; i = 1, \dots, n \quad (1.13)$$

$$D_j^- = \sqrt{\sum_{i=1}^n (v_{ij} - v_i^-)^2} \quad j = 1, \dots, m; i = 1, \dots, n \quad (1.14)$$

Finally, the relative closeness to the ideal solution for alternative  $j$  ( $C_j^*$ ) can be found as follows:

$$C_j^* = D_j^- / (D_j^* + D_j^-) \quad j = 1, \dots, m; i = 1, \dots, n; 0 < C_j^* < 1.0 \quad (1.15)$$

## 1.2 Critical Appraisal

Though several studies have been conducted on seismic resilience assessment of various structures and infrastructure systems in the last decade, there is still a need for comprehensive component-level model for functionality assessment and resilient quantification of building structures. The new models need to be consistent with current well-established models such as FEMA P-58 component-based approach for loss estimation. In the case of building structures, they need to include the consequence of seismic damage to various structural and non-structural components that impact building occupancy as well as all components impacting water, electricity, etc. services in the building. These models need to advance the current state-of-knowledge and provides quantitative methods to assess and compare resilience and functional recovery for various design alternatives.

Over the past three decades, multiple studies have been done on the sustainable-based design of buildings and Leadership in Energy and Environmental Design (LEED) and other agencies provide practical methods to consider sustainability in design. However, incorporating sustainability in resilience-based design is relatively new and there are have been a few limited studies on energy simulation considering seismic hazard. Using LCA,

the major contributor to the greenhouse gas emissions can be identified and the total environmental impact can be compared for different design alternatives. Yet, there is a need for multi-disciplinary decision models to compare and contrast these alternatives. Considering that buildings consume over 40% of energy in the US, a comprehensive building design method needs to combine architectural energy-based design with structural resilience-based design to achieve energy- and performance-efficient outputs.

A decision-making module is mostly absent in the current frameworks. Converting all these metrics into monetary loss, which is the current common practice, adds unnecessary uncertainties to the problem and limits applicability of the methodology to various case studies and site locations. Multi-criteria decision making has been used in construction and system management, but few researchers have used it for integrated resilience and sustainability assessment. Given various criteria involved in building design as mentioned above, a comprehensive resilience- and sustainability-based framework needs to utilize innovative multi-criteria decision models to concurrently include resilience measures such as monetary loss, downtime, and casualty and sustainability measures such as greenhouse emissions and energy consumption.

Due to their excellent lateral stiffness and aesthetic features, diagrids have the potential to become a more widely-used structural system in low- to high-rise buildings. An impediment to their widespread application is the lack of specific design provisions and performance criteria under extreme loads particularly seismic load. In this regard, specific seismic response factors and performance criteria for various damage states of diagrids

need to be quantified for loss analysis. Research in these areas will open up new horizons for creation of novel resilient and smart tubular structural systems. Seismic loss analysis will provide better understanding of robust and structurally efficient diagrid configurations as well as undesirable configurations in terms of seismic consequences.

Structural health monitoring models are a great tool to evaluate structural performance particularly absorption and adaption capability of the structure during an earthquake. Monitoring systems will reduce the need for inspection and minimize the cost and time. In recent years, researchers have studied seismic performance and loss of instrumented structures (Celebi et al. 2004; Cremen and Baker 2018; Hwang and Lignos 2018; Porter et al. 2006). Resilience quantification is a needed extension of these studies. Given the advances in system identification methods, localized sensor networks are the best choice for advancing current state-of-the-study.

### **1.3 Research Objectives**

The overall objective of this research is to develop a comprehensive framework for resilience- and sustainability-based analysis of smart building environments using multi-criteria decision methods. Based on the current state-of-the-art and the research needs, the focus of the research will be on functionality-based resilience quantification under seismic hazard. In short, the following objectives are set for this research:

1. Integrating resilience and sustainability assessment methods into a coupled assessment methodology considering resilience measures such as monetary loss, downtime, and

- casualty and sustainability measures such as greenhouse gas emissions and energy consumption.
2. Developing a risk-informed multi-criteria decision model that incorporates various resilience and sustainability measures considering the risk involved in decision analysis as well as vulnerability and loss analyses.
  3. Developing a model for damage detection and measurement and a quantitative method for post-earthquake rapid safety evaluation considering the data acquired from a localized sensor network.
  4. Creating a new quantitative framework for multi-dimensional functionality recovery analysis of buildings and residential facilities considering asset, occupancy, and serviceability losses due to seismic hazard.
  5. Presenting new seismic performance criteria for diagrid frames consistent with FEMA P-58 loss methodology and implementing the criteria for loss analysis of diagrid buildings.

## **1.4 Organization and Outline**

The material presented in Chapters 2-5 of this dissertation is from published or submitted journal articles. The main objective of this dissertation is to develop a comprehensive decision framework seismic resilience and sustainability of building structures. This framework is presented in Chapters 3 and 4 for steel diagrid and reinforced concrete case studies, respectively. Given that there are few reports on seismic performance and loss analysis of steel diagrid structures, Chapter 1 focuses on diagrid performance and

loss estimation. To further expand the contribution of this dissertation and propose a method for use of health monitoring data in resilience assessment, a new method for resilience quantification and rapid safety evaluation is also developed considering the data obtained from a localized health monitoring system, which is presented in Chapters 5 and 6 of this dissertation. The contents of the chapters of this dissertation are summarized below.

**Chapter 2** presents a comprehensive investigation into the nonlinear performance of steel diagrid structures using static, time-history dynamic, and incremental dynamic analyses. A framework for seismic performance assessment and loss estimation of steel diagrid buildings is developed. Illustrative and quantitative criteria for performance and damage assessment of diagrid frames is introduced and employed to estimate the seismic loss of archetype diagrid buildings. Also, the effects of building height, diagonal angle, and incomplete diagrid modules on performance and loss are studied.

**Chapter 3** introduces a coupled resilience- and sustainability-based decision-making framework for seismic design and rehabilitation of building structures. FEMA method for intensity-based and time-based loss, downtime, and casualty estimation are used to evaluate seismic asset, time, and life losses. The economic input-output life-cycle assessment method is adapted to evaluate the environmental loss due to earthquakes, as well. An MCDM framework is proposed based on analytic hierarchy process, multi-attribute utility theory, and technique for order preference by similarity to ideal solution (TOPSIS). The framework is used to study the resiliency and sustainability of archetype

steel diagrid buildings in a high seismic region. Six scenarios with different objectives including minimum asset, time, life, or environmental loss and maximum resilience are studied. A survey is conducted to find the weight factors for each criterion for each scenario.

**Chapter 4** integrates structural seismic resilience and sustainability assessment methods with whole-building energy simulation techniques to present a new comprehensive decision model for the design of building environments. Risk-based multi-attribute utility theory and analytic hierarchy process are used to develop a multi-criteria decision-making (MCDM) framework considering various economic, social, and environmental measures involved in the design of buildings. The model is implemented for a number of RC buildings and the influence of building configuration on the environment, seismic performance, and energy consumption is studied.

**Chapter 5** integrates component-based resilience quantification methods and SHM techniques to present a new probabilistic framework for seismic structural system evaluation and decision analysis. A trilateral framework is introduced which uses the data obtained from a localized sensor network to detect and locate damage, develops component-based functionality curves to quantify the seismic resilience of the structure, and makes post-quake rapid decisions based on a multi-criteria safety evaluation method. A nonlinear autoregressive exogenous (ARX) model is used to identify structural response and a statistical damage-sensitive coefficient is used to detect, locate, and measure damage in the system. Minor damages due to corrosion and major damages due to past extreme

events are studied considering a life-cycle approach for functionality assessment. Two groups of archetype structures located in a high seismic region are studied, namely steel diagrid and special reinforced concrete structures.

**Chapter 6** presents a new multi-dimensional framework for functional recovery analysis and resilience quantification of building facilities. Three measures defining the seismic functionality of a building facility are considered, which are asset, occupancy, and serviceability losses. The model is consistent with FEMA P-58 approach for loss analysis and considers the loss and downtime due to various structural and non-structural components of the building in resilience quantification. The framework is implemented on two groups of steel and reinforced concrete (RC) buildings archetypes located in a highly seismic region using a scenario-based approach.

**Chapter 7** presents a summary of the dissertation and major conclusions and possible future studies on the topic.

## Chapter 2

### 2. Seismic Performance Assessment and Loss Estimation of Steel Diagrid Structures<sup>2</sup>

#### 2.1 Introduction

Diagrid structural systems have become an increasingly attractive choice for mid-to-high-rise buildings around the world. Diagrid frames form the perimeter of the building creating a tubular structure with a distinctive outlook and an open façade to absorb natural sunlight. Like any other tubular system, the diagrid provides plenty of rentable open space inside. The main distinction between diagrids and conventional structural systems is the absence of vertical members/columns in the structure, replaced with inclined brace-shaped

---

<sup>2</sup> The material presented in this chapter was previously published in *Journal of Structural Engineering* and is re-used herein with permission from the publisher. See Appendix I for documentation of permission to republish this material.

Asadi, E., Li, Y., Heo, Y. A. (2018). Seismic Performance Assessment and Loss Estimation of Steel Diagrid Structures, *Journal of Structural Engineering*, 144(10), 04018179, [https://doi.org/10.1061/\(ASCE\)ST.1943-541X.0002164](https://doi.org/10.1061/(ASCE)ST.1943-541X.0002164).

members called diagonals. Diagonals efficiently carry both the gravity and lateral loads. Figure 2.1 (a) shows the main components of a diagrid frame alongside its basic triangular element. Diagonals connect to ring beams at diagrid nodes every a few floors forming diagrid modules (see 3-story modules in Figure 2.1 (a)). Apart from these advantages, diagrids are distinctively versatile such that complex geometrical shapes can be created by modifying their basic triangular elements. By changing the diagonal angle (the typical angle between the diagonal and horizontal axis), length, and inclination (the out-of-plane angle between the diagonal and vertical axis), various forms can be created which is particularly desirable to architects and stakeholders alike. Figure 2.1 (b) shows the 46-story Hearst Tower, an iconic diagrid building in New York City known for its sustainability and structural efficiency (Milana et al. 2015).

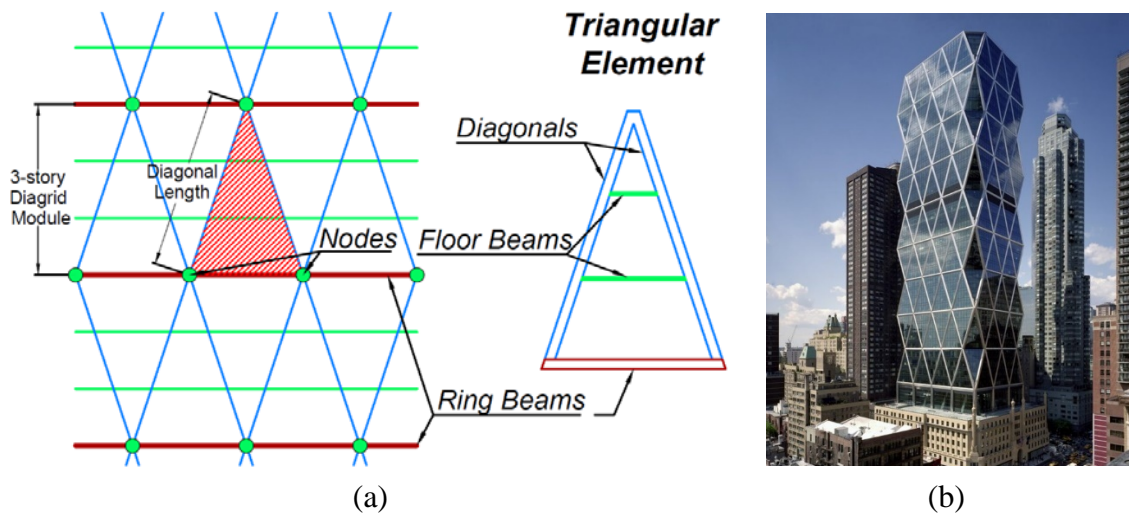


Figure 2.1 (a) Main components of a diagrid frame and its triangular base element; and (b) the Hearst Tower, New York City. (Reprinted from ArchDaily (2012), with permission from Chuck Choi)

A few research papers are published focused on diagrid performance assessment under extreme events. Asadi and Adeli (2017) discuss the state-of-the-art and the current

research trend for diagrid systems. The optimal diagonal angle and preliminary design of diagrids are among researchers' main interests (Kim and Lee 2012; Montuori et al. 2014; Moon et al. 2007; Zhang et al. 2012). They report that the optimal diagonal angle for high-rise diagrid buildings with 36- to 60-story is in the range of  $55^\circ$  to  $75^\circ$ . Their findings are used to choose the proper diagrid configuration for archetypes in this study. Kim and Lee (2012) present a comparative study of the seismic nonlinear performance of circular- and square-shaped diagrids but they focus on the effect of diagonal angle and overall nonlinear response of the structure and provide no specific criteria for performance assessment of diagrids. Milana et al. (2015) compare 40-story steel diagrids with conventional tubular structure and outriggers. They report an overall performance improvement in terms of strength, stiffness, and ductility once diagrids are used. Their main models, however, experience limited nonlinear deformation and little stiffness reduction in pushover analyses. Their building models are in a region with moderate seismic activity per ASCE Standard ASCE/SEI 41-13: Seismic Evaluation and Retrofit of Existing Buildings (2014) ( $S_{DS}$  and  $S_{D1}$  of 0.433g and 0.232g, respectively). Other researchers study the progressive collapse of high-rise diagrids and report that diagrids show high resistance against the failure of one or a few diagonals compared to conventional tubular structures (Kim and Kong 2013; Kim and Lee 2010; Kwon and Kim 2014). Notably, Kim and Lee (2010) highlight the importance of corner diagonals. They report that progressive collapse formed in their archetype, a 36-story steel diagrid, when more than 11% of the diagonals in the first story fails; once corner diagonals are involved, this ratio is reduced to 8%. Yet, they do not consider aleatoric or epistemic uncertainties on diagrid performance. Bhuiyan and

Leon (2016) study performance of a 64-story diagrid structure using Nonlinear Time-History Analysis (NTHA) and considering aleatoric (record-to-record) uncertainty. Yet, they provide little information about the ground motion records they used, the diagrid numerical model, and performance or damage criteria required for a reliable performance assessment.

FEMA P-58: Seismic Performance Assessment of Buildings (2012) describes seismic performance assessment procedure in terms of probable casualties, damages, losses, and repair/replacement time. It provides a comprehensive database of fragility specifications for various structural and non-structural components in addition to Performance Assessment Calculation Tool (PACT) to perform loss, downtime, and casualty estimation analyses. Different parameters may be used to evaluate the fragility function of a structure including maximum inter-story drift ( $IDR_{max}$ ), maximum absolute floor acceleration (ACC) (particularly for non-structural components), and plastic rotation demand at possible hinges. These key measures called Engineering Demand Parameters (EDPs) typically have a lognormal and in some cases normal or Weibull fragility distribution (Ramirez et al. 2012). A probabilistic estimation of loss functions ideally involves performing thousands of fragility analyses on models consisting of structural and non-structural components with stochastic properties. Performance of any structure can be assessed in terms of Probability Distribution Function (PDF) of economic losses and casualties caused by a specific stochastic seismic event (Yamin et al. 2017).

The effect of aleatoric and epistemic uncertainty on performance and loss estimation of various conventional structural systems have been extensively studied including steel Concentrically Braced Frames (CBFs) (Dyanati et al. 2015; Hwang and Lignos 2017b; Kinali and Ellingwood 2007), steel Moment-Resisting Frames (MRFs) (Dong and Frangopol 2016; Li et al. 2014), tall steel-framed buildings (Molina Hutt et al. 2015), and reinforced concrete frame buildings (Han et al. 2014; Heo 2009; Ramirez et al. 2012). Among them, Ramirez and Miranda (2012a) highlight the impact of residual drift on the expected total loss where severe unreparable damage to the structure is likely to cause significant demolition loss. Hwang and Lignos (2017a; b) used the probabilistic method introduced by Ramirez and Miranda (2012a) to assess the structural, nonstructural, and demolition losses in CBFs and MRFs, respectively. Yamin et al. (2017) propose a vulnerability loss estimation method and use it to produce seismic vulnerability in terms of repair cost and time. In the case of diagrid structures, however, no specific criteria are introduced for their performance assessment and no study has been reported on loss estimation of them. Given that the main cause of casualties in an extreme event is partial or total building collapse (FEMA 2012), performance acceptance criteria and damage states are among the most important properties of any structural system and need to be investigated thoroughly.

The objective of this paper is to introduce a framework for performance assessment and loss estimation of steel diagrid buildings. A comprehensive study on the nonlinear probabilistic performance of steel diagrid structures is conducted to develop new performance criteria for steel diagrid structures. To reflect major changes in behavior,

various archetype performance groups with different heights (4-, 8-, 15-, 30-story) and diagonal angles ( $45^\circ$ ,  $63^\circ$ , and  $72^\circ$ ) are studied. Nonlinear static and time-history dynamic analyses per FEMA-356: Prestandard and commentary for the seismic rehabilitation of buildings (2000), FEMA-440: Improvement of nonlinear static seismic analysis procedure (2005), FEMA P-695: Quantification of building seismic performance factors (2009) and ASCE/SEI 41-13, and Incremental Dynamic Analysis (IDA) per FEMA P-695 and P-58 are used to study diagrid performance and collapse mechanism. Collapse fragility functions are used to illustrate uncertainties in demand and performance. The proposed framework is implemented in FEMA P-58 PACT and used to evaluate the loss distribution functions of archetype steel diagrid buildings. The significance of each structural and non-structural component on the expected total monetary loss is assessed. The loss is estimated using an intensity-based approach as per FEMA P-58, considering two hazard levels, which are Design Basis Earthquake (DBE) with a 10% probability of exceedance in 50 years and Maximum Considered Earthquake (MCE) with a 2% probability of exceedance in 50 years according to United States Geological Survey (USGS) hazard maps.

## **2.2 Archetype Diagrid Buildings**

Four groups of typical diagrids archetype buildings with different heights, i.e. 4-, 8-, 15-, and 30-story and three different diagonal angles, i.e.  $45^\circ$ ,  $63^\circ$ , and  $72^\circ$ , are considered to represent a wide range of typical application of steel diagrids. The 15- and 30-story archetypes are studied under static nonlinear analysis only. As is common in diagrid structures, the diagrid frames form the perimeter of the building and central columns carry

a part of gravity loads. Figure 2.2 shows the typical floor plans of archetypes. The archetypes are labeled based on the number of stories and diagonal angle. For example, 4-45 archetype model has 4 stories and its diagonal angle with the horizon is approximately  $45^\circ$ .

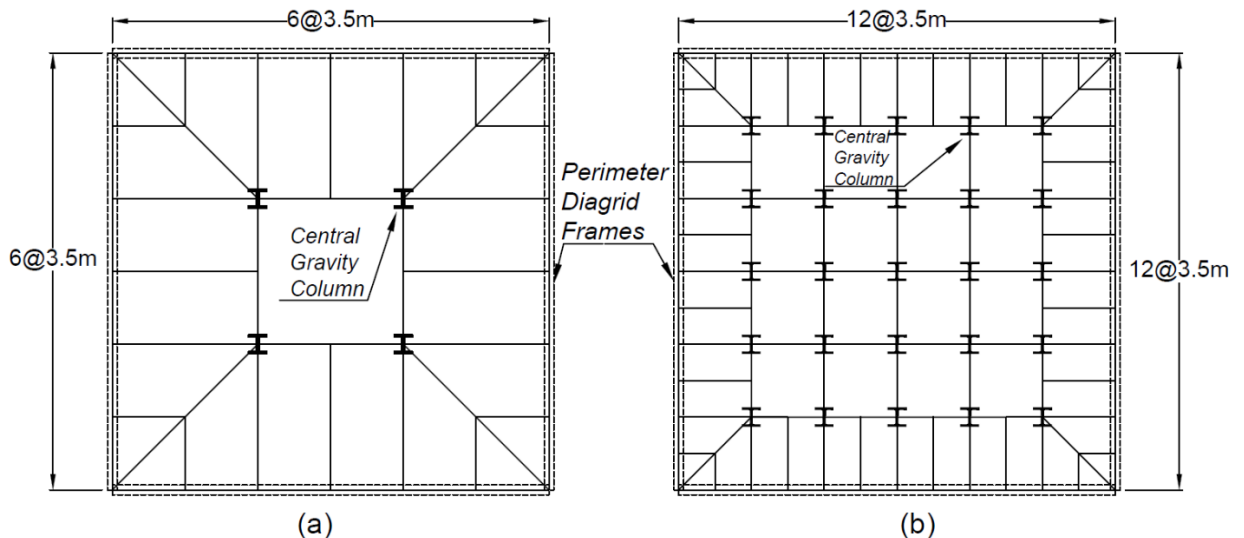


Figure 2.2 Typical floor plan for (a) 4-, 8-, and 15-story (b) 30-story diagrid archetypes

All archetypes are designed per the AISC Load and Resistance Factor Design (LRFD) (2011) and ANSI/AISC 360-10: Specification for Structural Steel Building design provisions using the software package SAP2000 (AISC 2010; CSI 2011). Current codes of design including ASCE/SEI Standard No. 7-10: Minimum Design Loads for Buildings and Other Structures (2010) provide no specific design criteria for diagrid structures. Hence, the response modification (R) factor is assumed 3.0 for the initial design of diagrid frames. This generally conservative assumption is used in several previous studies on diagrids including Kim and Lee (2010, 2012), Kim and Kong (2013), and Kwon and Kim (2014). In addition, ANSI/AISC 341-10: Seismic Provisions for Structural Steel Buildings (2016a)

provides no special seismic consideration for steel diagrids. Nor does other literature as pointed out in recent literature reviews on the topic (Asadi and Adeli 2017; Liu et al. 2018). In absence of specific special seismic considerations, the diagrids are designed as ordinary CBFs then checked as ordinary MRFs. Nevertheless, the special seismic load combinations of sections B2 and D1.4a of AISC 341-10 are considered. The standard W-shaped sections are used for beams, columns, and diagonals. The diagonal sections are changed every 2 or 3 stories to follow customary grouping practice in the construction of steel structures.

Due to large axial forces in diagonals, the main factor in the load capacity and performance of each diagonal is the cross-sectional area not the moment of inertia or other geometric properties of the member. Therefore, the required slenderness ( $KL/r$  where  $K$ ,  $L$ , and  $r$  are the effective length coefficient, the unbraced length, and the radius of gyration, respectively) for diagonal section is typically low, below the slender limit between elastic and inelastic buckling ( $KL/r = 4.71\sqrt{E/F_y}$  equal to 113 for grade 50 steel). Hence, in this study, the slenderness is limited to  $KL/r \leq 4\sqrt{E/F_y}$  per AISC 341-10 section F1 requirements for ordinary CBFs and non-compact sections are intentionally avoided in the design process to limit partial or global buckling.

Since diagrids are commonly used for carrying large lateral loads, a high seismic region is selected. The design loads are evaluated for an office/commercial building located in southern California, near Los Angeles city with  $S_s$  (spectral response acceleration at 0.2 sec) and  $S_l$  (spectral response acceleration at 1 sec.) of 2.461g and 1.127g, respectively. Dead and Live loads are 4 and 2.4  $kN/m^2$ , respectively (Gholipour et al. 2015; Kim and Lee

2012). The gravity loads, Dead and Live loads, are proportionally distributed among the floor beams, connected to columns and diagrid frames.

Three types of nonlinear analyses are conducted including pushover analysis on three-dimensional (3D) models in SAP2000 (CSI 2011) and NTHA and IDA on planar diagrid models in OpenSees (Mazzoni et al. 2006). In planar models, the web-dia-grid frame is under in-plane vertical and lateral loads. The diagrid frame parallel to the direction of lateral load is called web diagrid and the one perpendicular to it is called flange diagrid. Note that the archetype buildings are symmetric. Also, diagrid behavior is mostly governed by the behavior of web frames (Moon et al. 2007). The OpenSees and SAP2000 models are compared in detail to ensure consistent results. Figure 2.3 shows a comparison of SAP2000 model with lumped Plastic Hinges (PHs) and OpenSees model with fiber elements under pushover analysis for the 4-45 archetype. The horizontal axis in Figure 2.3 shows the average inter-story drift ratio ( $IDR_{avg}$ ). The SAP2000 lumped hinge approach shows a slightly larger lateral stiffness (approximately 3% larger initial lateral stiffness in Figure 2.3). It can be partly attributed to the differences in element used for each approach. The OpenSees model has fiber elements where distributed plasticity can be studied while the SAP2000 model shows only concentrated plasticity. The ultimate lateral load capacity of both models is close as well (2.7% difference in Figure 2.3). These small differences indicate good consistency between two approaches despite their dissimilarities.

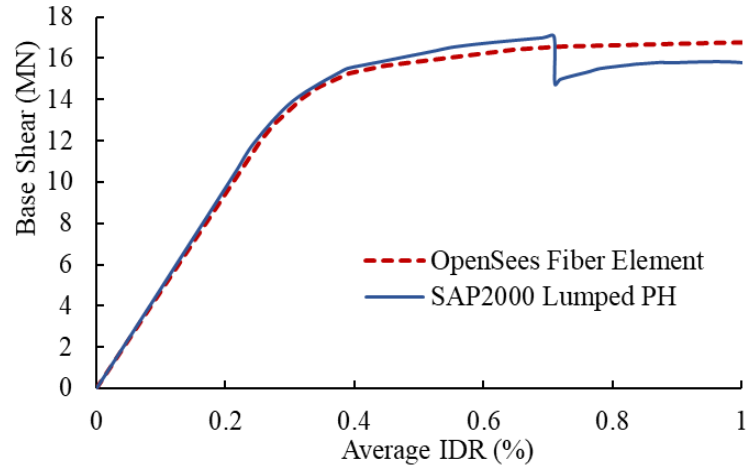


Figure 2.3 Comparison of SAP2000 model having lumped PHs with OpenSees model having fiber elements under pushover analysis for 4-45 archetype

For pushover analysis, three levels of performance are defined for each structural member: Immediate Occupancy (IO), Life Safety (LS), and Collapse Prevention (CP) per FEMA 356. Geometric nonlinearity ( $P-\Delta$  effect) is included in models. FEMA 356 recommendations for plastic acceptance criteria and modeling parameters of braces in compression are adapted since little experimental data is published on seismic performance of diagrids.

In OpenSees, beams and diagonals are modeled as beam-column fiber elements using Menegotto-Pinto hysteretic model with 0.02 hardening (Mazzoni et al. 2006). Figure 2.4 illustrates some modeling assumptions and the diagrid configurations. Uriz (2005) and Uriz and Mahin (2004) proposed a method for modeling material and geometric nonlinearity of CBFs is adapted here which considers low cycle fatigue and imposes small initial camber on beam-column elements to induce buckling and benefits from distributed plasticity of fiber elements for further precision. Accordingly, the corotational formulation is used for

all members. Local buckling is not considered explicitly. A leaning column, shown in Figure 2.4, carrying gravity loads is linked to the main frame to simulate the P- $\Delta$  effect (Li et al. 2014; Moghaddasi B and Zhang 2013). Similar to Uriz et al. (2008), the buckling and post-buckling behavior of the models are verified by Black et al. (1980) experiment. Figure 2.5 shows a comparison between Black et al. (1980) experiment on a 4-in tube strut and numerical model used here for diagonal members.

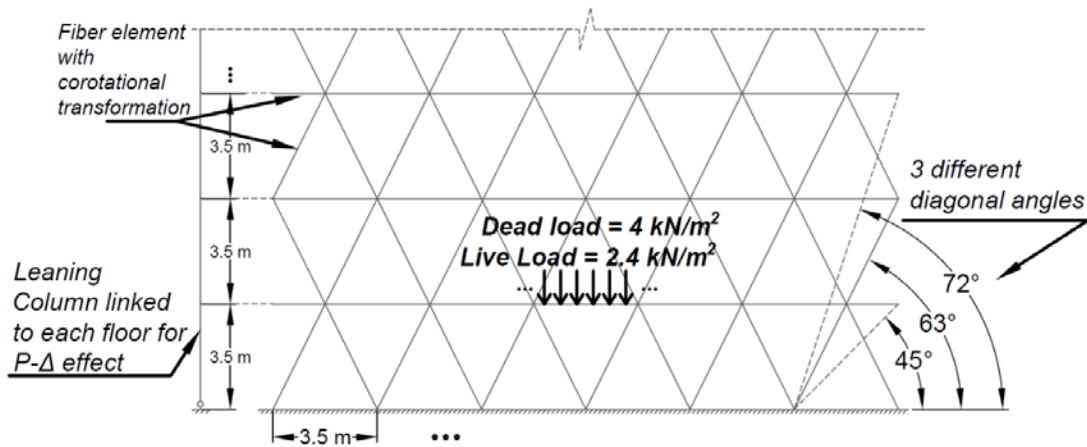


Figure 2.4 Schematic of diagrid archetype models

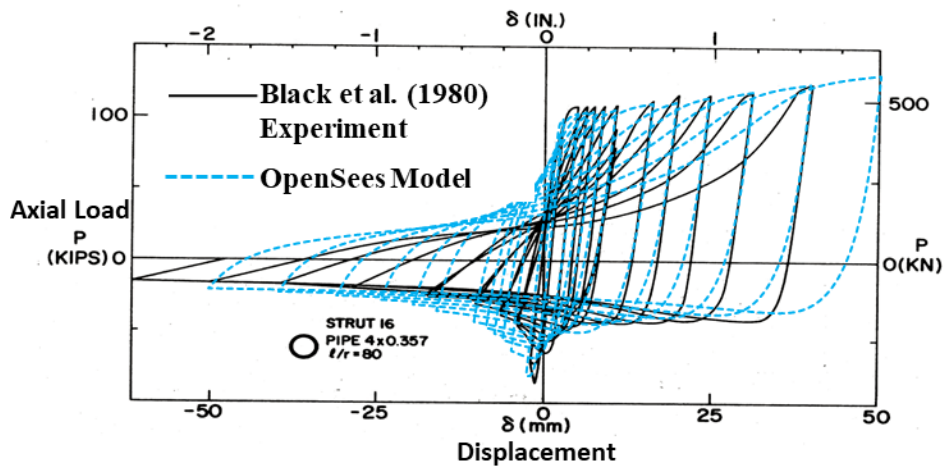


Figure 2.5 Comparison between experimental hysteresic response (Black et al. 1980) and current numerical model results

Diagrid connections are unique in terms of configuration where each joint connects at least 6 members, 4 diagonals with large axial force and 2 beams, together. Figure 2.6 depicts the schematic of a diagrid connection proposed by Kim et al. (2011). A few experimental studies (Kim et al. 2010, 2011) are reported on diagrid steel connections but no design criteria are introduced, yet. Thus, the diagrid joints are not modeled explicitly. Different modeling approaches including using moment-resisting connections and hinged connections are compared though. It is found that both design and failure of diagonal members is governed primarily by axial internal forces and their flexural moment has a negligible effect on their behavior regardless of joint modeling method, i.e. whether they are modeled as moment-resisting or hinged. These results are consistent with previous studies on the topic (Kim and Lee 2012; Mele et al. 2014; Moon et al. 2007). Moreover, as required by capacity-based design approach of AISC 360-10 and AISC 341-10, steel connection should be designed such that the plastic behavior initiates in brace or beam elements, not the connections (FEMA 2012; Hwang and Lignos 2017a). Accordingly, the connections are assumed post-Northridge welded moment resisting connections and the base nodes are fixed. Further details on numerical modeling of diagrids are discussed in Asadi and Adeli (2017, 2018b).

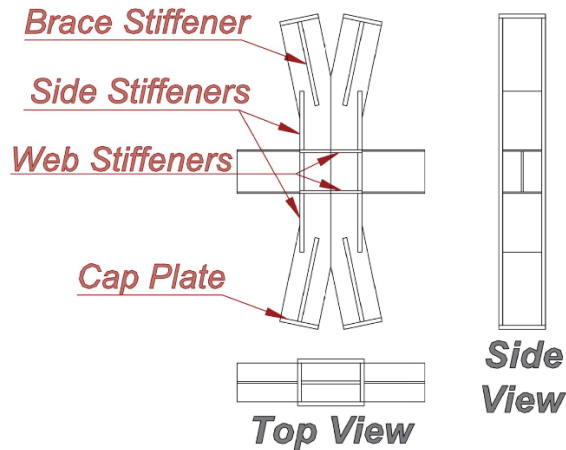


Figure 2.6 H-section steel diagrid connections adapted from Kim et al. (2011)

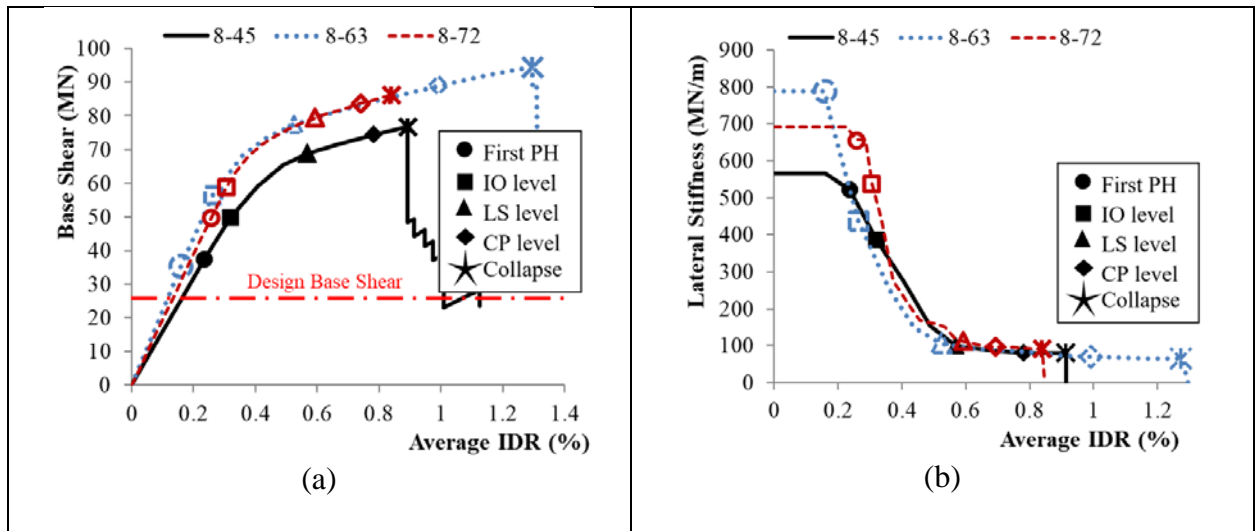
## 2.3 Seismic Nonlinear Performance of Diagrid Structures

### 2.3.1 Static Nonlinear Analysis

This section provides an overview of the nonlinear static performance of steel diagrid structures. A thorough study of the nonlinear static behavior of steel diagrids is presented in Asadi and Adeli (2018b). A series of static nonlinear analyses (pushover) is conducted on all models via SAP2000 software package based on provisions of FEMA 356 and P-58 and ASCE/SEI 41-13. This software package has been used in several other studies on diagrid structures (Kim and Kong 2013; Kim and Lee 2012; Kim et al. 2010; Mele et al. 2014; Moon et al. 2007).

Figure 2.7 shows the pushover curves for all four archetype groups in addition to the lateral stiffness versus  $IDR_{avg}$ , which is the slope of the pushover curve, for the 8-story models. Diagrids show considerable overstrength in pushover analyses. Such that the design base shear obtained using the Equivalent Lateral Force (ELF) method of ASCE7-10 for 8-45 (shown in Figure 2.7 (a) with a dash-dotted line) is approximately 1/3 of the

ultimate base shear which led to the collapse of the 8-45 structure. This large overstrength factor similarly observed in other models is partly due to the assumed  $R$  factor in the design procedure. As mentioned earlier, in this research the lowest suggested  $R$  factor of 3 is used for diagrids since the ASCE7-10 provides no specific response performance factor for diagrids. Table 2.1 summaries the key EDPs of all archetypes obtained from the static analysis. Generally, diagrid structure demonstrates to have a distinctively large lateral stiffness with mean  $IDR_{max}$  and  $IDR_{avg}$  of 0.35% and 0.24% under seismic design load, respectively. Notably, studied diagrid models, except for 4-72 model, show a smaller fundamental period than what the recommended ASCE7-10 equation  $T_a = C_t h_n^x$  gives. This may lead to a non-conservative estimation of design base shear per ASCE7-10 Eq. 12.8-3.



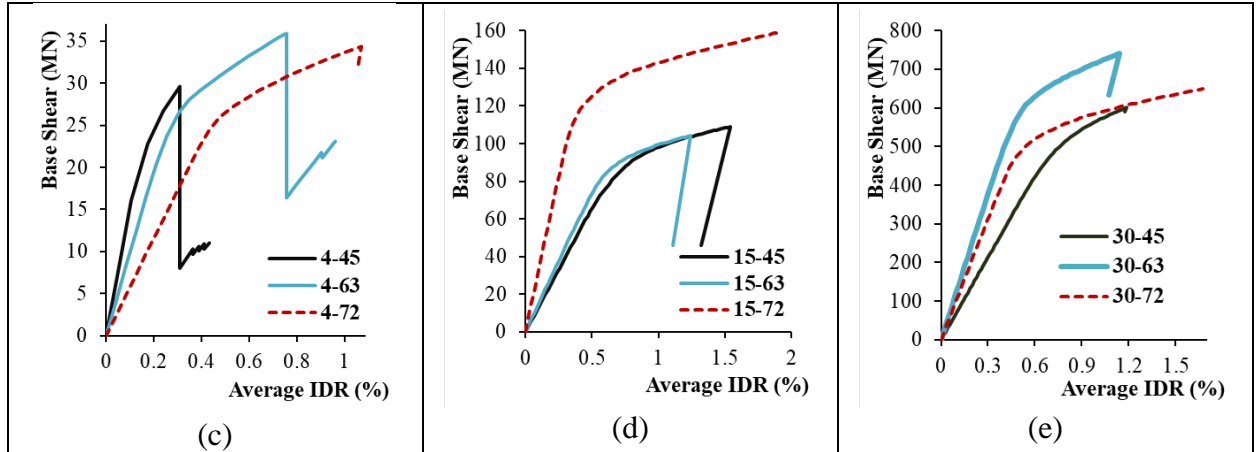


Figure 2.7 (a) Pushover curves and (b) lateral stiffness versus total drift curves for 8-story models and pushover curves for (c) 4- (d) 15- (e) 30-story archetypes

Table 2.1 Engineering demand parameters under static analysis

EDP	4-45	4-63	4-72	8-45	8-63	8-72	15-45	15-63	15-72	30-45	30-63	30-72
Fundamental period (sec)	0.23	0.29	0.38	0.41	0.37	0.40	0.77	0.73	0.57	1.39	1.26	1.29
Fundamental period using ASCE7-10 equation (sec)	0.35	0.35	0.35	0.59	0.59	0.59	0.95	0.95	0.95	1.60	1.60	1.60
Maximum IDR under seismic design load (%)	0.10	0.14	0.24	0.25	0.21	0.40	0.54	0.46	0.39	0.62	0.29	0.58
Average IDR under seismic design load (%)	0.08	0.13	0.21	0.21	0.17	0.23	0.38	0.35	0.24	0.40	0.19	0.33
Average IDR at collapse (%)	0.31	0.76	1.07	0.89	1.3	0.83	1.54	1.22	1.89	1.19	1.14	1.67

The slope of pushover curve decreases substantially as the first PH forms in corner diagonals (shown by a circular marker in Figures 2.7 (a) and (b)). The lateral stiffness of the structure continually decreases as PHs are formed in several diagonals in different stories. As the lateral load increases step by step, the PHs reach higher performance levels: IO, LS, and CP one after another. The load capacity of the structure increases up to an

ultimate load beyond which its load capacity drops suddenly indicating the formation of a failure mechanism. In Figure 2.7, a failure mechanism is formed in the diagrid frame if all diagonals of a story fully yield or reach global buckling critical axial load. At this point, labeled as the collapse point in Figures 2.7 (a) and (b), failure of all lateral-load-carrying members leads to a sharp reduction of lateral stiffness and excessive deformation of the frame. The average IDR is 1.15% at this point, which is notably smaller than IDR of special or ordinary CBFs at collapse, that is 2.5% and 1.78% respectively per FEMA P-58.

To study gravity loads, new numerical models are developed considering an upper bound gravity load on the frame. The original Dead and Live loads are increased to  $5 \text{ kN/m}^2$  (assuming a larger thickness for the concrete floor and heavier partition walls) and  $4.79 \text{ kN/m}^2$  (assuming a lobby and storage area for all floors), respectively. The pushover curves for the new upper-bound gravity loads for 8-45 archetype is presented in Figure 2.8. The archetypes with larger gravity loads generally require heavier sections for diagonals and internal columns. The resulting structure is heavier than the original one (8.6% larger in case of the 8-45 archetype) and can carry a larger ultimate base shear as shown in Figure 2.8. However, the IDRs representing different performance levels are basically the same. Consequently, the gravity loads affect the required cross-section and axial stiffness for diagonals, but it has an insignificant effect on key EDP of the system which is IDR. Following a different approach, the gravity loads are increased as mentioned but the structure was not designed again (keeping the original sections for members). This case is labeled as “original with larger gravity loads” in Figure 2.8. In this approach, we study a case where the building is being constructed with a material or used for an application other

than the initial design. In this approach, the whole pushover curve is basically the same as the original curve with merely 0.6% reduction in ultimate load-carrying capacity in case of the 8-45 archetype. The small impact of larger gravity load in this approach can be attributed to the significance of lateral seismic load compared to the gravity loads.

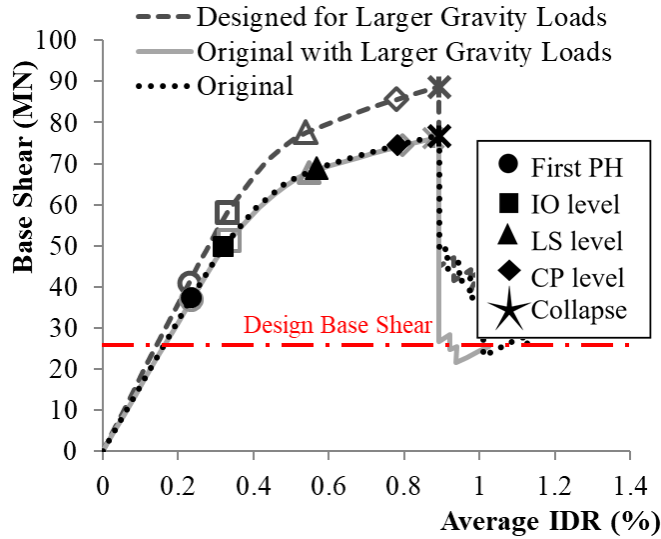


Figure 2.8 Pushover curves for 8-45 archetype considering different cases for gravity loads

## 2.3.2 Nonlinear Time-history Analysis

### 2.3.2.1 Earthquake Ground Motions

For dynamic analyses in OpenSees, a set of 22 far-field (located at greater than or equal to 10 km from the fault rupture site) ground motions recommended for collapse assessment of building structures by FEMA P-695 is used to study record-to-record variability in NTHA and IDAs. These records are carefully selected to properly represent record-to-record uncertainty (Ghafory-Ashtiany et al. 2011).

The ground motion set includes records on soft rock and stiff soil (Site Class C and D) with magnitudes between M6.5 and M7.6 taken from 14 different events. As recommended by FEMA P-695, the records are normalized with respect to peak ground velocity (PGV), then scaled such that the median spectrum of the record set matches the design response spectrum at structure fundamental period. The scaled response spectrums of all records are depicted in Figure 2.9 along with their median spectrum and the ASCE7-10 design spectrum matched at the fundamental period of the 4-45 diagrid structure. The spectrums include records with approximately 4.4g spectral acceleration and have significant variability across the design spectrum to reflect the record-to-record uncertainties.

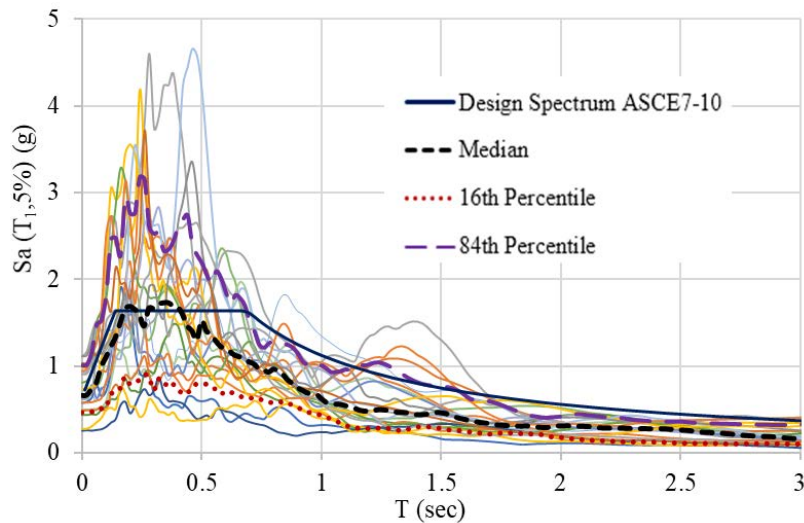


Figure 2.9 Response spectrum of all records normalized and scaled to match ASCE7-10 design response spectrum in the site for 4-45 archetype

### 2.3.2.2 Performance of Diagrids under Nonlinear Time-history Analysis

Dynamic analysis under well-selected ground motions produces valuable information on the performance of structure under extreme events. NTHA is conducted for two hazard

levels, DBE and MCE, and the results are used to assess diagrid performance and estimate the expected loss per FEMA P-58. The NTHAs are performed on OpenSees models of 4- and 8-story archetype buildings. Mean and maximum IDRs are used to assess the soft-story failure of diagrids.

As observed in nonlinear static analyses, a sharp reduction of diagonal axial strength between adjacent stories may lead to undesirable soft-story failure mechanism in diagrid structures. To investigate this failure mechanism, the ratio of  $IDR_{max}$  to  $IDR_{avg}$  is used as an indicator of possible soft-story mechanism. The  $IDR_{avg}$  is the peak displacement of the roof for each ground motion record divided by the total height of the structure. Table 2.2 presents the median expected EDPs, i.e.  $IDR_{max}$  and  $IDR_{avg}$  and their ratio and normalized pseudo-spectral displacement and acceleration based on 5% damped design spectra for the region at the fundamental period of the building structure, that is  $S_d(T_1, 5\%)$  and  $S_a(T_1, 5\%)$  respectively.

Table 2.2 Response spectrum of all records normalized and scaled to match ASCE7-10 design response spectrum in the site for 4-45 archetype

Model	DBE (10%/50-yr)					MCE (2%/50-yr)				
	$IDR_{max}$ (%)	$IDR_{avg}$ (%)	$IDR_{max}$ / $IDR_{avg}$	$S_d(T_1, 5\%)$ (cm)	$S_a(T_1, 5\%)$ (g)	$IDR_{max}$ (%)	$IDR_{avg}$ (%)	$IDR_{max}/$ $IDR_{avg}$	$S_d(T_1, 5\%)$ (cm)	$S_a(T_1, 5\%)$ (g)
4-45	0.50	0.44	1.16	4.64	1.65	0.71	0.62	1.17	10.43	3.71
4-63	0.55	0.47	1.17	5.68	1.65	0.93	0.69	1.41	8.52	2.47
4-72	3.04	0.86	3.49	8.47	1.90	5.03	1.41	3.54	12.70	2.85
3-72- EIM	1.85	0.62	2.98	8.47	1.90	3.85	1.06	3.65	12.70	2.85
8-45	1.24	0.96	1.25	19.26	1.57	1.77	1.48	1.19	28.90	2.35
8-63	0.65	0.54	1.26	11.64	1.69	0.95	0.75	1.31	17.46	2.53
8-72	1.61	0.58	2.76	8.95	1.62	2.70	0.86	3.39	13.43	2.42
6-72- EIM	0.53	0.34	1.55	8.95	1.62	0.71	0.44	1.62	13.43	2.42

The mean  $IDR_{max}$  for studied diagrids under DBE- and MCE- level NTHA is 1.27% and 2.02% respectively. Given that the structures are in a high seismic region, these values are relatively low compared to similar structural systems such as CBFs having an  $IDR_{max}$  of 1.46% and 2.78% under DBE and MCE (according to Chen et al. (2008) for 3-story special CBFs). In addition, if diagrids with  $72^\circ$  diagonal angle are excluded the mean  $IDR_{max}$  will be much smaller, i.e. 0.74% and 1.09% respectively. It clearly shows the distinctively large lateral stiffness of diagrid structures as reported in the literature (Ali and Moon 2007; Milana et al. 2015) and previously discussed in the static nonlinear analysis section. In case of  $72^\circ$  models, the diagrid is divided into a number of 3-story modules; but the uppermost module is an incomplete module with 1 or 2 stories instead of 3. The incomplete module, shown in Figure 2.10, causes a sharp reduction in stiffness of those stories and an increase and concentration of deformation in them. This distinctive configuration also affects the location of PHs. Thus, as noted in Table 2.2, it also causes an increase in the  $IDR_{max}$  and  $IDR_{max}$  to  $IDR_{avg}$  ratio. A similar configuration is noticeable on façade of Macquarie Bank in Sydney, Australia. Because of architectural limitation and requirements, this configuration might be used though. Further, this behavior indicates the significant effect of diagonal angle on the performance of a diagrid structures. Finding an optimal angle will improve both elastic and inelastic behavior of diagrid and should be an imperative part of the diagrid design process.

Excluding the incomplete modules, the EDPs for lower complete modules of 4-72 and 8-72 archetypes are also presented in Table 2.2. They are labeled 3-72-EIM (the lower module is a 3-story frame) and 6-72-EIM (the lower modules form a 6-story frame)

respectively. As indicated in Table 2.2, the excessive EDPs in 72° archetypes is mostly concentrated in the uppermost incomplete diagrid modules, i.e. 4<sup>th</sup> floor in 4-72 archetype and 7<sup>th</sup> and 8<sup>th</sup> floors in the 8-72 archetype. The lower section of 8-72 archetype shows a considerably smaller  $IDR_{max}$  and  $IDR_{avg}$  than the original one. This reduction is not significant in case of 4-72 archetype though. Designers are recommended to use dynamic nonlinear analysis if an incomplete module is used in diagrid configuration. Special considerations may be required in these modules including an increase in the design story shear or addition of supplemental load-carrying components for the floors affected.

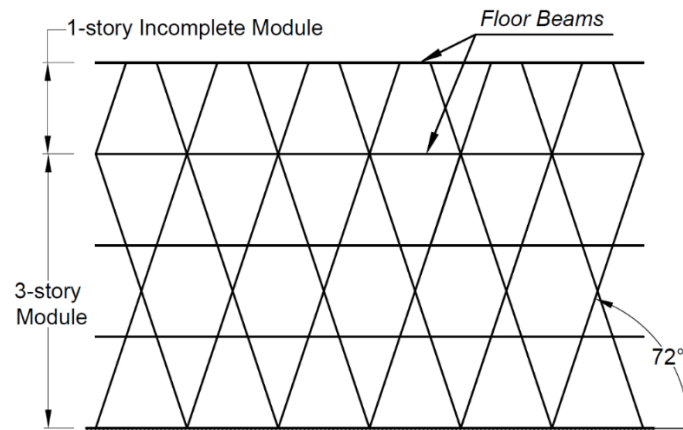


Figure 2.10 Elevation of 4-72 model with uppermost incomplete module

The 8-72 archetype shows better performance with smaller  $IDR_{max}$  values compared to 4-72 one, yet its  $IDR_{max}$  is much larger than 8-45 and 8-63 archetypes. The 8-63 archetype shows smaller  $IDR_{max}$  and  $IDR_{avg}$  than both other 8-story cases and the 8-45 archetype has the largest  $IDR_{avg}$ . Generally, the 4-45 and 8-63 archetypes show a better performance among 4- and 8-story archetypes, respectively. The optimal diagonal angle depends largely on the height to width ratio of the building (Moon et al. 2007).

Higher  $IDR_{max}$  to  $IDR_{avg}$  ratio implies a more concentrated damage in a single story and higher likelihood of soft-story formation (Chen et al. 2008). The  $IDR_{max}$  to  $IDR_{avg}$  ratio for diagrid archetypes is generally smaller than that of CBFs (reported in (Chen et al. 2008)) if the 72° models are excluded. This indicates that diagrids are less vulnerable to soft-story failure if the undesirable incomplete module configuration, as explained earlier, is avoided. Nonetheless, having an incomplete uppermost module make diagrids vulnerable to soft-story in those uppermost stories.

## **2.4 Performance Criteria and Damage States**

The ASCE/SEI 41-13 and FEMA P-58 provide a detailed list of the illustrative and quantitative performance criteria at each performance level or damage state for different structural systems. Here, the findings from previous sections together with collapse fragility analyses are used to develop practical performance criteria for steel diagrid frames.

### ***2.4.1 Collapse Fragility***

The fragility function shows the relationship between probability of collapse or failing a limit state and a demand indicator such as ground motion intensity (IM). Collapse fragility functions is a well-accepted approach to illustrate uncertainties in performance and vulnerability of the structure (ATC 2009). Lognormal cumulative distribution functions (CDFs) have been used for fragility analyses of various structural systems (Baker 2015; Ghafory-Ashtiany et al. 2011; Kinali and Ellingwood 2007). The probability of collapse given a certain demand ( $P(C | IM=z)$ ) is defined as follows:

$$P(C|IM = z) = \Phi\left(\frac{\ln(z/\mu)}{\beta}\right) \quad (2.1)$$

where  $\Phi(\cdot)$  is the normal CDF and  $\mu$  and  $\beta$  are mean and standard deviation of the fragility functions.

#### 2.4.1.1 Incremental Dynamic Analysis

To explicitly study the effect of record-to-record uncertainty, IDA (Azarbakht and Dolšek 2010; Vamvatsikos and Cornell 2002) is used to develop collapse fragility functions for steel diagrid archetypes. Figure 2.11 shows IDA curves for the 4-45 archetype where the vertical axis is the normalized pseudo-spectral acceleration based on 5% damped design spectra for the region at the fundamental period of the building structure ( $S_a(T_1, 5\%)$ ) and the horizontal axis is the maximum recorded IDR for each ground motion record in each analysis. The diagrid models display a sharp initial stiffness where all members are elastic, manifested as inclined lines in the initial part of the IDA curves, highlighted in Figure 2.11.

In the IDA curves, there are a few backward jumps (reversals) which have been reported in previous studies (Azarbakht and Dolšek 2010; Baker 2015; Li et al. 2010) and are in part due to the variability of ground motion records and sensitivity of analytical parameters considered here.

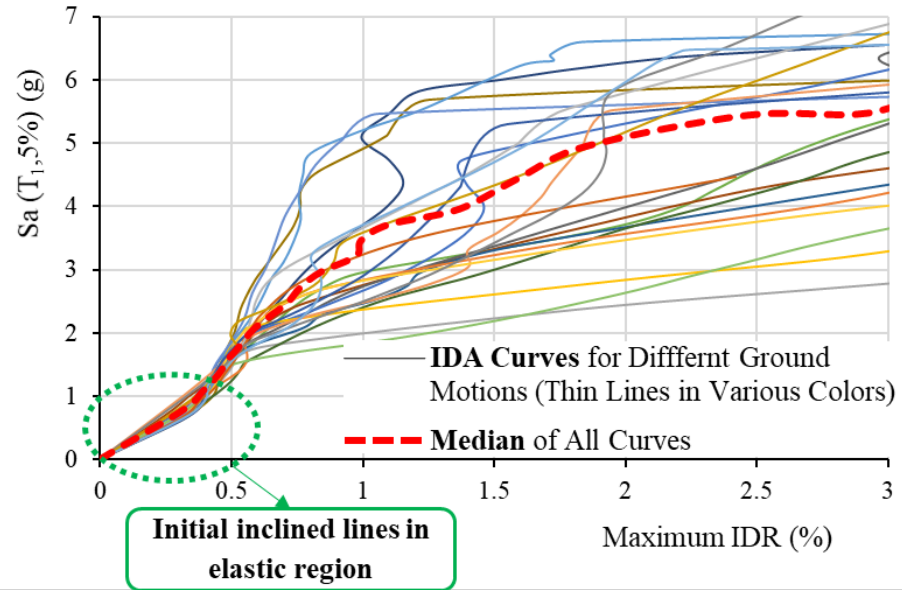


Figure 2.11 Incremental dynamic analysis curves for 4-45 archetype

#### 2.4.1.2 Collapse Capacity and Demand

Figure 2.12 shows the empirical CDF of collapse capacity for different archetypes each obtained from 748 NTHAs and the fitted lognormal fragility functions. In IDA, collapse is achieved if a slight increase of spectral acceleration significantly increases the maximum IDR which manifests as a sharp reduction in the slope of IDA curve. The collapse is presumed where 1) the slope of the fragility curve reaches 20% of its initial slope, a reduction of 80%, 2) the model reaches a numerical instability due to excessive nonlinear deformation in structural members (Vamvatsikos and Cornell 2002; Yamin et al. 2017).

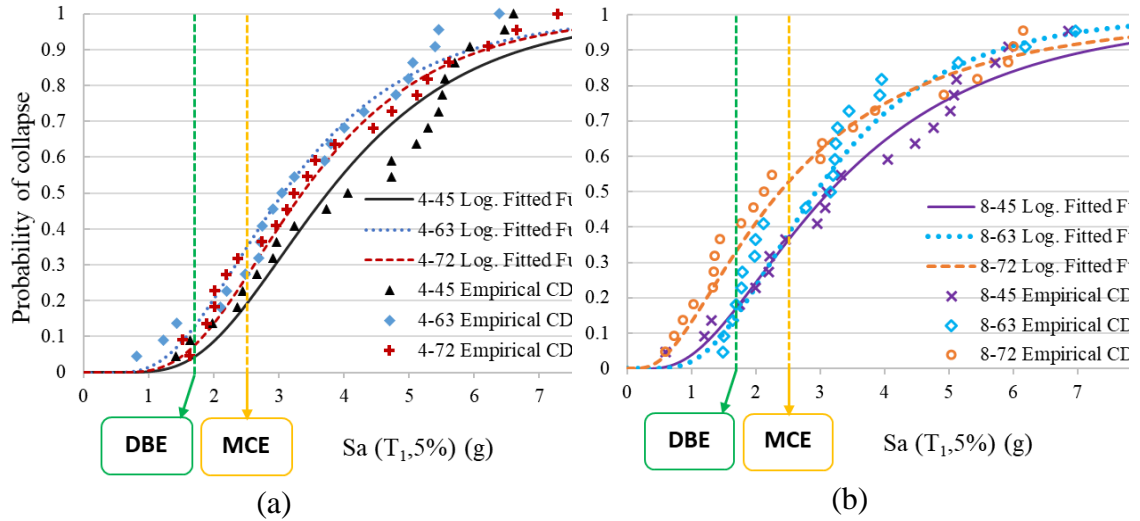


Figure 2.12 Empirical CDF of  $Sa(T_1,5\%)$  and fitted lognormal fragility functions for (a) 4-story and (b) 8-story archetypes

In Table 2.3, expected collapse capacity,  $\hat{S}_{CT}$ , expected collapse IDR, their corresponding logarithmic dispersions (standard deviations),  $\beta_{S_a}$  and  $\beta_{IDR}$  respectively, and the probability of collapse under DBE and MCE are listed. The diagrid models show a considerably large reserve capacity against collapse and undertake large spectral acceleration, a mean value of 3.1g and a dispersion of 0.42, before reaching the collapse point. As illustrated in Figure 2.12, the expected collapse capacity,  $\hat{S}_{CT}$ , is larger than DBE and MCE spectral acceleration except for 8-72 archetype. In addition, the 4-63 archetype shows slightly larger probability of collapse than the 4-72 and 4-45 archetypes and the 4-45 one shows the least probability of collapse. Among 8-story archetypes, 8-63 shows the least probability of collapse under DBE and the probability of collapse under MCE for 8-45 and 8-63 archetypes is very close. The 8-72, however, shows the largest probability of collapse.

A part of diagrid large capacity stems from the small  $R$  factor assumed here and the overstrength caused by it. But, the main part of it is due to substantial load capacity and stiffness of diagrid frames. Such that, in every span of a diagrid frame, inclined diagonal members carry a large portion of lateral load creating a distinctively stiff structure. This is a particularly desirable behavior in mid- to high-rise buildings under large lateral loads in which lateral displacement is a key concern. On a smaller scale, braced frames show similar behavior as they have a comparatively high lateral stiffness among steel structures as well (Hwang and Lignos 2017a).

Table 2.3 Expected collapse capacity and IDR, the corresponding dispersion and the probability of collapse under DBE and MCE based on logarithmic fragility CDF

Model	$\hat{S}_{CT}$ (g)	$\beta_{S_a}$	Collapse IDR <sub>max</sub> (%)	$\beta_{IDR}$	Prob. of collapse (%) under	
					DBE	MCE
4-45	3.75	0.46	1.16	0.53	3.7	18.1
4-63	3.07	0.52	1.50	0.62	11.4	33.6
4-72	3.35	0.47	5.91	0.42	6.6	25.7
8-45	3.15	0.65	1.37	0.41	15.8	35.3
8-63	2.93	0.52	1.25	0.57	13.4	36.9
8-72	2.37	0.77	2.60	0.74	31.7	51.8

Figure 2.13 shows the variation of collapse capacity and maximum recorded IDR and the corresponding logarithmic trendlines for all cases. The effect of the diagonal angle on expected collapse capacity ( $\hat{S}_{CT}$ ) is noticeable but not significant. However, its influence on collapse IDR<sub>max</sub> is comparably significant causing a dispersion of 2.16 and 0.61 for 4- and 8-story archetypes, respectively. The main contributor to this dispersion is the diagrid with 72° diagonal angle which has, as discussed, an incomplete module. If 72° case is

excluded, the collapse  $IDR_{max}$  of steel diagrids is 1.32% in average which is relatively small compared to other structural systems such as MRFs and CBFs (Chen et al. 2008; FEMA 2012). The mean collapse  $IDR_{max}$  is about 15% larger than the mean collapse  $IDR_{max}$  obtained from static nonlinear analyses, i.e. 1.15%. The IDA is a more comprehensive and realistic analysis which explicitly takes the effect of record-to-record uncertainty into account, though. Therefore, the results from IDA is considered for developing damage criteria which will be discussed later. The low collapse  $IDR_{max}$  may lead to low ductility which is not desirable in high seismic regions. In these regions, the low ductility can be mitigated by passive and semi-active control systems. In terms of dispersion, the 8-72 archetype shows larger variability with 0.77 dispersion on collapse capacity and 0.74 dispersion on collapse  $IDR_{max}$  followed by 4-63 archetype.

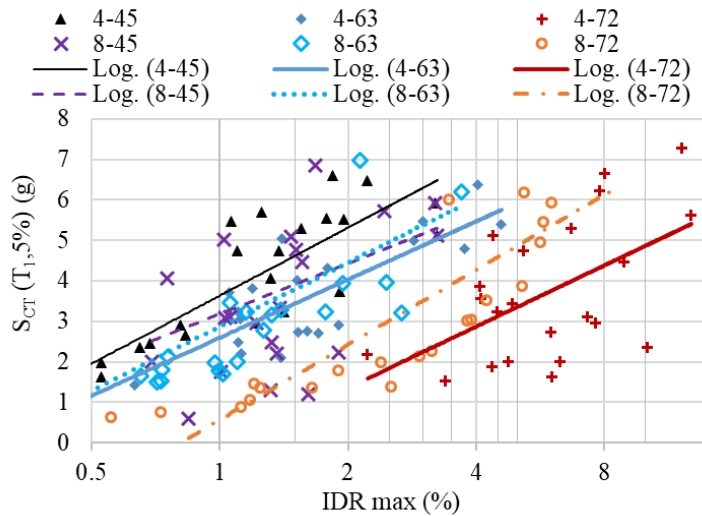


Figure 2.13 Variation of collapse capacity and  $IDR_{max}$  for different archetypes

Further, the collapse  $IDR_{max}$  obtained from IDA are noticeably different from values obtained from static nonlinear analyses. As noted, analysis criteria for IDA and static

analysis are not similar. In static analyses, collapse is achieved if all diagonal members of a story reach the full-yield or critical axial load limit. This limit is used given that the lateral displacement increases substantially, and the load-carrying capacity of the structure decreases considerably if all diagonals of a story fail (a soft-story collapse mechanism forms). On the other hand, in IDA, an 80% reduction in the slope of IDA curve and/or numerical instability indicate collapse (Vamvatsikos and Cornell 2002; Yamin et al. 2017).

#### ***2.4.2 Proposed Seismic Performance Levels and Damage States***

FEMA P-58 typically uses practicable EDPs such as maximum IDR and ACC to catalogue damage state of structural components.  $IDR_{max}$  has been effectively used as the damageability indicator to assess the performance of the various structural systems (Han et al. 2014; Li et al. 2010; Yamin et al. 2017). In case of diagrids which are used in mid-to high-rise buildings particularly because of their large lateral stiffness or small lateral displacement,  $IDR_{max}$  is the key indicator of their damageability and performance. Thus, the expected maximum IDR obtained from IDA is used as the main EDP to develop structural damage state and evaluate the seismic loss of the diagrid structures.

As discussed earlier, diagrids are particularly similar to CBFs with single diagonal brace in terms of configuration and damageability where the diagonals act like the diagonal braces and the gradual yielding and buckling of them under lateral loading leads to ultimate failure of the structure. Therefore, the FEMA P-58 recommendations for special CBFs with single diagonal braces are used to develop performance criteria and damage states for diagrid structures. Note that this similarity is mostly in component-level between diagonals

and diagonal braces. Apart from that, the absence of columns and the tubular form of diagrids has a significant influence on the behavior of diagrids, in particular, their lateral stiffness.

Based on static and dynamic analyses discussed earlier and the similarities between diagrid and CBFs, the performance of steel diagrid frames is categorized into five damage states: that is undamaged ( $DS_0$ ), minor damage ( $DS_1$ ), moderate damage ( $DS_2$ ), severe damage ( $DS_3$ ), and collapse (completely damaged) ( $DS_4$ ) states which are described in detail in this section. Clearly, the following criteria need to be verified by proper experimental studies.

The failure of the diagrid frames typically initiates from yielding or buckling of corner diagonals. Generally, the axial force is larger in corner diagonals compared to the middle ones which indicate the critical role of corner diagonals in diagrids. This behavior known as the shear lag effect is common in tubular structural systems (Ali and Moon 2007; Kim and Lee 2012). Shear lag is a non-uniform nonlinear distribution of the internal forces across the side of a tube-shaped structures or structural members. The result is large internal forces in corner members compared with the middle ones. As minor yielding or local buckling spread to a few diagonals and beams, the lateral stiffness of the structure decreases sharply indicating a significant change in performance. The  $IDR_{avg}$  is insignificant, approximately 0.3 percent, and it causes no or slight damage to the non-structural components. No global buckling in diagonals or yielding/fracture in connection should be

observed. This point is interpreted as DS<sub>1</sub> damage state where the structure leaves the IO performance level and enters the LS level.

As the lateral load increases several diagonal members yield or buckle locally. The lateral stiffness decreases step by step, but the load capacity of the structure is still increasing. The yielding reaches the depth of the beams and a few diagonals across the width and the height of the structure as well as a few central columns. The residual drift is noticeable, and the IDR and ACC may cause visible damage to non-structural components. According to analyses discussed earlier, the mean transient  $IDR_{avg}$  at this point is larger than 0.55%. Some yielding or minor cracks might be noticeable in connections. This point indicates the DS<sub>2</sub> damage state and passing the LS performance.

At the CP level, extensive global buckling or full yield of diagonals, beams and central columns cause a sharp decrease in lateral stiffness of the structure. Many diagonals and their connection fail but not all diagonals of a specific story. Extensive transient IDR and ACC cause severe non-structural damage. Approximately an  $IDR_{avg}$  of 1% represents the DS<sub>3</sub> damage state for diagrids. This is followed by an overall collapse (DS<sub>4</sub>) approximately at  $IDR_{avg}$  of 1.3%. The diagrid structure collapses when most diagonals of a specific story reach full yield or global buckling while most diagonals and beams of other stories are partially yielded or buckled. Literature shows similar values for  $IDR_{avg}$  at the collapse and sharp reduction of stiffness once the diagonals fail (Kim and Kong 2013; Kim and Lee 2010, 2012).

Table 2.4 summarizes the proposed damage states criteria and the corresponding  $IDR_{max}$  limit representing them for an ordinary steel diagrid frame with w-shaped diagonals. The  $IDR_{max}$  limit is approximated based on the performance of diagrids under static and dynamic nonlinear analyses. The  $72^\circ$  archetypes are excluded in approximation since the configuration pose an adverse impact on performance and should be avoided in practice. Note that diagrids experience a considerably large spectral acceleration while desirably confining the IDRs (see section 3 and subsection 4.1). This large spectral acceleration may cause damage to non-structural components vulnerable to excessive acceleration such as elevators and chillers. Here, a slightly more stringent criterion on  $IDR_{max}$  is considered to reduce possible damages to non-structural components vulnerable to excessive acceleration. Furthermore, the proposed dispersion values ( $\beta_D$ ) are based on dispersion observed for  $S_a(T_1, 5\%)$  in each damage state and represents the uncertainty in demand. Specifically, it is the arithmetic average of logarithmic dispersion of  $S_a(T_1, 5\%)$  for each damage state for studied archetypes. A full list of mean and logarithmic dispersion of  $S_a(T_1, 5\%)$  for each damage state and model is presented in Table 2.5.

Table 2.4 Damage criteria and illustrative description of damage states for steel diagrid frames

Damage State	$IDR_{max}$ limit (%)	$\beta_D$	Descriptive Damage criteria	
			Primary structural components	Non-structural components
DS <sub>1</sub>	0.25	0.27	Minor yielding or local buckling in a few diagonal members and beams. No global buckling in diagonals or fracture in connection.	The residual drift is negligible. IDR causes minor or no nonstructural damage.

DS <sub>2</sub>	0.55	0.24	Several diagonals yield or buckle but do not fail. Yielding reaches the depth of beams and a few diagonals and central columns. Some yielding or cracks in connections.	The IDR and ACC may cause visible damage to non-structural components.
DS <sub>3</sub>	0.95	0.30	Extensive global buckling or full yield of diagonals, beams and central columns. Many diagonals and their connection fail but not all diagonals of a specific story.	Extensive residual drift. Extensive IDR and ACC cause severe non-structural damage.
DS <sub>4</sub>	1.25	0.32	Most diagonals of a specific story reach full yield or global buckling.	The structure collapses.

Table 2.5 Mean and logarithmic dispersion of  $S_a(T_1, 5\%)$  for each damage state

Damage State	4-45		4-63		4-72		8-45		8-63		8-72	
	$\mu$	$\beta_D$										
DS <sub>1</sub>	0.65	0.14	0.64	0.23	0.27	0.40	0.43	0.45	0.53	0.14	0.39	0.27
DS <sub>2</sub>	1.93	0.13	1.55	0.21	0.45	0.36	0.86	0.42	1.14	0.15	0.75	0.19
DS <sub>3</sub>	3.08	0.29	2.31	0.30	0.69	0.36	1.69	0.41	2.21	0.27	1.14	0.17
DS <sub>4</sub>	3.59	0.32	2.77	0.32	0.86	0.38	2.44	0.40	2.77	0.30	1.36	0.20

Using the abovementioned damage criteria and the results from IDA, the fragility function for each damage state is estimated and their corresponding fragility curves are depicted in Figure 2.14 for each archetype model. The fragility curves in Figure 2.14 illustrates the probability of exceeding a certain damage criterion conditioned on a certain intensity indicated by  $S_a(T_1, 5\%)$ .

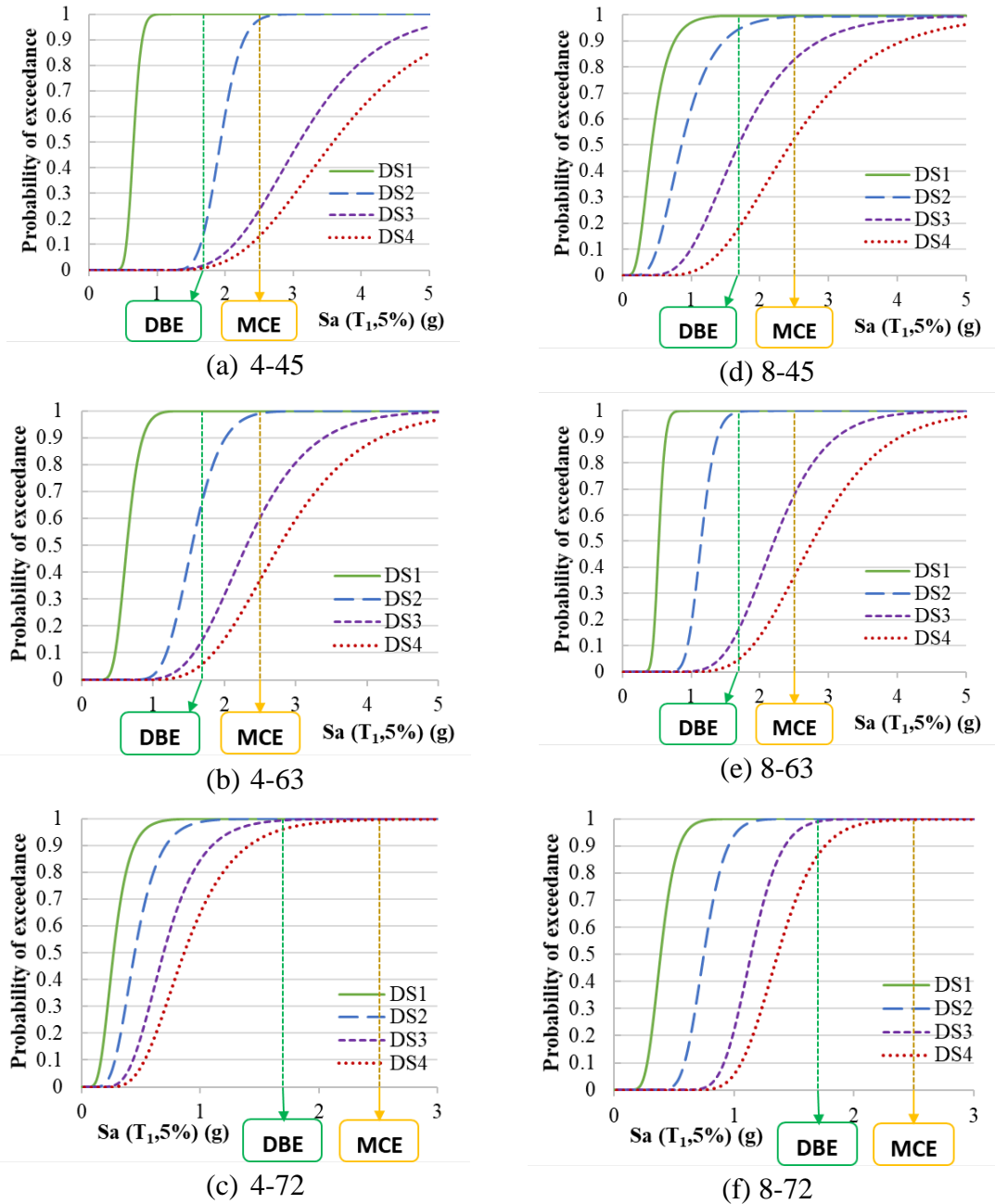


Figure 2.14 Seismic fragility curves for each damage state for (a) 4-45 (b) 4-63 (c) 4-72 (d) 8-45 (e) 8-63 (f) 8-72 archetype

The fragility curves for damage state divides the performance spectrum of the structure into different performance regions (Ellingwood and Kinali 2009). Hence in Figure 2.14, the structure is respectively in IO, LS, CP, and imminent collapse regions

before reaching the DS<sub>1</sub>, DS<sub>2</sub>, DS<sub>3</sub>, and DS<sub>4</sub> damage states. As illustrated in Figure 2.14, the 4-45 model is mostly in LS and CP region under DBE and MCE respectively, which adheres to conventional force-based design approach. Whereas, the 4-63 model may pass the LS region with 60% probability and even reaches imminent collapse point with 37% probability under MCE. This exemplifies the significance of diagonal angle in behavior and failure of diagrid frames. Generally, the 45° and 63° models show the relatively close probability of exceedance for the same intensity for different damage states. The 4-63 and 8-45 archetypes show the largest probability of exceedance for the same intensity among 4- and 8-story archetypes, respectively. The 72° archetypes, however, shows a much smaller probability than other cases. As discussed earlier, the 72° model experience much larger  $IDR_{max}$  before reaching the imminent collapse region which is mostly due to the incomplete uppermost diagrid module. Accordingly, the proposed criteria underestimate the response of diagrids with incomplete uppermost modules. As indicated in Table 2.5, the dispersion generally increases in higher damage states particularly in collapse damage state, DS<sub>4</sub>, which shows more significant uncertainty in higher damage states. Higher dispersion is reflected as a wider range of  $S_a(T_1, 5\%)$  covered by each fragility curve in Figure 2.14.

## 2.5 Seismic Loss Estimation

### 2.5.1 Methodology

The total probability of loss at a given earthquake intensity (IM) for mutually exclusive seismic events is defined as follows (Ramirez and Miranda 2012a; Yamin et al. 2017):

$$\begin{aligned} & Pr(L_T > l_i | IM = z_i) \\ &= \int_{EDP} \int_{DS} Pr(L_T > l_i | DS = DS_{ij}) PDF_{DS}(DS | EDP = d) PDF_{EDP}(EDP | IM = z) dDS dEDP \quad (2.2) \end{aligned}$$

where  $Pr(L_T > l_i | IM = z)$  is the probability of having a total loss greater than  $l_i$  given that hazard intensity is equal to  $z$ ,  $Pr(L_T > l_i | DS = DS_{ij})$  is the probability of having a total loss greater than  $l_i$  given that damage state of  $DS_i$  is achieved,  $PDF_{DS}(DS | EDP = d)$  is the PDF of achieving a damage state given that the EDP reaches a certain value of  $d$ , and  $PDF_{EDP}(EDP | IM = z)$  is the PDF of the EDP conditioned on a certain hazard intensity,  $z$ . The fragility function is used to find the probability that each damageable component reaches a certain damage state as follows.

$$\begin{aligned} & Pr(DS_n = DS_{ij} | EDP = d) \\ &= \begin{cases} 1 - F_{DS_{ij}|EDP=d_j} & \text{for } j = 0 \text{ (undamaged)} \\ F_{DS_{ij}|EDP=d_j} - F_{DS_{i(j+1)}|EDP=d_j} & \text{for } 1 \leq j < n \\ F_{DS_{ij}|EDP=d_j} & \text{for } j = n \text{ (collapse)} \end{cases} \quad (2.3) \end{aligned}$$

where  $F_{DS_{ij}|EDP=d_j}$  is the fragility function of the  $i$ th component in the  $j$ th damage state given that the EDP is equal to a certain value  $d$ .

The loss estimation methodology implemented in PACT is used to estimate the total loss distribution function. PACT, developed by ATC as a part of the ATC-58 project, can perform loss estimation analyses using Monte Carlo simulation method.

### 2.5.2 Criteria for Loss Estimation Analysis

As described, five damage states are considered for estimating the loss due to the failure of the diagrid frame, that is undamaged ( $DS_0$ ), slightly damaged ( $DS_1$ ), moderately damaged ( $DS_2$ ), extensively damaged ( $DS_3$ ), and completely damaged (collapsed) ( $DS_4$ ) states. The seismic loss is estimated as a CDF of economic loss due to cost for a given earthquake hazard level (Yin and Li 2010). The repair loss is assumed as a percentage of Total Replacement Cost (TRC). The land cost is not included, and the property cost is 50% of the building value. Based on RSMeans cost estimation data for southern Los Angeles, California (RSMeans 2018), the replacement cost for a steel commercial building with 4 and 8 stories is \$213.81 and \$206.40 per *sq. ft.* (approximately \$2301.4 and \$2221.7 per *sq. m*), respectively. The key assumptions for loss estimation along with their source are presented in Table 2.6.

Table 2.6 Building specification and assumptions for loss estimation

<b>Parameter</b>	<b>Value</b>	<b>Source</b>
Total Replacement Cost	US\$ 4,071,000 for 4-story buildings US\$ 7,860,000 for 8-story buildings	RSMeans (2018)
Height Factor Premium	1.08 for 5 <sup>th</sup> to 10 <sup>th</sup> floor 1.16 for 11 <sup>th</sup> and higher floors	FEMA P-58

Together with FEMA P-58, a Performance Assessment Calculation Tool (PACT) is also developed which contains the fragility specification database. The proposed fragility criteria for diagrids are implemented in PACT and used to assess the loss of archetype steel

diagrid buildings. Residual drift used for repair cost is found per section 5.4 of FEMA P-58 as a function of median transient IDR.

For diagrid frames, three new performance group is implemented into PACT for three different diagonal weights, i.e. diagonal weight less than 40 *lb. per ft.* (PLF), between 41 and 99 PLF, and greater than 100 PLF. The fragility specifications for especial CBFs frames with single diagonal (code B1033.002 in FEMA P-58) is modified according to performance criteria explained in section 4 to implement the new performance groups. Also, the connections are post-Northridge welded steel moment connection without reduced beam section (RBS) detailing.

As for non-structural components, each building has two hydraulic elevators, one 500-Ton (500 BTU/hr/12,000) chiller and air-handling unit on the roof, and a seismically-rated independent pendant lighting for each 4-*sq. m* of the floor. The perimeter of the building is covered with generic midrise stick-built curtain wall in each span, the interior wall partitions are partial or full-length gypsum walls with metal studs, and the floor and the ceiling are covered with seismically-rated raised access floor and suspended ceiling, respectively. A full list of structural and non-structural components considered in loss estimation analyses are presented in Table 2.7.

Table 2.7 Structural and non-structural fragility and cost specifications

Description	Unit	EDP	Damage state	Fragility Parameters		Fragility specification code	Average repair cost (US\$)
				$\mu^a$	$\beta^b$		
Diagrid Frame with w-shaped diagonals, $w < 40$ PLF	EA	IDR (rad)	DS <sub>1</sub>	0.0025	0.26	adapted from	44,530
			DS <sub>2</sub>	0.0055	0.23	B1033.002a	48,650
			DS <sub>3</sub>	0.0095	0.32		48,960

			DS <sub>4</sub>	0.0125	0.34	of FEMA P-58	48,960
Diagrid Frame with w-shaped diagonals, 41 PLF < w < 99 PLF	EA	IDR (rad)	DS <sub>1</sub>	0.0025	0.26	adapted from	44,530
			DS <sub>2</sub>	0.0055	0.23	B1033.002b	53,590
			DS <sub>3</sub>	0.0095	0.32	of FEMA P-	57,340
			DS <sub>4</sub>	0.0125	0.34	58	57,340
Diagrid Frame with w-shaped diagonals, w > 100 PLF	EA	IDR (rad)	DS <sub>1</sub>	0.0025	0.26	adapted from	44,530
			DS <sub>2</sub>	0.0055	0.23	B1033.002c	60,470
			DS <sub>3</sub>	0.0095	0.32	of FEMA P-	67,340
			DS <sub>4</sub>	0.0125	0.34	58	67,340
Post-Northridge welded steel moment connection other than RBS, beam one side, beam depth <= W27	EA	IDR (rad)	DS <sub>1</sub>	0.03	0.3	B1035.021	20,880
			DS <sub>2</sub>	0.04	0.3	(FEMA P-	35,160
			DS <sub>3</sub>	0.05	0.3	58)	35,160
Post-Northridge welded steel moment connection other than RBS, beams both sides, beam depth <= W27	EA	IDR (rad)	DS <sub>1</sub>	0.03	0.3	B1035.031	42,000
			DS <sub>2</sub>	0.04	0.3	(FEMA P-	62,760
			DS <sub>3</sub>	0.05	0.3	58)	62,760
Curtain Walls - Generic Midrise Stick-Built Curtain wall, Config: Monolithic	ft <sup>2</sup>	IDR (rad)	DS <sub>1</sub>	0.0338	0.4	B2022.001	2,060
			DS <sub>2</sub>	0.0383	0.4	(FEMA P-58)	2,60
Wall Partition, Type: Gypsum with metal studs, Full Height, Fixed Below, Fixed Above	based upon 13'x10 0' Panels	IDR (rad)	DS <sub>1</sub>	0.0021	0.6	C1011.001a	2,730
			DS <sub>2</sub>	0.0071	0.45	(FEMA P-	5,190
			DS <sub>3</sub>	0.012	0.45	58)	7,940
Wall Partition, Type: Gypsum + Wallpaper, Partial Height, Fixed Below, Lateral Braced Above	based upon 9'x100' Panels	IDR (rad)	DS <sub>1</sub>	0.0064	0.3	C3011.001b (FEMA P-58)	3,510
Raised Access Floor, seismically rated	ft <sup>2</sup>	ACC (g)	DS <sub>1</sub>	1.5	0.4	C3027.002 (FEMA P-58)	130
Suspended Ceiling, SDC D, E (Ip=1.0), Area (A): A < 250, Vert & Lat support	each 600 ft <sup>2</sup>	ACC (g)	DS <sub>1</sub>	1.0	0.4	C3032.003a	1,230
			DS <sub>2</sub>	1.8	0.4	(FEMA P-	10,220
			DS <sub>3</sub>	2.4	0.4	58)	19,760
Suspended Ceiling, SDC D, E (Ip=1.0), Area (A): 250 < A < 1000, Vert & Lat support	each 250 ft <sup>2</sup>	ACC (g)	DS <sub>1</sub>	0.7	0.4	C3032.003b	470
			DS <sub>2</sub>	1.15	0.4	(FEMA P-	3,770
			DS <sub>3</sub>	1.8	0.4	58)	7,830

Independent Pendant Lighting - seismically rated	EA	ACC (g)	DS <sub>1</sub>	1.5	0.4	C3034.002 (FEMA P-58)	640
Hydraulic Elevator – Applies to most California Installations 1976 or later	EA	ACC (g)	DS <sub>1</sub>	0.5	0.3	D1014.021 (FEMA P-58)	11,990 <sup>c</sup>
HVAC Galvanized Sheet Metal Ducting less than 6 sq. ft., SDC D, E, or F	based upon 1000 ft. segment	ACC (g)	DS <sub>1</sub> DS <sub>2</sub>	1.5 2.25	0.4 0.4	D3041.011c (FEMA P-58)	1,300 12,700
Control Panel - Capacity: all - Equipment that is either hard anchored or is vibration isolated	EA	ACC (g)	DS <sub>1</sub>	3.0	0.4	D3067.013b (FEMA P-58)	4,570
Fire Sprinkler Drop Standard Threaded Steel	per 100 units	ACC (g)	DS <sub>1</sub> DS <sub>2</sub>	1.5 2.25	0.4 0.4	D4011.053a (FEMA P-58)	550 550
Chiller - Capacity: 350 to <750 Ton	EA	ACC (g)	DS <sub>1</sub>	0.72	0.2	D3031.013h (FEMA P-58)	280,720
Air Handling Unit - Capacity: 25000 to <40000 CFM	EA	ACC (g)	DS <sub>1</sub>	1.54	0.6	D3052.013k (FEMA P-58)	206,800 <sup>d</sup>

a  $\mu$  = Median of component fragility curve

b  $\beta$  = Lognormal standard deviation (dispersion) of component fragility curve

c Collective cost

d Collective cost

Note: EA = per unit

### 2.5.3 Expected Loss at a Given Earthquake Intensity

The loss estimation analyses are done for two earthquake intensities, DBE (10%/50-yr) and MCE (2%/50-yr) using PACT. To simplify the figures and illustrations, the components listed in Table 2.7 are categorized into three groups: 1) structural components, 2) non-structural components vulnerable to excessive IDR, 3) non-structural components vulnerable to excessive ACC. The main contributor to loss caused by damage to structural

components is the diagrid frame. The non-structural components vulnerable to IDR includes the perimeter curtain walls and the interior partial- or full-length wall partitions. The third group consists of the all other equipment and decoration which are vulnerable to extreme acceleration.

Depending on the structural response under each intensity, substantial unreparable residual drift is likely to cause the cumulative loss to exceed the TRC threshold. In these cases, it is assumed that the building will be demolished even if it has not collapsed. The corresponding loss due to demolition, called demolition loss in Figure 2.15, varies based on the probability of exceeding the TRC threshold. In studied archetype, the demolition loss found to be insignificant except for 72° archetypes. Figure 2.15 shows the expected total loss due to each performance group as well as demolition loss for each archetype as a percentage of TRC. Also, Table 2.8 summaries the expected loss caused by each performance group as a percentage of TRC.

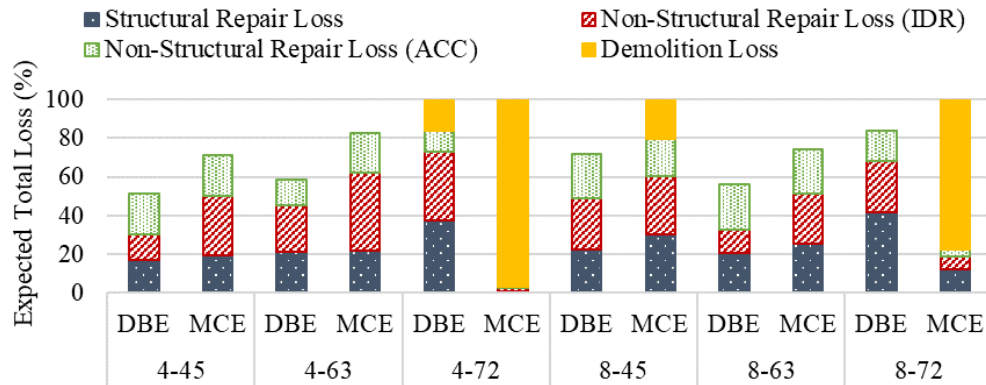


Figure 2.15 Expected total loss caused by various components as a percentage of total replacement cost

Table 2.8 Expected loss for different archetypes and intensities

Archetype	Intensity	Repair Loss (% of TRC)			Demolition Loss (% of TRC)	Median Loss (% of TRC)	Percent of realizations with collapse
		Structural	Non-Structural (IDR)	Non-Structural (ACC)			
4-45	DBE	17.0	12.9	21.4	0.0	51	2.0
	MCE	19.7	30.2	21.6	0.0	71	15.0
4-63	DBE	21.0	24.1	13.4	0.0	59	6.5
	MCE	22.1	40.0	20.5	0.0	83	31.5
4-72	DBE	37.3	35.7	11.1	15.4	99	4.0
	MCE	0.8	1.6	0.8	96.8	99	23.0
8-45	DBE	22.5	26.5	23.2	0.0	72	12.5
	MCE	30.5	30.0	19.0	19.9	99	36.5
8-63	DBE	20.6	12.3	23.5	0.0	56	12.5
	MCE	25.2	25.9	23.2	0.0	74	30.5
8-72	DBE	41.9	26.0	16.1	0.0	84	37.0
	MCE	12.1	6.4	4.0	77.4	100	46.5

The DBE causes an expected cumulative total loss equivalent to 51% of TRC to the 4-45 archetype. The total loss is relatively high considering the negligible probability of collapse under DBE for this archetype, that is 3.7% (see Table 2.3). The main contributor to the expected total loss is the non-structural components vulnerable to ACC with 21% contribution out of 51%. Compared to the 4-45 archetype, the expected total loss is larger for 4-63 archetype, up to 58%, and for 4-72, it reaches the TRC threshold. On the other hand, among 8-story archetypes, the 8-63 archetype has the least expected total loss, approximately 56% of TRC. This is consistent with the findings in previous sections where the 8-63 and 4-45 archetype display smaller IDR and ACC and a generally better performance.

As discussed earlier, diagrid frames have a large  $\hat{S}_{CT}$  which indicates they experience a large amount of spectral acceleration before reaching collapse. Even though the structure can undertake larger acceleration, the damage and loss to non-structural components may

become too large to overlook. In all cases, the loss due to non-structural components vulnerable to IDR increases significantly under MCE compared to DBE. Clearly, larger IDR causes the curtain wall and wall partitions, which are seismically rated and laterally supported, to reach a higher damage state leading to larger total loss under MCE hazard level. The loss due to ACC is slightly larger under MCE compared to DBE for most cases except for archetype whose expected total loss reaches the TRC. Once the expected total loss reaches the TRC threshold, the cumulative loss due to structural components is the most significant portion.

In general, the 4-63 archetype suffers larger expected total loss compared to the 4-45 archetype. It is consistent with the results of previous sections where the 4-63 archetype building shows a smaller collapse capacity and a larger probability of collapse under DBE and MCE. Compared to the 4-45 building, the structural and non-structural losses caused by IDR is increased in 4-63 but the loss caused by ACC is notably reduced particularly under MCE. In case of 4-72 archetype, the IDR of the structure is so large that the repair cost for some realization exceeds the TRC; Hence under DBE, about 15% of expected total loss is due to demolition loss. This value increases to about 99% in MCE which means the deformation and acceleration of 4-72 structure at MCE intensity level causes such a severe damage to structural and non-structural components that most likely the total repair cost exceeds the TRC threshold. For 4-72, a considerable number of realizations leads to unrepairable residual drift, specifically 36.5% and 53.5% of realizations under DBE and MCE respectively. This large unrepairable residual drift, particularly in the incomplete module, leads to considerable demolition losses for the 4-72 archetype. The unrepairable

residual drift in 4-45 and 4-63 is negligible. Furthermore, the loss caused by severe ACC in 4-72 archetype under DBE is smaller than that of 4-63 and 4-45 ones which indicates the significance of IDR in diagrid archetypes with  $72^\circ$  diagonal angle and the adverse impact of uppermost incomplete diagrid module in these structures. Similar behavior is observed for 8-72 archetype but on a smaller scale. The unreparable residual drift causing demolition loss is smaller for 8-72 archetype compared to the 4-72 case. The loss in 8-72 archetype is mostly due to large IDR in the incomplete module, i.e. 7<sup>th</sup> and 8<sup>th</sup> floors. In case of 8-72 archetype under DBE, the demolition loss is negligible and structural components is the largest portion of the expected total loss. Yet, the expected total loss under MCE exceeds the TRC threshold. The adverse effect of incomplete uppermost module mitigates in taller diagrid frames since the uppermost stories have a less significant impact on the overall behavior of the structure and these stories carry a smaller portion of cumulative base shear compared to middle and lowermost ones.

The 8-45 archetype also reaches the TRC threshold under MCE and about 20% of its expected total loss stems from demolition loss. This archetype also shows a larger  $IDR_{avg}$  which is partly due to small demand to capacity ratio ( $PM_u/PM_n$ ) of diagonals in this archetype. But more significantly, the expected total loss depends on how close the diagonal angle is to the optimal angle. The 8-63 archetype is close to the optimal configuration since it shows a considerably less amount of loss under both DBE and MCE.

Table 2.8 also lists the percent of realizations which leads to collapse in each case. These values are consistent with, but generally smaller than, the corresponding values for the probability of collapse under DBE and MCE in Table 2.3. For instance, the probability

of collapse for 4-72 archetype under DBE and MCE is 6.6% and 25.7% while the corresponding percent of realizations leading to collapse is 4% and 23%. This difference can be attributed to the additional uncertainty involved in loss estimation analysis due to non-structural components. Note that the probability of collapse presented in Table 2.3 is found based on fragility analyses on the complete structure considering the uncertainty in ground motion acceleration. Whereas, the values presented in Table 2.8 are based on Monte Carlo simulation used for loss estimation considering fragility function for all structural and non-structural components as listed in Table 2.7.

Figure 2.16 shows the lognormal CDF of total loss for different archetypes considering uncertainty in demand and collapse capacity. The vertical axis represents the probability of exceeding a certain total loss (C) and the horizontal one shows the total loss values as a percentage of TRC. Note that the 50% probability of exceedance in Figure 2.16 for each archetype represents the corresponding value shown in Figure 2.15. The 4-45 and 8-63 archetypes show the least probability of exceedance of a certain total loss both for DBE and MCE among 4- and 8-story archetypes, respectively. As noted in Table 2.3, these two cases show the least amount of collapse  $IDR_{max}$  (the key EDP for diagrids) among 4- and 8-story archetypes as well, respectively. Also, the expected total loss for them is smaller than other corresponding cases as illustrated in Figure 2.12. They are followed by the 4-63 and 8-45 archetypes, respectively while the 72° archetypes have the largest probability. This is again consistent with collapse  $IDR_{max}$  values presented in Table 2.3. The large  $IDR_{max}$  in 4-72 and 8-72 archetypes increases the unreparable residual drift and

leads to total demolition of the structure in most of the realization of Monte Carlo simulation for these cases.

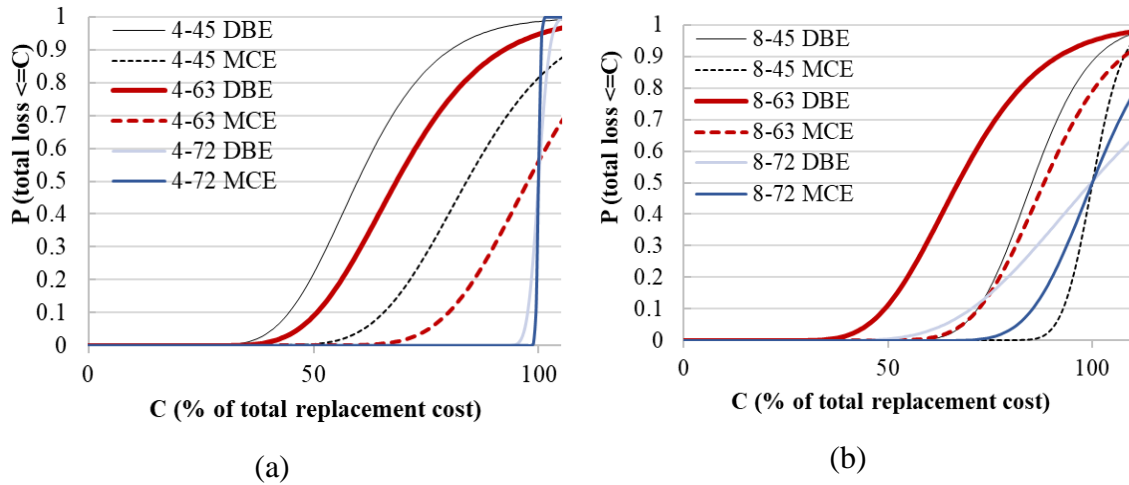


Figure 2.16 CDF of total loss for different intensities for (a) 4-story (b) 8-story archetypes

## 2.6 Conclusions

Diagrid seismic behavior is dictated by two key parameters: 1) the axial capacity of diagonals especially the corner ones and 2) the diagonal angle. Corner diagonals are where the initial yielding and/or local buckling occurs and failure or even partial yielding of them significantly decreases the lateral stiffness. Further, the diagonal angle has a major impact on maximum and average inter-story drift values as well as expected total loss. Therefore, a key step in diagrid design process is to find the optimal diagonal angle based on building configuration and height to width ratio of the building.

Having an incomplete module in diagrid frames adversely impact the diagrid performance causing substantial structural and non-structural damage and loss such that the expected total loss may exceed the total replacement cost threshold. The expected

collapse maximum inter-story drift of steel diagrids is comparatively small (e.g. 1.32% in average) compared to other structural systems such as MRFs and CBFs (Chen et al. 2008; FEMA 2012).

The diagrid structures show a substantial reserve capacity against collapse and undertake a large maximum absolute spectral acceleration, a mean value of 3.1g, before reaching the collapse point. In addition, they show significant overstrength in nonlinear static and time-history analyses. This substantial capacity is mostly due to the unique efficient configuration of diagrids in which diagonals carry both the gravity and the lateral loads through large axial forces. The large collapse capacity of diagrids may reduce the expected loss due to structural components, but the loss caused by excessive spectral acceleration to non-structural components will increase leading to a possible increase in the total expected loss.

Among the archetypes studied, the 4-story diagrid with 45° diagonal angle and the 8-story with 63° diagonal angle shows a smaller expected total loss and smaller collapse inter-story drift than other cases. In general, the main contributor to expected total loss of diagrid frame under design-based seismic hazard is the non-structural components vulnerable to excessive spectral acceleration. While under maximum considered hazard intensity, the contribution of non-structural components vulnerable to excessive inter-story drift (curtain walls and partitions) is more significant.

## Chapter 3

### 3. Multi-criteria Decision-making for Seismic Resilience and Sustainability Assessment of Diagrid Buildings<sup>3</sup>

#### 3.1 Introduction

Sustainability, as the Bruntland Report (Keeble 1988) firstly described, refers to the “development that meets the needs of the present without compromising the ability of future generations to meet their own needs”. In structure and infrastructure engineering, it is commonly quantified in terms of economic, social, and environmental gains achieved by using a sustainable approach in design, construction, and maintenance. Sustainable design

---

<sup>3</sup> The material presented in this chapter was previously published in the *Engineering Structures* and is re-used herein with permission from the publisher. See Appendix I for documentation of permission to republish this material.

Asadi, E., Salman, A. M., Li, Y. (2019). Multi-Criteria Decision-Making for Seismic Resilience and Sustainability Assessment of Diagrid Buildings, *Engineering Structures*, 191, 229-246, <https://doi.org/10.1016/j.engstruct.2019.04.049>.

of structures can substantially decrease the life-cycle economic and environmental loss whilst improving the resiliency of buildings (Bocchini et al. 2014). Seismic environmental consequences can be significant in seismic regions and need to be an essential part of a comprehensive performance assessment framework (Menna et al. 2013). Using innovative and efficient structural systems such as diagrids can effectively improve the sustainability and resiliency of buildings (Asadi and Adeli 2017; Liu et al. 2018; Milana et al. 2015).

Due to their substantial lateral stiffness and aesthetically appealing form, diagrids have been used as the primary load carrying system in several iconic buildings around the world including the 42-story Hearst Tower in New York City, the 36-story Capital Gate in Abu Dhabi, UAE, and the 11-story Macquarie Bank in Sydney, Australia (Ali and Moon 2007). Figure 3.1 shows the main components of a diagrid frame. Diagrid frames, commonly located on the perimeter of a building, form a tube-shaped stiff structure against large wind and earthquake loads while providing a large open rentable/usable space inside. Instead of columns and braces, diagrids consist of several inclined members called diagonals to carry both service and extreme loads. Having no vertical members (columns), they benefit from a wide-open façade which allows more sunlight to enter reducing the heating energy consumption. To improve sustainability, sky gardens and atriums can be located between the perimeter diagrid frames and the floors as seen in The Bow tower in Calgary, Canada (Charnish and McDonnell 2008).

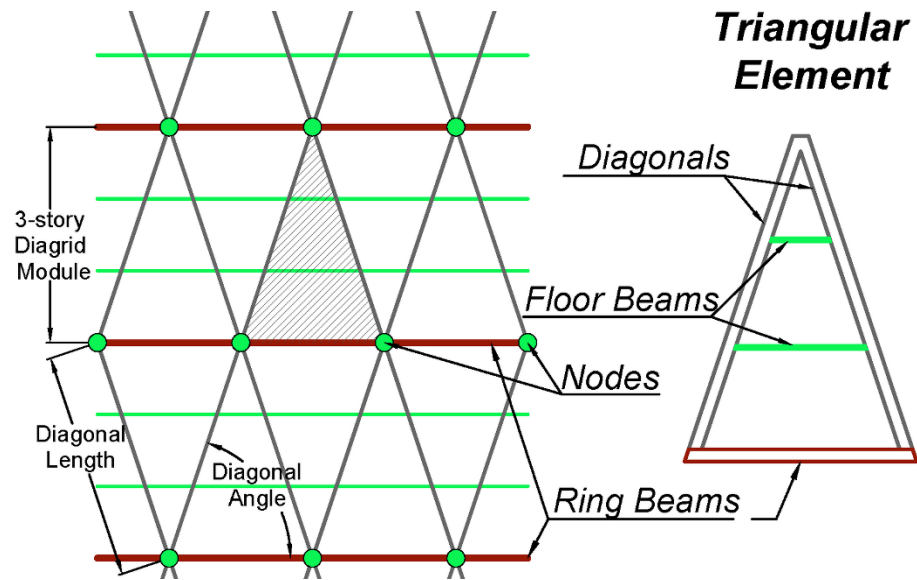


Figure 3.1 Main components of a diagrid frame and its triangular base element

Diagrids carry both lateral and gravity loads through large axial forces in diagonals leading to an efficient structure and possible reduction of required structural material (Ali and Moon 2007; Milana et al. 2015). Milana et al. (2015) compared 40-story steel diagrids with conventional tubular structure with outriggers and report considerable weight reduction (up to 33% for diagrid with an optimal diagonal angle) and overall performance improvement in terms of strength, stiffness, and ductility if diagrid is used. Moon et al. (2007) and Zhang et al. (2012) study diagrid configuration and tried to find the optimal or most efficient diagonal angle (the angle between diagonals and horizon) for archetype diagrids. Finding the optimal diagonal angle will improve the performance and reduce the required material for a structure; thus, it should be an imperative part of diagrid design process. Liu et al. (2018) and Asadi and Adeli (2017) present literature reviews on diagrid structures. Despite the worldwide trend and demand for resilience and sustainable design of buildings, none of the previous publications investigate the loss, downtime, and casualty

in diagrid structures after extreme events or propose a framework for their resilience or sustainability assessment.

Several researchers have aimed to incorporate environmental consequences of earthquakes into a comprehensive performance or resilience assessment framework for other conventional structural systems (Chhabra et al. 2018; Dong and Frangopol 2015, 2016; Feese 2013; Menna et al. 2013; Padgett and Li 2016). A few employed a component-level assessment approach considering fragility functions for various structural and non-structural components (Chhabra et al. 2018; Dong and Frangopol 2016). FEMA P-58 (2012) provides a comprehensive fragility specification database which can be used for component-level assessment of structures and a Performance Assessment Calculation Tool (PACT) which performs Monte Carlo analyses to estimate loss, downtime, and casualty of buildings.

A number of studies have focused on time-based resilience and sustainability consequence of earthquakes. Dong and Frangopol (2015) present a framework for time-based resilience and sustainability assessment of highway bridges. Han et al. (2016, 2017) and Tesfamariam and Goda (2015) studied seismic loss estimation of non-ductile reinforced concrete structures considering mainshock-aftershock effects. Han et al. (2016) proposed a framework for post-quake decision-making and Han et al. (2017) performed a cost-benefit analysis for base-isolation retrofitting of 3- and 6-story reinforced concrete structures. The total loss included economic loss, downtime, and fatalities converted into a monetary loss. Feese et al. (2013) studied the repair cost and environmental consequences

due to earthquakes for a commercial building located in a highly-seismic region. Athena was used for LCA while HAZUS-MH was used for loss estimation. Bocchini et al. (2014) proposed a unified sustainability and resilience assessment framework considering their similarities. Dong and Frangopol (2016) studied the seismic performance of base-isolated and conventional steel framed buildings in terms of repair loss, fatality, downtime, and CO<sub>2</sub> emissions. Dong and Li (2017) proposed a framework for quantifying resilience of residential communities against hurricanes in terms of economic loss, morbidity, social disruption, and environmental loss considering the potential effect of a changing climate. However, few discussed the post-assessment decision-making and none of them proposed a multi-criteria decision-making (MCDM) framework for post-assessment decision making.

Menna et al. (2013) highlighted the need for multi-criteria and multi-disciplinary decision-making approach in future studies due to various criteria involved in the design and seismic assessment of structures. Due to multiple disproportionate and in some cases conflicting criteria, finding the optimal solution in MCDM problems is challenging. Several methods are proposed to deal with MCDM problems including multi-attribute utility theory (MAUT), weighted sum approach, and sequential optimization (Frangopol and Liu 2005; Lounis and McAllister 2016). Among various MCDM methods, MAUT provides more flexibility and efficiency for problems involving uncertainty, risk, performance assessment, and subjective probability (Dyer et al. 1992; Keeney and Wood 1977; Mateo 2012). In MAUT, one choice or subset of the possible solutions is evaluated based on two or more attributes (criteria). Uncertainty can be included effortlessly with

discrete or continuous variables. The goal commonly is to maximize the total weighted utility function (Wallenius et al. 2008). MAUT has been used for various systems and engineering problems such as power systems expansion planning (Voropai and Ivanova 2002), seismic retrofit of concrete structures (Caterino et al. 2009), bridge and road construction (Zavadskas et al. 2007), and risk assessment for civil engineering facilities (Faber and Stewart 2003). Technique for order preference by similarity to ideal solution (TOPSIS) developed by Hwang and Yoon (1981) is another MCDM method used in the literature, for design and maintenance of road pavement (Chang et al. 2005), risk assessment of bridges (Wang and Elhag 2006), selecting a support structure for offshore wind turbines (Lozano-Minguez et al. 2011), and long-term energy planning and management (Ervural et al. 2018). In TOPSIS, the decision problem is viewed in a geometric space where the selected alternative should have the shortest  $n$ -dimensional ( $n$  = number of criteria) Euclidean distance from the ideal solution and the farthest distance from the worst possible solution (Chang et al. 2005; Mateo 2012). Hence, TOPSIS takes into account both the least acceptable and most acceptable solutions, similar to MAUT but in contrast to other methods such as cooperative game theory and weighted addition or product methods (Cheng et al. 2003; Zavadskas et al. 2007).

This paper presents a novel framework for seismic resilience and sustainability assessment of building structures using a comprehensive MCDM approach. A probabilistic model which incorporates variability in record-to-record ground motion, structural response, and component-level fragility is developed and employed for resilience and sustainability assessment of archetype diagrid buildings. The effect of diagonal angle is

studied by considering various archetypes with 45°, 63°, and 72° diagonal angles. Incremental dynamic analysis (IDA) is used to produce archetypes fragility curves. The probability distribution functions (PDFs) of loss, downtime, and casualty are evaluated using Monte Carlo simulation. FEMA P-58 method for intensity-based and time-based assessment are used to evaluate the seismic asset, time, and life loss. Component-level total repair cost and repair time (downtime) with short-track (parallel) and long-track (serial) planning are quantified for each floor. The EIO-LCA model of Carnegie Mellon University (CMU GDI 2018) is adapted to evaluate the environmental loss due to earthquakes. Furthermore, a risk-based MCDM framework is proposed based on the analytic hierarchy process (AHP), MAUT and TOPSIS which integrates all four losses into a total utility function or relative closeness score to make decisions about building design or retrofit. Sensitivity analysis is performed to demonstrate the framework application for various scenarios.

### **3.2 Proposed MCDM Framework**

The proposed framework consists of three main modules: 1) System Concept and Criteria (SCC) Module, 2) Resilience and Sustainability Assessment (RSA) Module, 3) Decision Making (DM) Module. Figure 3.2 depicts the main components of the framework and their connections. The framework works in a feedback loop (note the red arrows in Figure 3.2).

Once the decision is made it can be updated or optimized using new data acquired periodically from inspection or monitoring devices. Note that the decision analysis can be

updated periodically considering evolving conditions such as changes to frequency and intensity of hazards due to climate change and increasing vulnerability of the system caused by material deterioration, corrosion, aging, and so on (Lee et al. 2018).

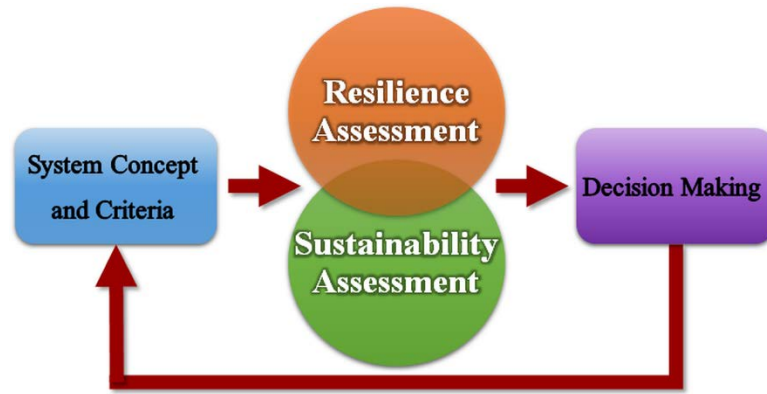


Figure 3.2 Main components of the proposed framework

### ***3.2.1 System Concept and Criteria Module***

In the SCC module, the project objective, specifications, and criteria including design, modeling, and analysis requirements will be specified. Also, the scope of the assessment including the effective factors and indicators and their importance/weight need to be identified. These criteria depend mainly on the objective of the project and historical/experimental data available about the system (ATC 2009). Figure 3.3 depicts the proposed flowchart for this module in the case of a structural system.

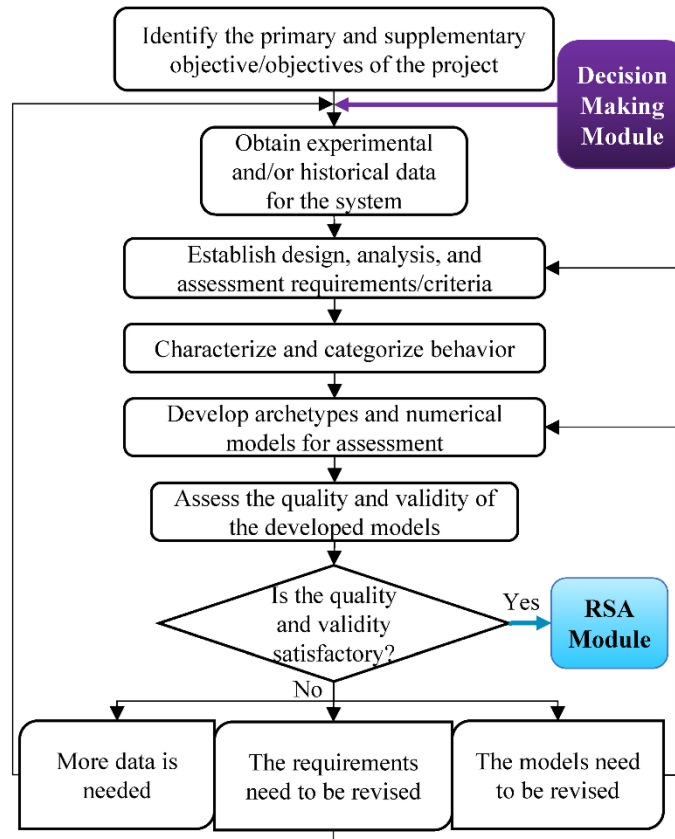


Figure 3.3 Flowchart for System Concept and Criteria (SCC) Module and its connection with other modules

## 3.2.2 Resilience and Sustainability Assessment Module

### 3.2.2.1 Resilience Assessment

Resilience is the ability of a system to rapidly recover from a damaged state caused by a stochastic hazard to the initial undamaged state and gain its pre-hazard functionality (Venkittaraman and Banerjee 2014). After an earthquake, it takes a period of time (downtime) to repair the damages, regain the losses and bring the building back to its primary functionality. The functionality of the building depends on its damage state after the event. Three to five damage states are typically considered for buildings based on damages to primary and secondary structural and non-structural components. The damages

are estimated according to damage indicators, called Engineering Demand Parameters (EDPs), such as maximum inter-story drift ( $IDR_{max}$ ) and maximum absolute spectral acceleration ( $ACC_{max}$ ) (Yin and Li 2010). These indicators are evaluated by nonlinear fragility analyses.

Seismic resilience is commonly quantified in terms of expected economic and social impacts of an earthquake using resilience measures such as expected monetary loss, downtime, and the number of casualties (Bocchini et al. 2014; Han et al. 2017; Ramirez and Miranda 2012a). These measures are in different units making the decision-making process complicated. The probability of loss (economic, social, environmental) at a given earthquake intensity ( $IM$ ) for mutually exclusive seismic events is defined as follows (Lounis and McAllister 2016; Ramirez and Miranda 2012a; Yamin et al. 2017):

$$\begin{aligned}
 & P(L > l_i | IM = z_i) \\
 &= \int_{EDP} \int_{DS} P(L > l_i | DS = DS_i) P(DS | EDP = d) P(EDP | IM = z) dDS dEDP \quad (3.1)
 \end{aligned}$$

where  $P(L > l_i | IM = z)$  is the probability of having a loss greater than  $l_i$  given that hazard intensity is equal to  $z$ ,  $P(L > l_i | DS = DS_i)$  is the probability of having a total loss greater than  $l_i$  given that damage state of  $DS_i$  is achieved,  $P(DS | EDP = d)$  is the probability of achieving a damage state given that the EDP reaches a certain value of  $d$ , and  $P(EDP | IM = z)$  is the probability of the EDP conditioned on a certain hazard intensity,  $z$ . Fragility functions are used to find the probability that each damageable component reaches a certain damage state. Lastly, the time-based probability of loss,  $P(L > l_i)$ , can be

estimated using the convolution of the cumulative distribution function of loss conditioned on the intensity level ( $P(L > l_i | IM = z_i)$ ) and the probability of expected number of occurrences in a year for each intensity ( $P(IM = z_i)$ ) (Mazumder et al. 2018; Ramirez and Miranda 2012a):

$$P(L > l_i) = \int_{IM} P(L > l_i | IM = z_i) P(IM = z_i) dIM \quad (3.2)$$

In general, the loss ( $L$ ) in Equations (3.1) and (3.2) can be any kind of loss due to earthquake including monetary, time, life, or environmental loss. In a component-level analysis, the consequence function ( $P(L > l_i | DS = DS_{ij})$ ) in Equation (3.1) needs a database of repair cost/time for each component in each damage state, which is currently available for many structural and non-structural components in FEMA PACT (FEMA 2012).

Therefore, all consequences/losses due to an earthquake are a function of four conditional probability distribution functions: (1)  $P(L > l_i | DS = DS_i)$  which is obtained from FEMA P-58 PACT database, (2)  $P(DS | EDP = d)$  which is based on damage state limits recommended by FEMA P-58 and found using time-history dynamic analyses for each intensity, (3)  $P(EDP | IM = z)$  which is also based on finite element outputs of intensity-based time-history dynamic analyses, (4)  $P(IM = z_i)$  is the mean annual frequency of occurrence for each intensity adjusted for the fundamental period of the structure and 5% damping ratio. The latter is obtained from USGS hazard online hazard tool. FEMA P-58 PACT is used for loss, downtime, and casualty estimation analyses since

the conditional consequence database is already integrated in this program. To obtain the probability of loss, PACT uses a Monte Carlo process with hundreds of realizations. PACT reports the outputs for each component, each floor, and the whole building. It also provides the outputs of each realization individually.

A simple approach used in the literature to quantify and assess resiliency is to convert all losses into a monetary loss (Han et al. 2016, 2017; Mitrani-Reiser 2007). In this approach, the total loss is the summation of direct and indirect losses. For example, fatality is assumed to have an expected monetary loss of \$4.16M with a coefficient of variation (COV) of 0.4 (Mitrani-Reiser 2007), which is not accurate for all regions and all cases. The expected total downtime is used to estimate the economic loss due to the downtime considering a monetary loss of 960 USD per floor per day for a conventional commercial building (Dong and Frangopol 2016), which adds a considerable amount of uncertainty to the problem. The monetary loss per floor per day of 960 USD is based on studies by Dong and Frangopol (2016) and Beck et al. (1999) where the repair time of the building is a function of the number of workers (15 per floor is presumed), daily working hours (8 hours is presumed), and weekly workday ratio (5:7 is presumed). The steel buildings studied by (Dong and Frangopol 2016) are in Los Angeles, CA and have a uniform story height of 4.57 m and bay span of 9.14 m with an approximate floor area of 2000 m<sup>2</sup>. Given the assumptions and uncertainty involved, a comprehensive and more flexible approach is to use a multi-criteria decision-making framework by considering every resilience metric as a criterion.

### 3.2.2.2 Sustainability Assessment

Commonly, sustainability of a building is measured as a probabilistic function of environmental, economic, and social consequences of its construction and life-cycle maintenance. Considering the relationship between sustainability and resilience, these consequences can be incorporated through quantitative parameters such as embodied energy, economic loss, downtime, and casualties. The sustainability function ( $M_S$ ) can be defined as a summation of consequences (in terms of loss, casualty, carbon dioxide emission, etc.) caused by the collapse ( $C$ ) and non-collapse damage ( $NC$ ) under a given hazard intensity ( $IM$ ) (Dong and Frangopol 2016):

$$M_S = C_{Cons|C} P_{C|IM} + C_{Cons|NC} (1 - P_{C|IM}) \quad (3.3)$$

where  $C_{Cons|C}$  and  $C_{Cons|NC}$  are the cumulative distribution function (CDF) of total consequences due to collapse and non-collapse damage, respectively and  $P_{C|IM}$  is the probability of collapse for a given hazard intensity of  $IM$ . But here, a more general approach is used. Considering different damage states ranging from slight damage to collapse, the sustainability function is a function of the conditional consequence given a damage state at time  $t$  ( $C_{Cons|DS}(t)$ ), the conditional probability of a damage state given the EDP at time  $t$  ( $P_{DS|EDP}(t)$ ), the conditional probability of an EDP given a hazard intensity at time  $t$  ( $P_{EDP|IM}(t)$ ), and the annual mean rate of occurrence of hazard  $IM$  at time  $t$  ( $P_{IM}(t)$ ). Thus, based on the theorem of total probability, the general form for the sustainability function can be expressed as (Dong et al. 2013; Ellingwood 2005):

$$M_S = \int_{IM} \int_{EDP} \int_{DS} C_{Cons|DS}(t) P_{DS|EDP}(t) P_{EDP|IM}(t) P_{IM}(t) dDS dEDP dIM \quad (3.4)$$

Given the probabilistic nature of the analyses, Monte Carlo simulation can be used to evaluate the sustainability. The consequence functions,  $C_{Cons|DS}$ , are evaluated using the EIO-LCA model presented by Carnegie Mellon University (CMU GDI 2018) where the environmental impact of earthquakes is quantified based on the monetary cost of repair/replacement of the building. This method considers not only the direct impacts of the product/project but also all the indirect impacts in the supply chain. In this model, the entire economy is divided into a number of sectors (480 sectors for US economy) and modeled as a large input-output matrix where the rows and the columns are sectors of the economy (Ochoa et al. 2002). The required economic purchases from all sectors of the economy ( $\mathbf{Q}$ ) to produce a vector of desired outputs ( $\mathbf{F}$ ) can be defined as follows (Hendrickson et al. 1998; Ochoa et al. 2002):

$$\mathbf{Q} = [\mathbf{I} + \mathbf{M} + \mathbf{M}^2 + \mathbf{M}^3 + \dots] \mathbf{F} = (\mathbf{I} - \mathbf{M})^{-1} \mathbf{F} \quad (3.5)$$

where  $\mathbf{I}$  is an identity matrix and  $\mathbf{M}$  is the input-output total requirement matrix developed based on the US economy benchmark and data points. Desired outputs ( $\mathbf{F}$ ) is a vector which includes the amount of purchase from various sectors to produce the product/project. In Equation (3.5), the term “ $\mathbf{I} \times \mathbf{F}$ ” is the contribution from the desired outputs themselves, “ $\mathbf{M} \times \mathbf{F}$ ” is the direct contribution from first level suppliers, “ $\mathbf{M}^2 \times \mathbf{F}$ ” is the indirect contribution from second level suppliers, and so on. Once the vector of required inputs ( $\mathbf{Q}$ )

is calculated, it is multiplied by the average environmental impact for each sector and industry to find the environmental impact of the product/project.

### **3.2.2.3 Integrated Resilience and Sustainability Assessment**

Figure 3.4 shows the step-wise illustrative procedure for resilience and sustainability assessment used here. In the SCC module, a detailed performance model is defined for the desired building which includes the collection of available and assumed data on all damageable structural and non-structural components of the building. Each component is assigned to a proper performance group based on its damageability and vulnerability characteristic. For instance, the non-structural walls may be assigned to full or partial seismically-rated wall partitions performance groups vulnerable to excessive inter-story drift (IDR). The building models are analyzed under nonlinear time-history analysis and the structural response at different points for different intensities is evaluated in terms of peak EDPs. The last step is to evaluate resilience and sustainability in terms of loss, downtime, casualty, and environmental impacts using Monte Carlo simulation by creating hundreds to thousands of realizations. PACT (FEMA 2012) is used for loss, downtime, and casualty estimation analyses.

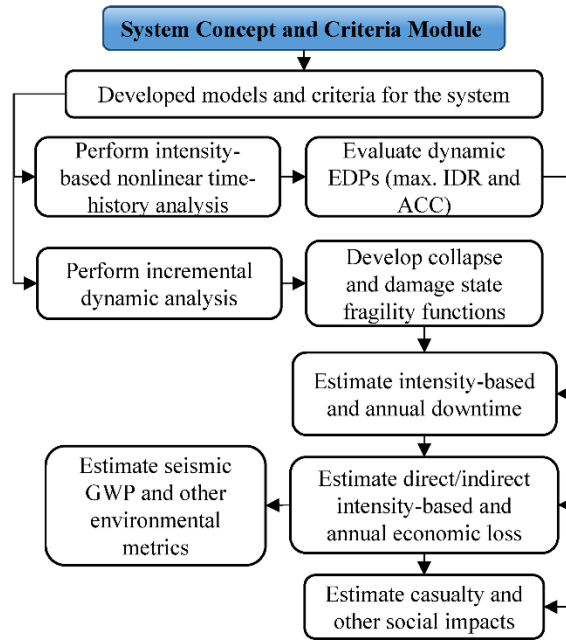


Figure 3.4 Flowchart for Resilience and Sustainability Assessment (RSA) Module

Due to the interrelation between the resilience and sustainability metric, a multi-criteria decision-making is the most sensible approach providing better flexibility and reliability for analyzing various scenarios and problems. Thus, in this research, a multi-criteria decision-making framework is introduced for post-assessment analysis.

### 3.2.3 Multi-Criteria Decision-Making Module

#### 3.2.3.1 Quadrilateral decision-making criteria

For the proposed decision model, the outputs of resilience and sustainability assessment are categorized and converted into four attributes: Asset Loss in million dollars, Time Loss in days, Life Loss in the number of casualties, and Environmental Loss in terms of global warming potential (GWP). The total expected asset loss in this study is the summation of direct repair/replacement costs of all damaged components. However, in

general, asset loss could also include indirect losses such as rent loss due to building closure.

The total expected time loss is the total repair/replacement time of the building. Yet, in general, some factors affecting loss are related to other structure and infrastructure systems in the community. For instance, the time it takes for a tenant or a business to settle in the building after repair/replacement is done depends on when roads (transportation system) are repaired, and water, gas, communication, and power services (infrastructure systems) are restored. For these cases, time loss represents the recovery time which is the repair/replacement time plus the indirect time loss due to interdependencies. Further, in a component-level analysis, time loss is the summation of expected repair, replacement or recovery time of each component on each floor considering a short-track (parallel) or long-track (serial) repair planning strategy.

The life loss contains the number of casualties, fatalities, and if the data is available Post-Traumatic Stress Disorder (PTSD) cases due to the earthquake. Finally, the total expected GWP, energy consumption, water withdrawal, and/or waste generation caused by earthquake damage can be considered as the environmental loss. Here, the number of casualties and fatalities are used for life loss and the expected GWP is used for environmental loss. Figure 3.5 depicts the quadrilateral decision-making criteria, i.e. asset, time, life, and environmental loss considered in the framework.

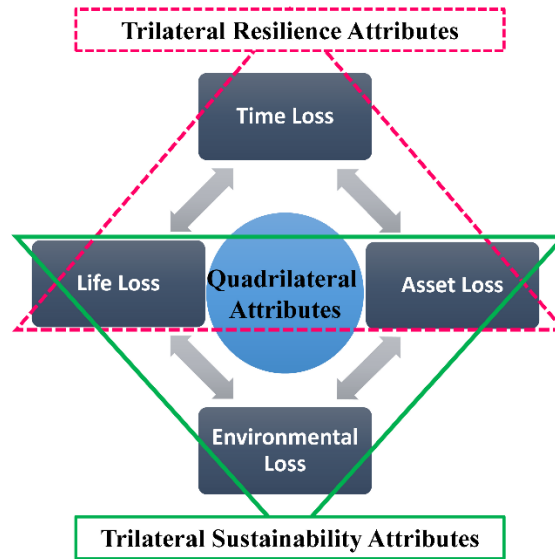


Figure 3.5 Quadrilateral decision-making attributes/criteria

### 3.2.3.2 Multi-Criteria Decision-Making Model

Converting all metrics into equivalent monetary loss imposes considerable uncertainties into the results as the conversion factors are mostly conservative assumptions based on a specific case and locality (Wallenius et al. 2008). In addition, decision making commonly involves identifying and choosing among different alternatives based on attributes which can be conflicting. Since resilience and sustainability assessment result in dissimilar and in some cases conflicting measures, an MCDM model is a more sensible approach. Therefore, a risk-based decision-making framework based on MAUT and TOPSIS is used for post-assessment decision making. MAUT is a practical and efficient approach for problems involving uncertainty, risk, performance assessment, and subjective probability (Dezfuli et al. 2010; Keeney and Wood 1977; Wallenius et al. 2008). Figure 3.6 depicts the main steps for using MAUT for decision-making for a building design/retrofit problem.

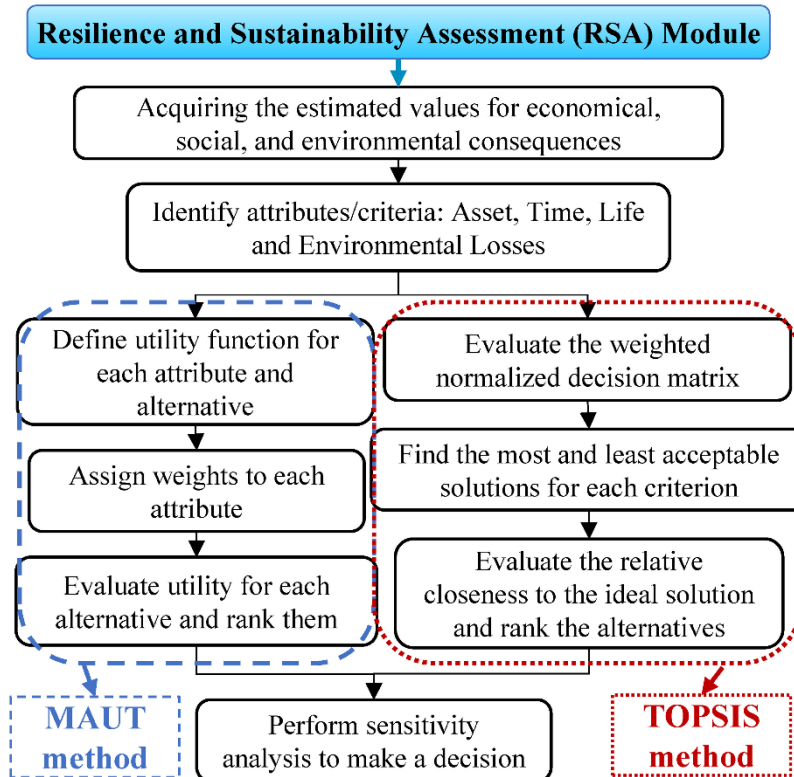


Figure 3.6 MCDM Flowchart for a design/retrofit decision problem using MAUT and/or TOPSIS methods

For MAUT, the utility functions defined over a set of attributes are used to quantify the decision maker’s preferences (Mateo 2012). The utility functions take a value from zero (for the worst outcome) to one (for the best outcome). They can be defined with three attitudes towards risk, which are risk aversion, risk neutral, and risk seeking. In this study, all four attributes (Asset, Time, Life, and Environmental Loss) need to be minimized as they are all undesirable consequences. Thus, to find the normalized utility values, the best outcome (minimum) of each attribute is assigned a utility value of 1 and the worst outcome (maximum) is assigned a utility of 0.

Then, normalized neutral utility values ( $u_i$ ) are calculated using the following formula for cost criteria (Wallenius et al. 2008):

$$u_i = \frac{A_{max} - A_{ij}}{A_{max} - A_{min}} \quad (3.6)$$

where  $A_{ij}$  is the score (resilience or sustainability metric) evaluated for an attribute  $i$  among  $n$  attributes for a certain alternative  $j$  among  $m$  alternatives, and  $A_{max}$  and  $A_{min}$  are the maximum and minimum scores evaluated for each attribute among all alternatives, respectively. Assuming utility independence, the overall unilateral utility function is formed using the following formula (Ferreira et al. 2009):

$$U_{t,j} = \sum_{i=1}^n w_i u_i(x_i) \quad j = 1, \dots, m; i = 1, \dots, n \quad (3.7)$$

where  $U_{t,j}$  is the overall utility of alternative  $j$ , and  $w_i$ ,  $u_i$ , and  $x_i$  are the importance factor, the utility function (using Equation (3.6)), and the value of the attribute  $i$ , respectively. The decision-maker need to find the best alternative based on importance factor of each criterion. The importance factor can be evaluated using lotteries between pairs of attributes, e.g. the decision maker compares the importance of cost and downtime and assigns the factors. The importance factor,  $w_k$ , for each attribute can be assigned based on historical data, engineering judgment, and problem objective. Three approaches are suggested for importance factor evaluation, which are ranking based on 1) judgment, 2) summation of weights (reversed rank/sum of ranks), and 3) order centroid weights (sum of reciprocal ranks/no. of ranks).

For TOPSIS, first the weighted normalized decision matrix needs to be developed using the following equation (Chang et al. 2005; Cheng et al. 2003):

$$v_{ij} = w_i A_{ij} / \sqrt{\sum_{j=1}^m A_{ij}^2} \quad j = 1, \dots, m; i = 1, \dots, n \quad (3.8)$$

where  $v_{kj}$  is an element of the weighted normalized decision matrix. Then, the ideal (most acceptable) and negative-ideal (least acceptable) are found. The ideal solution ( $A^*$ ) and negative-ideal solution ( $A^-$ ) are defined as:

$$A^* = \{v_1^*, \dots, v_n^*\} = \{(\max_j v_{ij} | i \in I'), (\min_j v_{ij} | i \in I'')\} \quad (3.9 - a)$$

$$A^- = \{v_1^-, \dots, v_n^-\} = \{(\min_j v_{ij} | i \in I'), (\max_j v_{ij} | i \in I'')\} \quad (3.9 - b)$$

where  $I'$  and  $I''$  are associated with benefit and cost criteria, respectively. Note that the hazard consequences/losses are considered as the cost criteria. Then, using n-dimensional Euclidean distances, the separation measures from ideal solution ( $D_j^*$ ) and from negative-ideal solution ( $D_j^-$ ) are evaluated:

$$D_j^* = \sqrt{\sum_{i=1}^n (v_{ij} - v_i^*)^2} \quad j = 1, \dots, m; i = 1, \dots, n \quad (3.10 - a)$$

$$D_j^- = \sqrt{\sum_{i=1}^n (v_{ij} - v_i^-)^2} \quad j = 1, \dots, m; i = 1, \dots, n \quad (3.10 - b)$$

Finally, the relative closeness to the ideal solution for alternative  $j$  ( $C_j^*$ ) can be found as follows:

$$C_j^* = D_j^- / (D_j^* + D_j^-) \quad j = 1, \dots, m; i = 1, \dots, n; 0 < C_j^* < 1.0 \quad (3.11)$$

### 3.3 Application to Diagrid Structures

#### 3.3.1 Archetype Diagrid Buildings

The proposed framework is implemented on a series of 4-story steel diagrid office/commercial buildings located in downtown Los Angeles, CA with  $S_s$  (spectral response acceleration at 0.2 sec) and  $S_l$  (spectral response acceleration at 1 sec.) of 2.481g and 0.862g, respectively. This high seismic region is selected since diagrids are commonly used for carrying large lateral loads. Dead and Live loads are 4 and 2.4 kN/m<sup>2</sup> following previous studies on diagrids and office buildings (Gholipour et al. 2015; Kim and Lee 2012). Three groups of diagrids with different diagonal angles are considered (45°, 63°, and 72° diagonal angles). The use of 72° diagonal angles in a 4-story diagrid building will result in a building with a 3-story complete module and a one-story incomplete module (see Figure 3.1 (a)). Previous studies showed that incomplete uppermost diagrid modules may lead to a sharp decline in lateral stiffness and a significant increase of deformations in the uppermost corresponding floors (Asadi et al. 2018). This configuration, however, might be used because of architectural limitation and requirements. A similar diagrid pattern is noticeable on the façade of Macquarie Bank in Sydney, Australia. Therefore, in addition to the 72° archetype, an alternate configuration is studied where the diagrid angle in the uppermost floors changes to avoid incomplete diagrid modules. This alternative configuration called 4-72A here is shown in Figure 3.7.

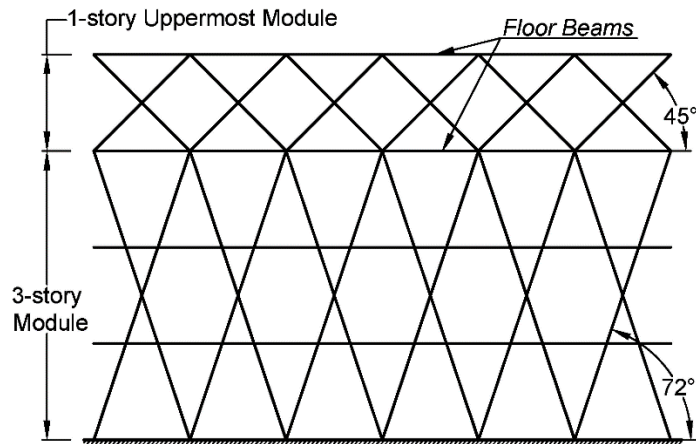


Figure 3.7 Diagrid modules of 4-72A archetype, an alternate configuration for 4-72 archetype

The archetypes are designed per AISC Load and Resistance Factor Design (LRFD)(AISC 2011, 2016b). The standard W-shaped sections are used for beams, columns, and diagonals. A seismic response modification factor ( $R$ ) of 4.0 is used in the initial design of diagrid frames (Asadi and Adeli 2018a).

Nonlinear time-history analyses and IDA are conducted on planar numerical models in OpenSees (Mazzoni et al. 2006). Beams and diagonals are modeled as beam-column fiber elements using Menegotto-Pinto hysteretic model with 0.02 hardening (Mazzoni et al. 2006). Uriz et al. (2008) method for modeling material and geometric nonlinearity is adapted. The buckling and post-buckling behavior of the models are verified using experimental results of Black et al. (1980). Further details on numerical modeling of diagrids and modeling validation are discussed in (Asadi et al. 2018). Figure 3.8 shows some modeling assumptions and three diagonal angles considered.

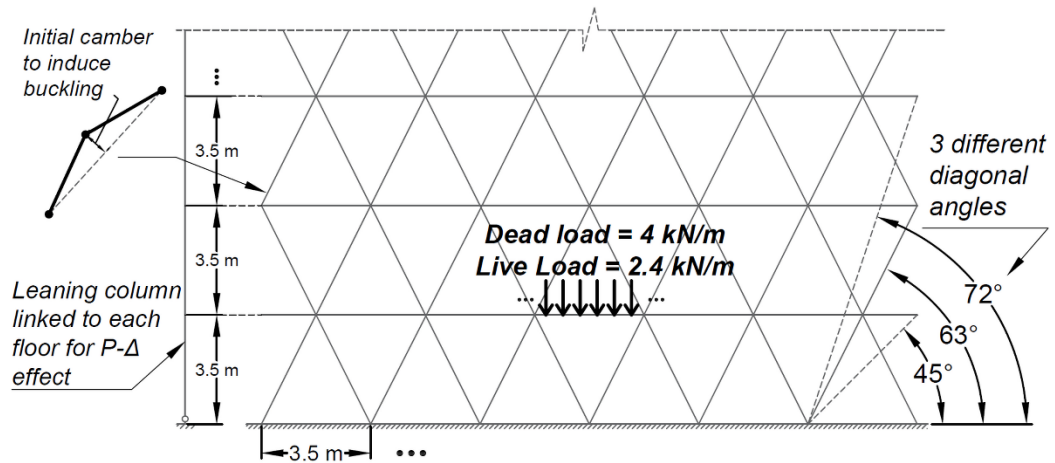


Figure 3.8 Schematic of diagrid archetype models

### 3.3.2 Fragility Analysis and Uncertainty Modeling

The aleatoric uncertainty in the performance of different structural and non-structural groups is included through their fragility parameters ( $\mu$ =median and  $\beta$ =lognormal standard deviation) for various damage states. PACT provides those parameters for various structural and non-structural components where every component is identified in a separate performance group. For the diagonal members, three performance groups with different weights are implemented into PACT, which are diagonal weight less than 40 lb/ft, between 41 and 99 lb/ft, and greater than 100 lb/ft (Asadi et al. 2018; FEMA 2012). Five damage states are considered for estimating the loss due to damage of the diagrid frame: undamaged ( $DS_0$ ), slightly damaged ( $DS_1$ ), moderately damaged ( $DS_2$ ), extensively damaged ( $DS_3$ ), and completely damaged (collapsed) ( $DS_4$ ) states. The performance group specifications are adapted from FEMA P-58 specifications for concentrically braced frames (code B1033.002a to c). Given that axial strength is a function of cross-sectional area and slenderness ratio, non-compact section with similar depth are selected for diagonals to

minimize the impact of slenderness ratio on performance. More discussion on the performance groups used are presented in (Asadi et al. 2018). A summary of damage and performance criteria is presented in Table 3.1. The connections are post-Northridge welded steel moment connection without reduced beam section (RBS) detailing with three damage states. As for non-structural components, each building has two hydraulic elevators, one 500-Ton (500 BTU/hr/12,000) chiller and air-handling unit on the roof, and a seismically-rated independent pendant lighting for each 4-sq. m of the floor. The perimeter of the building is covered with generic midrise stick-built curtain wall in each span, the interior wall partitions are partial or full-length gypsum walls with metal studs, and the floor and the ceiling are covered with seismically-rated raised access floor and suspended ceiling, respectively. A full list of damageable structural and non-structural components with their fragility parameters is presented in Table 2.7 (Asadi et al. 2018).

Table 3.1 Damage and performance criteria for steel diagrid frames (Asadi et al. 2018)

Damage State	DS <sub>1</sub>	DS <sub>2</sub>	DS <sub>3</sub>	DS <sub>4</sub>
IDR <sub>max</sub> limit (%)	0.25	0.55	0.95	1.25
$\beta$	0.27	0.24	0.30	0.32

Model uncertainty is due to inaccuracy in modeling the properties of the components, damping, mass, etc. FEMA P-58 associates this uncertainty with two factors: 1) accuracy of building definition and quality assurance of construction using a dispersion  $\beta_c$ , 2) completeness and accuracy of the nonlinear analysis model using dispersion  $\beta_q$ . Following

FEMA P-58, both standard deviation values are 0.25 assuming an average quality for both factors.

A set of 22 far-field ground motions recommended for collapse assessment of building structures by FEMA P-695 is used to study record-to-record variability in nonlinear time history analyses (NTHA) and IDAs. These records are carefully selected to properly represent record-to-record uncertainty (ATC 2009). The ground motion set includes records on soft rock and stiff soil (Site Class C and D) with magnitudes between M6.5 and M7.6 taken from 14 different events.

Collapse fragility is a well-accepted approach to illustrate the uncertainties in performance and vulnerability of structures (ATC 2009). Lognormal distribution is selected to model uncertainty in demand and performance since it has shown accuracy for fragility analyses of various structural systems (Han et al. 2016, 2017; Kinali and Ellingwood 2007; Li et al. 2010). IDA is used to develop lognormal collapse fragility functions for archetype buildings (Vamvatsikos and Cornell 2002). Figure 3.9 shows the lognormal fragility curves for all archetypes where the horizontal axis is the normalized pseudo-spectral acceleration based on 5% damped design spectra for the region at the fundamental period of the building structure,  $S_a(T_1, 5\%)$ . In Figure 3.9, the  $S_a$  for the Design Basis Earthquake (DBE) and the Maximum Considered Earthquake (MCE) are indicated with dashed lines. The collapse is presumed where 1) the slope of the fragility curve decreases to 20% of its initial slope or 2) numerical instability is achieved due to excessive nonlinear deformation in the structure (Li et al. 2014; Vamvatsikos and Cornell 2002).

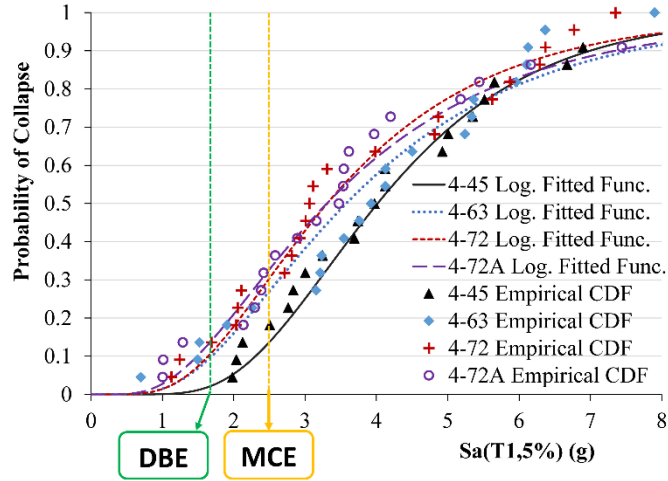


Figure 3.9 Empirical CDF of  $Sa(T1,5\%)$  and fitted lognormal fragility functions

In Table 3.2, expected collapse capacity,  $\hat{S}_{CT}$ , expected  $IDR_{max}$  at collapse, their corresponding logarithmic dispersions (standard deviations),  $\beta_{Sa}$  and  $\beta_{IDR}$  respectively, and the probability of collapse under DBE and MCE are listed.

The alternate configuration 4-72A has a slightly lower  $IDR_{max}$  at collapse point than 4-72 (6% lower). Their mean  $\hat{S}_{CT}$  is essentially the same (0.3% difference) but the 4-72A shows a noticeably larger dispersion leading to a larger probability of collapse under both DBE and MCE. Note that the “ $IDR_{max}$  at collapse” reported in Table 3.2 is the maximum recorded  $IDR$  for a single floor (including the 4<sup>th</sup> floor) at collapse. Thus, the larger  $IDR_{max}$  for 4-72 archetype is due to the concentration of lateral displacement in the upper floor. A detailed discussion of fragility analyses and performance of diaphragms under dynamic analyses can be found in (Asadi et al. 2018).

Table 3.2 Expected collapse capacity and  $IDR$ , the corresponding dispersion and the probability of collapse under DBE and MCE based on logarithmic fragility CDF

Model	$\hat{S}_{CT}$ (g)	$\beta_{Sa}$	$IDR_{max}$ at collapse (%)	$\beta_{IDR}$	Prob. of collapse (%) under	
					DBE	MCE

4-45	4.02	0.43	1.10	0.62	2.0	13.3
4-63	3.57	0.59	1.75	0.77	9.4	26.6
4-72	3.31	0.54	3.57	0.50	9.9	29.8
4-72A	3.30	0.62	3.37	0.50	13.2	32.3

### 3.3.3 Time-based Assessment

To evaluate the annual seismic losses, a time-based risk assessment approach is required. The probability of  $n$  occurrence of a seismic event with an intensity greater than  $z$  over a target design life ( $t_d$ ) can be modeled by a Poisson distribution (Chhabra et al. 2018):

$$P(IM > z, N = n, t_d) = \frac{(v_{IM} \times t_d)^n \times e^{-v_{IM} \times t_d}}{n!} \quad (3.12)$$

where  $v_{IM}$  is the mean annual frequency of exceedance of seismic intensity obtained from the hazard curves of the site. To evaluate the annual seismic consequences, a series of NTHAs for various intensities ranging from low intensity (with high Annual Frequency of Exceedance (AFE)) to high intensities (with low AFE) are conducted. As FEMA P-58 requires, the hazard curve is adjusted for the fundamental period of the structure and the site class and is divided into 10 segments (a minimum of 8 segments are required). Figure 3.10 shows the adjusted hazard curve for 4-63 archetype obtained from United States Geological Survey (USGS) online Hazard Tool (USGS 2017) with 10 intensities (each intensity is at the mid-point of the segment). For the 4-63 archetype, the minimum spectral acceleration ( $S_a^{\min}$ ) is equal to 0.05g and the maximum spectral acceleration ( $S_a^{\max}$ ) is 3.576g with mean AFE of 0.00003264 following the FEMA P-58 guidelines. The ground

motion records are scaled for the midpoint intensity in each segment of the hazard curve per FEMA P-58.

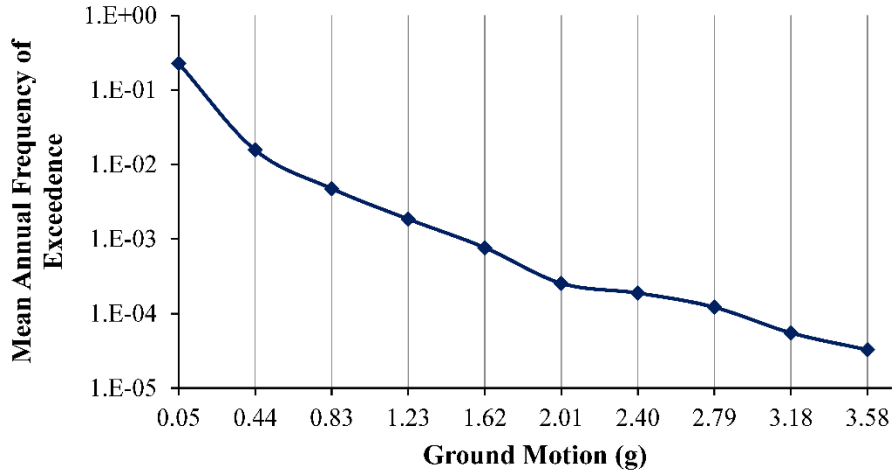


Figure 3.10 Adjusted hazard curve for 4-63 archetype obtained from USGS online Hazard Tool divided into 10 intensities

### 3.3.4 Seismic Resilience Assessment

In this section, the resiliency metrics including the component-level direct economic loss, the downtime, and the number of casualty and fatality caused by the earthquake is evaluated. The direct economic loss is calculated as the summation of repair costs of all structural and non-structural components using Equations (3.1) and (3.2). The downtime is evaluated based on the repair time required for each component at each floor. Two repair planning schemes: slow-track (serial planning) and fast-track (parallel planning) are considered for downtime analyses. The actual repair time is between this upper bound and lower bound depending on project planning and scheduling.

For assessing the number of casualties including fatality and injuries after an extreme event, a population model should be developed for the building. The population model

describes the number of people present in the building per 1,000 ft<sup>2</sup> (92.9 m<sup>2</sup>) of floor area at various times of a day. Typically, a peak population is defined based on the application of the building, e.g. commercial, residential, and the population during the day is presented in terms of fractions of the peak population (FEMA 2012). Based on FEMA P-58 recommendation, a peak population density of 4 per 1000 ft<sup>2</sup> (92.9 m<sup>2</sup>) with 0.2 dispersion is used. Considering the unoccupied areas such as utility and mailing room, 1/3 of the first floor and 1/6 of other floors is assumed unoccupied (Han et al. 2016; Mitrani-Reiser 2007).

The performance criteria developed by (Asadi et al. 2018) are implemented into PACT for loss, downtime, and casualty estimation of diagrid members. The repair loss is assumed as a percentage of Total Replacement Cost (TRC). Based on RSMMeans (2018) cost estimation data for southern Los Angeles, California, the replacement cost for a steel commercial building with 4 stories is \$213.81 per ft<sup>2</sup> (approximately \$2301.4 per m<sup>2</sup>). For estimating the downtime, a Total Replacement Time (TRT) of 720 days is considered. To be conservative, this TRT is slightly overestimated due to complications in the construction of diagrid frames (Ali and Moon 2007). The maximum number of workers for repair is assumed to be 0.002 per ft<sup>2</sup>, which is equal to 1 worker per 500 ft<sup>2</sup> (FEMA 2012). The key assumptions for resilience assessment along with their sources are presented in Table 3.3. Since the floor area, construction location, structural system, and the type of structural material are the same for all archetypes, the total replacement cost is assumed the same for all archetypes.

Table 3.3 Building specification and assumptions for resilience assessment

Parameter	Value	Source
Total Replacement Cost	US\$ 4,071,000 for 4-story buildings	RSMMeans (2018)
Total Replacement Time	720 days for 4-story buildings	FEMA P-58 (FEMA 2012)
Maximum number of workers per ft <sup>2</sup>	0.002 (1 worker per 500 ft <sup>2</sup> )	FEMA P-58 (FEMA 2012)

### 3.3.4.1 Loss Estimation

Considering the probability of occurrence of different earthquake hazard intensities, the annual CDF of total direct economic loss is evaluated in terms of monetary repair cost. Figure 3.11 depicts the annual economic loss for different archetypes as a summation of repair cost for each intensity (intensities are stacked upon each other). Note that this figure shows the cumulative rate of exceedance of all intensities considering their mean AFE. In this figure, lower areas belong to lower intensities. The largest portion of the annual loss in all archetypes is caused by intensity 2 which can be attributed to its considerable  $S_a$  (0.44g for 4-63 archetype) given its mean AFE (0.01566 for 4-63 archetype). Another key factor is the consequence functions. Even minor damages to structural or non-structural components can cause considerable repair cost. FEMA P-58 fragility database, which is used here, introduces 1-4 damage states for each structural and non-structural component. Each damage state has its consequence parameters, e.g. average repair cost and time. For most components, the average consequence for DS<sub>1</sub> (minor damage) is relatively large compared to the average consequence of more severe damage states. For example, for gypsum wall partitions, FEMA P-58 recommends three damage states (DS<sub>1</sub>, DS<sub>2</sub>, and DS<sub>3</sub>) with average repair costs of \$2730, \$5190, and \$7940 per 13'x100' panels, respectively.

Intensity 1 constitutes a small portion of total annual monetary loss except for 72° archetype where even this weak intensity causes noticeable annual loss. The incomplete module causes a sharp reduction in stiffness of the uppermost story and a concentration of deformation in the uppermost floor which leads to a noticeable increase in annual loss. The alternate configuration, 4-72A archetype, performs noticeably better having an approximately 30% less annual loss, as depicted in Figure 3.11 (d). The alternate configuration, 4-72A archetype, shows generally smaller lateral deformation compared to 4-72 archetype and deformation is not concentrated in the 4<sup>th</sup> story. Thus, the expected annual loss is decreased noticeably. In other words, larger lateral displacement in 4-72 archetype has caused larger damage and larger loss. A larger collapse  $IDR_{max}$  for 4-72 archetype compared to 4-72A archetype is not necessarily a sign of better performance since it is due to the concentration of lateral displacement in the 4<sup>th</sup> floor.

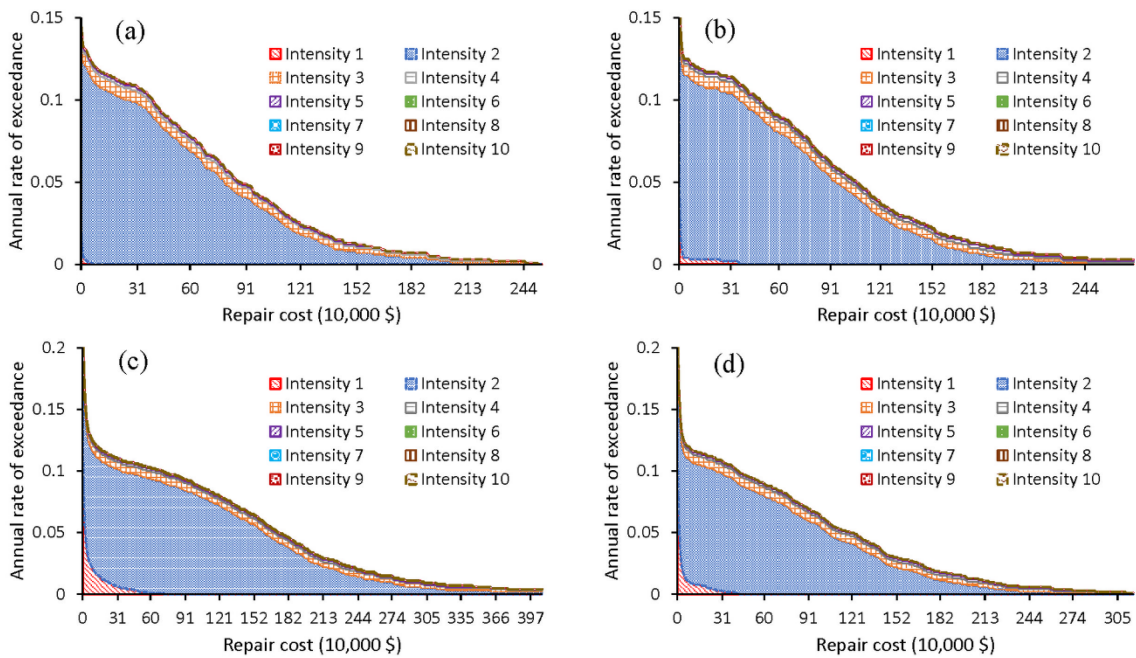


Figure 3.11 Annual repair cost for (a) 4-45, (b) 4-63 and (c) 4-72 (d) 4-72A archetypes

### **3.3.4.2 Downtime Estimation**

The time needed to regain the primary functionality (downtime) is a probabilistic function depending on the damage states, component-dependent repair time, and the number of workers available. Downtime is particularly important for commercial buildings and is the main metric for developing the functionality curve and the recovery path. Here, downtime is evaluated using two approaches: 1) intensity-based approach considering MCE and DBE, 2) time-based approach where the annual downtime is considered.

#### ***3.3.4.2.1 Intensity-Based Downtime***

The repair time for each floor of archetypes is evaluated and depicted in Figure 3.12. The expected repair time is reported as a percentage of TRT. The downtime is divided into three categories which are the repair time required for 1) structural components, 2) non-structural components vulnerable to IDR, 3) non-structural components vulnerable to acceleration. The downtime analysis is conducted using FEMA PACT (FEMA 2012). Note that the non-structural repair time reported for the roof is due to damage to the Chiller and Air Handling Unit installed on the roof.

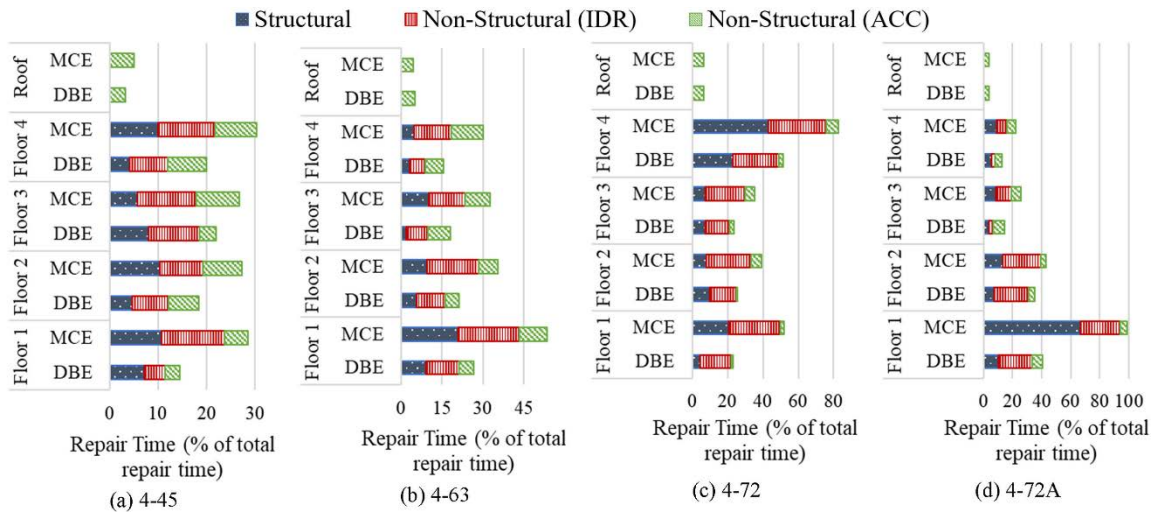


Figure 3.12 Repair time for different components and floors as a percentage of total replacement time

As depicted, the repair time for each story following a DBE-level earthquake for all archetypes except 72° archetypes remains under 25% of TRT. The 4-45 shows the smallest floor-wise repair time with up to 217 days (30% of TRT) for repairing the 4<sup>th</sup> floor under MCE.

Table 3.4 presents the median downtime for all studied cases with parallel and serial approach along with the expected required repair time (average of repair time for different floors) for each performance group. The structural components are a large percentage of the total repair time but in general, the non-structural components vulnerable to IDR (curtain walls and partitions) have the highest repair time. This shows the significance of non-structural loss which can be distinguished by component-level loss estimation only. The share of curtain walls and partition in total repair time increases under MCE.

Table 3.4 Total repair time for each component and median repair time for different intensities and models

Archetype	Intensity	Repair Time (Mean is in % of TRT)						Median Repair Time, Serial (% of TRT)	Median Repair Time, Parallel (% of TRT)
		Structural		Non-Structural (IDR)		Non-Structural (ACC)			
		Mean	COV	Mean	COV	Mean	COV		
4-45	DBE	6.0	0.27	7.5	0.30	4.8	0.42	74.2	22.5
	MCE	9.2	0.22	11.5	0.13	7.1	0.25	98.9	30.3
4-63	DBE	5.1	0.55	9.0	0.27	6.0	0.19	94.4	26.7
	MCE	11.4	0.52	17.1	0.23	8.5	0.31	99.2	53.6
4-72	DBE	11.2	0.64	18.1	0.26	2.5	0.80	99.2	51.4
	MCE	19.8	0.73	27.5	0.14	5.3	0.35	99.3	82.9
4-72A	DBE	6.5	0.38	13.3	0.78	5.4	0.32	98.8	40.4
	MCE	24.2	1.01	18.0	0.50	5.0	0.21	99.3	82.9

Floor to floor variation of the repair time is not significant except for the 72° archetypes. The repair time for structural components and to some extent non-structural components vulnerable to IDR under MCE is noticeably larger for the first floor of 4-63 compared to the second and the third floor. This indicates that large IDR in the first story has caused these components to reach severe damage in most realizations of the Monte Carlo simulation in PACT. Generally, the expected total floor repair times are consistent with the structural response under both the DBE and MCE. Note that structural and non-structural components on all floor are the same except for the roof which has non-structural components only, i.e. two hydraulic elevators, a chiller and an air-handling unit.

The 4-72 archetype shows a distinctively large repair time for the fourth floor which is caused by considerably larger deformation and acceleration in the uppermost incomplete module. It was found that grouping of diagonal members in the design process has a noticeable influence on diagrid behavior as well. Based on member grouping, smaller diagonals are used for the uppermost story of the 4-72 archetype which leads to a reduction

of stiffness in this story. This factor together with the effect of incomplete module caused a significant increase in repair time and loss for this floor. The diagrids are found to be particularly sensitive to the diagonal cross-sectional area and a sharp decrease of the cross-section between two adjacent floors may significantly affect the expected loss and downtime of the building. For 72° archetypes, the building experiences larger deformations and the repair time due to the structural components increase while the contribution of non-structural components to downtime is comparatively small (see Figure 3.12).

The repair time for the fourth floor of the 4-72A archetype reduces by about 75% compared to the 4-72 archetype, which shows that the alternate configuration can effectively reduce the damage to the uppermost incomplete module. The median repair time also reduces by about 21% for DBE. However, the median repair time increases by about 19% for MCE and the repair time for the first floor increases substantially (see Figure 3.12 (d)). Thus, the alternate configuration limits the loss and downtime in the incomplete floor; but it may increase them in lower floors. This indicates that the 72° diagonal angle is not an efficient choice for the studied archetype.

The least expected downtime (repair time) belongs to 4-45 archetype with a downtime of 162 days (22.5% of TRT) under DBE with parallel construction planning. With a serial construction planning, the respective downtime increases up to 534 (74.2% of TRT). Under MCE, the expected downtime for most cases increases substantially and if a serial construction is planned, the downtime reaches the TRT threshold. For 4-63 archetype, the expected downtime is larger than the optimal case, 4-45, and the main contributor to its downtime is the curtain walls and wall partitions.

### 3.3.4.2.2 Annual Seismic Downtime

The annual CDF of total downtime is evaluated in terms of repair time for each component at each floor considering a parallel construction planning and shown in Figure 3.13. The annual downtime follows a similar pattern as the repair cost (Figure 3.11) with the largest annual repair time caused by intensity 2. In general, the 4-45 archetype has lower annual probabilities of exceeding different downtimes. It also has little downtime due to intensity 1 with a  $S_a$  of 0.05g and a mean AFE of 0.2406 compared to other archetypes. The 4-72 and 4-72A both show high annual probabilities of exceeding different downtimes as seen in Figure 3.13 (c) and (d).

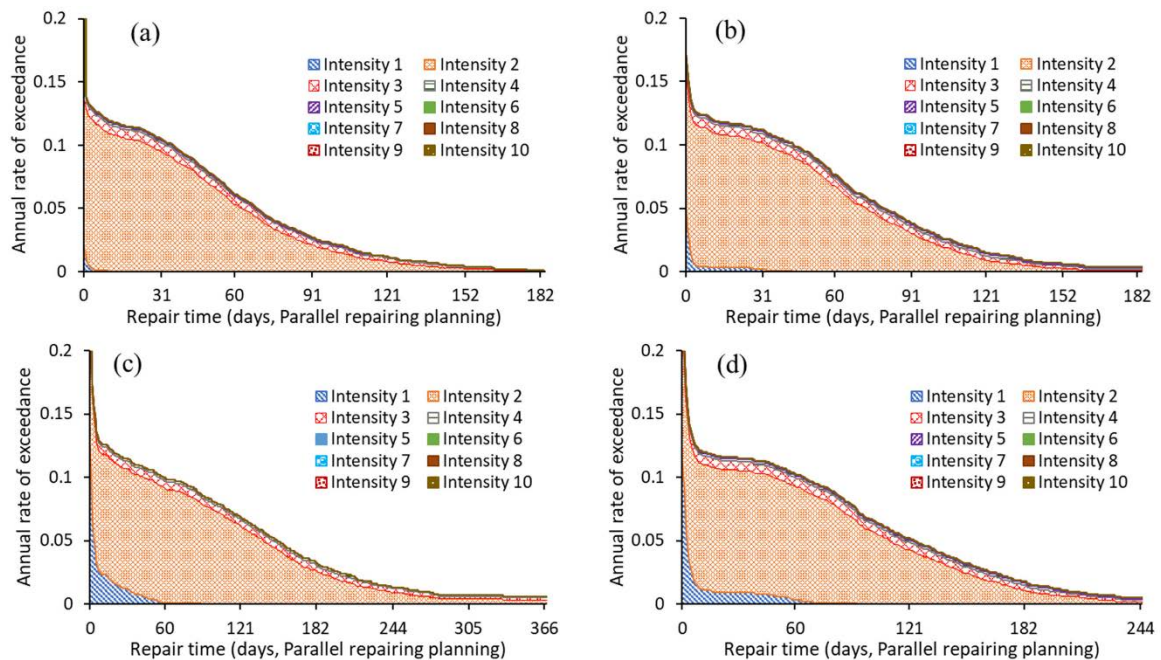


Figure 3.13 Annual downtime assuming parallel planning for (a) 4-45, (b) 4-63 and (c) 4-72 (d) 4-72A archetypes

### 3.3.4.3 Casualty Estimation

Figure 3.14 depicts the lognormal CDF of injuries for selected intensities for the 4-63 archetype. Clearly, the estimated number of injuries increases as the intensity increase

which shifts the median (50<sup>th</sup> percentile) of CDF of injuries to the right in Figure 3.14. Also, the dispersion/uncertainty of the estimated CDF increases with intensity which is manifested in wider CDFs for larger intensities in Figure 3.14. The main contributor to casualty is found to be non-structural components such as suspended ceilings vulnerable to excessive acceleration and in higher intensities, the wall partitions vulnerable to excessive IDR. Diagrids withstand large spectral acceleration while having a comparatively small IDR (Asadi et al. 2018). Therefore, structural and non-structural components vulnerable to excessive IDR mostly have not reached their corresponding severe damage state in smaller intensities. The injury and fatality occur mostly after these components reach severe damage state (FEMA 2012).

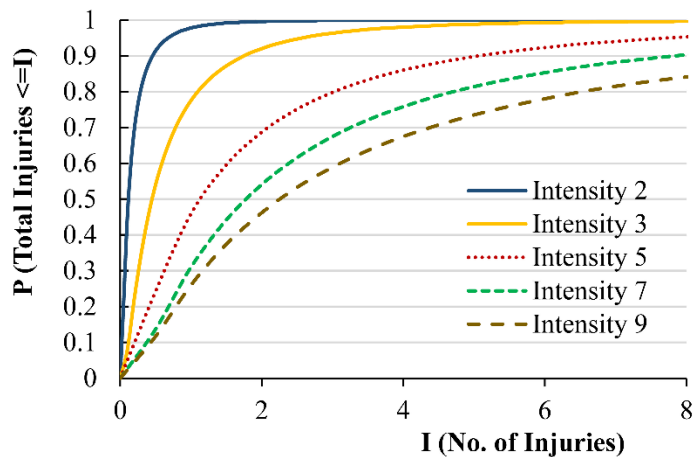


Figure 3.14 Cumulative distribution function of injuries for different intensities for 4-63 archetype

Figure 3.15 and 3.16 show the annual probability of injuries and fatalities under seismic hazard. Note that casualty outputs of FEMA P-58 method are not necessarily comparable with other models since the assumptions and component definition are not the same (Dong and Frangopol 2016; Sutley et al. 2016a; Wei et al. 2015). They are mostly

useful for comparison between cases analyzed using FEMA P-58 method (FEMA 2012). The current fatality models are not thorough either and do not include fatality due to all effective components which further limits their applicability. The injuries for intensity 2 is the largest as expected based on the repair cost and time observed previously followed by intensities 3 and 4, respectively. Intensity 1 shows a much lower annual probability of injuries indicating the negligible annual probability of damage for this intensity. While the injuries follow a relatively similar pattern with the repair time and downtime, the fatalities show a completely different pattern in term of the share of each intensity in the total annual fatality. Intensities 1 to 3 constitute a small portion of the total probability of fatality and intensities 4 and 9 constitute the largest portion of it. This difference can be attributed to the fact that fatalities in earthquakes are mostly caused by the total or partial collapse of the structure and it is unlikely that minor damage to a component causes fatality (Coburn et al. 1992; FEMA 2012). Partial collapse is presumed when a structural component reaches its collapse damage state (Han et al. 2016).

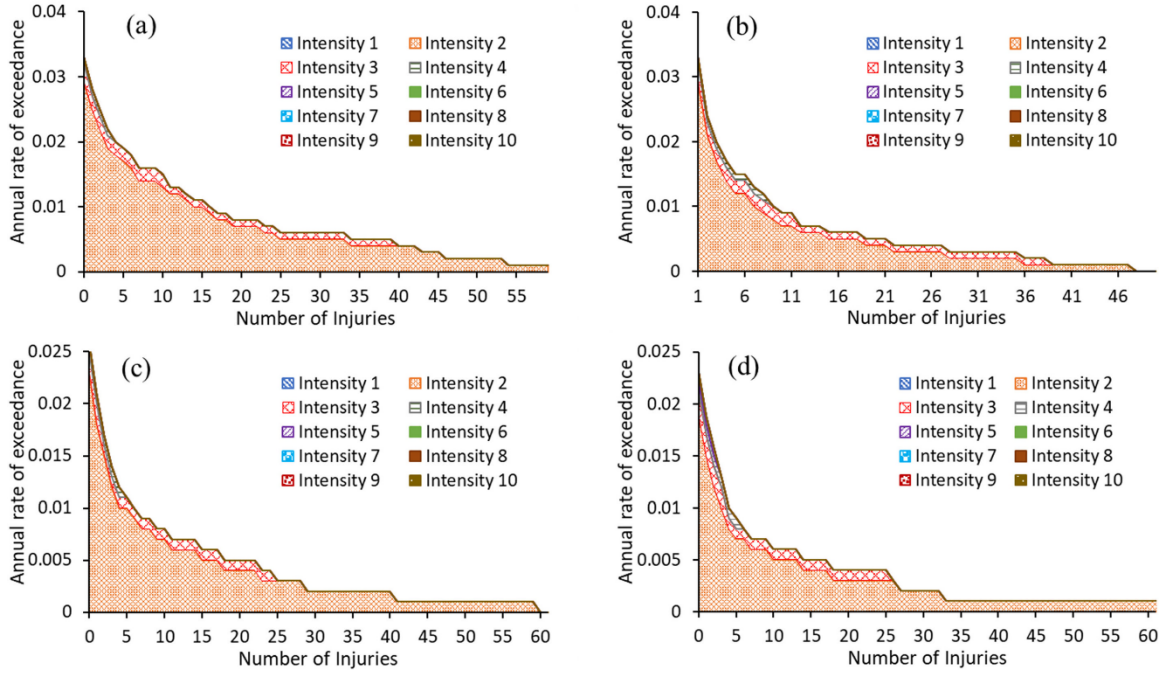


Figure 3.15 Annual rate of injuries for (a) 4-45, (b) 4-63 and (c) 4-72 (d) 4-72A archetypes under seismic hazard

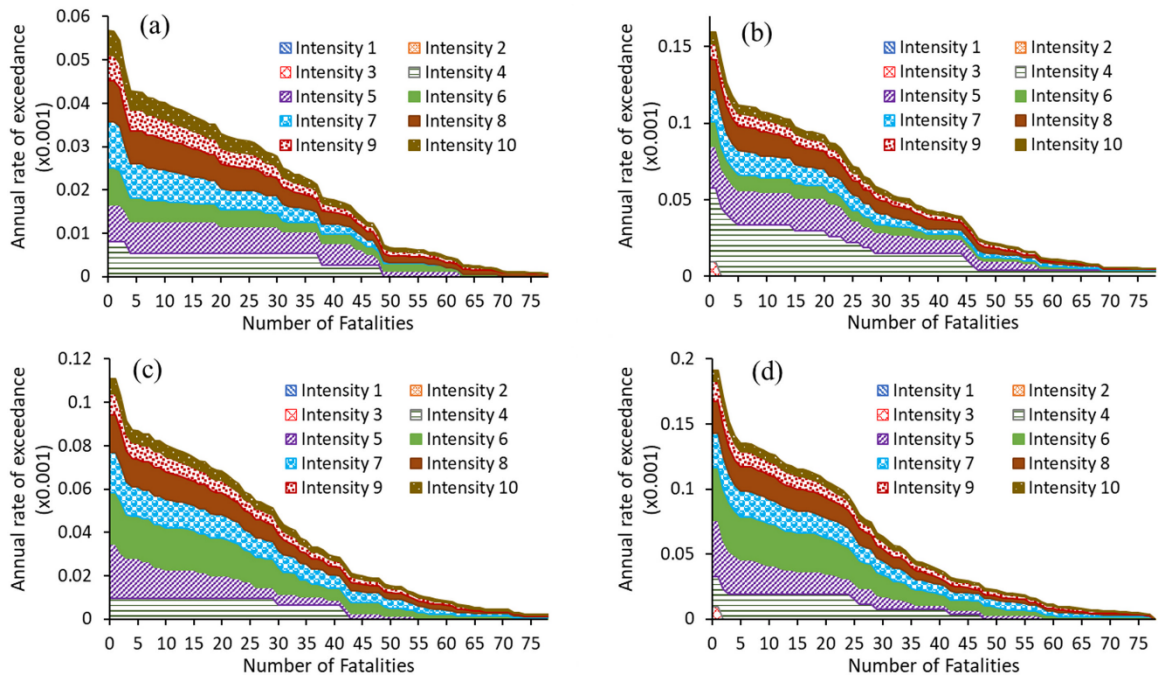


Figure 3.16 Annual rate of fatalities for (a) 4-45, (b) 4-63 and (c) 4-72 (d) 4-72A archetypes under seismic hazard

### ***3.3.5 Sustainability Assessment***

The EIO-LCA combines environmental data with historical economic data to resolve some of the issues with the process-based LCA, e.g. heavy data requirement, being time-consuming and costly, and system boundary selection. Due to its economic and industrial base, the EIO method provides more flexibility and can easily be combined with related studies in economics and insurance industry. Carnegie Mellon University has developed an EIO-LCA model based on historical economic-environmental data for various industry groups and sectors. The model used here is based on the most recent benchmark of the US economy (updated in 2010) which is built upon public data from the US Bureau of Economic Analysis, Department of Commerce, Census Bureau, Department of Energy, etc. (CMU GDI 2018). It has been used for LCA of various building and structural systems including commercial buildings (Junnila et al. 2006), residential Buildings (Ochoa et al. 2002; Sharrard et al. 2008), concrete and steel buildings (Guggemos and Horvath 2003), and transportation systems (Horvath 2006). Here, the repair/replacement cost due to earthquake calculated in the previous sections is used to estimate the environmental impacts of the earthquake considering construction industry and nonresidential maintenance and repair sector.

#### **3.3.5.1 Recycled/Reused Material**

Embodied energy, commonly measured in kg CO<sub>2</sub> equivalent per kg material, is the amount of energy needed for the life-cycle of a specific material including the energy required for extraction, processing, and transportation. Embodied energy can be reduced in three ways: 1) reducing the volume of material required, 2) using recycled materials,

and 3) efficient preparation and erection practice to reduce construction waste (Gallivan et al. 2010). Using efficient structural systems such as diagrids can effectively reduce the total required material and total embodied energy. Apart from that, using recycled steel or reusing steel which is the primary material for construction will reduce the total embodied energy. Recycled materials have several benefits: 1) they need less energy for production than virgin materials, 2) they are mostly construction waste that would otherwise be discarded hence harmful to the environment, 3) source of recycled material may be closer to the construction site reducing the energy required to transport the material to the site. In some cases, the material can come from a building set for demolition at the same site eliminating the need for transportation.

Most of the hot-rolled wide flange steel used in the US are produced using recycled materials. Averagely recycled content is about 93% of the hot-rolled structural shapes (AISC 2017). Structural steel can also be reused. Reusing steel is a cost-efficient and sustainable strategy but little study has been done on its sustainability impacts. Reusing structural steel will limit the environmental consequences due to the impacts caused by fabrication and transportation (AISC 2017). However, it may increase the uncertainty in the properties of the material and structural shapes (RSMMeans 2018; Wei et al. 2015). Therefore, the properties of steel being recovered or reused need to be evaluated according to AISC 360-16 Appendix 5 to make sure the reliability and performance of the structure will not be affected by the reused materials (Ochoa et al. 2002; Schmidt and Bartlett 2002). Here, three alternate archetypes 4-63R20, 4-63R50, 4-63R80 are also studied where 20%, 50%, and 80% of the structural steel is from reused material. For reused steel, two

processes, i.e. fabrication and transportation, are required and the GWP due to these processes form about 12% of total GWP produced from cradle to grave (AISC 2016c, 2017). Similar to the previous section, the repair cost of structural components is used to estimate the environmental consequences of the structural material.

### **3.3.5.2 Annual Environmental Consequences of Earthquake**

Table 3.5 lists the estimated environmental impacts due to initial construction and the annual seismic environmental consequences for different archetypes. The initial construction cost is presumed equal to the total replacement cost. Accordingly, the greenhouse gas emission from fossil fuel combustion sources constitutes the largest portion of the impacts for both initial construction and annual seismic repair. As expected, the 4-45 archetype has the least annual environmental impact followed by 4-63, 4-72A, and 4-72, respectively. Using reused steel for construction effectively reduces the GWP such that the annual seismic GWP for 4-63R20, 4-63R50, and 4-63R80 archetype reduces to 73.6, 68.3, and 63.4 tons CO<sub>2e</sub> (approximately 7.1%, 13.8%, and 20% reduction compared to 4-63 archetype), respectively. This reduction in seismic environmental consequences is achieved while the resilience metrics have little changes given that the quality testing requirements for reused sections are satisfied.

Table 3.5 Estimated environmental impacts due to initial construction and annual seismic damage repair

Environmental Metric	Greenhouse Gases						Energy	Conventional Air Pollutants					Water	
	Total GWP <sup>a</sup>	CO <sub>2</sub> Fossil <sup>b</sup>	CO <sub>2</sub> Process <sup>c</sup>	CH <sub>4</sub>	N <sub>2</sub> O	HFC/PFCs <sup>d</sup>	Total Energy	CO	NH <sub>3</sub>	NO	PM 10 <sup>e</sup>	PM 2.5 <sup>f</sup>	SO <sub>2</sub>	Water Withdrawals
Unit	ton CO <sub>2</sub> e	ton CO <sub>2</sub> e	ton CO <sub>2</sub> e	ton CO <sub>2</sub> e	ton CO <sub>2</sub> e	ton CO <sub>2</sub> e	TJ	ton	ton	ton	ton	ton	ton	kGal
Initial Construction														
4-story diagrid	2400	1970	250	119	38.7	17.7	34	21.6	0.222	7.64	4.19	1.43	3.82	20500
Annual Environmental Consequence due to Earthquake														
4-45	65.6	54.2	6.02	3.82	1.03	0.59	0.91	0.306	0.007	0.163	0.396	0.061	0.096	612
4-63	79.3	65.4	7.27	4.61	1.24	0.72	1.10	0.369	0.008	0.197	0.478	0.074	0.116	739
4-72	124	102.	11.4	7.20	1.94	1.12	1.73	0.577	0.013	0.307	0.747	0.116	0.182	1150
4-72A	86.7	71.6	7.95	5.04	1.36	0.79	1.21	0.404	0.009	0.215	0.523	0.081	0.127	808

a Global Warming Potential (GWP)

b Emissions of Carbon Dioxide (CO<sub>2</sub>) into the air from fossil fuel combustion sources

c Emissions of CO<sub>2</sub> into the air from sources other than fossil fuel combustion

d HFC/PFCs = Emissions of all high-GWP gases such as hydrofluorocarbons, perfluorocarbons, and sulfur hexafluoride into the air (100-year GWP values vary).

e PM 10 = Emissions of Particulate Matter (less than 10 microns in diameter) to the air

f PM 2.5 = Emissions of Particulate Matter (less than 2.5 microns in diameter) to the air

ton = metric tons

ton CO<sub>2</sub>e = metric tons of CO<sub>2</sub> equivalent

Using the variation of seismic repair cost shown in Figure 3.11, the variation of the annual probability of total greenhouse gas emissions for different archetypes is calculated and depicted in Figure 3.17. It clearly shows the difference between various archetypes in terms of annual earthquake consequences, specifically environmental consequences. Accordingly, the 4-63 and the 4-72A archetypes are likely to have similar seismic environmental consequences while the 4-72 case is more likely to have larger seismic environmental consequences. As depicted, these differences are more significant for annual total GWP greater than 220 tons CO<sub>2</sub>e. For instance, there is about 5.7% chance that the total CO<sub>2</sub>e produced by post-earthquake damage repair activities is more than 500 tons for the 4-45 archetype. This probability is 7.2%, 7.6%, and 9.7% for 4-63, 4-72A, and 4-72 archetypes, respectively. Given that the total CO<sub>2</sub> equivalent created by the initial construction is about 2400 tons, this probability implies that environmental impacts of earthquakes can be significant in a high seismic region like Los Angeles.

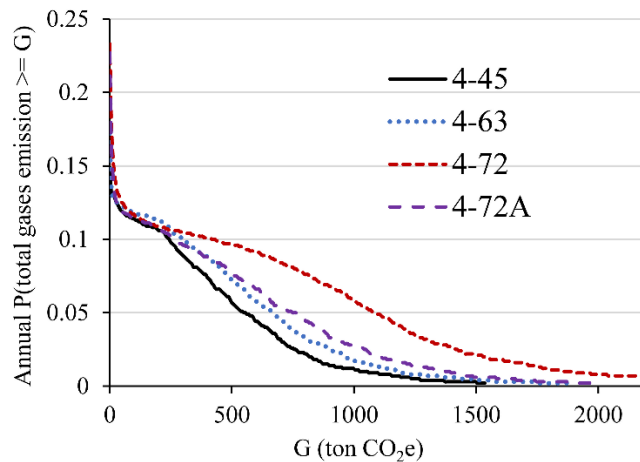


Figure 3.17 Annual probability of total greenhouse gas emission for different archetypes

### ***3.3.6 Multi-Criteria Decision Making***

Here the decision-making framework is applied to find the best option among various archetypes. The total expected asset loss due to the earthquake is quantified based on the annual seismic repair cost and the total expected time loss is calculated based on the annual seismic repair time. The indirect monetary loss due to closure and downtime is not added to the monetary loss since it will be considered in the time loss. Adding the monetary loss disproportionately increases the asset loss and may cause double counting of the downtime. The life loss contains the annual number of casualty and fatality due to the earthquake. Finally, the total annual GWP caused by the earthquake damage is considered as the environmental loss.

The importance factor assigned to each attribute is subjective depending on the project goals, client requirements, and decision-maker's experienced judgment. Assuming various decision-making scenarios, the sensitivity of final decision to the importance factor (IF) is studied. Six scenarios are studied: 1) lowest asset loss assuming a scenario where significantly valuable asset exists in the building, e.g. a warehouse with expensive stored asset, 2) lowest time loss assuming a scenario where the downtime is significantly costly and/or the building should remain functional after extreme event, e.g. building is a hospital, 3) lowest life loss where a large number of people will reside or work in the building, e.g. building is a school, 4) lowest environmental loss where due to client's requirements or official regulations the building should be eco-friendly, 5) high resilience where overall resilience of the building is the main criteria, and 6) neutral where all attributes have the same importance. The latest scenario is assumed for comparison only.

For each scenario, a pairwise comparison matrix is developed using a three-level AHP (Mateo 2012; Saaty 1990). The goal of each scenario is at the top level, the alternative design options (archetypes) are at the middle level, and the attributes/criteria are at the bottom level of the AHP. For importance/weight factors, three groups of experts from industry and academia (i.e., engineers, graduate students, and faculty members) were formed and a survey was conducted following similar studies on the topic (Ellingwood and Tekie 1999; Zavadskas et al. 2007). Participants were selected based on their familiarity with the topic. In the survey, the participants were asked to select the weight factor to best reflect the main goal of each scenario. The mean weight factor is used in this study disregarding the upper and lower bounds of the survey data. To express the relative importance or strength of one criterion over another, a numerical value between 1 to 9 (or their reciprocal) is assigned to each pair (Ferreira et al. 2009; Mateo 2012; Saaty 1990). For instance, for scenario 1 (least asset loss), asset loss may be strongly more important than time loss, weakly more important than life loss, and absolutely more important than the environmental loss in pair-wise comparison lottery between them. Hence, a scale factor of 5, 3, and 9 would be suggested by the participant to show the importance of asset loss over others, respectively. Tables 3.6-3.10 presents the comparison matrix for scenarios 1-5, respectively. The importance factors for scenario 6 are all 0.25 for all four attributes.

Table 3.6 Pairwise comparison matrix for Scenario 1- lowest asset loss

Attribute (Criteria)	Asset Loss	Time Loss	Life Loss	Envir. Loss	Importance Factor S1
Asset Loss	1	5	2	5	0.502
Time Loss	1/5	1	1	2	0.153
Life Loss	1/2	1	1	7	0.276
Envir. Loss	1/5	1/2	1/7	1	0.068

Table 3.7 Pairwise comparison matrix for Scenario 2- lowest time loss

Attribute (Criteria)	Asset Loss	Time Loss	Life Loss	Envir. Loss	Importance Factor S2
Asset Loss	1	1/2	1/2	3	0.184
Time Loss	2	1	3	4	0.442
Life Loss	2	1/3	1	7	0.304
Envir. Loss	1/3	1/4	1/7	1	0.070

Table 3.8 Pairwise comparison matrix for Scenario 3- lowest life loss

Attribute (Criteria)	Asset Loss	Time Loss	Life Loss	Envir. Loss	Importance Factor S3
Asset Loss	1	2	1/4	3	0.214
Time Loss	1/2	1	1/3	2	0.147
Life Loss	4	3	1	7	0.566
Envir. Loss	1/3	1/2	1/7	1	0.073

Table 3.9 Pairwise comparison matrix for Scenario 4- lowest environmental loss

Attribute (Criteria)	Asset Loss	Time Loss	Life Loss	Envir. Loss	Importance Factor S4
Asset Loss	1	2	1	1/3	0.197
Time Loss	1/2	1	1/3	1/3	0.108
Life Loss	1	3	1	1/2	0.244
Envir. Loss	3	3	2	1	0.450

Table 3.10 Pairwise comparison matrix for Scenario 5- highest resilience

Attribute (Criteria)	Asset Loss	Time Loss	Life Loss	Envir. Loss	Importance Factor S5
Asset Loss	1	3	1	4	0.384
Time Loss	1/3	1	1	3	0.209
Life Loss	1	1	1	7	0.340
Envir. Loss	1/4	1/3	1/7	1	0.068

The assets, time, life, and environmental losses, total utility ( $U_i$ ) for MAUT method, and relative closeness to ideal solution ( $C^*$ ) for TOPSIS method for various scenarios and alternative archetypes are listed in Table 3.11. The values in Bold indicate the highest score and best alternative for each scenario. The scores calculated based on MAUT and TOPSIS are very close and the best choice from either method is the same. For most scenarios, the 4-63R80 archetype is the best choice given its low environmental loss and life loss. Note

that 4-63R80 does not experience the least annual asset or time loss but it is second in terms of asset or time loss. For scenario 1 (least asset loss), the 4-63R80 archetype is found to be the best choice followed by 4-63R50 and 4-63R20 respectively. The 4-45 shows the least asset and time loss but receives a smaller overall score (9% in MAUT and 11% in TOPSIS methods compared to 4-63R80). It is mainly because the casualty is the highest for the 4-45 archetype and in the survey, most participants gave a high importance factor to life loss. This indicates that the environmental benefits of using reused steel may offset the resilience shortcomings due to the diagrid configuration, even if the asset loss is the priority. As expected, the 4-72 archetype shows the least  $U_t$  and  $C^*$  but noticeably, the 4-72A results in a much larger score for scenario 1 (1.9 and 1.3 times larger for MAUT and TOPSIS methods, respectively). Similarly, the 4-63R80 archetype is the best alternative for scenario 2 (least time loss) and the difference between the total utility for the 4-63R80 archetypes and the 4-45 case is much larger than scenario 1. It is mostly due to the relatively close annual repair time of these archetypes compared to large annual repair time for 4-72 and 4-72A.

For scenario 3 (least life loss), the 4-72A archetype has the best score followed by 4-63R80. The 4-63R80 shows a slightly better score than the other 4-63 and a noticeably better score than the 4-45 archetype. The total number of injuries which constitutes the largest portion of the number of casualties is the highest for 4-45 archetype making this alternative the worst case in terms of life loss. It is found that the 4-45 archetype experiences large spectral acceleration while minimizing the IDR. This large spectral acceleration causes substantial damage to the non-structural components particularly the

suspended ceilings which contributes significantly to the number of injuries. The 4-72A archetype has a larger score than the 4-72 one as well (by 40% and 25% for MAUT and TOPSIS methods, respectively).

As expected, the 4-63R80 archetype is the best choice in terms of environmental loss followed by 4-63R50 and 4-63R20. Note that based on the survey, in the hierarchy pairwise matrix for this scenario, a larger weight is assigned to life loss than time and asset loss to reflect the interrelationship between social and environmental consequences in a sustainability assessment framework. This has led to a notably small score for 4-45, 4-72, and 4-72A archetypes for scenario 4.

For the highest resilience scenario, the environmental loss has the smallest importance factor, i.e. 0.068. Despite that, the 4-63R80 achieve a noticeably better score than others which indicates that the benefits of sustainable strategies such as reusing steel may offset its cost. Note that the reduction in construction cost due to reusing steel and the increase in cost due to additional required testing are not included in the assessment. The 4-72 archetype shows a much smaller score value than 4-72A for scenario 5.

Further, for all scenarios, the 4-72A archetype results in a larger total utility value than the 4-72 archetype which demonstrates that the proposed alternate configuration can improve the resilience and sustainability of the diagrid building. For scenario 6, the 4-63R80 has the best overall score indicating again the importance of sustainable design strategies, if an MCDM is used.

Table 3.11 Evaluation matrix obtained from RSA module, total utility ( $U_i$ ) for MAUT method, and relative closeness to ideal solution ( $C^*$ ) for TOPSIS method

Attribute (Expected Annual)	4-45	4-63	4-63R20	4-63R50	4-63R80	4-72	4-72A							
Asset Loss (Thousand \$)	105.22	127.06	127.06	127.06	127.06	198.49	139.02							
Time Loss (Days)	8.47	9.95	9.95	9.95	9.95	19.44	15.21							
Life Loss (# of Casualty)	0.052	0.0354	0.0354	0.0354	0.0354	0.0327	0.0295							
Envir. Loss (ton CO <sub>2</sub> e)	65.6	79.3	73.6	68.3	63.4	124	86.7							
Total utility ( $U_i$ ) for MAUT method and relative closeness to ideal solution ( $C^*$ ) for TOPSIS method														
Scenario	$U_i$	$C^*$	$U_i$	$C^*$	$U_i$	$C^*$	$U_i$	$C^*$	$U_i$	$C^*$	$U_i$	$C^*$	$U_i$	$C^*$
Scenario 1	0.721	0.687	0.771	0.770	0.778	0.771	0.784	0.772	<b>0.789</b>	<b>0.773</b>	0.237	0.280	0.698	0.652
Scenario 2	0.693	0.691	0.799	0.828	0.806	0.830	0.812	0.831	<b>0.818</b>	<b>0.831</b>	0.261	0.276	0.635	0.508
Scenario 3	0.431	0.369	0.762	0.753	0.769	0.754	0.776	0.756	0.782	0.756	0.486	0.587	<b>0.804</b>	<b>0.787</b>
Scenario 4	0.739	0.707	0.757	0.747	0.799	0.810	0.839	0.858	<b>0.875</b>	<b>0.879</b>	0.209	0.255	0.689	0.644
Scenario 5	0.658	0.609	0.775	0.777	0.781	0.778	0.787	0.779	<b>0.793</b>	<b>0.780</b>	0.292	0.354	0.707	0.650
Scenario 6	0.741	0.685	0.777	0.784	0.800	0.809	0.822	0.825	<b>0.842</b>	<b>0.833</b>	0.214	0.280	0.660	0.586

### 3.4 Conclusions

A multi-criteria decision-making framework for resilience and sustainability assessment of building structures subjected to earthquake hazard is introduced considering uncertainty in demand, modeling, and component-level fragility. Three decision models are utilized: analytic hierarchy process, multi-attribute utility theory (MAUT), and Technique for order preference by similarity to ideal solution (TOPSIS). The framework is implemented on a series of steel diagrid buildings in a high seismic region. For demonstration purpose, only a neutral (linear) utility function is used for MAUT.

The diagrid structures show a substantial reserve capacity against collapse and experience a large maximum absolute spectral acceleration, a mean value of 3.6g, before reaching the collapse point. This large spectral acceleration results in substantial damage to non-structural components vulnerable to excessive acceleration which increases the expected number of injuries. The diagonal angle and the configuration are key factors in the performance of the diagrid frames (Asadi and Adeli 2017; Moon et al. 2007). Incomplete uppermost diagrid modules significantly increase monetary loss and downtime. An alternate configuration is proposed where diagonal angle changes in the uppermost floors to avoid having an incomplete diagrid module. This alternate configuration found effective in reducing seismic loss, particularly life loss, achieving much better scores (total utility) than original archetype (4-72) for various decision-making scenarios.

Though, it has little impact on resilience metrics, reusing steel has a significant influence on environmental metrics and can be a cost-efficient construction strategy. The benefits of sustainable design are more evident with an MCDM framework. Such that the

environmental benefit may outweigh the shortcomings due to structural configuration and nonlinear performance. For instance, the 4-63R80 archetype (with 80% reused steel) achieved the highest score among all alternatives when the objective is to maximize overall resiliency (scenario 5) as well as when it is to minimize environmental loss (scenario 4). Other sustainable design strategies such as using energy-efficient walls/roofs or walls/roof with high thermal mass which affects energy consumption of the building can be explored as well. Further, the proposed quadrilateral MCDM framework can be extended and calibrated for the cost-benefit analysis of other structures such as bridges or infrastructure systems such as water distribution systems.

The FEMA P-58 method used here does not include fragility specification for many structural systems such as steel plate shear walls or many light-weights exterior walls. Thus, this approach may not be applicable to all building structures. Though the quadrilateral loss model described here may include various losses due to earthquakes or other hazards, the required data can be obtained only through detailed case-based studies or through a community-oriented resilience assessment approach, which is out of the scope of this paper and an important topic for future studies. For instance, the recovery time may be longer than repair/replacement time as it depends on the recovery time of the community. The FEMA casualty and fatality models used here are limited and are mostly suitable for comparison purposes. Multi-criteria decision models have advanced significantly over the past decade. Among recent studies, using fuzzy logic with TOPSIS method (Ervural et al. 2018) and Bayesian adaptive decision models (Lee et al. 2018) can improve the flexibility and applicability of the proposed model.

## Chapter 4

### **4. Risk-informed Multi-criteria Decision Framework for Resilience, Sustainability, and Energy Analysis of Reinforced Concrete Buildings<sup>4</sup>**

#### **4.1 Introduction**

Mounting evidence of human-induced climate change and increasing loss due to various natural hazards have reinforced experts' efforts to develop new tools and techniques for sustainable and resilient design and construction of civil infrastructure. Global warming driven primarily by increased carbon dioxide concentration in the atmosphere has amplified the frequency and intensity of weather and climate hazards. Meanwhile, irregular variation of temperature, precipitation, and humidity has increased

---

<sup>4</sup> The material presented in this chapter is submitted for possible publication to the *Journal of Building Performance Simulation*.

Asadi, E., Shen Z., Zhou H., Salman, A. M., Li, Y. (20XX). Risk-informed Multi-criteria Decision Framework for Resilience, Sustainability, and Energy Analysis of Reinforced Concrete Buildings, *Journal of Building Performance Simulation*, Submitted.

the vulnerability of the infrastructure systems (Melillo et al. 2014). Weather and climate disasters have caused over 800 billion USD loss in the past 10 years in the US (NOAA 2019). On the other hand, to reduce the carbon footprint and other environmental impacts, several studies aimed to include sustainability criteria in the design of various structure and infrastructure systems (Kamali et al. 2018; Moussavi Nadoushani et al. 2017; Padgett and Li 2016). Other natural hazards, especially earthquakes, also cause billions of dollars of economic loss and claim thousands of lives every year. Seismic risk has increased due to significant population/industry growth in earthquake-prone urban regions and increasing vulnerability of aging buildings and infrastructure (FEMA et al. 2017). To mitigate environmental impacts while addressing the increasing risk due to seismic hazard, recent studies advocate for an integrated approach which includes both sustainability and resilience criteria in design/rehabilitation of structure and infrastructure systems (Belleri and Marini 2016; Bocchini et al. 2014; Phillips et al. 2017; Simonen et al. 2018).

All critical economic, social, health, and security services of a community depend, directly or indirectly, on buildings, making buildings an integral part of future resilient and sustainable communities (Roostaie et al. 2019). Seismic resilience of buildings and other structures have been extensively studied in recent years (Asadi et al. 2018; Bocchini et al. 2014; Bruneau et al. 2003; Roostaie et al. 2019). In 2012, FEMA published FEMA P-58 report providing a uniform approach for estimating key seismic resilience metrics, namely repair/replacement cost, downtime, and number of casualties (Belleri and Marini 2016; FEMA 2012). This report also provides a component-level fragility specification database and a Performance Assessment Calculation Tool (PACT) to quantify those metrics. Whilst the building sector is also one of the main consumers of energy produced in the US,

accounting for over 40% of total energy, and produces about 38% of greenhouse gas (GHG) emissions in the country (Basbagill et al. 2013; Belleri and Marini 2016). About 30% of all the energy consumed in a building during its lifespan is in the form of embodied energy (Ibn-Mohammed et al. 2013). Process-based bill-of-material (BOM) and economic input-output (EIO) life cycle assessment (LCA) methods are commonly used for quantifying embodied energy (FEMA 2012; Sharrard et al. 2008). Carnegie Mellon University has developed an EIO-LCA method based on the most recent benchmark of the US economy (updated in 2010) and public data from the US Bureau of Economic Analysis, Department of Commerce, Census Bureau, Department of Energy, etc. (CMU GDI 2018). This method has been used for LCA of various building and structural systems including commercial concrete and steel buildings (Guggemos and Horvath 2003; Junnila et al. 2006) and residential Buildings (Sharrard et al. 2008). Simonen et al. (2018) developed a database of environmental impacts of seismic damage to building components based on EIO-LCA method of (CMU GDI 2018) and FEMA P-58 database (FEMA 2012). In addition to embodied energy, buildings consume substantial operational energy for indoor environment conditioning (heating, cooling, ventilation), powering equipment, lightening, etc., over their life cycle. Increasingly, whole-building energy simulation is being conducted to achieve energy-efficient design. Yet, to achieve a holistic design framework, sustainability needs to be studied considering its interrelation and overlaps with resiliency (Asadi et al. 2019b; Belleri and Marini 2016; Park et al. 2018).

To quantify the total life-cycle cost, a simple approach used in the literature is to convert all losses, including environmental, life, and time loss, into a monetary loss (Han et al. 2016; Mitrani-Reiser 2007). This approach, however, adds to epistemic uncertainty

because of regional and case-based assumptions required for such conversion (Chau et al. 2015; Lloyd and Ries 2007). Given the uncertainties, adding all converted losses together may yield inaccurate conclusions. Another approach is multi-criteria decision models (MCDM) where the sustainability and resilience metrics, criteria, or attributes are kept in their original unit/space. MCDM provide more flexibility for problems where the objective is not solely minimizing monetary losses, e.g. a problem where the objective is to minimize the number of casualties. Multi-criteria decision analysis has been used in the past in the architectural design and construction industry (Baglivo et al. 2014; Hopfe et al. 2013; Invidiata et al. 2018). Invidiata et al. (2018) used complex proportional assessment (COPRAS) and analytic hierarchy process (AHP) decision models to find the best alternative design based on building environment criteria such as thermal comfort, energy demand, and monetary cost of construction. In their study, EnergyPlus was used for energy consumption analysis. Baglivo et al. (2014) used MCDM to find the optimal wall configuration based on sustainability factors such as thermal performance, operational energy use, embodied energy, productivity, and construction cost. Hopfe et al. (2013) also used AHP for building energy performance assessment considering the energy use, acoustical and thermal-comfort performance, and indoor air quality. But, they all focus on architectural criteria leaving out structural performance, resilience against natural hazards, and environmental consequence of construction and maintenance. Few studies used MCDM for building design based on both resilience and sustainability criteria.

This paper integrates recent resilience, sustainability, and energy analysis methodologies for buildings and presents a new comprehensive trilateral decision-making framework for their design. The proposed trilateral model uses both AHP and risk-based

MAUT to include various resilience, sustainability, and energy criteria in decision analysis. A survey is conducted to quantify the importance factor for each criterion considering seven different scenarios/objectives. Criteria quantified for seismic resilience include asset loss, time loss, number of casualties and fatalities. For sustainability, life-cycle construction and maintenance cost and GHG emission are studied. Using whole-building energy simulation, annual energy consumption, cost, and associated GHG emission are studied. The framework is implemented for two groups of commercial reinforced concrete (RC) buildings located in Los Angeles (LA), CA and Boston, MA.

## 4.2 Proposed Multi-Criteria Decision-Making Framework

The proposed decision-making framework consists of three main modules: (1) System Concept and Criteria (SCC) Module, (2) Resilience, Sustainability, and Energy Analysis (RSEA) Module, (3) Multi-Criteria Decision Making (MCDM) Module. Figure 4.1 depicts its main components and their inter-connections. The model consists of a feedback loop to update decisions based on new data obtained from monitoring and inspection, or due to change in hazard, vulnerability, or loss parameters. Monitoring and inspection through feedback loop are not studied here.



Figure 4.1 Main components of the proposed framework

### ***4.2.1 System Concept and Criteria (SCC) Module***

The project objectives, system properties, and analysis and design specification and assumptions will be defined in the SCC module. Similarly, the scope of assessment and the importance of each metric over others (e.g. monetary loss importance over GHG emission) are defined in this module according to decision-maker's preference and the objectives of the project. The output of this module is the archetype models ready for vulnerability, life-cycle, and energy-consumption analyses. The models include all structural and non-structural components of the building for component-level resilience and sustainability assessment and the thermal zone arrangement, material properties for walls, roof, façade, etc., and HVAC, lighting, and shading components for whole-building energy simulation. More details on SCC module is presented in (Asadi et al. 2019b). Numerical models developed in SCC module goes to RSEA module where they are analyzed for various measures depending on project requirements.

### ***4.2.2 Resilience, Sustainability, and Energy Analysis (RSEA) Module***

The integrated core module, RSEA, consist of three sub-modules where resilience, sustainability, and whole-building energy metrics are quantified. Figure 4.2 shows the step-wise illustrative procedure for the RSEA module. The simulation models are analyzed, and the output is transferred to the MCDM module where decision analysis is performed.

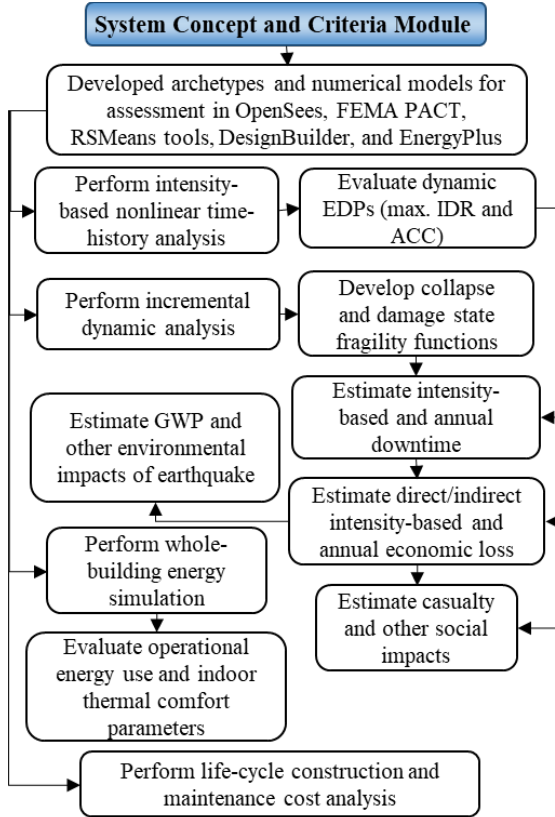


Figure 4.2 Seismic resilience, sustainability, and energy-consumption analysis (RSEA) Module

#### 4.2.2.1 Resilience Assessment

Resilience ( $R$ ) can be quantified as the integration of functionality ( $Q$ ) over a time interval ( $T_R$ ) after the occurrence of an event at time  $t_0$  (Cimellaro et al. 2010):

$$R = 1/T_R \int_{t_0}^{t_0+T_R} Q(t) dt \quad (4.1)$$

$$Q(t) = (1 - L_t) \times f_R \quad (4.2)$$

where  $L_t$  is the whole-building loss function and  $f_R$  is the recovery function. Loss is the key parameter in the above formula embodying earthquake consequences. For mutually exclusive seismic events, the total probability of seismic loss at a given earthquake

intensity is defined in the following (Belleri and Marini 2016; Ramirez and Miranda 2012b).

$$P(L > l_i | IM = z) = \int_{EDP} \int_{DS} P(L > l_i | DS = DS_{ij}) P(DS | EDP = d) P(EDP | IM = z) dDS dEDP \quad (4.3)$$

where  $P(L > l_i | IM = z)$  is the probability of having a loss greater than  $l_i$  given that hazard intensity is equal to  $z$ ,  $P(L > l_i | DS = DS_{ij})$  is the probability of having a total loss greater than  $l_i$  given that damage state of  $DS_i$  is achieved for component  $j$ ,  $P(DS | EDP = d)$  is the probability density function (PDF) of achieving a damage state given that the engineering demand parameter (EDP) reaches a certain value of  $d$ , and  $P(EDP | IM = z)$  is the PDF of the EDP conditioned on a certain hazard intensity,  $z$ . For component-level loss estimation, the conditional consequence function,  $P(L > l_i | DS = DS_{ij})$ , requires a database of repair cost/time and other consequence functions for every component, which is provided alongside FEMA P-58 in FEMA PACT (FEMA 2012). The fragility functions obtained from nonlinear dynamic analysis are used to find the probability of reaching a certain damage state for each damageable component.

For time-based loss estimation, the annual probability of loss,  $P(L > l_i)$ , given the annual probability of each earthquake intensity,  $P(IM = z)$ , will be:

$$P(L > l_i) = \int_{IM} P(L > l_i | IM = z) P(IM = z) dIM \quad (4.4)$$

The loss ( $L$ ), in equations above, may be any kind of loss due to any stochastic hazard including monetary, time, life, or environmental loss due to earthquake.

#### 4.2.2.2 Sustainability Assessment

Sustainability involves a broad range of metrics, but it is commonly quantified using three main measures: environmental, economic, and social consequences of the product or process. Some criteria are both a resilience and sustainability measure and some are both sustainability and energy measure. Considering this inter-relationship, these consequences can be incorporated through quantitative parameters such as embodied energy, operational energy use, construction and maintenance costs, and economic loss, downtime, and casualties due to natural or manmade hazards.

The initial cost of the buildings was analyzed using data-based life-cycle cost estimator tools, the construction cost of all structural and non-structural components of a building can be estimated accurately. Particularly, RSMeans Data Online (2018) was used To estimate the construction cost includes substructure cost, shell cost, interiors cost, services cost, and contractor and architectural fees. The tasks and periodicities recommended by Whitestone cost reference (Abate et al. 2009) is used for estimating building maintenance cost. The Whitestone database was used for estimating ecological footprint due to operation and maintenance of residential buildings (Basbagill et al. 2013; Martínez-Rocamora et al. 2017).

Maintenance and energy costs and benefits need to be discounted to a present value. The net present value of a future cost  $C(t)$  at the year  $t$ , can be calculated as (Zheng and Lai 2018):

$$C(t) = \sum_{t=1}^n \frac{B_t - M_t}{(1 + r)^t} \quad (4.5)$$

where  $r$ ,  $B_t$ ,  $M_t$ , and  $n$  are annual monetary discount rate, monetary benefit gained, maintenance cost, and number of years considered.

All construction, operation, maintenance activities will have environmental impacts as well which need to be considered in an MCDM framework. Based on the theorem of total probability, the sustainability function ( $M_S$ ) function can be expressed as a function of conditional consequence functions as follows (Belleri and Marini 2016; Ellingwood 2005):

$$M_S = \int_{IM} \int_{EDP} \int_{DS} C_{Cons|DS}(t) P_{DS|EDP}(t) P_{EDP|IM}(t) P_{IM}(t) dDS dEDP dIM \quad (4.6)$$

where  $C_{Cons|DS}(t)$ ,  $P_{DS|EDP}(t)$ ,  $P_{EDP|IM}(t)$ , and  $P_{IM}(t)$  are the conditional consequence given a damage state, the conditional probability of a damage state given the EDP, the conditional probability of an EDP given a hazard intensity, and the annual mean rate of occurrence of hazard  $IM$ , all at time  $t$ , respectively. The consequence functions,  $C_{Cons|DS}$ , are evaluated using the EIO-LCA model presented by Carnegie Mellon University (CMU GDI 2018). The EIO-LCA uses both environmental and historical economic data aiming to answer shortcomings of process-based LCA such as requiring heavy data, being time-consuming and expensive, and selecting proper system boundaries. EIO-LCA method provides more flexibility since it can effortlessly be used along with related studies in economics and insurance industry. EIO-LCA calculates the environmental consequences of the building construction, maintenance, and seismic repair using their corresponding cost. It considers both the direct impacts of the product/project and the indirect impacts in the supply chain (Ochoa et al. 2002).

### **4.2.2.3 Energy Consumption and Cost Analysis**

The whole-building energy analysis is performed in widely-used EnergyPlus (ASHRAE 2016a; Invidiata et al. 2018; Robati et al. 2017). Through concurrently solving the heat balance equations of thermal zones and plant systems of the building, EnergyPlus calculates energy consumption for indoor heating and cooling, water heating, ventilation, lighting, and plug and process loads (Crawley et al. 2001). EnergyPlus considers both source and site energy consumption in various units including kWh. The source energy is the energy used to generate the electricity, e.g. natural gas or coal, which has a significant impact on the GHG emissions due to energy consumption. The site energy is the energy consumed in the building in the form of electricity or natural gas. To estimate the current cost of energy, the yearly average price data is collected from (US BLS 2018) and future cost is discounted using Equation (4.5). National Institute of Standards and Technology (NIST) also provides the projected energy price indices and discount factors for life-cycle cost (LCC) analysis which is used to verify the cost estimation (Lavappa and Kneifel 2018).

## ***4.2.3 Multi-criteria Decision-making Module***

### **4.2.3.1 Trilateral Criteria/Attributes**

The effective metrics/attributes are categorized into three sets, i.e. resilience, sustainability, and energy, to match the RSEA module outputs creating a trilateral decision analysis framework. The set of resilience metrics incorporate three attributes which are asset, time, and life losses due to the hazard, here earthquake hazard. The seismic asset loss (AL) measured in US Dollars may include all direct and indirect monetary losses such as repair/replacement cost, closure cost, and relocation cost due to earthquake. The time loss (TL), commonly measured in number of days, is the time it takes for the building to return

to its original functionality after an extreme event. Depending on the system being studied, it may also be referred to as restoration or recovery time, or downtime. The life loss (LL) represents the social impacts of earthquake and is commonly measured in terms of number of casualties, injuries, fatalities, and if data is available number of Post-Traumatic Stress Disorder (PTSD) cases and displaced households. Note that all or some of these metrics can be included in the decision model depending on available data and project specification.

Sustainability involves social, economic, and environmental metrics. Given its overlap with resilience in this study, the emphasis for the sustainability submodule is on the environmental consequence and construction and maintenance costs. A component-level approach is recommended for initial construction cost (ICC) evaluation where the replacement cost of all structural, non-structural, and utility components of the building is included. ICC is also evaluated in US dollars. Cost of repairing and maintaining interior finishes, exterior closure, plumbing, conveying, fire, and electrical equipment, etc. due to aging is also an economic criterion of sustainability. Here, maintenance costs are evaluated in US dollars for a 50-year lifespan, abbreviated MC.

Moreover, an environmental loss (EL) due to construction, operation, maintenance, and seismic repair/replacement is considered. EL can be measured in terms of ton CO<sub>2</sub> equivalent GHG emission, m<sup>3</sup> or kGal water withdrawal, ton waste or pollution produced, etc. depending on the project requirement and/or decision maker's preference.

The third set of criteria includes energy-consumption metrics such as annual operational energy consumption in kWh or annual operational energy cost (OEC) in US

dollars. These metrics depend on construction materials, glazing type, and wall thickness, HVAC specification, age of the building, number of occupants, and maintenance/repair plan. These metrics are evaluated through whole-building simulation. Figure 4.3 depicts the three-level AHP model used and categorizes the trilateral sets of criteria/attributes considered. The AHP shows the relationship between the objective of the project, the criteria, and the alternative choices the decision maker has (Mateo 2012). The elements of each level need to be compared to each other from bottom to top to achieve the AHP-based goal. At the lowest level, the criteria are to be compared to each other to create pairwise comparison matrices. These matrices are used to find the importance/weight factors for each criterion compared to others. These factors are then used to evaluate the utility functions, as described in the next section.

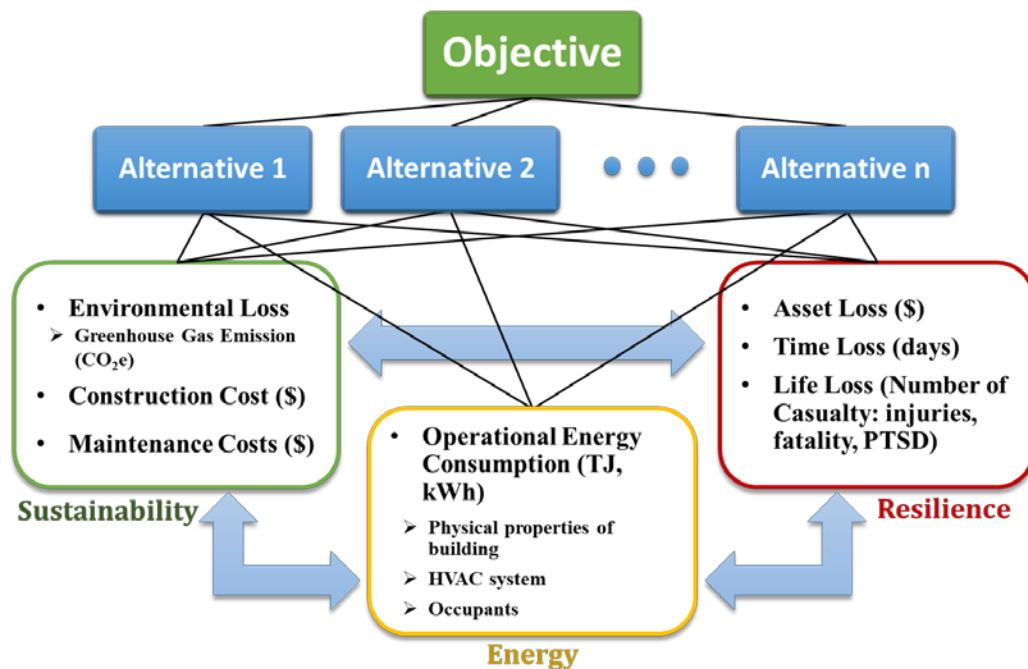


Figure 4.3 Analytic hierarchy model considered for decision analysis and the trilateral sets of criteria/attributes

#### 4.2.3.2 Multiple Criteria/Attribute Decision Making

In MAUT, utility functions measuring the preference over a set of criteria/attributes need to be defined for each alternative and each attribute. Utility takes a value of 0 (for the worst outcome) to 1 (for the best outcome). To achieve a risk-informed decision, utility can be defined with three attitudes towards risk: risk aversion, neutral (linear), and risk seeking. For risk neutral attitude the utility function ( $u_{ij}$ ) can be find as follows for a minimization criterion:

$$u_{ij(x)} = \frac{A_{max,i} - x_{ij}}{A_{max,i} - A_{min,i}} \quad (4.7)$$

where  $x_{ij}$  is the score (resilience, sustainability, or energy metric) for criteria/attribute  $i$  ( $i = 1, \dots, n$ ) and alternative  $j$  ( $j = 1, \dots, m$ ).  $A_{max,i}$  and  $A_{min,i}$  are the maximum and minimum scores evaluated for each  $i$  attribute among all  $m$  alternatives, respectively. For risk aversion and seeking utility functions an exponential equation is used (Ellingwood and Lee 2016; Lee et al. 2018; Wood and Khosravanian 2015):

$$u_{ij(x)} = \frac{1 - \exp(-r \times x_{ij})}{1 - \exp(-r)} \quad (4.8)$$

where  $r$  is a non-zero risk aversion factor. Positive values for  $r$  give convex functions (risk aversion) and negative  $r$  values give concave functions (risk seeking), as depicted in Figure 4.4.

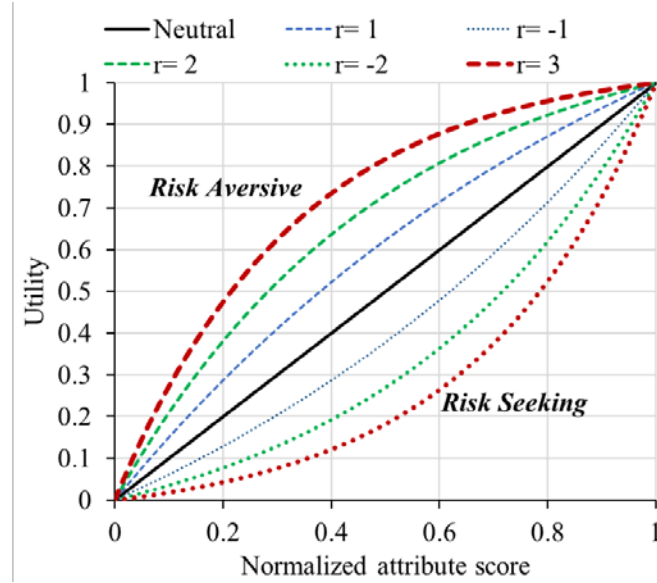


Figure 4.4 Utility curves with different attitude towards risk using exponential utility function adapted from (Wood and Khosravianian 2015)

As described, utility functions are developed for all outputs of the RSEA module. As is common with consequence functions, the additive model is used to formulate the total utility function. Assuming utility independence, the overall unilateral utility function is formed using the following formula (Ferreira et al. 2009):

$$U_{t,j} = \sum_{i=1}^n w_i u_{ij}(x) \quad i = 1, \dots, n; j = 1, \dots, m \quad (4.9)$$

where  $U_{t,j}$  is the total utility of alternative  $j$ , and  $w_i$  is the importance/weight factor ( $w_i$ ). Decision maker uses lotteries between pairs of criteria/attributes to find the  $w_i$ . The  $w_i$  values are assigned based on historical data, engineering judgment, and problem objective. Commonly, a numerical value between 1 (for equally important) to 9 (for absolutely more important) or their reciprocal is assigned to each pair of attributes to express the importance of one over the other. Similarly, 3, 5, and 7 mean objective  $i$  is weakly more important, strongly more important, and very strongly more important than objective  $j$ , respectively (Ferreira et al. 2009; Mateo 2012; Wallenius et al. 2008). For instance, if the objective of

the project is to minimize the asset loss, the decision maker compares the importance of the asset loss over the environmental loss and may assign a value of 9 to their pair to express absolute importance of the former over the later.

#### **4.2.3.3 Objectives, Scenarios and Weight Factors**

A major advantage of multi-criteria decision models is their flexibility to deal with various decision scenarios, objectives, and criteria. Here, seven scenarios with different objectives are studied: (1) minimum asset loss (AL), (2) minimum time loss (TL), (3) minimum life loss (LL), and (4) minimum environmental loss (EL), (5) maximum resilience, (6) minimum annual operational energy cost (OEC), and (7) neutral scenarios. An example for Scenario 1, minimum AL, is a case where significantly valuable properties exists in the building, e.g. a warehouse with expensive stored asset. Scenario 2, minimum TL, applies to cases where the downtime is significantly costly and/or building should remain functional after an extreme event, e.g. building is a hospital. Minimum LL, the objective of Scenario 3, is the primary goal of current design codes and is important particularly if a large number of people will reside or work in the building, for example if the building is a school. Scenario 4, minimum EL, is considered for a situation where due to client's requirements or official regulations the building should be eco-friendly. For Scenario 5, overall resilience of the building is the objective. Scenario 6 represents a case in a cold region with low seismicity where cost of energy is extremely high. For Scenario 7, all criteria/attributes have the same importance. The last scenario is assumed for comparison only.

Given the number of criteria involved and the interdependency between them, pair-wise lotteries are used to find the  $w_i$  for each criterion over the others for various scenarios.

Following previous studies on multi-criteria decision analysis (Ellingwood and Tekie 1999; Zavadskas et al. 2007), a survey was conducted among experts to find the  $w_i$  values. Participants include civil engineers, graduate students, and faculty members who were selected due to their familiarity with the topic. Participants were asked to select a weight factor to best represent the main goal of each scenario. The mean weight factor obtained from the survey is used, ignoring the upper and lower bounds of the data. Tables 4.1-4.6 lists the pairwise comparison matrices and the weight factors for Scenarios 1-6, respectively. The  $w_i$  values for Scenario 7 are all 1/7.

Table 4.1 Pairwise comparison matrix for Scenario 1- minimum asset loss

Criteria	AL	TL	LL	EL	ICC	OEC	MC	$w_i$ for S1
AL	1	5	3	5	5	5	5	0.365
TL	1/5	1	1/3	2	2	3	2	0.103
LL	1/3	3	1	7	7	7	7	0.300
EL	1/5	1/2	1/7	1	2	3	2	0.082
ICC	1/5	1/2	1/7	1/2	1	1/2	1	0.045
OEC	1/5	1/3	1/7	1/3	2	1	2	0.059
MC	1/5	1/2	1/7	1/2	1	1/2	1	0.045

Table 4.2 Pairwise comparison matrix for Scenario 2- minimum time loss

Criteria	AL	TL	LL	EL	ICC	OEC	MC	$w_i$ for S2
AL	1	1/2	1/2	3	3	3	3	0.155
TL	2	1	3	4	4	5	4	0.312
LL	2	1/3	1	6	7	7	7	0.298
EL	1/3	1/4	1/6	1	2	2	2	0.078
ICC	1/3	1/4	1/7	1/2	1	1/2	1	0.047
OEC	1/3	1/5	1/7	1/2	2	1	2	0.062
MC	1/3	1/4	1/7	1/2	1	1/2	1	0.047

Table 4.3 Pairwise comparison matrix for Scenario 3- minimum life loss

Criteria	AL	TL	LL	EL	ICC	OEC	MC	$w_i$ for S3
AL	1	3	1/4	3	3	3	3	0.171
TL	1/3	1	1/7	1	2	2	2	0.084
LL	4	7	1	8	8	8	8	0.499
EL	1/3	1	1/8	1	2	3	2	0.091
ICC	1/3	1/2	1/8	1/2	1	1/2	1	0.046
OEC	1/3	1/2	1/8	1/3	2	1	2	0.063
MC	1/3	1/2	1/8	1/2	1	1/2	1	0.046

Table 4.4 Pairwise comparison matrix for Scenario 4- minimum environmental loss

Criteria	AL	TL	LL	EL	ICC	OEC	MC	$w_i$ for S4
AL	1	3	1	1/4	3	2	3	0.158
TL	1/3	1	1/2	1/3	2	2	2	0.096
LL	1	2	1	1/3	6	6	6	0.225
EL	4	3	3	1	5	5	5	0.359
ICC	1/3	1/2	1/6	1/5	1	1/2	1	0.047
OEC	1/2	1/2	1/6	1/5	2	1	2	0.069
MC	1/3	1/2	1/6	1/5	1	1/2	1	0.047

Table 4.5 Pairwise comparison matrix for Scenario 5- maximum resilience

Criteria	AL	TL	LL	EL	ICC	OEC	MC	$w_i$ for S5
AL	1	3	1	4	4	4	4	0.273
TL	1/3	1	1	2	3	3	3	0.160
LL	1	1	1	7	7	7	7	0.323
EL	1/4	1/2	1/7	1	2	3	2	0.088
ICC	1/4	1/3	1/7	1/2	1	1/2	1	0.046
OEC	1/4	1/3	1/7	1/3	2	1	2	0.063
MC	1/4	1/3	1/7	1/2	1	1/2	1	0.046

Table 4.6 Pairwise comparison matrix for Scenario 6- minimum operational energy cost

Criteria	AL	TL	LL	EL	ICC	OEC	MC	$w_i$ for S6
AL	1	2	1/5	2	1/2	1/7	1/2	0.064
TL	1/2	1	1/5	1/2	1/2	1/7	1/2	0.040
LL	5	5	1	3	7	1	7	0.317
EL	1/2	2	1/3	1	1	1/8	1	0.065
ICC	2	2	1/7	1	1	1/6	1	0.070
OEC	7	7	1	8	6	1	6	0.373
MC	2	2	1/7	1	1	1/6	1	0.070

### 4.3 Case Studies

#### 4.3.1 Design and Numerical Modeling of Archetype RC Buildings

Two groups of typical RC shear wall archetype buildings located in downtown Los Angeles, CA and Boston, MA are considered. Three different configurations are considered for each group to represent typical shear wall ratio of RC buildings. The LA site is selected for its extreme seismic activity but warm weather with  $S_s$ , spectral response acceleration at 0.2 sec, and  $S_1$ , spectral response acceleration at 1 sec, of 2.481g and 0.862g, respectively, and ground snow load of 0 to 5 psf (0.24 kN/m<sup>2</sup>). The Boston site is selected

for its low seismicity but cold weather requiring considerable energy consumption, where  $S_s$  and  $S_I$  are 0.217g and 0.069g, respectively, and snow load of 40 psf (1.92 kN/m<sup>2</sup>). Figure 4.5 shows the typical floor plans adapted from AlHamaydeh et al. (AlHamaydeh et al. 2017a). The building footprint is 30 m × 30 m, with 6 m long spans. The typical story height is 4 m. Two types of window glazing configurations, i.e., a double glazing (BG) and a low-e triple glazing (HG), are considered. The double glazing represents the base line and the triple low-e glazing represents a high-performance energy saving glazing. Archetypes are labeled based on location, configuration, and glazing type. For example, LA-SF-BG is the archetype located in LA with a Special RC Moment Frame and base glazing. Similarly, B-SWm-HG is the archetype located in Boston with a shear wall in the middle of outer frames (see Figure 4.5 (c)) and high-performance glazing.

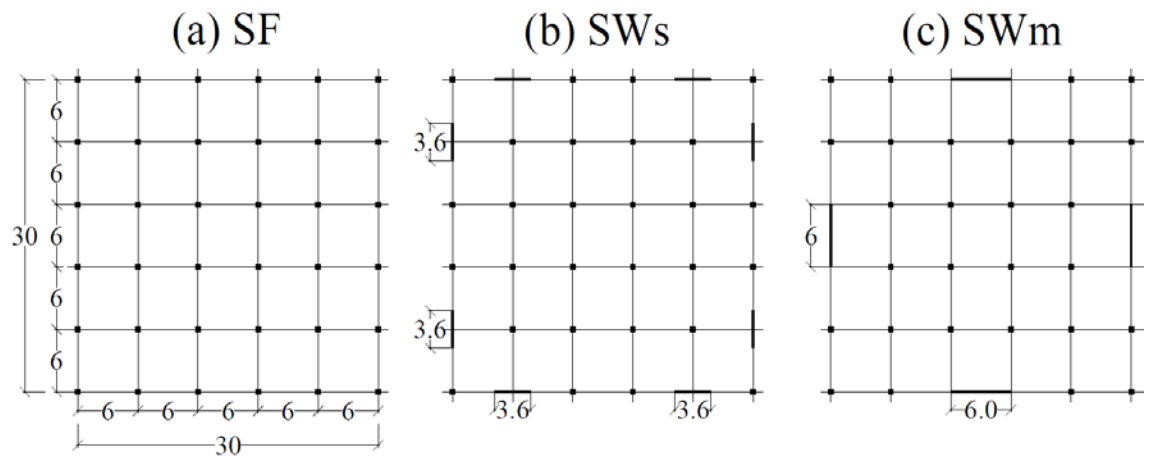


Figure 4.5 Floor plans of archetype RC building with different shear wall ratios, (a) SF archetype with no shear wall, (b) SWs archetype with 2 shear walls, and (c) SWm archetype with one shear wall on each side (dimensions are in meters)

Structures are designed based on ACI 318-14 (2014) and ASCE7-16 (2017a). The designed RC frames are modeled in OpenSees (Mazzoni et al. 2006) as planar frames using fiber elements for beams and columns and SFI-MVLEM elements for shear walls. The SFI-MVLEM element recently developed by Kolozvari et al. (2014) captures nonlinear

interaction between shear and axial/flexural behavior of RC walls and columns under cyclic loading. Models are validated with Tran and Wallace (2015) experiment on RC shear walls.

#### ***4.3.2 Specifications for Life-cycle Cost Analysis***

The construction cost is calculated using Building Construction category of RSMeans (2018) considering both material and labor costs. The non-structural construction costs include the cost of exterior items such as windows and curtain walls as well as interior items such as partitions and ceiling. Installation costs of windows are also estimated per RSMeans (2018), and glazing material costs differences are considered using Building Energy Optimization Tool (BEOpt) (Christensen et al. 2006). For maintenance costs, a commercial building template of Whitestone cost reference (Abate et al. 2009) is adapted given the occupancy of the buildings. It considers annual repair costs and periodic replacement costs of various structural and non-structural components. For instance, the replacement period, i.e. life, of the glazing material is presumed 30 years and windowed curtain walls are assumed to have an annual cleaning/washing fee of 0.1 \$/ft<sup>2</sup> in LA, and 0.11 \$/ft<sup>2</sup> in Boston to account for slightly higher labor cost in Boston.

The seismic monetary loss is estimated as a Cumulative Distribution Function (CDF) of repair cost due to earthquake. The replacement cost is based on the construction cost estimated by RSMeans database (2018). This value includes the structure, exterior closure, and utility infrastructure and is called the core and shell replacement cost. To account for tenant improvements and asset, this value is increased by 25% following FEMA P-58 assumptions for its example buildings (FEMA 2012). For estimating the downtime, a Total Replacement Time (TRT) of 720 days is considered. The maximum number of workers for

repair is assumed 0.002 per ft<sup>2</sup> equal to 1 worker per 500 ft<sup>2</sup> (1 worker per 46.45 m<sup>2</sup>) per FEMA recommendations (FEMA 2012). The initial construction, total replacement, and 50-year cumulative maintenance costs are presented in Table 4.7.

Table 4.7 Estimated life-cycle cost of studied archetypes

<b>Archetype</b>	<b>Initial Construction Cost (1000\$)</b>	<b>Total Replacement Cost (1000\$)</b>	<b>Cumulative Maintenance Cost in 50 years (1000\$)</b>
LA-SF-BG	7,962	9,954	3,249
LA-SF-HG	8,190	10,238	3,363
LA-SWm-BG	8,248	10,310	3,249
LA-SWm-HG	8,475	10,594	3,363
LA-SWs-BG	8,388	10,485	3,249
LA-SWs-HG	8,615	10,769	3,363
B-SF-BG	7,796	9,746	3,254
B-SF-HG	8,026	10,033	3,369
B-SWm-BG	8,053	10,066	3,254
B-SWm-HG	8,283	10,353	3,369
B-SWs-BG	8,121	10,151	3,254
B-SWs-HG	8,351	10,439	3,369

The main non-structural components considered in seismic loss estimation include two hydraulic elevators, one 350-Ton (BTU/hr/12,000) chiller and air-handling unit on the roof, and a seismically-rated independent pendant lighting for each 4-sq. m of the floor, perimeter stick-built curtain wall, interior gypsum wall partitions with metal studs, seismically-rated raised access floor and suspended ceiling, and fire sprinkler. FEMA P-58 typically uses practical EDPs such as maximum interstory drift ratio (IDR) and maximum absolute floor acceleration (ACC) to catalogue damage state of structural and non-structural components. FEMA P-58 database is used to define the fragility specification for each component.

### ***4.3.3 Energy Analysis Settings***

Each floor of the archetype buildings is divided into nine thermal zones to study the influence of the shear wall distributions and building orientation on energy consumption and thermal comfort. The three-dimensional (3D) view of the special frame (SF) building and its thermal zones include a core of 18 m × 18 m at the center and eight boundary zones on the perimeter of the building, as shown in Figure 4.6. The envelope, floor, HVAC, fenestration, etc. are designed per ASHRAE 90.1 requirements for the climate zones 3B (LA) with a Mediterranean climate and 5A (Boston) characterized by its cold and humid climate (ASHRAE 2016b; a). The occupancy, lighting, equipment, ventilation and HVAC settings and schedules are adapted from ASHRAE reference building for middle and large office (ASHRAE 2016a). Following previous studies, the whole building architecture is modeled in DesignBuilder (DesignBuilder 2016) to create the input files for EnergyPlus (Crawley et al. 2001). The building has an occupancy of 18.51 m<sup>2</sup>/person and lighting and office equipment intensities of 10.76 and 8.08 W/m<sup>2</sup>, respectively. The HVAC system is a variable air volume (VAV) with reheat system. The AC heating and cooling setpoint temperature are 21.1°C (70°F) and 23.9°C (75°F) with heating back temperature of 15.6°C (60°F) and 29.4°C (85°F), respectively. The weather data of the Los Angeles International Airport (WMO #722950) and Boston-Logan International Airport (WMO #725090) are used as the input, which provides the seasonal temperature variations and precipitation schedules needed for building energy analysis.

Glazing materials play a critical role in the energy efficiency of window curtain wall buildings (Carmody and Haglund 2012). Solar heat gain coefficient (SHGC) and U-factor are the two most important parameters that differentiate window assemblies. While SHGC

controls the transmission of solar heat through a window assembly, the U-factor dictates the heat loss/gain of it. Lower U-factor can efficiently reduce the heat flow between indoor and outdoor space, and therefore saving energy consumption. Two types of glazing materials, i.e. double glazing and triple low-E glazing are studied. Their solar thermal properties and costs are listed in Table 4.8. The double-glazing represents a base case (BG) and costs of 267 \$/m<sup>2</sup>, while the triple low-E glazing represents a high-performance case (HG) and costs of 394 \$/m<sup>2</sup> (Christensen et al. 2006). For estimating CO<sub>2</sub> equivalent due to energy generation, the site energy (i.e. energy consumed by building) is converted into source energy using EnergyPlus conversion factors, which are 3.167 and 1.084 for electricity and natural gas, respectively.

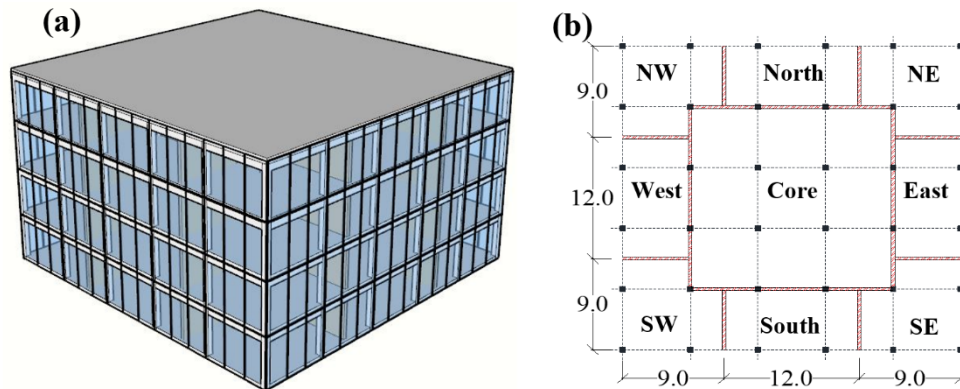


Figure 4.6 (a) SF archetype 3-dimensional (3D) view built in DesignBuilder and (b) Typical thermal zone designation for all archetypes (dimensions in meters)

Table 4.8 Window glazing properties and costs

Glazing	SHGC <sup>a</sup>	Direct solar transmission	Light transmission	U-factor (m <sup>2</sup> -K/W)	Cost (\$/m <sup>2</sup> )
Double glazing	0.25	0.21	0.31	2.58	267
Triple low-E glazing	0.14	0.07	0.30	1.07	394

a SHGC = Solar Heat Gain Coefficient

#### 4.3.4 Vulnerability Assessment

For dynamic analyses in OpenSees, a set of 22 far-field (located at greater than or equal to 10 km from the fault rupture site) ground motions recommended by FEMA P-695 (ATC 2009) for collapse analysis are used. Records are on soft rock and stiff soil (Site Class C and D) with magnitudes between M6.5 and M7.6 taken from 14 different events. The records are normalized with respect to PGV and scaled such that the median spectrum of the record set matches design response spectrum (ASCE 2017a; ATC 2009).

Incremental Dynamic Analysis (IDA), a widely-accepted method to study the record-to-record variability of earthquake hazard, is used to evaluate performance and collapse capacity of the archetypes (Azarbakht and Dolšek 2010). The collapse capacity,  $\hat{S}_{CT}$ , obtained from IDA is used to find the empirical CDF of collapse fragility functions. Then, maximum likelihood method is used to fit a lognormal distribution function over the empirical CDF. The empirical CDF and the fitted lognormal collapse curve are illustrated in Figure 4.7 for various archetypes where horizontal axis shows the normalized pseudo-spectral acceleration based on 5% damped design spectra for the region at the fundamental period of the building structure, i.e.  $S_d(T_1, 5\%)$ . Table 4.9 also summarizes the expected collapse capacity and IDR and their logarithmic dispersion ( $\beta$ ). All archetypes marginally satisfy ASCE7-16 (ASCE 2017a) requirement for conditional probability of failure caused by the maximum considered earthquakes (MCE), which is 10% for risk category of I. Note that the glazing type of curtain walls are assumed to have little impact on the collapse capacity.

Table 4.9 Expected collapse capacity and collapse IDR and their corresponding logarithmic dispersion

Archetype	$S_{CT}(T_1,5\%)$ (g)	$\beta_{S_{CT}}$	Collapse IDR (%)	$\beta_{IDR}$
LA-SF	2.98	0.51	7.13	0.46
LA-SWm	3.17	0.71	0.82	0.87
LA-SWs	3.13	0.59	0.79	0.63
B-SF	0.97	0.84	6.55	0.66
B-SWm	1.34	0.81	0.71	1.08
B-SWs	1.32	0.61	0.85	0.46

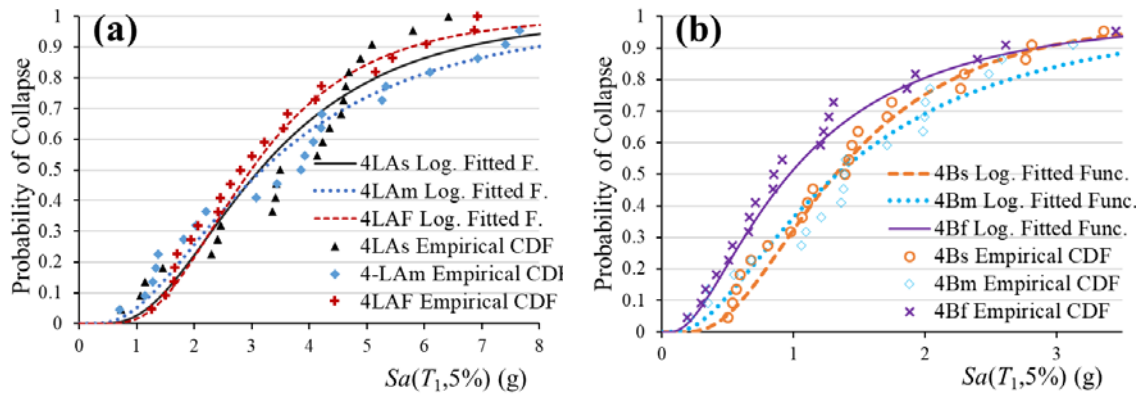


Figure 4.7 Empirical CDF of  $Sa(T_1,5\%)$  and fitted lognormal fragility functions for (a) LA and (b) Boston archetypes

### 4.3.5 Seismic Loss Estimation

FEMA PACT database of fragility parameters, repair cost/time, casualty and fatality consequence function for various structural and non-structural components is used to perform Monte Carlo simulations for loss estimation (FEMA 2012). The resiliency metrics including the component-level direct economic loss, downtime, and number of casualty (injuries and fatality) caused by intensity-based and time-based earthquake hazard are evaluated. The direct economic loss is calculated as the summation of repair/replacement costs of all structural and non-structural components. Similarly, the downtime is the summation of repair time required for all components on each floor. Two repair planning

schemes: slow-track (serial planning) and fast-track (parallel planning) are considered for downtime analysis. As noted, a commercial population model is considered for the building to estimate the casualty. Considering the unoccupied areas such as utility and mailing room, 1/3 of the first floor and 1/6 of other floors are assumed unoccupied (Han et al. 2016). The component-level casualty consequence functions of FEMA PACT are used for casualty estimation.

Time to repair the damages caused by earthquake and restore the functionality of the building is a main indicator of robustness and resilience of the system. Figures 4.8 and 4.9 depict the cumulative annual repair time and number of injuries for various archetypes considering a fast-track repair scheme, respectively. As expected, earthquake causes an insignificant annual loss for Boston archetypes compared to LA ones. For instance, the annual probability of repair time exceeding 10 days for B-SF-BG archetype is about 0.00047, much smaller than that of corresponding LA case (LA-SF-BG) which is 0.078. As shown in Figure 4.8 and 4.9, glazing type has little impact on repair time and casualty. It has a minor impact on repair cost, however.

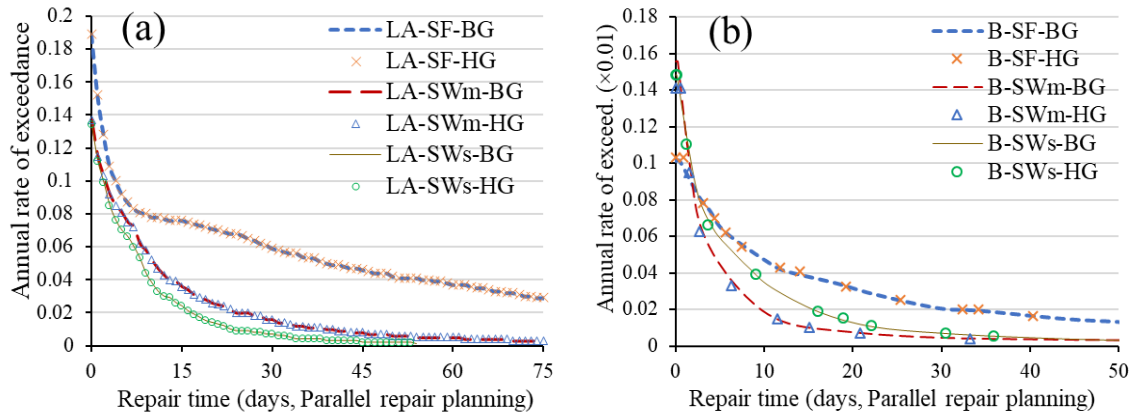


Figure 4.8 Cumulative annual repair time for various (a) LA and (b) Boston archetypes

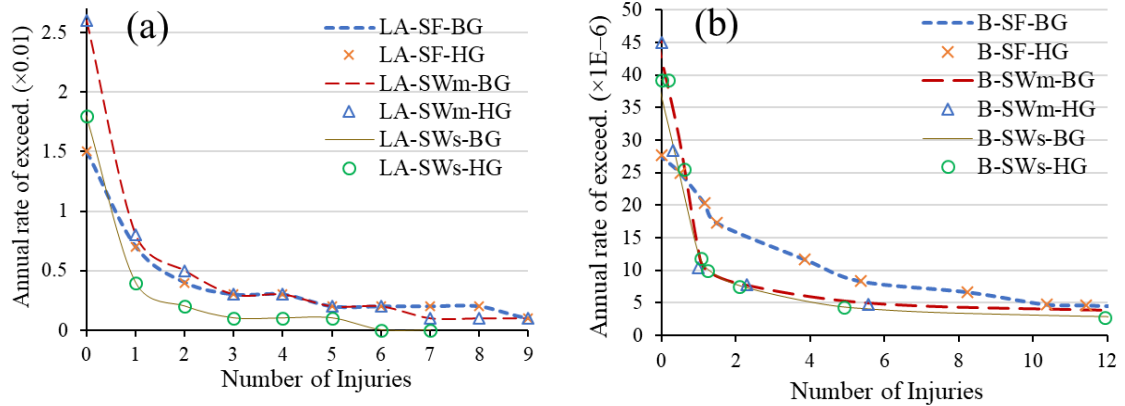


Figure 4.9 Cumulative annual number of injuries for various (a) LA and (b) Boston archetypes

Shear walls have a major impact on all losses. In both cities, framed RC buildings require a longer repair/replacement time compared to shear wall archetypes. This is true for repair/replacement costs as well, but not for injuries and fatalities due to earthquake. RC framed buildings, SF archetypes, has much smaller lateral stiffness compared to the shear wall RC buildings. This leads to a noticeable increase in IDR and considerable damage to non-structural components even in low seismic intensities (0.05-0.2g) as shown in Figure 4.10. Figure 4.10 shows the annual rate of exceedance of repair cost and fatalities for LA-SF-BG archetype. The horizontal axes show the earthquake intensity in terms of  $S_d(T_1,5\%)$  and the loss in terms of repair cost (Figure 4.10 (a)) or number of fatalities (Figure 4.10 (b)). As depicted, most of the monetary loss and downtime of RC buildings at a high seismic region like LA is due to low- to mid-intensity earthquakes with  $S_d(T_1,5\%)$  between 0.1-0.6g. Note that while the ground motion intensity is not significant in that range, the mean annual frequency of exceedance (MAFE) of that intensity range is significant, i.e. about 0.02 or a return period of 50 years. At low to mid intensities, non-structural components such as wall partitions and suspended ceilings are the main contributor to the loss and casualty.

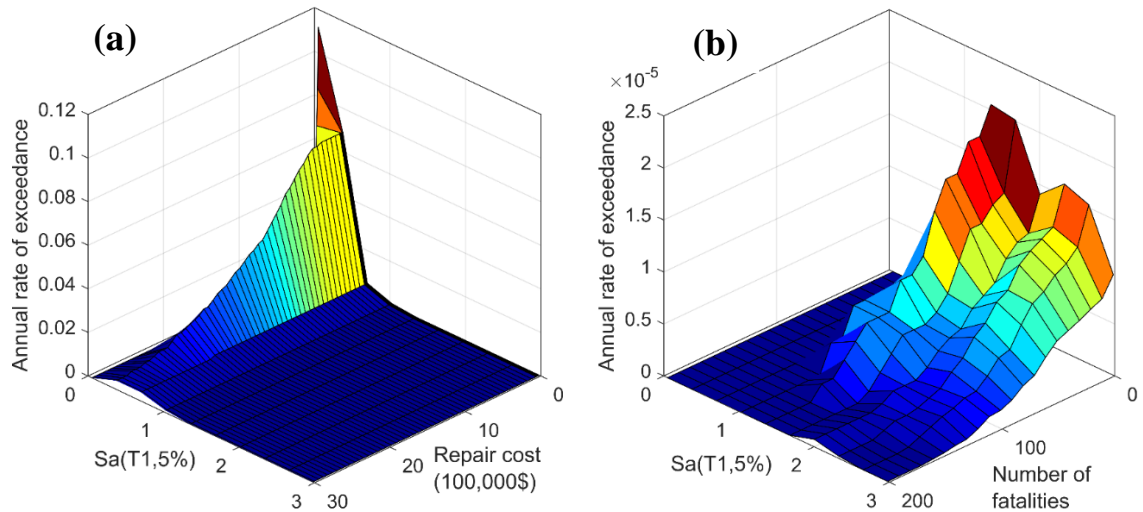


Figure 4.10 Annual rate of exceedance of (a) repair cost and (b) fatalities for LA-SF-BG archetype

#### 4.3.6 Energy Cost Analysis and CO<sub>2</sub> eq Emissions

The whole building energy analysis is performed in EnergyPlus (Crawley et al. 2001) and the annual energy consumptions are obtained. Figure 4.11 compares the energy consumption for HVAC cooling and heating, lighting, and equipment for various archetypes of LA and Boston. As depicted, heating constitutes the major part of annual energy use in Boston while cooling is a significant end use for both sites. The RC framed buildings consume noticeably more energy for both cooling and heating (16% and 14% less on average for LA and Boston buildings with BG, respectively). The difference is less significant for HG, high performance glazing, though (6% and 9% less HVAC energy use on average for LA and Boston buildings with HG, respectively). This is mainly caused by the combined effects of the thermal mass and shading effects of shear walls. It highlights the positive influence of shear walls on energy consumption in addition to their advantages in terms of structural performance and overall monetary loss and downtime, as discussed earlier. Yet, the energy use for lighting increases in shear wall buildings since solid shear walls reduce the natural lights entering the building. Given that lighting is a minor part of

annual energy use compared to HVAC, shear walls archetypes have a clear advantage in terms of energy consumption. In general, SWs archetypes show smaller energy use for HVAC than SWm archetypes. However, this difference is also slightly diminished by the increase in energy use for lighting. Table 4.10 summarizes the energy consumption and cost and CO<sub>2</sub> eq emission due to energy consumption for various archetypes.

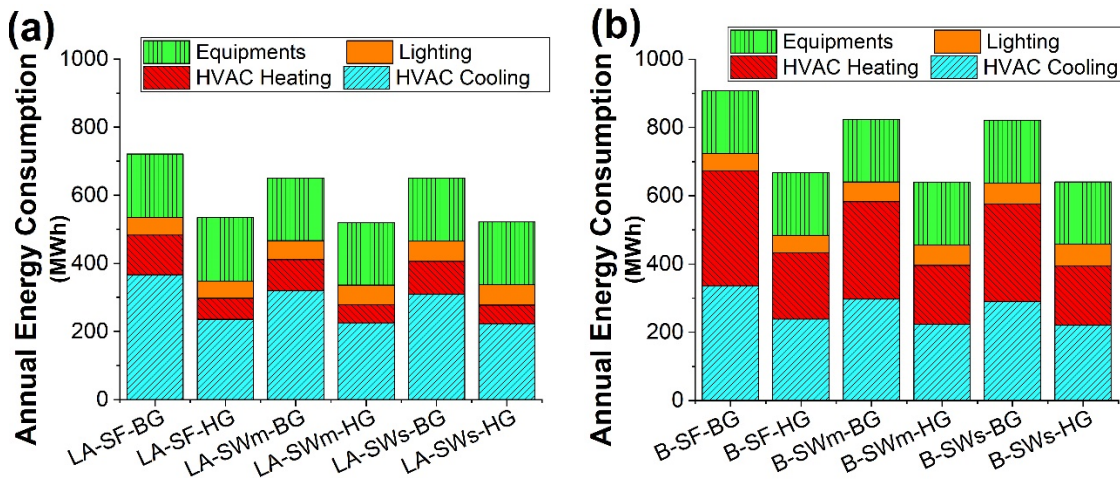


Figure 4.11 Annual energy consumptions for various archetype buildings in regions: (a) Los Angeles and (b) Boston

Table 4.10 Annual energy consumption, cost, and CO<sub>2</sub> eq emission due to energy consumption for various archetypes

Archetype	Consumption (MWh)	Cost (1000\$)		CO <sub>2</sub> eq (ton)
		Electricity	Natural Gas	
LA-SF-BG	721	109	5	177
LA-SF-HG	533	85	3	133
LA-SWm-BG	651	101	4	162
LA-SWm-HG	522	85	2	130
LA-SWs-BG	650	100	4	161
LA-SWs-HG	524	85	2	131
B-SF-BG	907	125	15	316
B-SF-HG	670	104	9	247
B-SWm-BG	826	118	13	293
B-SWm-HG	641	103	8	240
B-SWs-BG	823	117	13	291
B-SWs-HG	643	103	8	240

Figure 4.12 depicts the annual energy costs due to various uses for various archetypes. Due to difference in type of energy (i.e. electricity or gas) used, the energy cost of heating is noticeably smaller than energy cost of cooling. Similar to energy consumption, the buildings with shear wall show smaller overall energy cost compared to framed buildings for both sites. The difference is more significant for Boston, particularly for heating cost. Considering the source and type of energy in LA and Boston, the annual CO<sub>2</sub> eq emission due to energy used is also presented in Table 4.10.

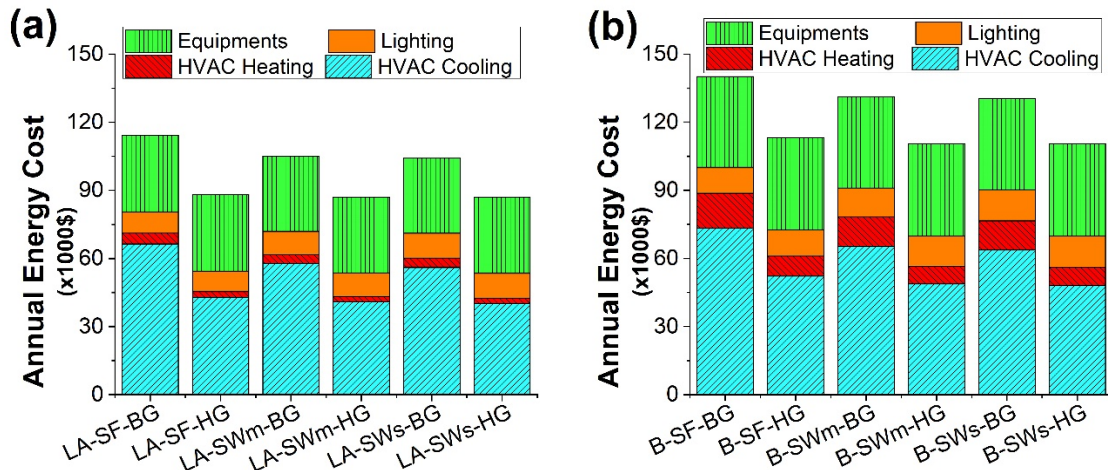


Figure 4.12 Annual energy costs for various archetype buildings in regions: (a) Los Angeles and (b) Boston

The properties of the glazing determine the solar heat gain, direct solar transmission, and light transmission of heat and light from windows. Note that glazing significantly affects the heating and cooling energy use, energy cost, and CO<sub>2</sub> eq emission. Using high-performance triple low-e glazing (i.e. HG cases) reduces the energy use, cost, and CO<sub>2</sub> eq emission between 27-38% compared to double glazing (i.e. BG cases) for HVAC heating and cooling. As such, while glazing has little impact on resilience, it has a significant impact on sustainability and energy consumption. These conflicting attributes of BG and HG archetypes can be better studied in a multi-criteria decision-making framework.

### ***4.3.7 Risk-informed Multi-Criteria Decision Making***

The proposed decision model is used to find the optimal choice among all design alternatives. All criteria quantified in the RSEA module are the input parameters of the decision-making module, listed in Tables 4.11 and 4.12 for LA and Boston archetypes, respectively. Here, asset loss (AL) is the monetary cost of repair/replacement due to earthquakes and time loss (TL) is repair/replacement time required for restoring the building to its original condition. For life loss (LL), the weighted addition method is used to combine the annual injury and fatality outputs (Mateo 2012). To reflect the significance of fatality over injuries in total LL, a weight factor of 15 is assumed for fatalities. This factor is based on the difference between fatality comprehensive cost and mean injury comprehensive cost suggested by (FHWA 1994; Sutley et al. 2016a). Environmental loss (EL) is the GHG emissions due to initial construction, seismic repair/replacement, maintenance activities, and operational energy consumption. Initial construction cost (ICC), quantified using RSMeans LCC estimator, is the construction cost of all structural and non-structural components including substructure, shell, interiors, services, and other equipment. Operational energy cost (OEC) is the life-cycle cost of energy consumed for heating, cooling, lighting, and equipment considering a 50-year life-cycle. MC is the life-cycle cumulative cost of maintaining the building including its plumbing, conveying, fire, electrical equipment, interior finishes, exterior closure, etc. given they are aging and require periodic inspection and maintenance to function.

Risk is also incorporated in the decision model through the decision maker's attitudes towards risk, which can be risk aversion, neutral, or risk seeking. Based on the objective/s of the project, the decision maker may take or avoid a certain level of risk in decision

analysis. This improves the adaptability of the model in dealing with subjective and conflicting criteria and provides new avenues to stakeholders in risk and resource management. The level of risk can be adjusted with factor  $r$  in Equation (4.8). Figure 4.13 and Tables 4.11 and 4.12 show the total utility ( $U_i$ ) scores for various cases studied. For demonstration, an  $r$  factor of 2 is used in these Tables and Figure.

For most scenarios, the RC buildings with two shear walls (SWs-BG and SWs-HG archetypes) are the best alternatives as they achieved the highest scores. This is mostly due to their small seismic loss (monetary cost, downtime, and casualty) as well as their comparable energy costs compared to other archetypes. They have the least AL, TL, and LL making them the best alternative for LA site. From a sustainability viewpoint, the initial construction cost of archetypes with shear wall is slightly larger than framed buildings (up to 5%), however. In an MCDM framework, all these conflicting outputs can be taken into account, systematically. As such, the minor difference in initial cost does not affect the overall utility score. Note that the significant thermal mass of shear walls helps with energy consumption as well reducing the cost of operational energy and improves the scores for SWs and SWm alternatives.

Table 4.11 Evaluation matrix obtained from RSEA module and total utility ( $U_i$ ) scores for various scenarios with risk averse (RA), neutral (N), and risk seeking (RS) attitudes for LA archetypes

Criteria	LA-SF-BG		LA-SF-HG		LA-SWm-BG		LA-SWm-HG		LA-SWs-BG		LA-SWs-HG							
	Annual Seismic Resilience Criteria																	
AL (10 <sup>3</sup> \$)	148.4		153.8		50.6		50.8		31.8		32.0							
TL (Days)	7.126		7.130		2.276		2.276		1.477		1.477							
LL (# of Casualties)	0.050		0.050		0.078		0.078		0.036		0.036							
Life-cycle Environmental Criteria due to Construction, Maintenance, Repair, and Energy Use																		
EL (ton CO <sub>2</sub> e)	4,690		4,820		4,860		4,990		4,940		5,070							
EL - Const.	6,660		6,900		3,610		3,680		3,020		3,100							
EL - M & R <sup>a</sup>	41,761		32,494		38,539		32,156		38,261		32,169							
Life-cycle Construction, Maintenance, and Repair Cost and Energy Criteria																		
ICC (10 <sup>3</sup> \$)	7,963		8,190		8,248		8,475		8,388		8,615							
OEC (10 <sup>3</sup> \$)	4,627		3,555		4,251		3,513		4,221		3,513							
MC (10 <sup>3</sup> \$)	3,249		3,363		3,249		3,363		3,249		3,363							
Total utility ( $U_i$ ) scores with risk averse (RA), neutral (N), and risk seeking (RS) attitudes																		
Scenarios	RA			N			RS			RA			N			RS		
	RA	N	RS	RA	N	RS	RA	N	RS	RA	N	RS	RA	N	RS	RA	N	RS
S1	0.380	0.303	0.223	0.421	0.340	0.239	0.615	0.527	0.416	0.600	0.544	0.464	0.938	0.895	0.856	0.909	0.909	0.909
S2	0.361	0.296	0.222	0.421	0.340	0.240	0.617	0.531	0.422	0.601	0.547	0.468	0.937	0.894	0.854	0.906	0.906	0.906
S3	0.529	0.425	0.305	0.601	0.480	0.331	0.424	0.353	0.272	0.413	0.377	0.329	0.934	0.888	0.845	0.908	0.908	0.908
S4	0.299	0.248	0.191	0.609	0.494	0.347	0.618	0.484	0.340	0.682	0.639	0.578	0.868	0.761	0.654	0.906	0.906	0.906
S5	0.392	0.316	0.233	0.450	0.363	0.255	0.591	0.505	0.397	0.578	0.526	0.450	0.934	0.889	0.847	0.907	0.907	0.906
S6	0.414	0.351	0.275	0.751	0.657	0.535	0.482	0.356	0.239	0.564	0.539	0.511	0.805	0.687	0.585	0.859	0.859	0.859
S7	0.420	0.386	0.348	0.506	0.423	0.319	0.707	0.583	0.448	0.612	0.554	0.486	0.849	0.750	0.661	0.714	0.714	0.714

a Environmental consequences due to maintenance activities and seismic damage repair

b Environmental consequences due to operational energy use

Table 4.12 Evaluation matrix obtained from RSEA module and total utility ( $U_t$ ) scores for various scenarios with risk averse (RA), neutral (N), and risk seeking (RS) attitudes for Boston archetypes

Criteria	B-SF-BG		B-SF-HG		B-SWm-BG		B-SWm-HG		B-SWs-BG		B-SWs-HG							
	Annual Seismic Resilience Criteria																	
AL (10 <sup>3</sup> \$)	0.4864		0.5046		0.3173		0.3217		0.3409		0.3440							
TL (Days)	0.0255		0.0255		0.0163		0.0163		0.0164		0.0164							
LL (# of Casualties)	4.47E-4		4.48E-4		4.96E-4		4.98E-4		3.87E-4		3.91E-4							
Life-cycle Environmental Criteria due to Construction, Maintenance, Repair, and Energy Use																		
EL (ton CO <sub>2e</sub> )	4,590		4,730		4,740		4,880		4,780		4,920							
EL - Const.	2,050		2,120		2,040		2,110		2,040		2,110							
EL - M & R <sup>a</sup>	48,740		40,299		45,970		39,593		45,670		39,601							
Life-cycle Construction, Maintenance, and Repair Cost and Energy Criteria																		
ICC (10 <sup>3</sup> \$)	7,796		8,026		8,053		8,283		8,121		8,351							
OEC (10 <sup>3</sup> \$)	5,734		4,612		5,359		4,500		5,326		4,500							
MC (10 <sup>3</sup> \$)	3,254		3,369		3,254		3,369		3,254		3,369							
Scenarios	Total utility ( $U_t$ ) scores with risk averse (RA), neutral (N), and risk seeking (RS) attitudes																	
	RA	N	RS	RA	N	RS	RA	N	RS	RA	N	RS	RA	N	RS	RA	N	RS
S1	0.374	0.264	0.173	0.379	0.292	0.202	0.634	0.585	0.547	0.618	0.606	0.592	0.905	0.832	0.747	0.887	0.845	0.777
S2	0.333	0.246	0.169	0.379	0.291	0.202	0.636	0.587	0.549	0.619	0.610	0.602	0.914	0.855	0.795	0.893	0.869	0.829
S3	0.473	0.337	0.215	0.529	0.393	0.259	0.437	0.381	0.338	0.420	0.411	0.403	0.908	0.847	0.786	0.893	0.865	0.816
S4	0.282	0.212	0.152	0.609	0.527	0.432	0.568	0.458	0.371	0.692	0.683	0.675	0.787	0.665	0.555	0.894	0.873	0.836
S5	0.373	0.267	0.178	0.405	0.312	0.216	0.607	0.556	0.515	0.594	0.584	0.572	0.904	0.835	0.760	0.889	0.854	0.798
S6	0.374	0.292	0.217	0.698	0.583	0.454	0.472	0.351	0.255	0.560	0.550	0.542	0.780	0.657	0.553	0.852	0.838	0.813
S7	0.414	0.365	0.324	0.490	0.411	0.321	0.693	0.594	0.510	0.606	0.586	0.570	0.817	0.705	0.602	0.705	0.686	0.656

a Environmental consequences due to maintenance activities and seismic damage repair

b Environmental consequences due to operational energy use

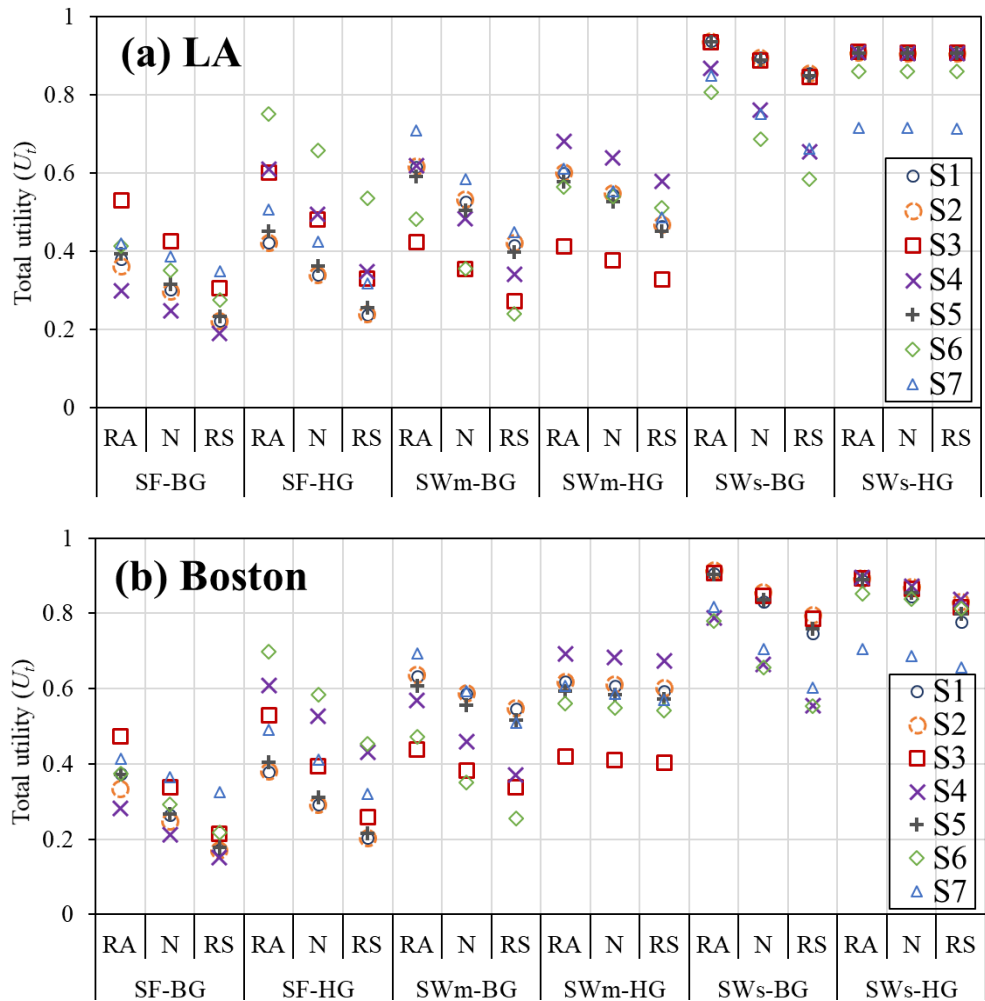


Figure 4.13 Total utility ( $U_t$ ) scores for various scenarios for (a) LA and (b) Boston buildings with risk averse (RA), neutral (N), and risk seeking (RS) attitudes

As shown in Figure 4.13, the  $U_t$  scores for scenarios 1,2, and 5 (minimum asset loss and time loss and maximum resilience) for both sites follow a very similar variation. This indicates the close interdependency between the AL, TL, and resiliency in general. Scenario 3, minimum casualty, changes differently for various archetypes, however. For Scenario 3, the  $U_t$  scores of LA-SF is noticeably larger than that of for LA-SWm. The difference is more evident for risk aversion case. This is mainly due to smaller LL in case of RC framed buildings compared to buildings with one centerline shear wall on each side.

It is also partly due to the importance/weight factor assigned to life loss as well. In the survey conducted to quantify the importance factors, most participants gave a larger pairwise importance factor to life loss compared to other losses such as AL or TL.

For all cases, averting risk result in a higher score, as expected. But, this change to scores differs from one archetype to another. For SF archetypes, the  $U_t$  scores drops noticeably if the decision maker wants to seek risk whereas for SWm and SWs cases, the  $U_t$  score decreases slightly. The drop in  $U_t$  scores is generally less significant for archetypes with high-performance glazing (HG cases). HG archetypes achieve a better score than archetypes with base glazing (BG) for most scenarios considering the conflicting factors of initial cost and energy consumed. For Scenarios 6, in particular, where minimum operational energy is the objective, they achieve a considerably larger score (between 7% larger in case of LA-SWs with risk aversion attitude to 214% larger in case of LA-SWm with risk-seeking attitude).

#### **4.4 Conclusions**

This paper presents a novel multi-criteria framework for design of buildings considering various resilience, sustainability, and energy measures. Building upon recent advancement in loss analysis and energy simulation, it provides a quantitative risk-based decision model for integrated structural and architectural performance assessment and design. The framework is implemented on a series of RC buildings in seismic and cold regions and the impact of shear wall ratios on asset, time, life, and environmental loss as well as energy consumption is studied.

Compared to RC buildings with shear wall, RC framed buildings consumed noticeably more energy for cooling and heating (on average 12%). This is partly due to the shading effect provided by the wall and, to a lesser extent, due to the significant thermal mass of shear walls. Archetype buildings with shear wall experience less monetary seismic loss and downtime as well resulting in high total utility scores in the decision analysis. As such, for most cases, buildings with symmetric side shear walls ranked first in decision analysis even though they require a higher initial construction cost. Nonetheless, shear walls block the natural light resulting in slightly more energy use for lighting. Further, glazing has little impact on resilience but significant influence on heating and cooling energy use and cost. As such, using triple low-e glazing reduced the energy use, cost, and corresponding CO<sub>2</sub> eq emission as much as 48% compared to regular double glazing. Averting risk result in a higher utility score, particularly in case of regular double glazing. As discussed, these trade-off between various criteria, i.e. different cost, loss, and energy measures, can be studied in a multi-criteria framework even if they yield conflicting outputs.

As an extension to this study, multi-variable formal optimization techniques can be used to find the optimal member size, location, and cost given various economic, social, and environmental criteria such as estimated direct/indirect loss or cradle to grave cost. Nature-based algorithms for global optimization such as swarm intelligence, multi-agent models based on behavior of social swarm, and evolutionary computation, multi-dimensional models based on biological evolution theory, can be used for such studies (Ekici et al. 2019; Jafari and Valentin 2018; Sutley et al. 2016a; Wang et al. 2019). Furthermore, the trilateral decision model proposed here can be applied to other structure

or infrastructure systems as well and be the basis for a computer program which automatically makes decisions on structural and architectural design/retrofit projects.

## Chapter 5

### 5. Localized Health Monitoring System for Seismic Resilience Quantification and Safety Evaluation of Smart Structures<sup>5</sup>

#### 5.1 Introduction

With the advent of the Internet of Things (IoT), new opportunities emerge to improve the performance, resilience, and sustainability of structures and infrastructure systems. The smart cities and IoT paradigm extend the current Internet communication to various everyday devices including transportation, water, communication, power systems, and buildings (Abreu et al. 2017). Smart buildings, equipped with a sensor network, can monitor structural health in addition to energy and water consumption. To effectively utilize the data acquired from monitoring devices, multi-disciplinary studies need to

---

<sup>5</sup> The material presented in this chapter will be submitted for possible publication to the *Structural Safety*. Asadi, E., Salman, A. M., Li, Y., Yu, X. (20XX). Localized Health Monitoring System for Resilience Quantification and Safety Evaluation of Smart Structures, *Structural Safety*, ready for submission.

interconnect resilience quantification techniques with smart system technologies to minimize risk and optimize the life-cycle cost of structural systems.

Seismic risk, in particular, has increased markedly over years, which is primarily due to significant population growth and industrial development in earthquake-prone regions and increasing vulnerability of aging buildings and infrastructure (FEMA et al. 2017). Among 128 significant earthquakes (M7.0 or greater) that occurred worldwide in the last decade, the M9.0 Tohoku, Japan earthquake in 2011 alone caused about 220 billion USD damage (FEMA et al. 2017; NGDC/WDS 2019). Researchers have proposed various tools and techniques to evaluate, manage, and mitigate seismic risk and improve resilience (Bruneau et al. 2003; Burton et al. 2016; Lee and Ellingwood 2017; Sutley et al. 2016a). Thanks to recent component-based loss estimation methods, structural and infrastructure engineers can quantify various engineering demand parameters (EDP) of the desired system and illustrate a meaningful and thorough description of its performance (Bruneau et al. 2017; Cimellaro et al. 2010; FEMA 2012).

As early as the 1970s, the term resilience has been used to refer to system robustness, redundancy, rapidity, and/or resourcefulness (4 R's) against abnormal disturbances (Bocchini et al. 2014; Holling 1973). These four capabilities of the system, called dimensions of resilience, are used to define and partly quantify resilience. Seismic resilience of buildings and other structural systems have been extensively studied in recent years (Bocchini et al. 2014; Cimellaro et al. 2010; Dong and Frangopol 2016; Han et al. 2016). A common approach to quantify resilience, which is adopted and well-developed

for civil infrastructure, is to use functionality curves and define resilience as a function of loss due to extreme event and recovery path.

In 2012, FEMA published FEMA P-58 report providing a uniform approach for loss estimation of building structures under earthquake hazard (FEMA 2012). The report is accompanied by a comprehensive component-based fragility specification database and a Performance Assessment Calculation Tool (PACT), which can be used to perform Monte Carlo simulation for estimation of seismic loss, downtime, and other seismic measures. Quantifying these measures requires extensive and reliable data on system properties and performance. Though system properties and performance can be simulated and estimated using historical data or periodic inspections, these methods are time-consuming and increase the epistemic uncertainty affecting reliable decision making. An online monitoring system, however, (1) minimizes the uncertainty in our knowledge of the system, (2) increases the robustness and resourcefulness of the system by reducing the reaction time, (3) improves the accuracy and timeliness of decisions, and (4) provides high-quality data for future system design (Ansari 2005; Cremen and Baker 2018; Naeim et al. 2006; Shankaranarayanan and Cai 2006).

Aiming to develop an online structural health monitoring (SHM) system, extensive research has been conducted on vibration-based structural health monitoring (SHM) of various structures, listed in several literature reviews on the topic (Amezquita-Sanchez and Adeli 2016; Fan and Qiao 2011; Goyal and Pabla 2016; Lynch and Loh 2006). Among various methods proposed, autoregressive (AR) and AR exogenous (ARX) methods use a statistical damage-sensitive coefficient to detect damage under ambient vibration. Damage

can be identified and measured by comparing coefficients obtained from undamaged and damaged structures (Sohn and Farrar 2001). These methods can effortlessly be utilized in localized sensor networks (Ling et al. 2009; Xing and Mita 2012). Other researchers have used wavelets for performance assessment or loss estimation. Porter et al. (2006) proposed a Bayesian-based method to estimate seismic loss in instrumented buildings. Hwang and Lignos (2017a, 2018) proposed a wavelet-based damage identification method for seismic loss assessment and risk management. Celebi et al. (2004) implemented an SHM system on a 24-story building in San Francisco, CA to record inter-story drift ratio and estimate performance level of the structure per FEMA 273 (FEMA 1997) criteria. Saini and Tien (2018) proposed a probabilistic method to predict earthquake parameters such as moment magnitude and lateral displacement of a structure based on the first 3 seconds of recorded acceleration. This method can be used for earthquake early warning which has been extensively studied in past two decades (Allen et al. 2009; Cheng et al. 2014; Kanamori 2005; Wu and Kanamori 2008). Cremen and Baker (2018) studied uncertainty and errors in post-quake damage and loss quantification when a building is instrumented. Yet, studies on SHM systems are focused on damage identification and as noted by Cremen and Baker (2018), a few applied SHM in loss estimation. None, to the best authors' knowledge, explored post-event resilience quantification given the resilience quantification methodologies themselves are among current subjects being debated by the research community.

In conventional models, SHM systems collect the data and send it to a processing or fusion center for analysis and decision making. In decentralized and localized SHM, however, each sensor processes the data locally and mostly communicates with

neighboring sensors, which reduce the communication cost and improves system redundancy. If damage is detected, however, the refined data will be transferred to a Central Console for decision making. As such, sensor networks are categorized into four groups: (1) centralized infrastructure where all sensors send raw data to a processing center, (2) distributed infrastructure where refined data from all sensors are sent to a fusion center, (3) hierarchical infrastructure where several sensors send data to a cluster head which makes the decision and sends it to a Central Console, and (4) localized infrastructure, used here, where decisions on damage are made at the sensors and transferred to a Central Console. Figure 5.1 compares these four network patterns (Ling et al. 2009). Further, among various practices to employ the network, wireless sensor network (WSN) is an inexpensive and easy-to-deploy method compared to a wired network using coaxial wires (Glaser et al. 2007).

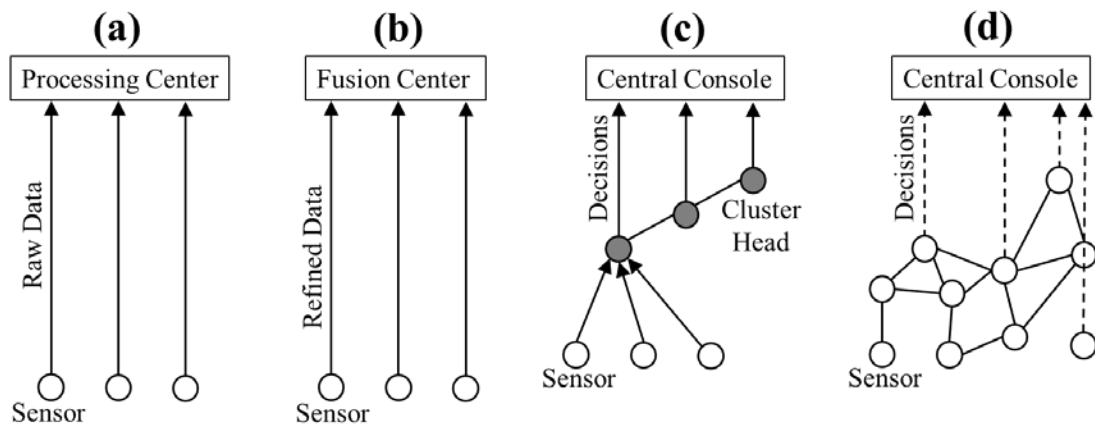


Figure 5.1 Four different network infrastructure patterns: (a) centralized, (b) distributed, (c) hierarchical, (d) localized infrastructures, adapted from (Ling et al. 2009)

This paper integrates an advanced functionality assessment method with recent nonlinear ARX system identification models to propose a new framework for post-quake resilience quantification and rapid decision analysis of structural systems. First, a trilateral

seismic assessment and decision-making framework is introduced. The method is calibrated on Van Nuys building, an instrumented building in California. Then, it is used to identify minor and major damages to archetype structures considering three practical EDPs which are absolute maximum floor displacement (Disp), floor acceleration (ACC), and inter-story drift ratio (IDR). Component-based functionality curves are developed for archetype steel diagrid and special reinforced concrete structures and used to quantify a resilience index for a scenario earthquake. Further, a quantitative method is proposed for post-quake safety evaluation and evacuation decision making.

## **5.2 Trilateral Framework for System Assessment and Decision Analysis**

Resilience incorporates measures reflecting a system's ability to resist a disturbance, mitigate the damage, and recover efficiently (Bocchini et al. 2014; Bruneau et al. 2003). The objective is to minimize economic loss, downtime, as well as casualties. These losses are caused directly or indirectly by an abnormal disturbance or an extreme event, e.g. earthquakes, floods, and/or hurricanes. Time-based deterioration due to aging, corrosion, and exposure may increase these losses.

The proposed framework consists of three main modules: (1) System Concept and Criteria (SCC) module, (2) Trilateral module consisted of Resilience, Monitoring, and Control submodules, (3) Decision Making (DM) module. Figure 5.2 depicts the main components of the framework and their connections. By linking the Monitoring submodule to SCC module, it is possible to update the numerical models during normal operation of the SHM system. Note that this model updating requires SHM to be calibrated for damage characterization. By linking the Monitoring submodule to Resilience submodule, it is

possible to directly calculate the EDPs when an extreme event occurs. Control submodule, which is not studied in this paper, can be used to minimize structural response based on the output of the DM module. Note that the model also includes a feedback loop to use the obtained results and decisions to update the initial numerical models and assumptions. In addition, dynamic changes in vulnerability, hazard intensity, or loss specifications can be incorporated using the feedback loop. The vulnerability of the system may change due to aging, deterioration, corrosion, and damages incurred in minor earthquakes.

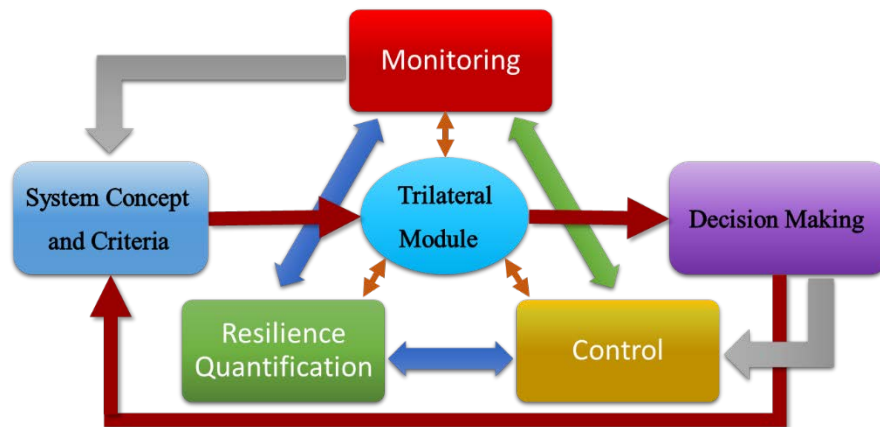


Figure 5.2 Main components of the proposed framework for Assessment and Decision Analysis

The SCC module is where the initial numerical models are developed and periodically updated in each feedback cycle. The numerical models for resilience assessment are developed based on project objectives, system properties, and analysis and design specifications. Scope and limitations of the assessment and the weight factors for decision analysis are also assigned in this module. As shown in Figure 5.3, the numerical models are reexamined to ensure they meet the project objectives and requirements and decision maker’s preferences. Figure 5.3 depicts a typical procedure for SCC module.

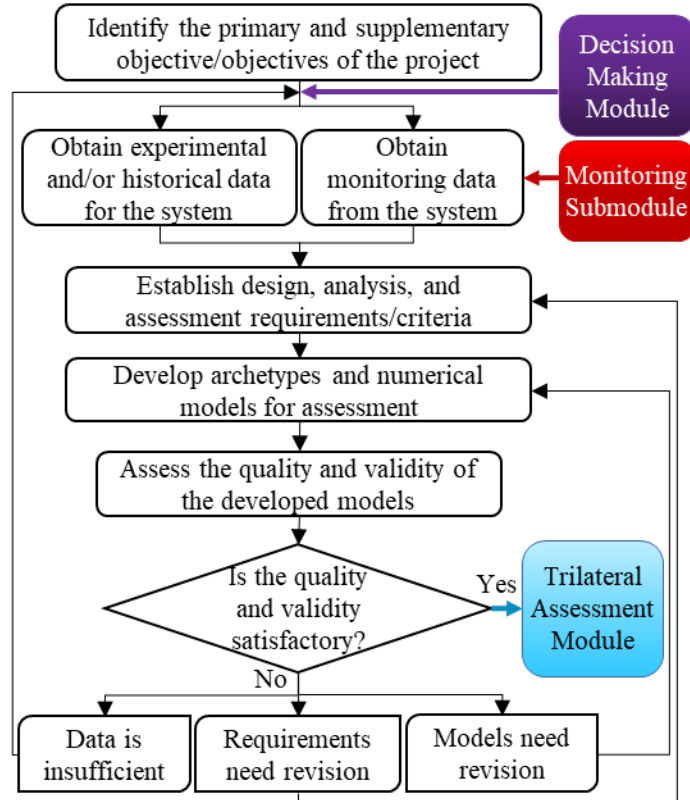


Figure 5.3 Flowchart for System Concept and Criteria (SCC) Module and its connection with other modules

### 5.2.1 Life-cycle Functionality Assessment

Seismic resilience is commonly quantified as the integration of functionality ( $Q$ ) over a certain control time,  $t_c$ , after an abnormal disturbance such as an earthquake occurs at time  $t_0$  (Cimellaro et al. 2010).

$$R = 1/t_c \int_{t_0}^{t_0+t_c} Q(t)dt \quad (5.1)$$

Functionality, also called quality and serviceability, depends on loss and recovery functions. Total loss ( $L_t$ ) is the summation of all losses incurred by all damageable structural and non-structural components over  $t_c$  due to an earthquake. Recovery path to restore functionality depends largely on the rapidity and robustness capabilities of the

system. Formally, the recovery path can be incorporated through a recovery function into functionality calculation, as follows (Cimellaro et al. 2010; Karamlou and Bocchini 2017).

$$Q(t_E < t < t_R) = [1 - L_t(IM, t_R)] \times f_R(t, t_E, t_R) \quad (5.2)$$

where  $t_E$ ,  $t_R$ , and  $IM$  are earthquake effective occurrence time, recovery time, and earthquake intensity, respectively. Using functionality curves, dimensions of resilience can be quantified as well (Cimellaro et al. 2010). Rapidity, one of four dimensions of resilience, is the slope of the functionality curve. On average, rapidity or recovery rate is the ratio of loss ( $L_t$ ) over net recovery time ( $t_R - t_E$ ), as shown in Figure 5.4. Robustness, another dimension of resilience, is defined as the residual functionality of the system once the earthquake strikes (at time  $t_{E1}$  and  $t_{E2}$  in Figure 5.4 for mainshock and aftershock, respectively).

$$\text{Rapidity} = \frac{dQ(t)}{dt} \quad (5.3)$$

$$\text{Robustness} = 1 - L_t \quad (5.4)$$

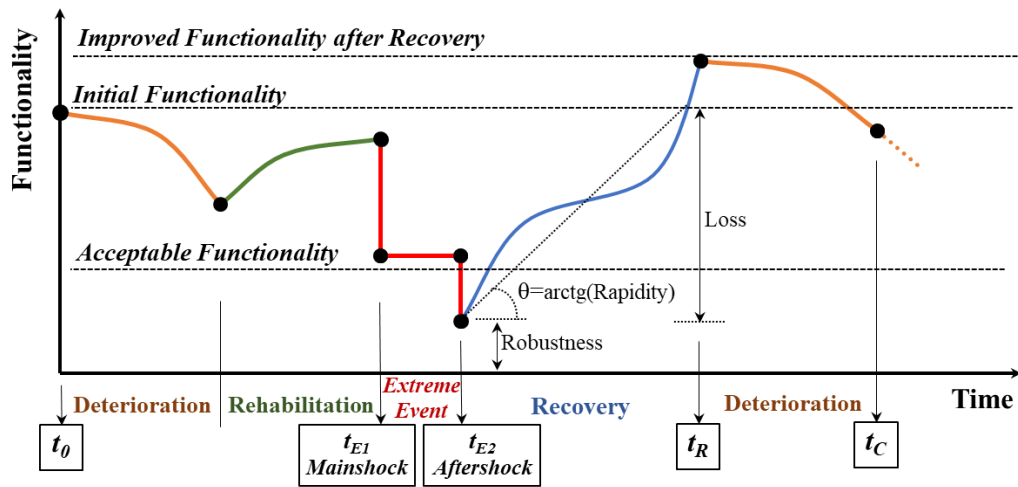


Figure 5.4 Life-cycle functionality of a system and the effect of evolving conditions on the functionality (not to scale)

A more comprehensive approach is to study the functionality of the system over its whole life-cycle given the extreme event and post-event recovery is a part of its life-cycle. Figure 5.4 illustrates major life-cycle activities and events which may affect functionality. They are categorized into four time-based stages: deterioration, rehabilitation, and recovery activities and extreme events. As such, expected functionality may reduce due to aging, deterioration, and material corrosion of structural and non-structural components. Extreme events such as earthquake diminish functionality drastically, possibly below acceptable functionality as shown in Figure 5.4. Following an earthquake, the inspection, repair, and recovery activities start to restore functionality to its initial state or an improved one. Throughout system life-cycle, accurate functionality estimation is possible if accurate and updated data is available on system properties and capacity.

### ***5.2.2 Monitoring and Control***

The trilateral module consists of three submodules, including Monitoring submodule which is an SHM system and structural Control submodule which is an active or semi-active control system. SHM submodule/system can detect, locate, and measure damage in the structure. Control system minimizes the damage through dissipating, absorbing, and reflecting the energy caused by dynamic loads such as an earthquake. Control system may include a wide range of devices from passive control systems such as sliding friction pendulum isolators to hybrid control systems such as tuned mass damper equipped with an active actuator (Lu et al. 2018; Saaed et al. 2015). Though proposed as a possible part of a comprehensive assessment and decision framework, the control submodule is not studied here.

Accurate and reliable assessment of a dynamic system requires periodic data on its properties and performance which in case of a building can be acquired through inspection or sensing network. Inspection needs trained specialist familiar with potential damage and probable hazards in the region which is costly and time-consuming (Lynch and Loh 2006; Suo and Stewart 2009). An online monitoring network, on the other hand, can provide real-time data on system performance minimizing the epistemic uncertainty and increasing the confidence level of performance prediction analyses (Ling et al. 2009; Stewart 2001).

SHM systems operate in three stages: (1) normal operation, (2) during extreme event, (3) post-event. Figure 5.5 depicts a step-wise schematic of SHM system operation. Damage detection and measurement are conducted in the localized sensor network while loss analysis which requires more computational resources is performed in the Central Console (see Figures 5.1 and 5.5). During normal operation of the structure which may include deterioration and rehabilitation stages as noted in Figure 5.4, the SHM system periodically collects data on the health condition of the structure and updates the presumed numerical models. These updated models can be used to improve loss and functionality estimates and help in repair and/or rehabilitation decision making. At this stage, the SHM system works on low-power given WSN power-consumption is a concern in SHM projects (Ling et al. 2009).

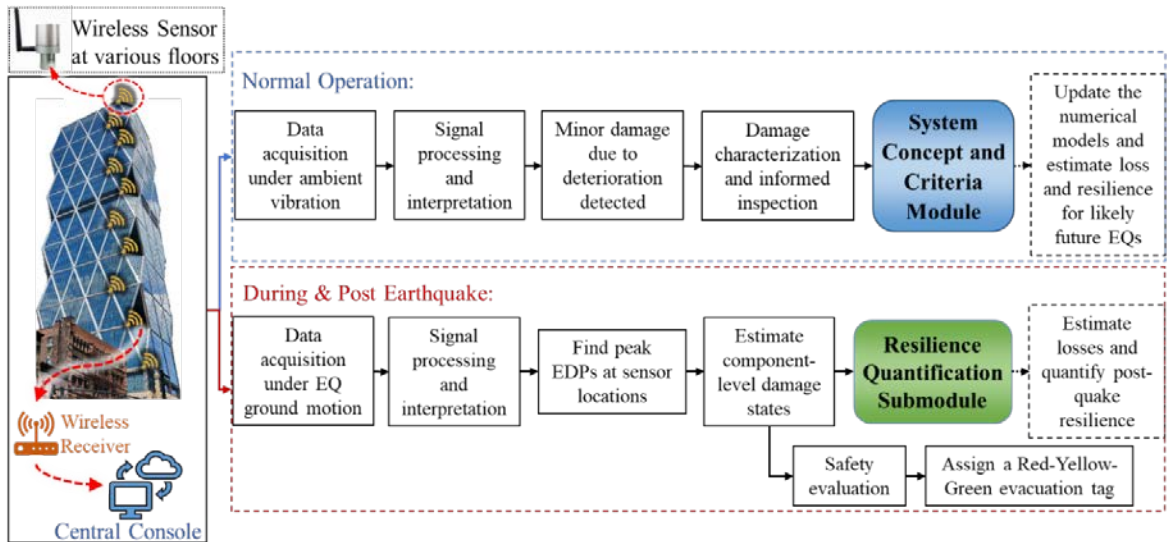


Figure 5.5 Schematic of SHM system for operating in normal stage or during/post-earthquake, Diagrid building in the left is the Hearst Tower in New York City

However, when an extreme event occurs, it provides real-time data on system performance which is used to accurately estimate the incurred damage, loss, functionality, and ultimately resilience in near real-time. The data acquired from instruments are structural EDPs. For instance, the instrument monitors floor acceleration and displacement during and after the event which are used to find key EDPs required for loss analysis such as absolute maximum floor displacement (Disp), floor acceleration (ACC), inter-story drift ratio (IDR). In this stage which is triggered by sharp changes in EDPs or frequency shift, the direct outputs of the sensors will be used for loss analysis. The EDPs are deterministic in this stage, hence, the analysis requires much less computational resource and time (Cremen and Baker 2018; Naeim et al. 2006). After an extreme event, sensor direct outputs will be used to assess the post-event condition of the structure and report to the authorities for recovery planning. Note that detection of a failed sensor node in a network may indicate a failure or damage in the structure given the location of the node (Mahapatro and Mohan Khilar 2013). Therefore, SHM system minimizes the need for post-event inspection,

improves the post-event emergency management and planning, and improves the accuracy and timeliness of recovery decisions.

### 5.2.2.1 Localized Structural Health Monitoring and Damage Detection

Localized transfer function models such as ARX models have been used to detect damages to multi-story structures (Ling et al. 2009; Ohata et al. 2006; Sohn and Farrar 2001). Here, a local nonlinear ARX model is developed to identify the response of the structure and detect damage via statistical damage indicators provided the response is stationary. If  $y[.]$  and  $u[.]$  are sensor output and the input to the structure respectively, then an ARX model can be defined as follows to predict the response (Ohata et al. 2006; Takewaki et al. 2012).

$$\begin{aligned} y[k] + a_1 y[k - 1] + a_2 y[k - 2] + \dots + a_{n_a} y[k - n_a] \\ = b_1 u[k - 1] + b_2 u[k - 2] + \dots + b_{n_b} u[k - n_b] + \epsilon[k] \end{aligned} \quad (5.5)$$

where  $k$  is the discrete time step,  $n_a$  and  $n_b$  are the order of output and input of the ARX model and  $\{a_i\}$  and  $\{b_i\}$  are vectors of weights/coefficients for output and input, respectively. The term  $\epsilon$ , called residual error, is the difference between the actual measured signal ( $y$ ) and the prediction using the ARX model ( $\hat{y}$ ). For error prediction, parameters (coefficients) vector ( $\theta$ ) and the data (input and output signal) vector ( $\phi$ ) are described as follows (Takewaki et al. 2012).

$$\theta = [a_1 \quad \dots \quad a_{n_a} \quad b_1 \quad \dots \quad b_{n_b}]^T \quad (5.6)$$

$$\phi[k] = [-y[k - 1] \quad \dots \quad -y[k - n_a] \quad u[k - 1] \quad \dots \quad u[k - n_b]]^T \quad (5.7)$$

Then, the predicted output ( $\hat{y}$ ) and corresponding error ( $\epsilon$ ) are found as follows:

$$\hat{y}[k] = \boldsymbol{\theta}^T \boldsymbol{\varphi}[k] \quad (5.8)$$

$$\epsilon[k] = y[k] - \hat{y}[k] = y[k] - \boldsymbol{\theta}^T \boldsymbol{\varphi}[k] \quad (5.9)$$

The above equations can describe the system in damaged and undamaged conditions. Initially, while modeling the SHM system, the structure is known to be undamaged. Hence, the undamaged ARX coefficients are evaluated under ambient vibration (Gaussian random variable with zero mean) and stored in the sensor database (baseline output). The baseline coefficients and corresponding residual error are labeled  $\{a_i\}_{st}$  and  $\{b_i\}_{st}$  and  $\epsilon_{st}$ . During system operation, either normal operation or when an extreme event occurs, sensors receive an unknown (damaged or undamaged) signal. SHM system evaluate the ARX coefficients  $\{a_i\}_u$  and  $\{b_i\}_u$  and the residual error  $\epsilon_u$  for the unknown signal at each sensor. Residual error is a damage-sensitive feature which can be used to identify and measure damage. Previous studies have found the ratio of the variances of the residual errors to be an accurate indicator of the damage (Bornn et al. 2010; Ling et al. 2009; Sohn and Farrar 2001). Therefore, the following ratio is used as a damage indicator ( $DI$ ):

$$DI = \frac{\sigma^2(\epsilon_u)}{\sigma^2(\epsilon_{st})} \quad (5.10)$$

where  $\sigma^2(\cdot)$  is the variance. If the structure is undamaged, the residual errors will remain invariant with a Gaussian distribution and  $DI$  has an F-distribution given the input excitation is Gaussian white noise. If the structure is damaged, however, the coefficients of the ARX model will change leading to an increase in the variance of the residual error which can be identified via  $DI$ . The data studied here are structural EDPs such as Disp, ACC, and IDR obtained from instruments.

### 5.2.2.2 Sensor Failure Detection

Real data are susceptible to bad disturbance caused by transmitter or sensor failure which needs to be accounted for, so they have minimal effect on the outputs of the SHM system. Localized WSNs are evidently more robust compared to hierarchical and centralized networks since damage identification is conducted in each sensor instead of cluster head or processing center (see Figure 5.1). Localized models, used here, use intrinsic sparsity of damage across the building for detection and failure of a few sensors does not affect the performance of the whole SHM system noticeably (Ling et al. 2009). Cloud-computing for central console, where the loss analysis is performed, minimizes SHM system risk as well. Further, most signal processing tools provide options to minimize bad disturbance. For example, MATLAB provides an advanced error threshold option, called `LimitError`, for robustification of error criterion which minimizes those negative effects. Filtering the data, commonly low- or band-pass filters, to focus on required frequency bands also diminishes the effects. Yet, data need to be examined for infrequently large residual error and smoothed if needed. To detect failure, note that if a part of data shows bad disturbance, it is likely due to the failure of a sensor or absence of excitation (source of input). Missing data is also a sign of sensor or data acquisition failure (Ljung 2007).

Using FEMA P-58 approach for loss estimation, post-quake functionality and resilience assessment can be done with as few as one instrument at each floor. In case of instrument failure or if the floor is not instrumented, cubic spline interpolation, as follows, can be used to estimate the EDPs (Limongelli 2003; Naeim et al. 2006).

$$y(h_i) = x_3 h_i^3 + x_2 h_i^2 + x_1 h_i + x_0 \quad (5.11)$$

where  $x_0$  to  $x_3$  are interpolation coefficients such that output  $y$  at floor  $i$  matches acquired data and  $h_i$  is the height of floor  $i$ . Clearly, missing data adds to the uncertainty in loss and resilience analyses and minimizes the benefits of SHM system in reducing uncertainty. Yet, for any  $n > 1$  (if  $n$  is the number of available instruments), the data acquired from instrumentation improves the accuracy and reliability of the analyses (Cremen and Baker 2018).

### 5.2.3 Resilience Assessment

Resilience is quantified based on the functionality of the system and loss caused by hazards. In general, cumulative distribution function (CDF) of loss ( $P(L > l_i)$ ) for each component of the system can be quantified as follows (Bocchini et al. 2014; Ramirez and Miranda 2012a; Yamin et al. 2017).

$$\begin{aligned} &P(L > l_i) \\ &= \int_{IM} \int_{EDP} \int_{DS} P(L > l_i | DS) P(DS | EDP) P(EDP | IM) P(IM) dDS dEDP dIM \quad (5.12) \end{aligned}$$

In Equation (5.12),  $P(L > l_i | DS)$  is the consequence function conditioned on the damage state obtained from fragility database of FEMA P-58 for various consequences (FEMA 2012). The term  $P(DS | EDP)$  is the probability of reaching a damage state given EDP reaches a certain value evaluated based on limit states recommended by FEMA P-58 using dynamic time-history analyses and the term  $P(EDP | IM)$  is the probability of reaching a certain EDP given a hazard intensity of  $IM$  which is also obtained from time-history dynamic analysis. Lastly,  $P(IM)$  is the mean frequency of exceedance in a year for

each intensity obtained from the United States Geological Survey (USGS) online hazard tool and adjusted for the fundamental period of the structure and 5% damping ratio. Figure 5.6 shows a step-wise flowchart to quantify various resilience measures in the Trilateral module and their connection with the Monitoring submodule. Here, OpenSees is used for seismic dynamic nonlinear analyses, FEMA PACT fragility specification database is used for loss estimation, and RSMeans life-cycle cost estimator is used for cost estimation.

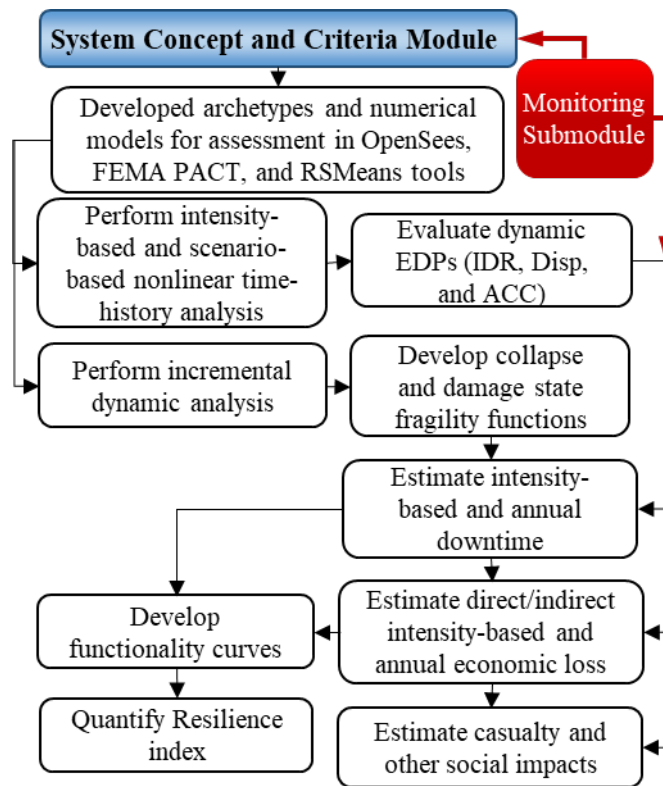


Figure 5.6 The flowchart for the Resilience Submodule and its connection with other modules

#### 5.2.4 Post-quake Safety Evaluation and Evacuation Decision-making

Conventionally, post-quake safety evaluation is done manually through visual inspection of damages to critical structural components. ATC-20 (Rojah 2005) provides a three-level guideline for post-quake safety evaluation and decision-making on evacuation

which includes rapid, detailed, and engineering evaluations. ATC-20 methods involve assessment of story leaning, racking damages to walls and other structural components, falling hazard like parapet and chimney, ground slope movement, and partial and full collapse. Inspections, however, are subjective and time-consuming taking several weeks to complete, as was the case for 2006 Hawaii and 2003 San Simeon earthquakes (Chock 2007; Zhu et al. 2011). The outputs of SHM systems largely reduce the need for post-quake inspection.

Based on the losses incurred at each assessment interval, the building will receive a tag using traffic light tagging method (Han et al. 2015; Rojah 2005). This method gives a clear description of the building condition and streamlines post-event decision-making. Green, yellow, and red colors are used to identify tolerable, intermediate, intolerable damages to the buildings (Guéguen and Tiganescu 2018). This color code matches with the Applied Technology Council (ATC) method where building receives green–inspected, yellow–restricted use, or red–unsafe placards (Rojah 2005).

To assign those tags based on computational simulation outputs, researchers provide various methods assuming criteria on EDP and/or damage state limits (Guéguen and Tiganescu 2018; Han et al. 2015; Naeim et al. 2006). Among them, (Han et al. 2015), adapted here, suggests a series of component-based damage criteria for post-quake safety evaluation of buildings. Accordingly, for a green tag three criteria shall be met: (1) no minor or more significant damage to exterior beam or column, (2) no severe residual IDR (unrepairable IDR) in any story, (3) no fracture of fire sprinkler units. An additional criterion is considered here which is (4) no moderate or more significant damage to curtain

walls and wall partitions. A red tag is assigned for any case with (1) severe damage to exterior beam or column, (2) severe residual IDR on a floor, (3) severe damage of fire sprinkler units, and (4) severe damage or collapse of curtain walls and wall partitions. If a building does not comply with either red or green tag, a yellow tag is assigned.

### **5.3 Van Nuys Instrumented Building**

To benchmark the proposed model, the 7-story Van Nuys Hotel building located in Southern California is studied. This building was instrumented during the 1971 San Fernando and 1994 Northridge earthquake and its seismic performance has been extensively studied throughout last decades (Cremen and Baker 2018; Krawinkler 2005). In particular, it is used for seismic performance assessment testbed project by Pacific Earthquake Engineering Research (PEER) center and details of their post-quake damages and observed EDPs are provided by (Islam 1996; Krawinkler 2005). Following (Krawinkler 2005; Paspuleti 2002), a numerical model is developed in OpenSees and seismic performance and recorded damages under 1994 Northridge earthquake are compared with observed data. Figure 5.7 depicts the lateral displacement at various floors in longitudinal (West-East) and transverse (North-South) directions and compares them with displacement recorded by instruments. As depicted, in nonlinear time-history analysis, the model predicts the peak displacements well (with an error of 1, 3, 10, and 2% at roof and 6<sup>th</sup>, 3<sup>rd</sup>, and 2<sup>nd</sup> floors) and predicts the variation of displacement by time acceptably.

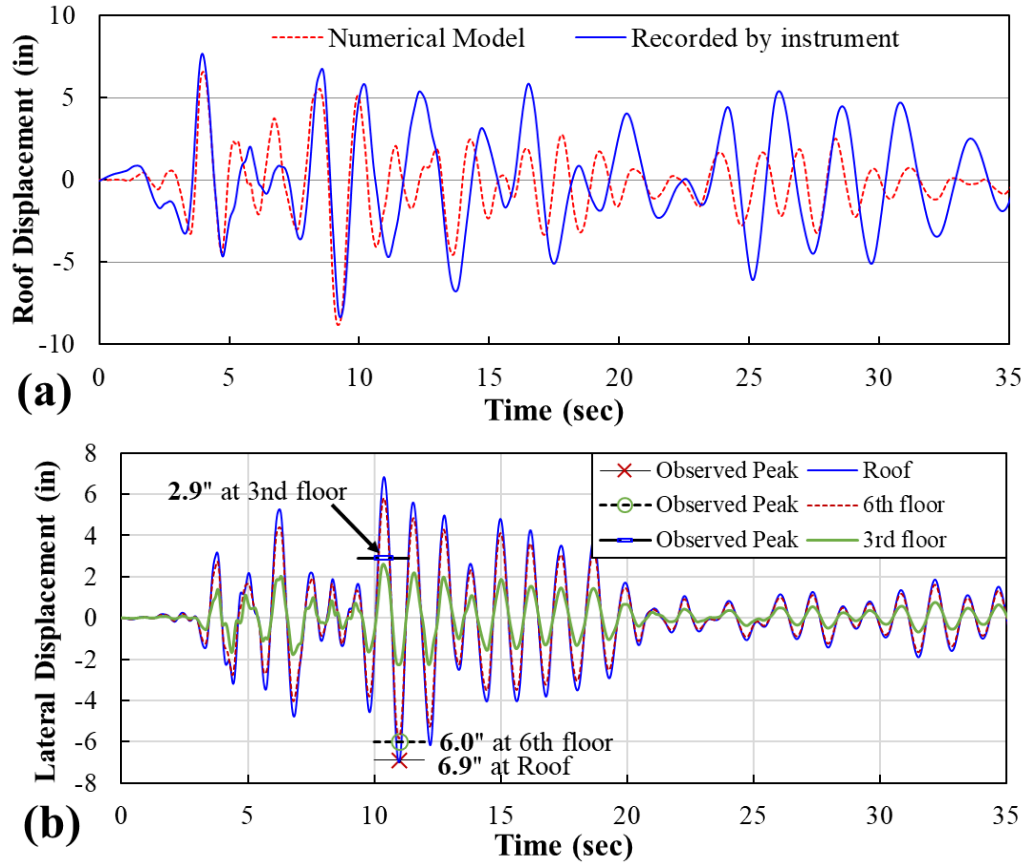


Figure 5.7 Lateral displacement from numerical models of Van Nuys Hotel during 1994 Northridge Earthquake compared with recorded displacement from instruments (a) at roof in the longitudinal direction and (b) at various floors in transverse direction, displacement values specified are peak values reported by (Islam 1996)

Based on the description provided for structural and non-structural components in (Krawinkler 2005; Paspuleti 2002; Trifunac et al. 1999), loss analysis is performed using FEMA P-58 fragility specifications and functionality curve and resilience index are quantified. (Paspuleti 2002; Trifunac et al. 1999) report extensive damage to columns of 5<sup>th</sup> story, minor to moderate damage to beam-column connections and perimeter frame, and non-structural damage to windows and partition walls particularly in the 4<sup>th</sup> and 5<sup>th</sup> stories. Accordingly, fragility specifications of structural components including columns, beams, and beam-column and slab-column connections are included in the loss analysis.

For non-structural components sensitive to IDR, first story exterior walls are considered masonry walls and others are considered generic curtain walls with windows (Cremen and Baker 2018). Interior partition walls are considered generic gypsum walls. For non-structural components sensitive to floor acceleration, suspended ceiling, fire sprinklers, Heating, ventilation, and air conditioning (HVAC) ducting and control panel, and an elevator are considered based on available data (Krawinkler 2005). Based on (Krawinkler 2005; Paspuleti 2002) reports on initial construction and repair costs, initial construction cost is presumed 1.43 M US\$ and to match the repair cost database of FEMA P-58, the current monetary cost is used considering a discount rate of 3% (FEMA 2012; Lounis and McAllister 2016).

Figure 5.8 (a) depicts the repair time for various floors of the Van Nuys Building under the 1994 Northridge earthquake. Consistent with the post-quake reports, the building incurs major damages in the structural components of the 4<sup>th</sup> and 5<sup>th</sup> floors which can be attributed to shear cracks reported by (Krawinkler 2005; Trifunac et al. 1999). It also incurs non-structural damage to the masonry walls of the 1<sup>st</sup> floor and wall partitions in various floors, both are sensitive to IDR, which are consistent with reports as well. Figure 5.8 (a) also depicts the repair time for non-structural components sensitive to ACC including an air handling unit considered on the roof, suspended ceilings, fire sprinklers, the elevator.

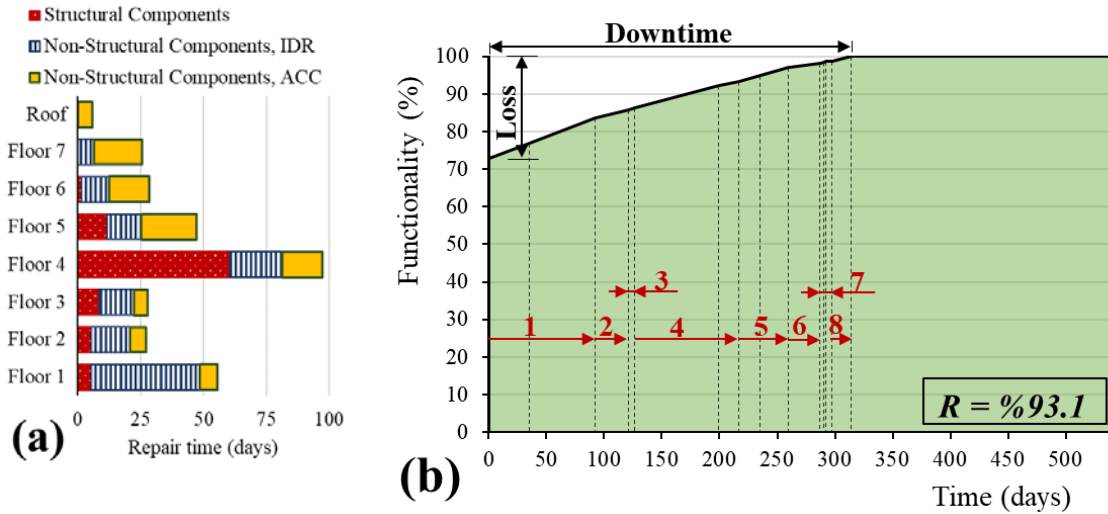


Figure 5.8 (a) Repair time for various floors of Van Nuys building and (b) Functionality curve for Van Nuys Building under 1994 Northridge earthquake (numbered arrows show the repair time for various components: (1) structural components, (2) masonry walls of 1<sup>st</sup> floor, (3) curtain walls, (4) full/partial interior wall partitions, (5) suspended ceilings, (6) independent pendant lighting, (7) elevator, ducting, air handling unit on the roof, and control panel, (8) fire sprinklers

To develop a functionality curve and quantify resilience index ( $R$ ) from Equation (5.1), downtime ( $t_R - t_E$ ) and total loss ( $L_t$ ) are required. FEMA P-58 provides a database of conditional seismic consequence functions ( $P(L > l_i | DS)$  in Equation (5.12)) for different structural and non-structural components which are used to quantify those repair/replacement time and cost for each component. Repair time and repair cost are used to develop functionality curves and quantify resilience index, as depicted in Figure 5.8 (b). Repair/replacement cost as a percentage of the total replacement cost on the vertical axis is used to describe functionality loss. Repair time is shown in days on the horizontal axis and total replacement time (540 days) is used as the control time ( $t_c$ ) (Krawinkler 2005). Figure 5.8 (b) presents a component-based functionality curve and indicates the corresponding resilience index ( $R$ ) of the Van Nuys building under the 1994 Northridge Earthquake. Numbered arrows and dashed lines in Figure 5.8 (b) show the stepwise repair

process of building components until the functionality is fully restored, considering a series repair scheme. As described in Figure 5.8 caption, repair starts with structural components and ends with non-structural components related to utility service. With the repair of each component, a part of functionality loss is restored. The area under the functionality curve is used to quantify  $R$  (Cimellaro et al. 2010). Accordingly, the resilience, robustness, and rapidity indices for the building are 93.1%, 72.8%, and 46.7%, respectively. Note that a 50% robustness indicates a total loss equal to half of the building replacement cost. Further, given severe damages to partition walls ( $IDR > 1.2\%$ ), moderate damage to beams and columns, and minor residual IDR, the building receives a Red tagging.

#### **5.4 Archetype Design, Modeling, and Components**

For demonstration, the proposed framework is implemented on two groups of buildings, steel diagrid framed (SDF) and special reinforced concrete framed (RCF) structures. Diagrid frames are an innovative structural system where both gravity and lateral loads are carried by inclined diagonal members. An iconic diagrid building in New York City named Hearst Tower is shown on the left side of Figure 5.5. In recent studies, they have shown excellent lateral stiffness and relatively efficient performance against lateral loads including earthquakes (Asadi and Adeli 2017; Liu et al. 2018). ANSI/AISC 341-16 (2016a) and similar standards, however, provide no special seismic design considerations for diagrids. They are selected to further study their seismic resiliency considering that they are capable of controlling lateral deformation and minimizing damage in high seismic regions (Kim and Lee 2012; Liu et al. 2018). Special RC frames, on the other hand, has a more ductile performance and can withstand larger lateral deformation before collapse

(Han et al. 2015). The buildings are designed based on ASCE 7-16 (2017b), ANSI/AISC 360-16 (2016b), ANSI/AISC 341-16 (2016a), and ACI 318-14 (2014) for Downtown Los Angeles, a highly seismic region.

Archetypes are commercial 4-story buildings with a typical story height of 4 m. Figure 5.9 illustrates the typical floor plan for diagrid and RC buildings adopted from previous studies (AlHamaydeh et al. 2017b; Asadi et al. 2018). RSMeans Data Online (2018) is used for calculating the total replacement cost of the buildings for loss analysis. The total replacement cost is the construction cost plus 25% to account for tenant improvements and asset following FEMA P-58 examples (FEMA 2012). Construction cost includes substructure cost, shell cost, interiors cost, services cost, and contractor and architectural fees. The buildings are modeled in OpenSees for dynamic analyses using fiber elements for beams, columns, and diagonals. Numerical models are verified by experimental studies (Black et al. 1980; Kolozvari et al. 2014). More details on building structures are presented in (Asadi et al. 2019b, 2020).

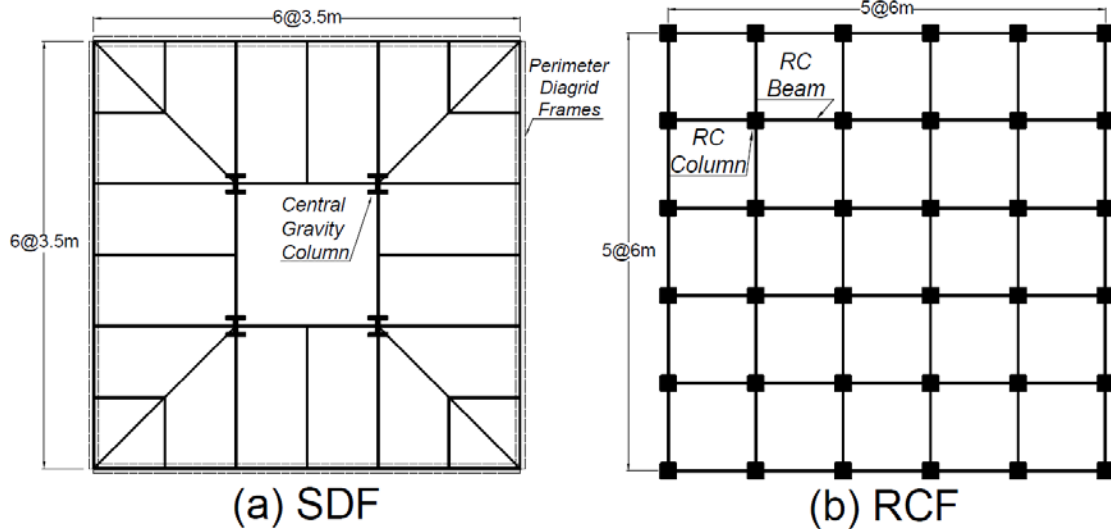


Figure 5.9 Typical floor plan for (a) steel diagrid framed (SDF) and (b) reinforced concrete framed (RCF) archetypes

## 5.5 Uncertainty Modeling and Fragility Analysis

An SHM system minimizes epistemic uncertainty as it provides data on system properties and performance. Yet, uncertainty in structure capacity, demand, and SHM failure need to be addressed properly. Uncertainty in capacity stems from uncertainty in material properties, member geometry, and modeling. In past decades, several experimental and analytical studies tried to estimate these uncertainties and proposed methods to minimize them (Jaquess and Frank 2002; Lu et al. 1994; Schmidt and Bartlett 2002). Here, uncertainty in material properties and member cross-section are included in the Monte Carlo simulation using Latin Hypercube Sampling method (Celik and Ellingwood 2010). Experimental studies on concrete and steel members are used to develop probability density function (PDF) for various member properties (Kappos et al. 1999; Lu et al. 1994; Schmidt and Bartlett 2002). Table 5.1 lists the normalized mean value ( $\mu_N$ ) and coefficient of variation (CoV) for various parameters considered.

Table 5.1 Variation of steel and concrete member properties randomly sampled using Latin Hypercube Sampling method and normalized by nominal value

	$t$	$b$	$h$	$f_y$	$\epsilon_{cu}$	$b$	$h$	$A_s$	$f_c'$	$f_{ys}$
	Steel members (Schmidt and Bartlett 2002)				Concrete members (Lu et al. 1994) and (Kappos et al. 1999)					
Dist.	LogN	LogN	LogN	LogN	Norm.	Norm.	Norm.	Norm.	Norm.	Norm.
$\mu_N$	1.04	0.998	0.999	1.11	0.994	1.00	1.00	1.00	1.12	1.10
CoV	0.025	0.004	0.002	0.063	0.358	0.02	0.02	0.04	0.18	0.06

Note:  $t$  = web/flange thickness;  $b$  = section width;  $h$  = section height;  $f_y$  = steel yield strength;  $\epsilon_{cu}$  = concrete ultimate strain for confined concrete;  $A_s$  = concrete reinforcement area–top and bottom;  $f_c'$  = concrete compressive strength;  $f_{ys}$  = reinforcement yield strength.

For record-to-record variability, a set of 22 far-field (located at  $\geq 10$  km from the fault rupture site) ground motion records are used which are recommended by FEMA P-695 (2009) for collapse and performance fragility evaluation. Records include ground motions of magnitudes M6.5 to M7.6 obtained from 14 different events on Site Class C and D. Collapse fragility curves are developed using Incremental Dynamic Analysis (IDA) (Vamvatsikos and Cornell 2002). Maximum likelihood method is used to fit a lognormal distribution function over the empirical collapse fragility curve. Collapse fragility curves for the undamaged and damaged (deteriorated due to corrosion) buildings are shown in Figure 5.10. The horizontal axis shows  $S_a(T_1, 5\%)$  which is the normalized pseudo-spectral acceleration for 5% damped design spectra for the region at the fundamental period of the building structure. Given the uncertainties involved, each curve required over 5,000 nonlinear time-history dynamic analyses. The mean and standard deviation of collapse capacity,  $\hat{S}_{CT}$ , and collapse IDR are also listed in Table 5.2.

To assess the damage detection capability of the ARX model in normal operation, damage due to corrosion with various severities are imposed on the building. Corrosion damages are commonly insignificant and difficult to detect making it a critical case to

assess the proposed ARX model (Melchers 1999). Ghosh and Padgett empirical model (2010) is adopted to estimate a reduction in web and flange thickness due to corrosion. As depicted in Figure 5.10, corrosion has a minimal impact on collapse capacity and IDR. After 25, 50, and 100 years of corrosion with no maintenance, the collapse capacity decreased by 3.0%, 5.4%, and 7.8%, respectively. SHM need to detect these small changes to capacity. To assess the ARX model under multiple damages due to an extreme event, a CRF archetype is considered where 2 columns of the first story, on 2<sup>nd</sup> and 5<sup>th</sup> axes, have been severely damaged (failed) due to a mainshock excitation. As depicted in Figure 5.10,  $\hat{S}_{CT}$  of damaged RCF considerably drops (about 35%) due to failure of those 2 columns.

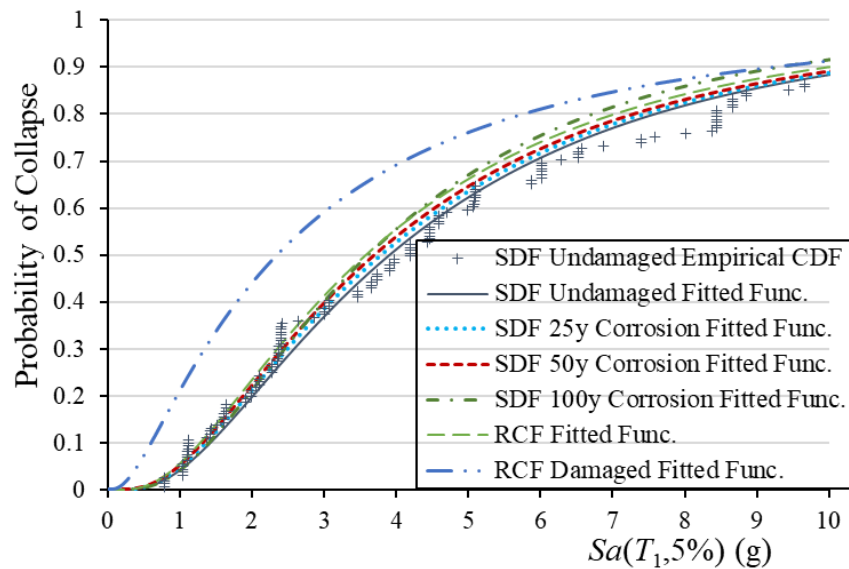


Figure 5.10 Empirical CDF of  $Sa(T_1, 5\%)$  and fitted lognormal fragility functions for various archetypes

Table 5.2 Expected collapse capacity and collapse IDR and their corresponding logarithmic dispersion

Archetype	$S_{CT}(T_1, 5\%)$ (g)	$\beta_{S_{CT}}$	Collapse IDR (%)	$\beta_{IDR}$
-----------	---------------------------	------------------	---------------------	---------------

SDF	3.91	0.79	2.40	1.05
SDF-25y	3.79	0.80	2.41	1.05
SDF-50y	3.69	0.81	2.38	1.04
SDF-100y	3.60	0.74	2.26	0.94
RCF	3.58	0.80	6.39	0.96
RCF-2Cols.Failed	2.34	1.07	3.69	1.17

The aleatoric uncertainty in performance and loss specification of structural and non-structural components is also included using the fragility specification database of FEMA P-58 (FEMA 2012). FEMA P-58 provides a comprehensive database of fragility specifications for seismic repair/replacement cost and time and other consequences due to damages to various components. These specifications, adopted in this study, include the mean and dispersion of those consequences for different component-based damage states. For diagrid frame members, the fragility specification and damage states developed in (Asadi et al. 2018) are adopted as FEMA PACT does not provide fragility specifications for diagrids. Steel connections are assumed post-Northridge welded steel moment connection without reduced beam section (RBS) detailing. Non-structural components for both steel and concrete buildings include two hydraulic elevators, one 500-Ton chiller and air-handling unit on the roof, and for each 4 m<sup>2</sup> a seismically-rated pendant lighting. Perimeter walls are generic midrise stick-built curtain wall and the interior walls are partial or full-length gypsum walls with metal studs. The ceiling is covered with seismically-rated suspended tiles. A full list of damageable structural and non-structural components with their fragility parameters is presented in (Asadi et al. 2018, 2020).

## 5.6 ARX System Identification

### 5.6.1 *Damage Detection and Damage Location*

The ARX SHM system is implemented on archetype frames to detect possible damages. For functionality, the literature focuses on functionality loss due to extreme events since deterioration has minimal impacts. Deterioration/degradation rate of building elements depends largely on the environmental conditions, material and construction quality, and extent of exposure. Proper construction, installation, and maintenance practices slow down the deterioration. Yet, a localized SHM system is able to detect these minor damages and update the numerical models to achieve a more reliable and accurate system assessment. Damage due to deterioration is used to assess the ARX model accuracy. Three EDPs including IDR, ACC, and Disp are studied to find the most reliable indicator of performance, damage, and damage location. The ratio of variance ( $DI$ ) is quantified for each EDP and their variation and sensitivity towards damage is studied. To simulate ambient vibration, Gaussian white noise is imposed on the foundation of the structure. For SDF archetype, a WSN is considered where sensors are installed on diagrid nodes at each floor level, as shown in Figure 5.11. To assess the ARX model accuracy in detecting both the damage and its location, it is assumed that two diagonal members of the first floor, as shown in Figure 5.11, are exposed to deterioration. It is expected that the sensor closest to the damaged members, Sensor (1,1), shows the largest  $DI$ .

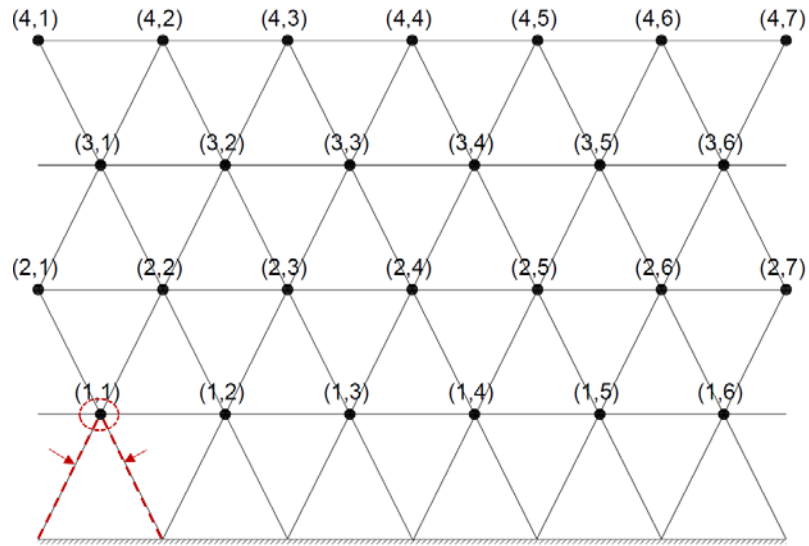


Figure 5.11 Sensors located at diagrid nodes and structural members affected by corrosion

Figure 5.12 (a) illustrates the variation of  $DI$  for ACC across the height and width of the SDF archetype for a case where corner diagonal members of the first floor are exposed to corrosion for 25 years. As expected, the sensor closest to the corroded members shows the largest changes in  $DI$  signifying the location of the damage. Note that larger  $DI$  denotes larger variance of identified EDP at that sensor compared to that of uncorroded structure. Variation of  $DI$  for other EDPs, i.e. Disp and IDR, also indicates damage in the structure.  $DI$  of Disp clearly identifies the damaged floor but not the exact sensor location. Therefore, ACC is found to be a better indicator of damage location for diagrid frames. The number of sensors on each floor is also studied. Figure 5.12 (b) illustrates the variation of  $DI$  for all EDPs having one sensor at each floor for the same damaged case. As depicted, even with one sensor at each floor,  $DI$  for all EDPs identifies the damage and  $DI$  for ACC and Disp locates the damaged floor.  $DI$  for IDR has a larger value on the top floor instead of the first floor which can be attributed to the way sensors are located on the frame. As shown in Figure 5.11, sensors are not located above each other due to the diagrid triangular form.

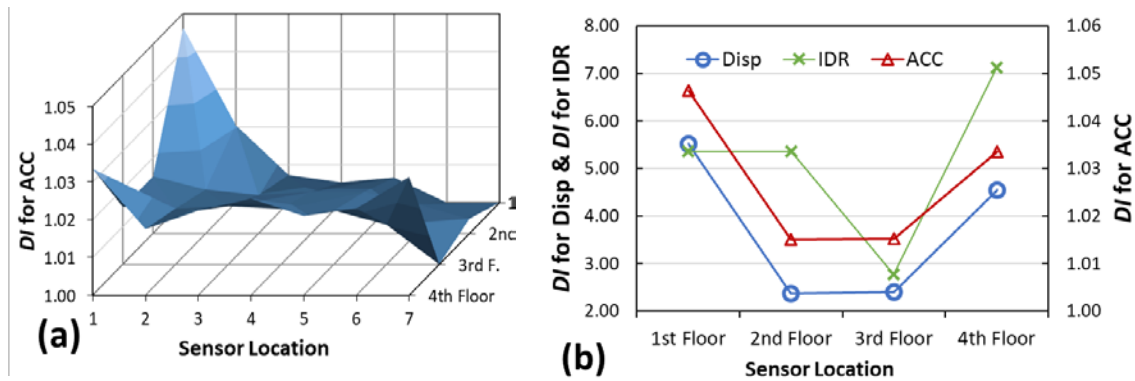


Figure 5.12 Variation of DI for (a) ACC with sensors at diagrid nodes and (b) all EDPs with one sensor at each floor of SDF archetype

For the damaged case of RCF archetype, multiple damage location is studied where two columns of the first floor (at the 2<sup>nd</sup> and 5<sup>th</sup> axes) have failed due to a mainshock earthquake. The ARX model accurately detected the presence of damage in the structures through a change in *DI*. As depicted in Figure 5.13, *DI* for Disp, ACC, and IDR detects the damaged floor as well. *DI* for ACC detects the location of one damaged column accurately (sensor #5 at axis 5 in Figure 5.13 (a)) and indicates damage around axis 1 and 2 (sensor #1 and sensor #2 in Figure 5.13 (a), respectively).

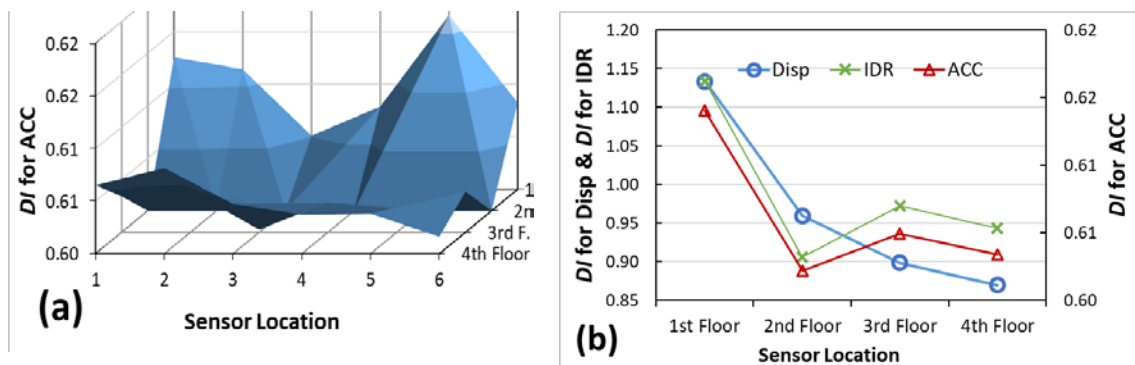


Figure 5.13 Variation of DI for (a) ACC with sensors at beam-column nodes and (b) all EDPs with one sensor at each floor of RCF archetype

### ***5.6.2 Damage Severity and Characterization***

Detecting and locating the damage are the primary benefits of current SHM systems. However, they may be used for damage severity and characterization. This measurement and characterization are valuable during normal operation to update the numerical models as well as during post-quake recovery planning to minimize the need for inspection and offline evaluation. The ARX model can measure damage severity and as discussed earlier detect the damage location but for damage characterization, commonly case-based experimental data are required (Lynch and Loh 2006; Sohn and Farrar 2001; Vidal et al. 2014). A practical approach is to use offline non-destructive evaluation techniques and inspection to characterize the damage after it is detected and located by the SHM system (Farrar and Worden 2007). As this inspection is based on detected damage and limited to the damaged location, this is an informed and efficient inspection.

Figure 5.14 shows the variation of mean  $DI$  for different EDPs with different damage severity for SDF archetype.  $DI$  in this figure is the average of  $DI$  for all sensors and all LHS segments. Following the previous discussion on life-cycle functionality assessment, corrosion severity at a certain age is used to indicate damage severity (at the two corner diagonals of the 1<sup>st</sup>-floor corresponding to analysis in the previous section). As depicted, mean  $DI$  increases as damage severity increases. Figure 5.14 also shows the CoV of  $DI$  as error bars which reveal that uncertainty in  $DI$  is also increasing as the damage severity increases. Different EDPs show similar capability in detecting the severity of the damage.

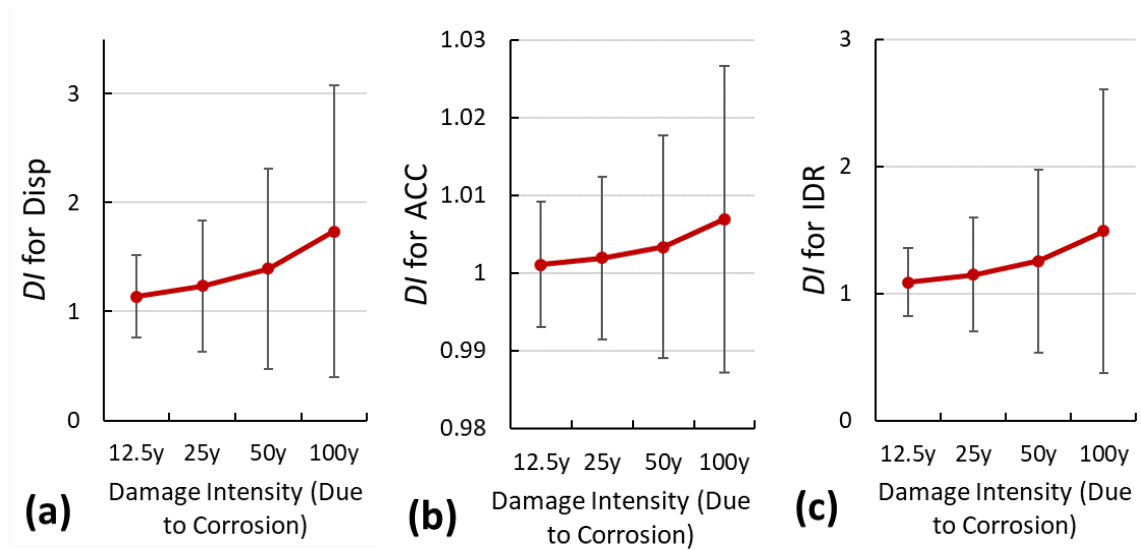


Figure 5.14 Variation of mean DI for (a) Disp, (b) ACC, and (c) IDR for all sensors

## 5.7 Resilience Quantification

### 5.7.1 Scenario-based Assessment

The functionality of the structures is studied using a scenario-based approach in the absence of real data on archetypes (ATC 2009; FEMA 2012). The ground-motion prediction equations (attenuation function) proposed by (Boore and Atkinson 2008) is used to find the spectral intensity at the building site given three scenario earthquakes: (1) an M6.5 earthquake with an epicentral distance of 40 km, (2) an M7 earthquake with an epicentral distance of 15 km, and (3) an M8 earthquake with an epicentral distance of 5 km from the building site all with a shear-wave velocity from the surface to 30 m ( $V_{S30}$ ) of 300 m/s (Burton et al. 2016). Accordingly, the median spectral acceleration intensity for scenarios 1-3 is 0.41 g, 0.83 g, and 1.55g for SDF archetype with fundamental periods of 0.36 sec and 0.31 g, 0.70 g, 1.60 g for CRF archetype with fundamental periods of 0.74 sec, respectively. The median spectral acceleration for scenario 1-3 is roughly 1/6, 1/3, and 2/3 of the maximum considered earthquake (MCE) spectral acceleration, respectively.

### ***5.7.2 Component-based Functionality Curve***

Figure 5.15 shows the component-based functionality curve of the SDF archetype. Total replacement time is presumed to be 720 and 950 days for SDF and RCF archetypes, respectively (FEMA 2012). Note that in the proposed framework, EDP outputs of sensors are used to perform the loss analysis, produce functionality curves, and estimate the resilience index but here, for demonstration, the outputs of calibrated numerical models are used. The SDF building shows 91.85% resilience under the scenario 2 which indicates an acceptable design for diagrid frame given the magnitude and the distance of the earthquake (an M7 earthquake with an epicentral distance of 15 km). However, it suffers from both structural and non-structural losses (approximately 10% structural loss and 22% non-structural loss). Structural components take about 99 days to repair. Among non-structural components, suspended ceilings vulnerable to excessive acceleration incur the bulk of the damage and constitute the largest portion of the downtime (about 103 days of total 447 days). Wall partitions are the second largest in terms of downtime with a repair time of about 83 days.

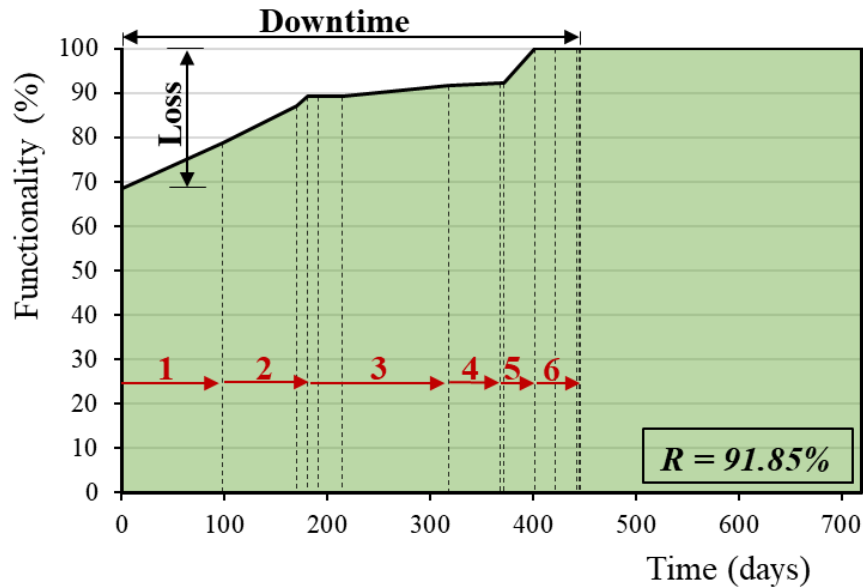


Figure 5.15 Functionality curve of original SDF archetype under scenario earthquake 2 (numbered arrows show the repair time for various components: (1) structural components including diagonals, beams, and connections, (2) curtain and partition walls, (3) raised access floors and suspended ceilings, (4) independent pendant lighting, (5) hydraulic elevator and chiller on the roof, (6) HVAC ducting, air handling unit, and fire sprinklers)

Figure 5.16 compares the functionality curve of various SDF and RCF archetypes under scenario earthquake 2. Four cases are shown for the SDF archetype including an SDF building with all or two corner diagonals of the 1<sup>st</sup> story damaged due to 25 and 100 years of exposure to corrosion. For the RCF, two columns of the 1<sup>st</sup> floor are assumed to fail due to a mainshock earthquake. Given the uncertainty involved in loss and vulnerability analyses, the recovery path for corroded archetypes is slightly different compared to the uncorroded case. The structural damage is noticeably larger for the corroded cases (up to 22% larger in case of SDF with 25-year corrosion for all diagonals and 95% larger in case of RCF with 2 failed columns).

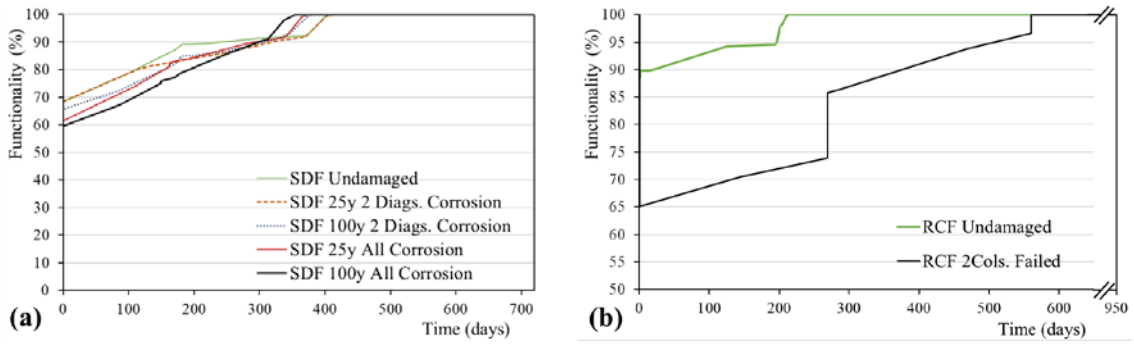


Figure 5.16 Comparison of functionality curves for (a) SDF and (b) RCF archetypes undamaged and various damaged cases under scenario earthquake 2

Table 5.3 lists the resilience, robustness, and rapidity indices, median repair time considering a parallel repair plan, and median monetary loss for various archetypes. Note that rapidity index is the ratio of total monetary loss (as a percentage of total replacement cost) to downtime (as a percentage of total replacement time). The resilience of the buildings against a scenario earthquake is generally decreasing as damage increases. The reduction is noticeable in the case of the SDF archetype exposed to a 100-year corrosion compared to the original SDF (0.6%, 3%, and 4% reduction in Scenario 1, 2, and 3, respectively) and it is even more noticeable in the case of the RCF with failed columns when compared to the original RCF (1.2%, 10%, and 25% reduction in Scenario 1, 2, and 3, respectively). This shows the impact of partial structural failure that occurred due to the mainshock on the resilience of the structure during the aftershock. Due to column failure, the median repair cost of the RCF archetype in scenario 2, for instance, has increased by nearly 207% while repair time has increased by about 139% compared to the undamaged case. Nonetheless, among the SDF cases, variation is not significant since the damage due to corrosion is insignificant as discussed in the collapse fragility analysis section. Similarly, robustness, which embodies the residual capacity of the system, decreases with damage.

As described in this section, the outputs of SHM system are used to produce detailed reports, containing functionality curves and resilience indices, for experts to further assess the health of the building and if needed, develop a rehabilitation plan. The report also identifies the location of the possible damages and the severity of the damages as well, as demonstrated in previous sections.

Table 5.3 Resilience, robustness, and rapidity indices, median monetary loss, and median repair time considering a parallel repair plan for various archetypes for Scenario 1, 2, and 3 earthquakes

Archetype	Resilience (%)			Robustness (%)			Rapidity (%/%)			Repair Cost (10,000\$)			Repair Time (Days)		
	S1	S2	S3	S1	S2	S3	S1	S2	S3	S1	S2	S3	S1	S2	S3
SDF	98	92	73	85	68	44	0.6	1.9	0.6	68	147	261	165	119	711
SDF-2Dia. 25y	98	91	75	85	68	44	0.6	2.2	0.6	68	172	260	166	119	711
SDF-2Dia. 100y	98	90	74	86	66	43	0.6	2.2	0.6	67	171	263	162	119	711
SDF-All 25y	97	90	75	85	61	43	0.6	2.2	0.6	69	174	265	167	121	711
SDF-All 100y	97	89	70	85	59	42	0.6	2.2	0.6	70	177	272	171	123	711
RCF	100	98	84	98	89	68	0.7	1.7	0.6	23	118	328	32	62	483
RCF-2Col. Failed	99	89	63	89	65	26	0.6	2.2	0.7	110	361	765	167	148	940

### 5.7.3 Post-quake Safety Evaluation

In the Central Console, results of damage detection, vulnerability assessment, and loss estimation are used for the post-quake decision on evacuation and repair/rehabilitation. In the proposed framework, after an earthquake, recorded EDP values will simply be used to find the damage state of each component, assess safety based on the criteria described in Subsection 2.4, and make a decision on evacuation. For safety evaluation under future earthquake scenarios, a multi-criteria probabilistic approach is used here to assign the

evacuation tags. Using component-based damage state criteria described earlier, the probability of reaching minor, moderate, or severe damage states for critical components are quantified, listed in Table 5.4. Given the uncertainty involved, here a 5% limit is used on the probability of each damage state instead of non-occurrence. These probabilities are used to assign a red/yellow/green tag to each archetype given a possible earthquake scenario. For residual IDR, per FEMA P-58, a median and dispersion of 1.0% and 0.3 are used. Also, IDR of 0.2%, 0.5%, and 1.0% represent minor, moderate, and severe damage states for stiff diagrid frames while IDR of 1.5%, 2.7%, and 4.1% represent those of ductile special RCF, respectively (FEMA 2012). As listed in Table 5.4, given that all archetypes incur minor damages under the Scenario 2 earthquake, none satisfies the green tag requirement. Yet, damages remain minor with a small amount of moderate damage to various components (up to 17% moderate damage for wall partitions of RCF archetype). Colored cells in Table 5.4 indicate the main damage states with high probability which lead to a yellow tag for the archetypes. For the SDF cases, fire sprinklers which are vulnerable to excessive acceleration incur larger moderate damage compared to other components. This is partly because of its stiff diagrid frame which is able to limit IDR but can experience large spectral acceleration as reported previously (Asadi et al. 2018; Kim and Lee 2012). The difference in probability of various damage states among various SDF archetypes is insignificant. Probabilities generally increase as damage increases with a few exceptions such as minor damage state due to residual IDR and different damage states for fire sprinkler. These exceptions are attributed to the uncertainty involved considering minimal differences between various cases. Ductile special RCF limits structural damages and RCF archetypes incur mostly non-structural damage to wall partitions and curtain walls which

are vulnerable to excessive IDR. Under Scenario 3, all archetypes received a Red tag. The SDF archetype received a Red tag because of about 11% probability of severe damage to fire sprinklers, which are sensitive to ACC. The RCF received a red tag because of up to 32% probability of severe damage to wall partitions which are sensitive to IDR.

Table 5.4 Probability of minor (DS<sub>1</sub>), moderate (DS<sub>2</sub>), or severe (DS<sub>3</sub>) damage states for critical components

Critical Component	Damage State	SDF	SDF-2Dia. 25y	SDF-2Dia. 100y	SDF-All 25y	SDF-All 100y	RCF	RCF-2Col. Failed
Probability of different damage states under Scenario 2								
Diagonals/ Columns and Beams	DS <sub>1</sub>	0.601	0.600	0.600	0.599	0.605	0.000	0.003
	DS <sub>2</sub>	0.031	0.034	0.034	0.043	0.057	0.000	0.000
	DS <sub>3</sub>	0.000	0.000	0.000	0.000	0.000	0.000	0.000
Curtain and Partition Walls	DS <sub>1</sub>	0.700	0.701	0.701	0.711	0.720	0.357	0.340
	DS <sub>2</sub>	0.034	0.008	0.007	0.008	0.014	0.168	0.164
	DS <sub>3</sub>	0.000	0.000	0.000	0.000	0.000	0.031	0.034
Fire Sprinkler	DS <sub>2</sub>	0.126	0.126	0.119	0.124	0.120	0.000	0.000
	DS <sub>3</sub>	0.034	0.016	0.016	0.015	0.011	0.000	0.000
Residual IDR	DS <sub>1</sub>	0.661	0.661	0.663	0.653	0.650	0.009	0.009
	DS <sub>2</sub>	0.074	0.074	0.076	0.089	0.110	0.000	0.000
	DS <sub>3</sub>	0.000	0.000	0.000	0.000	0.000	0.000	0.000
Safety Tags for various scenarios								
Scenario 1		Green	Green	Green	Yellow	Yellow	Green	Yellow
Scenario 2		Yellow	Yellow	Yellow	Yellow	Yellow	Yellow	Yellow
Scenario 3		Red	Red	Red	Red	Red	Red	Red

## 5.8 Conclusions

A component-based functionality assessment and resilience quantification method is proposed which matches well with FEMA P-58 loss estimation method. The framework uses the data obtained by a localized sensor network to identify different damages to the structure, produce a component-based functionality curve, quantify resilience, and make quantitative decisions on the evacuation of the building.

The proposed nonlinear ARX system identification model is capable of detecting, locating, and measuring negligible damages to the structure. The ratio of variances of residual errors ( $DI$ ), used as a damage-sensitive coefficient, was found to be an accurate indicator of damage in the structure. For both stiff diagrid frame and ductile reinforced concrete frame,  $DI$  of the maximum absolute floor acceleration (ACC) is more accurate in locating the damage than other engineering demand parameters including maximum interstory drift ratio (IDR) and maximum absolute floor displacement (Disp).  $DI$  of IDR and Disp signals are primarily suitable for damage detection and measurement, however. All three mentioned indicators can identify minor changes to damage severity. As damage severity increase, both the mean and the dispersion of  $DI$  increased. Using the ARX model, as few as one sensor at each floor can detect the damage and locate the damaged floor.

Using component-based functionality curves, resilience, robustness, and rapidity indices are calculated and scenario-based recovery path is studied. Given the uncertainty involved, the recovery paths of pre-event damaged and undamaged structures are dissimilar, and the resilience index can identify primarily moderate to major damages. In the studied archetypes, pre-event damage increased structural repair cost up to 20% in case of deteriorated diagrid frames and 368% in case of partially failed reinforced concrete frames. Failure of two of the 1<sup>st</sup> story columns of the studied concrete archetype caused about 10% reduction in resilience index while median repair cost increased by nearly 207% and repair time increased by about 139% compared to the undamaged case. A quantitative post-quake safety evaluation method is used to assign green/yellow/red tags on buildings based on the output EDP which can be directly obtained from SHM system after the earthquake or estimated for future scenario earthquakes. Although this method provides a

straightforward and meaningful decision for rapid post-quake evacuation, detailed results for resilience quantification are to be used for recovery planning.

As an extension to the current study, structural control models can be used to minimize loss and improve the functionality of the system. Further, the proposed safety evaluation method can be expanded to a risk-informed multi-criteria decision model which takes into account trade-off between various resilience metrics such as direct and indirect monetary loss, recovery time, and casualty as well as sustainability metrics such as construction cost and embodied energy to find an optimal repair/rehabilitation plan (Lee et al. 2018).

## 5.9 Appendix A.

Table 5.A.1 Structural and non-structural fragility and cost specifications for various components

Description	Used in	Unit	EDP	Damage state	Fragility Parameters		Fragility specification code	Average repair cost (US\$)
					$\mu^a$	$\beta^b$		
Diagrid Frame with w-shaped diagonals, w < 40 PLF	SDF	EA	IDR (rad)	DS <sub>1</sub>	0.0025	0.26	adapted from B1033.002a of FEMA P-58	44,530
				DS <sub>2</sub>	0.0055	0.23		48,650
				DS <sub>3</sub>	0.0095	0.32		48,960
				DS <sub>4</sub>	0.0125	0.34		48,960
Diagrid Frame with w-shaped diagonals, 41 PLF < w < 99 PLF	SDF	EA	IDR (rad)	DS <sub>1</sub>	0.0025	0.26	adapted from B1033.002b of FEMA P-58	44,530
				DS <sub>2</sub>	0.0055	0.23		53,590
				DS <sub>3</sub>	0.0095	0.32		57,340
				DS <sub>4</sub>	0.0125	0.34		57,340
Diagrid Frame with w-shaped diagonals, w > 100 PLF	SDF	EA	IDR (rad)	DS <sub>1</sub>	0.0025	0.26	adapted from B1033.002c of FEMA P-58	44,530
				DS <sub>2</sub>	0.0055	0.23		60,470
				DS <sub>3</sub>	0.0095	0.32		67,340
				DS <sub>4</sub>	0.0125	0.34		67,340
Post-Northridge welded steel moment connection other than RBS, beam one side, beam depth ≤ W27	SDF	EA	IDR (rad)	DS <sub>1</sub>	0.03	0.3	B1035.021 (FEMA P-58)	20,880
				DS <sub>2</sub>	0.04	0.3		35,160
				DS <sub>3</sub>	0.05	0.3		35,160
Post-Northridge welded steel moment connection other than	SDF	EA	IDR (rad)	DS <sub>1</sub>	0.03	0.3	B1035.031 (FEMA P-58)	42,000
				DS <sub>2</sub>	0.04	0.3		62,760
				DS <sub>3</sub>	0.05	0.3		62,760

RBS, beams both sides, beam depth <= W27									
ACI 318 SMF, Conc Col & Bm = 24" x 24", Beam both sides	RCF	EA	IDR (rad)	DS <sub>1</sub>	0.02	0.4	B1041.001b	27,800	
				DS <sub>2</sub>	0.0275	0.3		39,000	
				DS <sub>3</sub>	0.05	0.3		48,400	
Low rise reinforced concrete walls with boundary columns, 8" to 16" thick, height <15'	RCF	EA	IDR (rad)	DS <sub>1</sub>	0.0033	0.35	B1044.071	18,530	
				DS <sub>2</sub>	0.0087	0.2		36,200	
Reinforced concrete flat slabs- columns with shear reinforcing	RCF	EA	IDR (rad)	DS <sub>1</sub>	0.03	0.4	B1049.011	41,200	
				DS <sub>2</sub>	0.048	0.4		45,600	
Curtain Walls - Generic Midrise Stick-Built Curtain wall, Config: Monolithic	SDF,	ft <sup>2</sup>	IDR (rad)	DS <sub>1</sub>	0.0338	0.4	B2022.001 (FEMA P-58)	2,060	
	RCF			DS <sub>2</sub>	0.0383	0.4		2,60	
Wall Partition, Type: Gypsum with metal studs, Full Height, Fixed Below, Fixed Above	SDF,	based upon 13'x100' Panels	IDR (rad)	DS <sub>1</sub>	0.0021	0.6	C1011.001a (FEMA P-58)	2,730	
	RCF			DS <sub>2</sub>	0.0071	0.45		5,190	
				DS <sub>3</sub>	0.012	0.45		7,940	
Wall Partition, Type: Gypsum + Wallpaper, Partial Height, Fixed Below, Lateral Braced Above	SDF, RCF	based upon 9'x100' Panels	IDR (rad)	DS <sub>1</sub>	0.0064	0.3	C3011.001b (FEMA P-58)	3,510	
Raised Access Floor, seismically rated	SDF, RCF	ft <sup>2</sup>	ACC (g)	DS <sub>1</sub>	1.5	0.4	C3027.002 (FEMA P-58)	130	
Suspended Ceiling, SDC D, E (I <sub>p</sub> =1.0), Area (A): A < 250, Vert & Lat support	SDF, RCF	each 600 ft <sup>2</sup>	ACC (g)	DS <sub>1</sub>	1.0	0.4	C3032.003a (FEMA P-58)	1,230	
				DS <sub>2</sub>	1.8	0.4		10,220	
				DS <sub>3</sub>	2.4	0.4		19,760	
Suspended Ceiling, SDC D, E (I <sub>p</sub> =1.0), Area (A): 250 < A < 1000, Vert & Lat support	SDF, RCF	each 250 ft <sup>2</sup>	ACC (g)	DS <sub>1</sub>	0.7	0.4	C3032.003b (FEMA P-58)	470	
				DS <sub>2</sub>	1.15	0.4		3,770	
				DS <sub>3</sub>	1.8	0.4		7,830	
Independent Pendant Lighting - seismically rated	SDF, RCF	EA	ACC (g)	DS <sub>1</sub>	1.5	0.4	C3034.002 (FEMA P-58)	640	
Hydraulic Elevator – Applies to most	SDF, RCF	EA	ACC (g)	DS <sub>1</sub>	0.5	0.3	D1014.021 (FEMA P-58)	11,990 <sup>c</sup>	

California Installations  
1976 or later

HVAC Galvanized Sheet Metal Ducting less than 6 sq. ft., SDC D, E, or F	SDF, RCF	based upon 1000 ft. segment	ACC (g)	DS <sub>1</sub> DS <sub>2</sub>	1.5 2.25	0.4 0.4	D3041.011c (FEMA P-58)	1,300 12,700
Control Panel - Capacity: all - Equipment that is either hard anchored or is vibration isolated	SDF, RCF	EA	ACC (g)	DS <sub>1</sub>	3.0	0.4	D3067.013b (FEMA P-58)	4,570
Fire Sprinkler Drop Standard Threaded Steel	SDF, RCF	per 100 units	ACC (g)	DS <sub>1</sub> DS <sub>2</sub>	1.5 2.25	0.4 0.4	D4011.053a (FEMA P-58)	550 550
Chiller - Capacity: 350 to <750 Ton	SDF, RCF	EA	ACC (g)	DS <sub>1</sub>	0.72	0.2	D3031.013h (FEMA P-58)	280,720
Air Handling Unit - Capacity: 25000 to <40000 CFM	SDF, RCF	EA	ACC (g)	DS <sub>1</sub>	1.54	0.6	D3052.013k (FEMA P-58)	206,800 <sup>d</sup>

a  $\mu$  = Median of component fragility curve

b  $\beta$  = Lognormal standard deviation (dispersion) of component fragility curve

c Collective cost

d Collective cost

Note: EA = per unit

## **Chapter 6**

# **6. Multi-dimensional Functional Earthquake Recovery Analysis and Resilience Quantification of Building Facilities**

### **6.1 Introduction**

Rapid population growth and economic developments in earthquake-prone regions and increasing vulnerability of aging buildings and lifeline infrastructures have increased the seismic risk in the last decades (FEMA et al. 2017). Per National Geophysical Data Center (NGDC), 128 significant earthquakes (M7.0 or greater) have occurred worldwide in last decade which have claimed 335,000 lives, destroyed around 600,000 houses, and caused hundreds of billion USD damage (NGDC/WDS 2019). To minimize seismic loss and casualties, recent studies advocate an all-inclusive resilience-based approach that incorporates functional recovery on top of traditional safety-based approach (Bocchini et al. 2014; Bruneau et al. 2003; Burton et al. 2016; EERI 2019; Reinhorn and Cimellaro 2014).

Seismic resilience can be achieved by reducing the probability of failure, the seismic consequence/loss, and the time needed to restore the intended functionality (Bruneau et al. 2003). Post-event recovery time may include the time required for

inspection and safety evaluation, finance and engineering planning, repair of various structural and non-structural components, repair of access routes and utility services, and inhabiting the building again (Burton et al. 2016; Mitrani-Reiser 2007). For building environments, the consequence and loss due to an earthquake may include monetary loss, casualties, injuries, fatalities, and any other economic and social impacts. Asadi et al. (2019b) proposed a multi-criteria decision model to include various economic, social, and environmental criteria in resilience assessment. The model quantifies resilience indicators such as seismic loss and downtime discretely and then integrates them using multi-attribute utility theory. Reinhorn and Cimellaro (2014) considered two scales, i.e. spatial and temporal scales, for resilience evaluation of a community and proposed a seven-dimension framework for community functionality assessment which includes population, environmental, governmental, economic, and social/cultural dimensions. For their case study, they study a health care facility and used asset loss as an indicator of the functionality of a building facility. In a number of publications including a recent book, Cimellaro et al. provide various methodologies to assess community resilience and quantify resilience for based on asset losses (Cimellaro 2016; Cimellaro et al. 2006, 2010, 2016).

However, the function/purpose of a building system can be evaluated using other indicators/measures and each of these indicators/measures can be used to develop a functionality curve. Given that the primary function of a building is to provide safe housing for occupants, Burton et al. (2016) considered housing capacity (number of occupants) as an indicator of the functionality. They indicated that repairs associated with structural safety and internal access need to be completed to restore the occupancy after earthquakes. They propose three functioning states to model shelter-in-place housing capacity of the

buildings which includes (1) building is unsafe for occupancy hence non-functional which is equivalent to red tag of ATC-20 method (Rojah 2005), (2) building is safe for occupancy hence fully functional equivalent to green tag of ATC-20, and (3) building is safe but not fully functional. In their community-based approach, buildings can have one of the three conditions in terms of occupancy regardless of building internal components on each floor. Han et al. (2015) suggest a few damage criteria for normal, prudent, and imprudent occupants in case of evacuating a building after earthquake. Accordingly, normal occupants are likely to evacuate under damages such as (1) a beam or column reaches moderate damage state or higher, (2) a story shows significant IDR, (3) curtain wall or wall partition reaches significant damage state, (4) a sprinkler fractures, and (5) ceiling unit collapses. Prudent occupants, however, are more likely to evacuate under relatively minor damages such as (1) a beam or column incurs minor damage, (2) a story shows visible IDR, (3) a curtain wall or wall partition incurs visible damage, (4) a sprinkler fractures, and (5) a ceiling unit collapse. Imprudent occupants are likely to evacuate under more severe damages such as beams and columns incurring severe damage state and severe IDR.

Further, the new paradigm of functional recovery aims to introduce new design provisions based on recovery time, a much-needed supplement to the widely-integrated safety-based design provisions (EERI 2019; Sattar et al. 2018). Design for functional recovery is supported by National Earthquake Hazards Reduction Program (NEHRP) and Earthquake Engineering Research Institute (EERI) as an imperative element of resilience-based community management. Recent studies focus on community resilience (Burton et al. 2016; Dong and Li 2017; McAllister Therese 2016). However, building facilities are commonly designed as a discrete structure based on the owner's preference and design

standards. Therefore, a functional recovery design framework needs to present a quantitative method to find the recovery time for a distinct facility considering the interdependent impact of lifeline infrastructure. Moreover, damage to each infrastructure system may affect one or a few measures of building functionality and leave other measures intact. For instance, damage to the transportation system mostly affects the occupancy aspect since it limits the residents' ability to reenter the building or get access to lifeline facilities. Meanwhile, damage to water distribution system affects the serviceability aspect of the functionality given it limits occupants' ability to access to water/wastewater service even if the building is safe to occupy. This partial interdependency between buildings and lifeline systems further complicates the problem indicating the need for a multi-dimensional approach in resilience quantification of building facilities. For building facilities, the first objective following an earthquake is to reoccupy or re-enter the building and restore the shelter-in-place function of the building. The next step is to achieve functional recovery where all building's services need to be restored to attain the building's intended operation/function (EERI 2019). A practical interim design approach is to design for code-based safety requirements and control the system for functionality criteria.

This paper presents a new multi-dimensional framework for functional recovery analysis and resilience quantification of building facilities. Three measures defining the seismic functionality of a building facility are considered, which are asset, occupancy, and serviceability losses. The model is consistent with FEMA P-58 approach for loss analysis and considers the loss and downtime due to various structural and non-structural components of the building in resilience quantification. The framework is implemented on

two groups of steel and reinforced concrete (RC) buildings archetypes located in a highly seismic region using a scenario-based approach.

## **6.2 Proposed Framework**

### ***6.2.1 Life-cycle Functionality and Resilience***

Functionality, also called serviceability and quality, is an indicator of system robustness, redundancy, resourcefulness, and rapidity, which are four aspects of resilience (Bruneau et al. 2003; EERI 2019). As shown in Figure 6.1, throughout the life-cycle of a structure, functionality may be affected by various activities and events such as deterioration, rehabilitation, repair, and extreme events like earthquake ( $t_{E1}$  and  $t_{E2}$  for mainshock and aftershock in Figure 6.1, respectively). The key stage where functionality decreases drastically is when an extreme event such as a major earthquake strikes the building. At this stage, loss of functionality and the post-event recovery indicate the resilience of the system against that hazard. In addition to extreme events, structure may lose strength and consequently functionality because of corrosion, erosion, fatigue, and other time-based deterioration phenomena as well. Maintenance, repair, rehabilitation activities restore functionality up to its initial state and retrofit may improve it beyond that to an improved functional level.

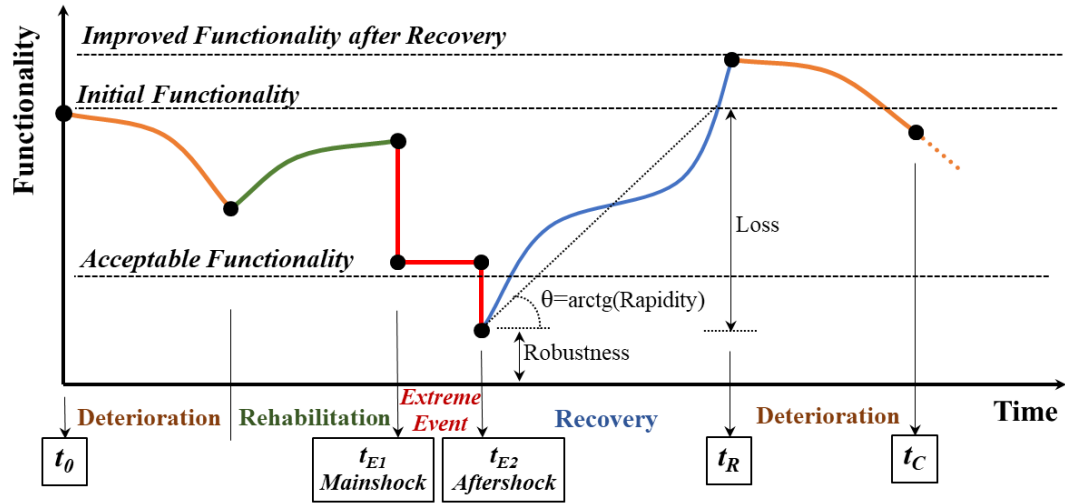


Figure 6.1 Life-cycle functionality of a system (not to scale)

Resilience is commonly quantified by integrating functionality over a time interval  $(t_C - t_0)$  (Cimellaro et al. 2010).

$$R = \frac{1}{t_C - t_0} \int_{t_0}^{t_0+t_C} Q(t) dt \quad (6.1)$$

where  $t_0$  marks the start time of life-cycle functionality assessment and  $t_C$ , control time, marks the end of the cycle or the effective life span of the system.  $Q(t)$  is the functionality, a non-stationary stochastic process. As such, the area under the functionality curve is an index of resilience. Furthermore, aspects of resilience can be quantified using functionality as well. The ratio of loss ( $L_t$ ) over recovery time is the average rapidity, as shown in Figure 6.1. Also, residual functionality after an extreme event is the robustness of the system (Bruneau et al. 2003).

## ***6.2.2 Multi-dimensional Functionality Assessment***

### **6.2.2.1 Functionality based on Loss of Occupancy**

As discussed, the area under the functionality curve is commonly used to quantify resilience. Functionality, however, depends on several measures each can be an indicator of system function/purpose and each can be used to develop a functionality curve. For instance, Burton et al. (2016) considered the number of occupants (housing capacity) as an indicator of the functionality. Occupancy (housing capacity) is measured in person-days for a community. To restore occupancy after an earthquake, they indicated that repairs associated with structural safety and internal access need to be completed. Considering a component-based approach for functionality assessment, damage to structural components and non-structural components such as partition walls and curtain walls affects the occupants' ability to reenter or reoccupy the building after an earthquake.

To evaluate occupancy based on outputs of numerical simulation, researchers have provided various criteria on EDPs and/or damage states (Guéguen and Tiganescu 2018; Han et al. 2015; Naeim et al. 2006). Han et al. (2015) recommended a series of component-based damage criteria for post-earthquake occupancy assessment of buildings. Accordingly, if a building experiences (1) severe damage to exterior beam or column, (2) severe residual IDR (unrepairable IDR) on a floor, or (3) severe damage of fire sprinkler units, it is unsafe for re-occupancy and a red tag will be assigned to the building based on ATC 20 safety tagging method (Rojah 2005). Also, if a building experiences (1) minor or more significant damage to exterior beam or column, (2) severe residual IDR in any story, or (3) fracture of fire sprinkler units, it needs to be evacuated for further investigation and a yellow tag will be assigned based on ATC 20 method. Considering that damage to curtain

walls and wall partitions also impacts the occupancy and may trigger evacuation, Asadi et al. (2019a) added another criterion to the above three criteria, which is (4) severe damage to curtain walls and wall partitions. Therefore, if any of the four criteria occurs on any floor, that floor needs to be evacuated.

To restore occupancy, the components affecting the occupancy need to be repaired, which include structural components such as beam, columns, shear walls, braces, slabs, and connections and non-structural components such as exterior walls, curtain wall with windows, roof finishes, chimney, partition, stairs, doors, suspended ceilings, floor finishes, etc. Hence, occupancy-based recovery function of the building,  $f_{R,Occ}$ , is a function of repair time of those components,  $t_{Rk,Occ}$ , on various floors. Assuming a floor-by-floor repair scheme, the total time to restore occupancy is the summation of the repair time of all occupancy-related components for all floors.

$$f_{R,Occ} = \sum_{f=1}^q \sum_{k=1}^p \int_{t_{Rk,Occ}} f_{Rk,Occ}(t, t_E, t_{Rk,Occ}) dt \quad (6.2)$$

where  $f = 1, \dots, q$  is the floor number,  $f_{Rk,Occ}$  is the repair time function for component  $k$  among all  $p$  occupancy-related components of floor  $f$ .

### 6.2.2.2 Functionality based on Loss of Serviceability

A primary function of buildings post-earthquake is to provide safe shelter-in-place. However, the functional recovery of the building is not achieved until all utility services are restored as well. In building facilities, two milestones are to be considered for restoring functional recovery after an earthquake. First, the repairs related to safety and occupancy need to be completed so the residents can reenter the building. The first step, occupancy

restoration, is discussed in the previous section. Next, services such as water/wastewater, electricity, conveying, air-conditioning, fire protection, gas, Internet, and equipment and furnishing need to be restored in order to achieve full functionality. The second step, serviceability restoration, is largely dependent on restoration time of water, power, and gas network of the community. Nonetheless, the non-structural components of the building which provide those services should be repaired as well. These components may include cold/hot water pipes, wastewater pipes, fire sprinklers, heat-generating systems, building's hot water and electricity supply systems, building's air, hot/cold water, electricity, and gas distribution system, elevators, chillers, and their control panels and instrumentation.

Similar to occupancy, loss of serviceability of a building is due to damage to the components providing those services. Most of the non-structural components which provide serviceability are vulnerable to excessive absolute floor acceleration (ACC). FEMA P-58 provides damage state specifications for common components of building facilities, which are used here to define the limit state that triggers serviceability loss. To restore serviceability, both the non-structural components required for each service and the corresponding supply network in the community need to be repaired if damaged. Serviceability-based recovery function of a building,  $f_{R, Serv}$ , can be defined as a function of repair time of serviceability-related components on various floors,  $t_{Rk, Serv}$ . Similar to occupancy, the total time to restore serviceability is the summation of the repair time of all related components for all floors.

$$f_{R, Serv} = \sum_{f=1}^q \sum_{k=1}^p \int_{t_{Rk, Serv}} f_{Rk, Serv}(t, t_E, t_{Rk, Serv}) dt \quad (6.3)$$

where  $f_{Rk, Serv}$  is the repair time function for component  $k$  among all components required for restoring serviceability to floor  $f$ .

### 6.2.2.3 Functionality based on Asset Loss

Given the building is an asset/property, Cimellaro et al. (2010) considered monetary loss as the main functionality indicator to produce the seismic functionality curve. They used the repair cost of an archetype building to find the post-earthquake immediate loss of functionality. Accordingly, functionality depends on (1) total loss,  $L_t$ , which is the summation of all monetary losses to all damageable structural and non-structural components due to earthquakes and (2) recovery function,  $f_R$ , which represents system rapidity. Recovery function can be developed using repair/recovery time and repair scheme which could be parallel, i.e. concurrent repairing all floors, or series, i.e. repairing each floor after completing the repair of lower floors. Therefore, functionality ( $Q$ ) is defined as follows (Cimellaro et al. 2010).

$$Q(t_E < t < t_R) = [1 - L_t(IM, t_R)] \times f_R(t, t_E, t_R) \quad (6.4)$$

where  $t_E$ ,  $t_R$ , and  $IM$  are earthquake effective occurrence time, recovery time, and earthquake intensity, respectively.

To systematically develop a functionality function/curve, component-level loss and recovery time are needed. FEMA P-58 Performance Assessment Calculation Tool (PACT) provides such a comprehensive component-level fragility specification database which is used here to estimate the seismic loss, downtime, and other consequences (FEMA 2012). They are used to find the total loss and recovery time and to develop a step-wise recovery

scheme. In general, any kind of loss due to seismic hazard can be calculated as follows (Asadi et al. 2019b; Bocchini et al. 2014; Mitrani-Reiser 2007).

$$P(L > l_i) = \int_{IM} \int_{EDP} \int_{DS} P(L > l_i | DS) P(DS | EDP) P(EDP | IM) P(IM) dDS dEDP dIM \quad (6.5)$$

where  $P(L > l_i | DS)$  is the conditional probability of loss given certain damage state which is obtained from FEMA P-58 fragility database,  $P(DS | EDP)$  is the probability of reaching each damage state given certain EDP,  $P(EDP | IM)$  is the probability of reaching a certain EDP given a hazard intensity of  $IM$ , and  $P(IM)$  is the probability of exceedance for each intensity which is acquired from the United States Geological Survey (USGS) online hazard tool and adjusted for a 5% damping ratio and the fundamental period of the structure.

#### 6.2.2.4 Multi-dimensional Functionality Hypersurface

In this study, the concept of functionality curves is extended to functionality surface, a 2-dimensional (2D) extension, or higher levels (3D, 4D, etc.) depending on the number of functionality indicators considered for the system. Using this new multi-dimensional functionality hypersurface, multiple indicators of functionality can concurrently be studied and used to quantify a multi-variant resilience index. As such, the following multiple integral is developed to quantify a new multi-dimensional resilience index for residential communities where the weighted summation of resilience indices for various facilities gives the overall resilience index of the community.

$$R = \frac{1}{N} \sum_{j=1}^N w_j \int_{T_1} \dots \int_{T_i} \dots \int_{T_n} \frac{1}{t_{R_i} - t_E} w_i [1 - L_{t_i}(IM, t_{R_i})] \times f_{R_i}(t, t_E, t_{R_i}) dT_i \quad (6.6)$$

where  $L_{t_i}$ ,  $f_{R_i}$ , and  $t_{R_i}$  are the total loss, recovery function, and recovery time for dimension  $i$  and  $i = 1, \dots, n$  indicates the number of functionality indicators (dimensions) involved.  $w_i$  is the weight factor assigned to dimension  $i$  and  $w_j$  indicates the significance of facility  $j$  in the overall functionality of the community which is consisted of  $N$  facilities. To normalize the resilience index ( $R$ ), summation of both  $w_i$  and  $w_j$  factors should be equal to 1.0.

For a facility with two functionality indicators, a functionality surface will be developed and the volume under the surface is  $R$  for that facility. Note that those two indicators plus the recovery time (three random variables overall) create a 3D surface for functionality. Similarly, the integration of an  $n$ D functionality function gives the resilience index of a facility with  $n$  functionality indicators. Thus, the functionality of the facility creates a hypersurface in  $\mathbb{R}^n$  space which is defined using a multivariate polynomial as follows.

$$Q(T_1, \dots, T_i, \dots, T_n) = [1 - L_{t_i}(IM, t_{R_i})] \times f_{R_i}(t, t_E, t_{R_i}) \quad (6.7)$$

## 6.3 Archetype Building Facilities

### 6.3.1 Configuration and Design of Archetypes

The proposed model is implemented on a series of steel diagrid (SD) and reinforced concrete (RC) buildings located in a small community near downtown Los Angeles, CA. Diagrid frames are an innovate tubular structural system which carry both lateral and gravity loads through their diagonal members. They provide substantial lateral load-carrying capacity and are an efficient choice for a high seismic region like LA (Liu et al. 2018). Diagrid system have been used for several iconic buildings around the world including the Hearst Tower in New York, shown in Figure 6.2, and Seattle Central Library

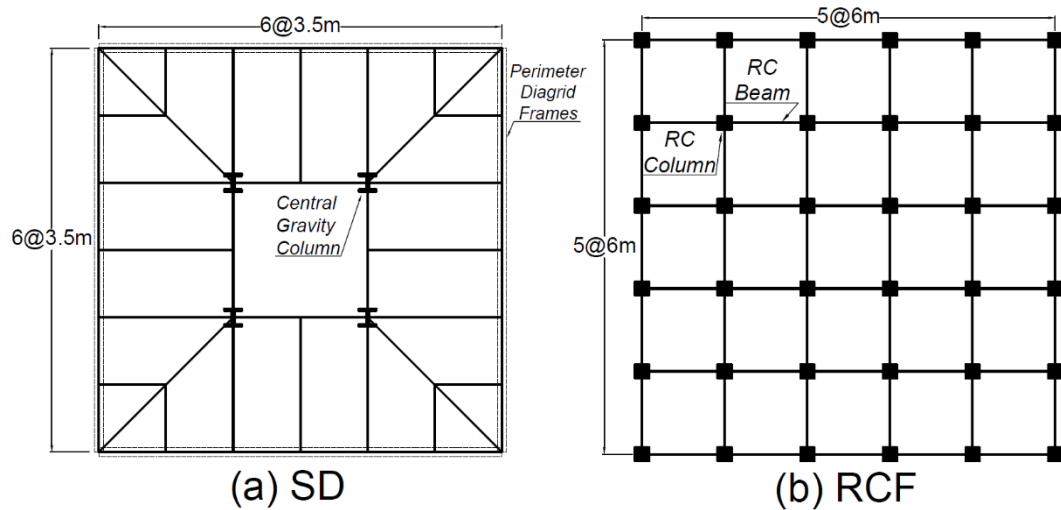
in Seattle (Asadi and Adeli 2017; Boake 2014). Despite their structural advantages and aesthetical features, there are a few reports on their seismic performance and design standards provide little specification for their design (Asadi and Adeli 2018b; Liu et al. 2018). They are selected to further study their seismic performance and resilience. Special RC frames has a more ductile performance and can withstand large lateral deformation before collapse (Han et al. 2015).



Figure 6.2 Hearst Tower, New York City, one the first iconic steel diagrid buildings

The 4-story archetypes are designed per ASCE 7-16 (2017b), ANSI/AISC 360-16 (2016b), ANSI/AISC 341-16 (2016a), and ACI 318-14 (2014) standards considering an  $S_s$  (spectral response acceleration at 0.2 sec) and  $S_l$  (spectral response acceleration at 1 sec.) of 2.481g and 0.862g, respectively. Three different diagrid configurations with 45°, 63°,

and  $72^\circ$  diagonal angles are considered given the diagonal angle has a major impact on diagrid performance. The angle between the diagonal members and the horizontal axis is called diagonal angle. Diagrid archetype plan and configuration are adopted from (Asadi et al. 2018). They archetypes are labeled based on diagonal angle, thus the steel diagrid archetype with  $45^\circ$  diagonal angle is labeled SD-45. For RC buildings, three configurations with different shear wall ratio are considered and typical floor plan is adapted from (AlHamaydeh et al. 2017a; Asadi et al. 2020). The RC archetype with no shear wall is labeled RCF, the RC archetype with 2 shear walls on each outer frame is labeled RC-2SW, and the last one with one shear wall at the middle of each outer frame is labeled RC-1SW (See Figure 6.3).



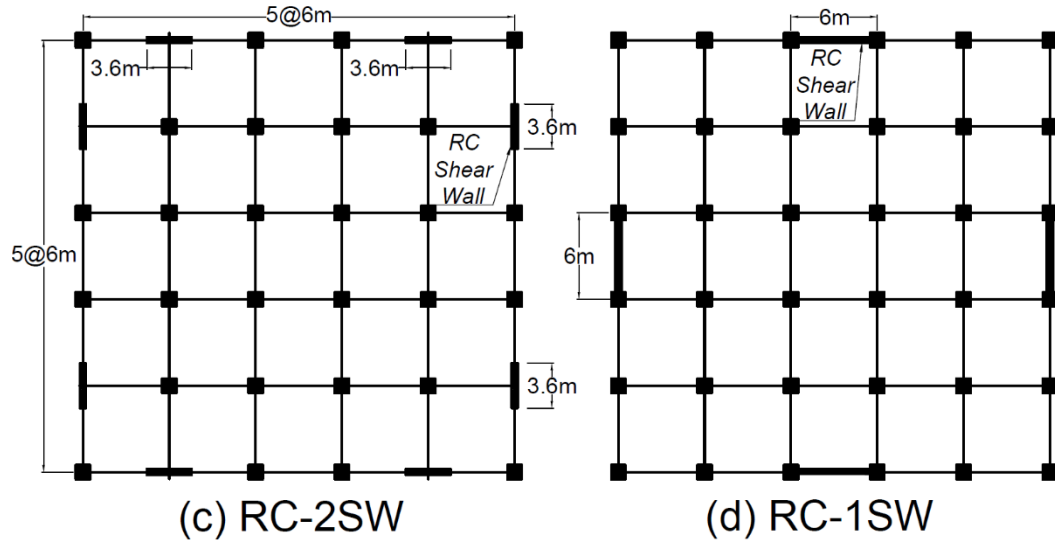


Figure 6.3 Typical floor plan for (a) steel diagrid archetypes (SD-45, SD-63, SD-72), (b) RCF, (c) RC-2SW, and (d) RC-1SW archetypes

## 6.4 Scenario-based Assessment

Seismic resilience of buildings is assessed using a scenario-based approach. To find seismic intensity at the site, Boore and Atkinson (2008) ground-motion prediction equations (attenuation function) are used. Three scenario earthquakes are considered: (1) an M6.5 earthquake with an epicentral distance of 40 km, (2) an M7 earthquake with an epicentral distance of 15 km, and (3) an M8 earthquake with an epicentral distance of 5 km from the building site all with a shear-wave velocity from the surface to 30 m ( $V_{S30}$ ) of 300 m/s (Asadi et al. 2019a; Burton et al. 2016).

## 6.5 Vulnerability Analysis

Nonlinear dynamic time-history analysis is used for scenario-based vulnerability assessment and incremental dynamic analysis (IDA) is used for collapse fragility assessment (Vamvatsikos and Cornell 2002). Numerical models are built on OpenSees platform using fiber elements for beams, columns, and diagonals (Mazzoni et al. 2006).

OpenSees models are validated by experimental studies (Black et al. 1980; Kolozvari et al. 2014). More details on building structures and numerical models are presented in (Asadi et al. 2019b, 2020). To account record-to-record variability, a set a 22 far-field ground motion records recommended by FEMA P-695 (ATC 2009) for fragility analysis are used. The records include 14 different events, Site Class C and D, and ground motions of magnitudes M6.5 to M7.6. The records are normalized and scaled to match the intensity of scenario earthquake (ATC 2009). Collapse fragility curves are developed using IDA and maximum likelihood method is used to fit a lognormal distribution function over the empirical collapse fragility curve. Collapse fragility curves of archetype buildings are depicted in Figure 6.4. The horizontal axis is  $S_a(T_1,5\%)$ , the normalized pseudo-spectral acceleration for 5% damped design spectra for the region at the fundamental period of the building structure.

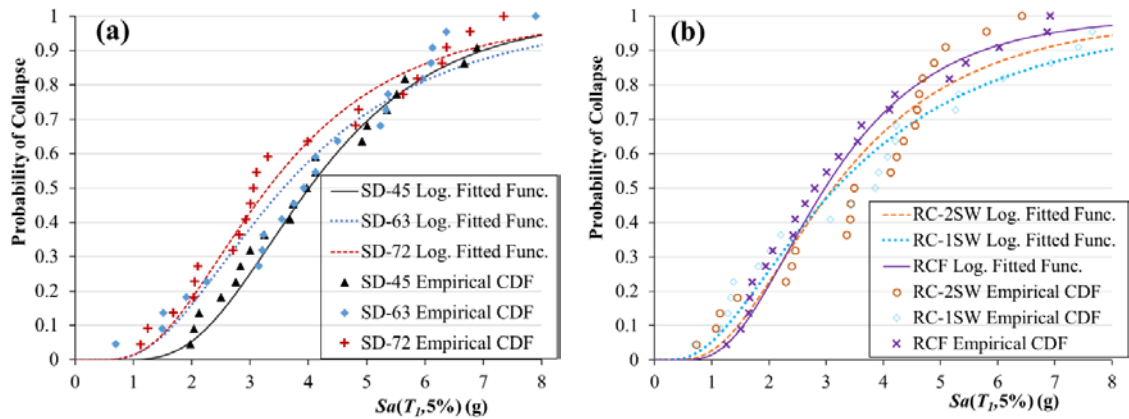


Figure 6.4 Empirical CDF of  $S_a(T_1,5\%)$  and fitted lognormal fragility functions for (a) steel and (b) RC building archetypes

The mean and standard deviation of collapse capacity,  $\hat{S}_{CT}$ , and collapse IDR are listed in Table 6.1. Among SD structures, diagrid with a diagonal angle of  $45^\circ$  shows the highest collapse capacity followed by SD-63 and SD-72 archetypes. Diagrids shows a

noticeably high collapse capacity considering no special design considerations were considered in their design process.

Table 6.1 Expected collapse capacity and collapse IDR and their corresponding logarithmic dispersion

Archetype	$S_{CT}(T_{1,5\%})$ (g)	$\beta_{S_{CT}}$	Collapse IDR (%)	$\beta_{IDR}$
SD-45	4.02	0.43	1.10	0.62
SD-63	3.58	0.59	1.75	0.77
SD-72	3.31	0.55	3.57	0.50
RCF	2.98	0.51	7.13	0.46
RC-1SW	3.17	0.71	0.82	0.87
RC-2SW	3.13	0.59	0.79	0.63

## 6.6 Loss and Downtime Analysis

FEMA P-58 comprehensive database of fragility specification is used to estimate component-based repair cost and time (FEMA 2012). For diagrid frame members, the fragility specification developed in (Asadi et al. 2018) is adopted given FEMA P-58 does not provide fragility specifications for diagrids. Steel connections are assumed post-Northridge welded steel moment connection without reduced beam section (RBS) detailing. Fragility specifications for RC columns and beams and low-rise RC walls are based on ACI 318 special RC frame requirements.

Non-structural components for both steel and concrete buildings include two hydraulic elevators, one 500-Ton chiller and an air-handling unit on the roof which is covered with concrete tiles, and for every 4 m<sup>2</sup> a seismically-rated pendant lighting. Cold and hot water and sanitary waste piping, HVAC ducting, fire sprinklers, diesel generator, desktop electronics, electricity control panels are also included. Perimeter walls are generic midrise stick-built curtain wall and the interior walls are partial or full-length gypsum walls with metal studs. The ceiling is covered with seismically-rated suspended tiles. A list of

damageable structural and non-structural components with their fragility parameters is presented in Appendix A of Chapter 5.

The building replacement cost is estimated based on RSMeans cost estimation data for southern Los Angeles, California (RSMeans 2018). The key assumptions for loss estimation along with their source are presented in Table 6.2.

Table 6.2 Building specification and assumptions for loss and downtime estimation

<b>Parameter</b>	<b>Value</b>	<b>Source</b>
Total Replacement Cost	US\$ 4,660,000 for SD buildings US\$ 10,338,000 for RC buildings	RSMeans (2018)
Total Replacement Time	720 days for SD buildings 950 days for RC buildings	FEMA P-58
Maximum number of workers per ft <sup>2</sup>	0.002 (1 worker per 500 ft <sup>2</sup> )	FEMA P-58

### ***6.6.1 Loss and Downtime Functions***

The loss and downtime analysis are performed for archetype buildings in FEMA P-58 PACT (FEMA 2012) using Monte Carlo simulation and component-based repair cost and time fragility functions. Three scenario earthquakes (S1, S2, and S3), described earlier, are considered. Figure 6.5 depicts the loss and downtime fragility functions for SD-63 archetype, as a sample of results. As depicted, the probability of exceedance for loss and downtime increases from S1 to S3 given S1, S2, and S3 are scenario earthquake with an approximate return period of 100, 750, and 3000 years for the studied site. The median repair cost increases from 16% of total replacement cost for S1 to 39% for S2 and 71% for S3 earthquake. Meanwhile, the downtime due to repair increases from 70 days for S1 to 150 days for S2 and 268 days for S3. This noticeable increase from S1 to S2 can be attributed to the damage to non-structural components such as wall partitions, suspended

ceiling as well, and chiller. For S3, however, moderate to severe damages to structural components are observed which has significantly increased the expected asset loss.

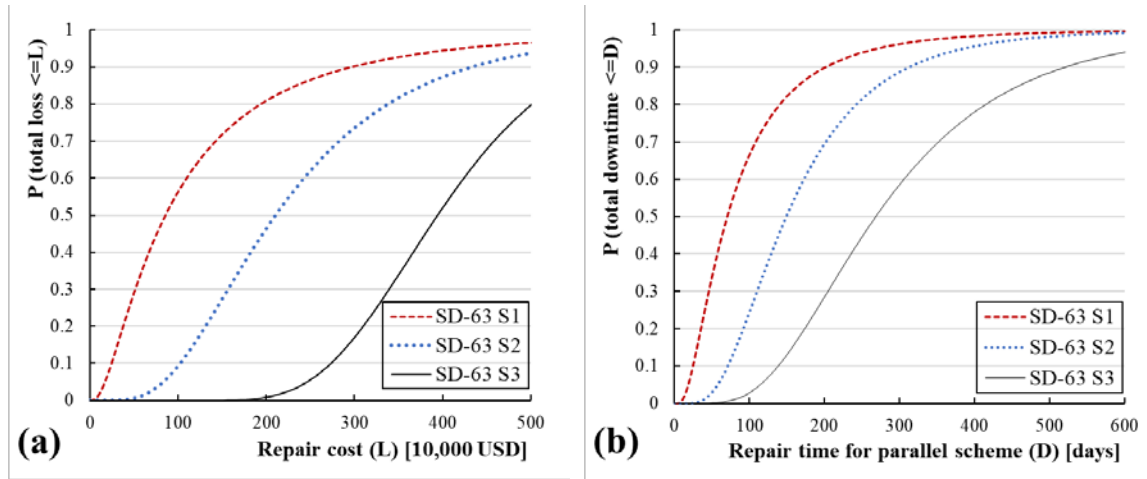


Figure 6.5 CDF of (a) loss and (b) downtime for SD-63 archetype for Scenario 1, 2, and 3 earthquakes

Figure 6.6 depicts the loss and downtime fragility functions for various archetypes under S2 earthquake. Among diagrid buildings, the SD-45 shows a generally better performance with a smaller median repair cost than other SD archetypes and a slightly smaller median repair time compared to SD-63 archetype. SD-72 shows a noticeably poorer performance in terms of expected loss and downtime which is attributed to the uncomplete upper diagrid module as reported in (Asadi et al. 2019b). Among RC archetypes, RCF shows a relatively larger repair cost and time which are partly due to lateral stiffness of the RC frame. RCF lateral stiffness is much smaller than cases with RC shear walls, RC-1SW and RC-2SW, which leads to larger IDR for RCF under the same earthquake load. Though RCF structural components can undertake large IDR, the damage to non-structural components vulnerable to IDR increases the overall loss and downtime. At the same time, the stiff RC shear wall archetypes experience a larger ACC at various

floors compared to RCF archetypes which slightly increases the loss due to non-structural components vulnerable to ACC.

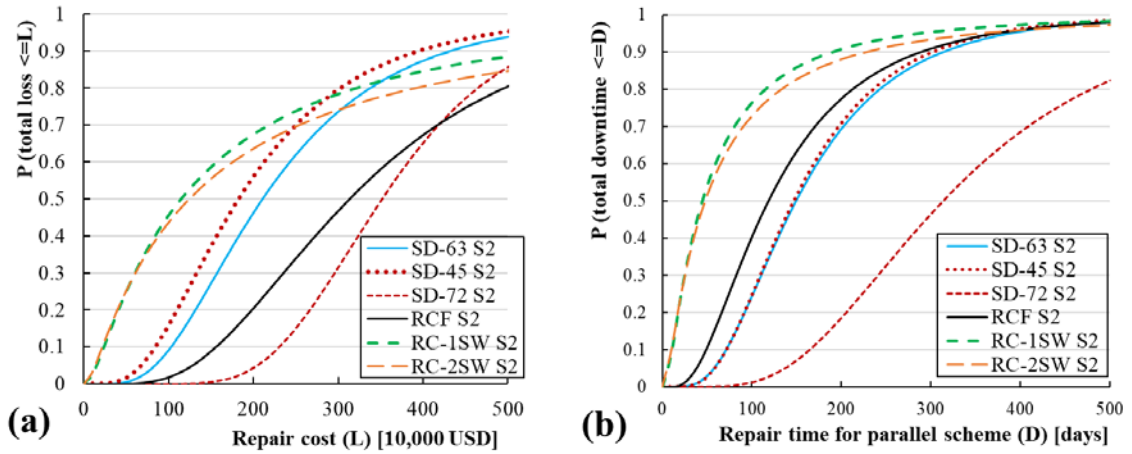


Figure 6.6 CDF of (a) loss and (b) downtime for various archetypes for Scenario 2 earthquake

### 6.6.2 Downtime for Occupancy and Serviceability

The proposed framework utilizes the repair time for components affecting occupancy or serviceability to quantify the downtime in terms of these dimensions of functionality. For either dimension, there are two main steps to find the downtime and related functionality loss, (1) identifying the occupancy or serviceability loss occurrence and (2) quantifying loss and downtime based on loss and downtime for various components affecting each dimension. First, a multi-criteria limit state is considered to determine whether the occupancy or serviceability loss has occurred on a certain floor (a binary variable). As described earlier, damage to key components is used to identify the loss of occupancy or serviceability. For occupancy, four conditions are controlled which are based on (Asadi et al. 2019a; Han et al. 2015; Rojahn 2005) criteria for loss of occupancy. However, components affecting serviceability, such as pipes, elevator, control panels, air conditioning system, and ducts are commonly vulnerable to ACC. Among them, hot water

pipes are particularly vulnerable to ACC and may experience leakage at joints at an ACC as low as 0.55g (FEMA 2012). This limit state is used here to identify the loss of serviceability.

After identifying the loss of functionality, the downtime and loss due to each effective component in each floor are quantified to find the floor-by-floor and the overall downtime. Figure 6.7 depicts the floor-by-floor repair time for structural and non-structural components affecting occupancy or serviceability for various archetypes. Non-structural damages are categorized to damages causing occupancy loss and damages causing serviceability loss. Structural damages primarily affect occupancy. Note that the non-structural damage and downtime shown at Roof are caused by damage to chiller and air-handling unit located on the Roof. As depicted, the downtime increases from S1, a low-intensity major earthquake, to S3, a significant earthquake. The SD-63 archetype suffers minor structural damage and moderate to severe non-structural damages in all S1 and S2 and the structural damage increases to moderate damages in S3. This leads to occupancy loss on all floors for S2 and S3 for this archetype. The non-structural damages for SD-63 are mostly to excessive ACC on the 1<sup>st</sup> and 4<sup>th</sup> floors. Large ACC leads to loss of serviceability as it causes damage to components providing serviceability. For the 4<sup>th</sup> floor of SD-63 archetype under S2, the downtime for occupancy components is smaller than all other floors but the downtime for serviceability components is much larger than other floors leading to the largest downtime for the 4<sup>th</sup> floor among all floors under S2.

The RC archetypes, however, experience little structural damage and downtime under S1 and relatively small non-structural damage and downtime under S2. This can be attributed to the ductile performance of special RC frames compared to steel diagrid

frames. Special RC frames can tolerate large lateral deformation before reaching minor damage limits. Particularly for RC-1SW archetype which has shear walls, the downtime due to both occupancy and serviceability components increases significantly under S3. This indicates that a number of non-structural components have reached the severe damage state under S3.

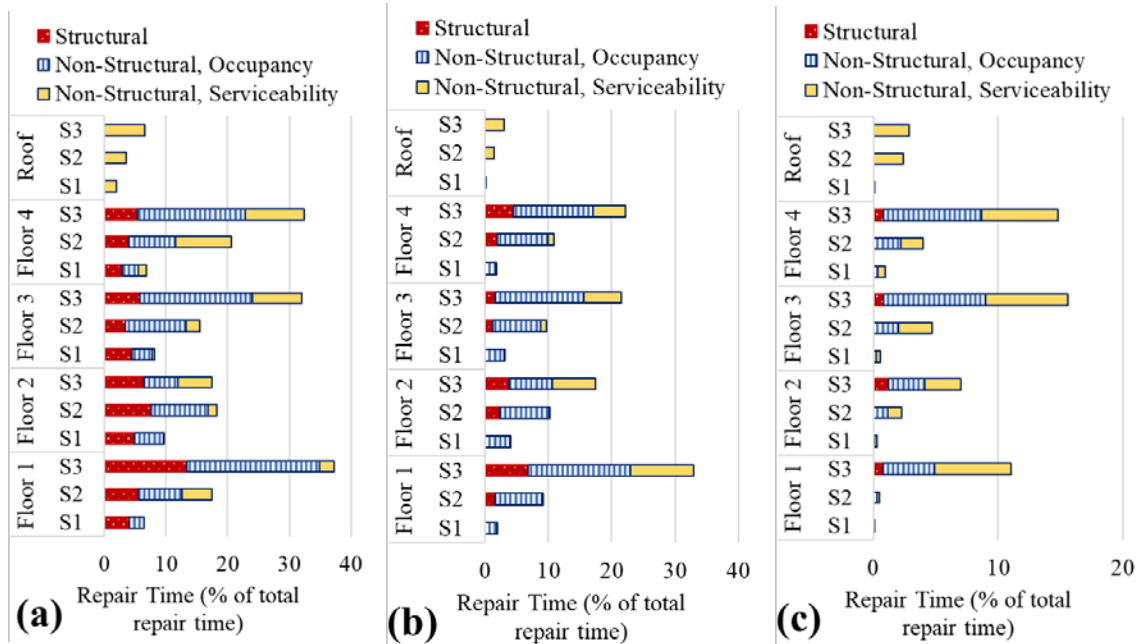


Figure 6.7 Floor-by-floor repair time for structural and non-structural components affecting occupancy and serviceability for (a) SD-63, (b) RCF, and (c) RC-1SW archetypes

## 6.7 Multi-dimensional Functionality Analysis

### 6.7.1 Functionality Curves

The component-based loss and downtime fragility functions and median outputs are used to develop multi-dimensional functionality curves for archetype building and calculate the resilience index  $R$ . Three groups of functionality curves are produced which are functionality curve based on asset loss, occupancy loss, and serviceability loss. For Functionality curve based on asset loss (FAL), the loss and downtime due to all

components of the building are included. The FAL is developed based on a repair scheme where first structural components, then non-structural components affecting occupancy, and last non-structural components affecting serviceability are repaired. Figure 6.8 shows a sample FAL for SD-63 archetype under S2. The numbered arrows show the repair time for various components and the process by which the initial functionality is restored. The components related to each numbered arrow are listed on the caption for Figure 6.8. The total replacement time (720 days for SD and 950 days for RC archetypes) is considered the control time in Equation (6.1). Asset loss is depicted as a percentage of total replacement cost.

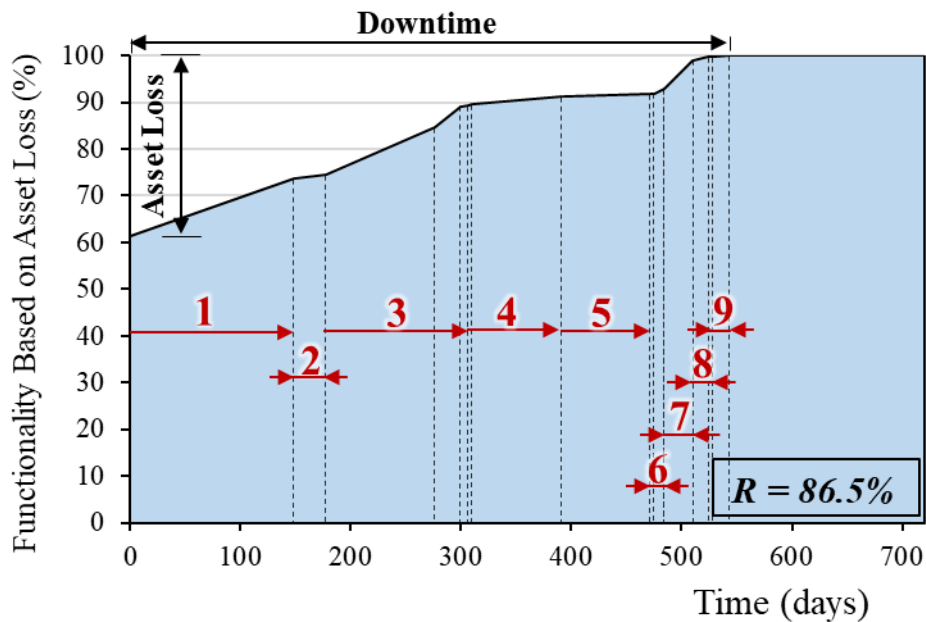


Figure 6.8 Functionality curve based on asset loss for SD-63 archetype under Scenario 2 earthquake, numbered arrows show the repair time for various components: (1) structural components, (2) concrete tile roof, (3) walls and stair, (4) suspended ceiling and raised access floor, (5) independent pendant lighting, (6) elevator and plumbing, (7) chiller, (8) HVAC, ducting, fire sprinkler, diesel generator, and control panels, (9) furniture

For SD-63, the majority of loss of functionality is due to structural components and non-structural components affecting occupancy. About 77% and 72% of total loss and

downtime for SD-63 is due to damage to components related to occupancy. Therefore, the greater part of the total downtime is to restore occupancy and a smaller portion (28% in case of SD-63 archetype) is required to restore serviceability of the building. Figure 6.9 shows the functionality curve based on occupancy loss (FOL) for SD-63 archetype under S2. Based on the proposed approach, it takes about 391 days (occupancy downtime) to repair occupancy-related components and re-occupy the building after an S2 earthquake assuming a floor-by-floor repair scheme. This key output is significantly important for post-earthquake decision-making and community resilience assessment and can be used as the critical parameter for functional recovery design of building facilities. For SD-63 archetype, the S2 earthquake has caused a loss of functionality on all floors. It is assumed that if a lower floor is unsafe for re-occupancy, the upper floors will remain unoccupied as well. The loss of occupancy is primarily due to minor damage to a number of diagonal members and to a lesser extent, moderate damage to internal partition walls. For SD-63, the occupancy downtime for the 2<sup>nd</sup> floor is the largest among all floors which is mainly due to damage to structural components. For the 4<sup>th</sup> floor, the damage to non-structural components vulnerable to ACC increases significantly which leads to significant loss of serviceability at this floor but not a significant loss in occupancy, as depicted in Figures 6.9 and 6.10.

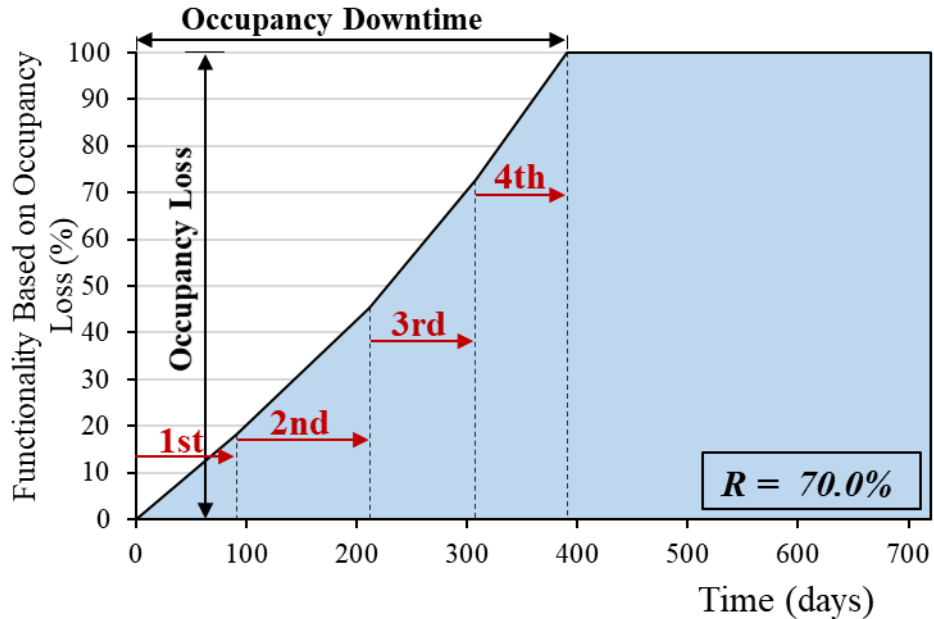


Figure 6.9 Functionality curve based on occupancy for SD-63 archetype under Scenario 2 earthquake, numbered arrows show the occupancy repair time for various floors

To achieve full functionality, components required for the intended service of the building need to be repaired as well. Figure 6.10 shows the functionality curve based on serviceability loss (FSL) for SD-63 archetype under S2. As depicted, the loss of serviceability is limited to the 2<sup>nd</sup> to 4<sup>th</sup> floor given that the median ACC is larger on these floors than the 1<sup>st</sup> floor and the median ACC for the 1<sup>st</sup> floor does not reach the serviceability loss limit state. Although the first floor is considered functional in terms of services, there are minor damages to the pendant lighting, HVAC ducting, and furniture which should be repaired. These damages are minor and do not affect main services of the building including water, electricity, sanitary waste, air conditioning, and resident's conveyance. As mentioned, the 4<sup>th</sup> floor of the SD-63 archetype experiences large ACC and as a result shows the largest serviceability downtime among all floors. The

serviceability loss and downtime at the Roof are due to damage to chiller and air-handling unit.

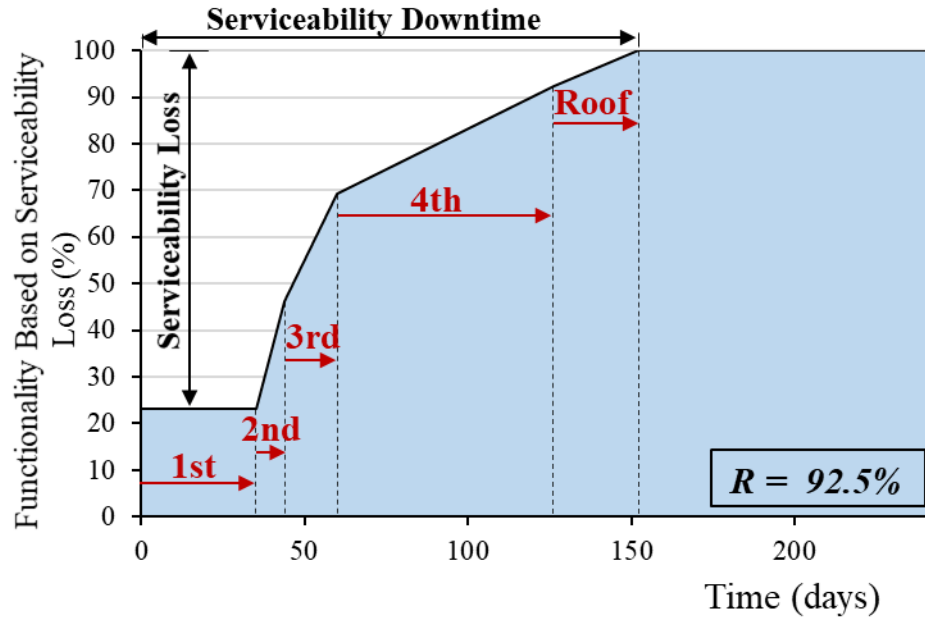


Figure 6.10 Functionality curve based on serviceability for SD-63 archetype under Scenario 2 earthquake, numbered arrows show the serviceability repair time for various floors

### 6.7.2 Functionality Surfaces

Using Equation (6.6), a multi-dimensional functionality surface for occupancy and asset loss and another functionality surface for serviceability and asset are developed and presented in Figure 6.11 (a) and (b), respectively. Figure 6.11 (a) is an integration of FAL and FOL and Figure 6.11 (b) is an integration of FAL and FSL functions. The volume under these figures is a resilience index of combined occupancy and asset or serviceability and asset, respectively. The weight factor for all dimensions is assumed 1.0. The full 4-dimensional (4D) functionality hypersurface will be an integration of Figure 6.11 (a) and (b) and the Lebesgue measure of the region covered by the 4D hypersurface is a comprehensive resilience index for building facilities considering all three dimensions. As

depicted, the downtime for occupancy is larger than that of serviceability and the downtime for asset loss is approximately equal to the summation of downtime for occupancy and serviceability.

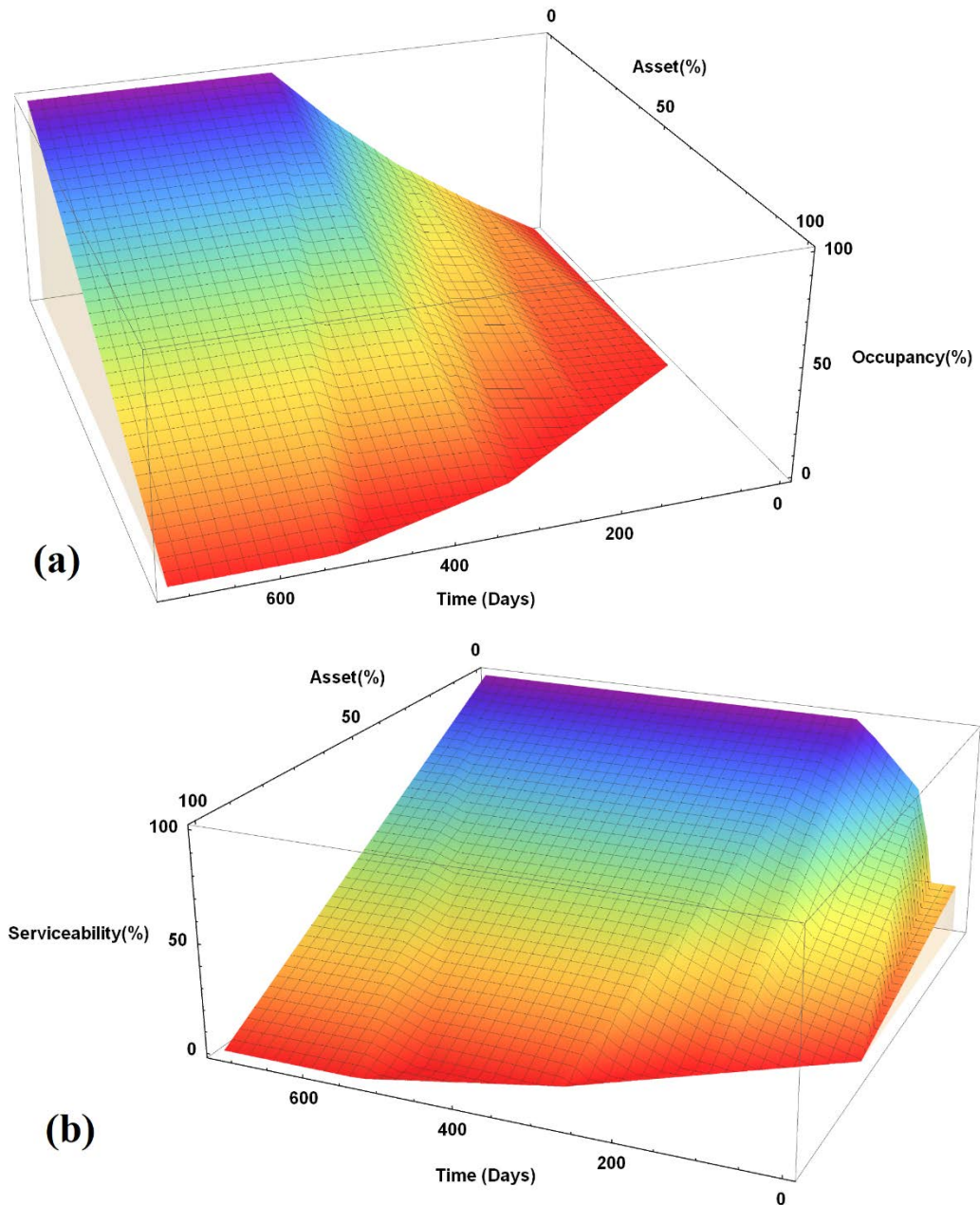


Figure 6.11 Functionality surfaces based on (a) occupancy and asset losses and (b) serviceability and asset losses for SD-63 archetype under S2 earthquake

### ***6.7.3 Multi-dimensional Resilience Indices***

Table 6.3 summarizes the resilience indices based on three dimensions and the dimension-based downtime and loss for each archetype. The total loss and downtime are approximately equal to the summation occupancy and serviceability loss and downtime, respectively. As listed, the downtime for occupancy and serviceability, quantified using the proposed approach, can be a design parameter in a functional recovery design approach. Accordingly, SD-45 archetype shows the largest resilience indices for various dimensions and earthquake scenarios among SD archetypes, except for resilience index for serviceability for S3 where SD-72 achieves a better  $R$ . This is mostly due to slightly smaller serviceability downtime (191 days compared to 193 and 231 days for SD-45 and SD-64 archetypes, respectively) and noticeably smaller serviceability loss (460,000 USD compared to 1,430,000 and 1,250,000 USD for SD-45 and SD-64 archetypes, respectively) for the SD-72 archetype under S3. Note that while the downtime and loss for serviceability for SD-72 are smaller than other SD cases, the downtime and loss for its occupancy are significantly larger than SD-45 and SD-63. Therefore, the overall resilience index of SD-72 is the lowest among SD archetypes indicating a poor seismic performance for this model as indicated in (Asadi et al. 2019b).

Table 6.3 Resilience index and median loss and downtime based on functionality curve for asset loss (FAL), occupancy loss (FOL), and serviceability loss (FSL) for various archetypes for Scenario 1, 2, and 3 earthquakes

Archetype	R per FAL (%)			R per FOL (%)			R per FSL (%)			Loss per FOL (10,000\$)			Loss per FSL (10,000\$)			Downtime per FOL (Days)			Downtime per FSL (Days)		
	S1	S2	S3	S1	S2	S3	S1	S2	S3	S1	S2	S3	S1	S2	S3	S1	S2	S3	S1	S2	S3
SD-45	98	91	63	100	85	64	99	96	91	22	113	126	39	44	143	129	287	541	36	122	193
SD-63	96	87	58	100	70	55	99	93	92	47	139	208	29	41	125	212	391	796	27	153	231
SD-72	91	69	52	70	61	52	96	74	96	142	233	416	11	64	46	451	811	1522	47	207	191
RCF	100	94	67	100	80	60	100	99	84	75	202	722	4	64	168	101	362	702	7	33	293
RC-1SW	100	99	90	100	100	86	100	98	89	3	54	178	6	47	192	7	54	282	11	78	234
RC-2SW	100	95	73	100	100	86	100	88	69	8	163	199	2	145	425	7	186	255	7	251	581

Special RC archetypes achieve better resilience indices for asset loss than steel diagrid which can be attributed to the special seismic considerations recommended by ACI 318 (2014) which are considered in the design and loss analysis. These considerations limit the seismic damage to structural components and as a result, they reduce the expected loss and downtime. Such seismic considerations are currently unavailable for diagrids. Nonetheless, SD archetypes show better resilience indices for occupancy and serviceability under S3 earthquake which is found to be caused by the difference in considered control time in  $R$  calculation (720 days for SD and 950 days for RC archetypes). Among RC archetypes, RC-1SW achieve better  $R$  for all dimensions.

## **6.8 Conclusions**

A new framework is introduced for multi-dimensional functionality assessment and resilience quantification of building facilities under seismic hazard. Three key dimensions of building functionality loss, i.e. asset, occupancy, and serviceability losses, are considered and a component-based method is presented to develop functionality curves and surfaces based on each dimension. The framework is implemented on a series of steel diagrid and RC building archetypes.

The proposed framework is consistent with FEMA P-58 loss analysis approach and uses FEMA P-58 component-based seismic fragility specifications to (1) identify the occurrence occupancy or serviceability loss in any floor and (2) quantify the monetary loss and downtime for occupancy, serviceability, and overall asset. Most non-structural components of the building which contribute to serviceability are vulnerable to floor acceleration. Therefore, floors with large floor acceleration are likely to have serviceability

loss. For instance, at the 4<sup>th</sup> floor of SD-63 archetype, large floor acceleration led to significant loss of serviceability compared to other floors while the occupancy loss and downtime of the 4<sup>th</sup> was less than 1<sup>st</sup> to 3<sup>rd</sup> floors.

The downtime for occupancy and serviceability are particularly important for risk-informed functional recovery design of building facilities and this framework identifies the tradeoffs and difference in occupancy loss and serviceability loss in various floors. The greater part of total downtime is to restore occupancy and the smaller part for restoring serviceability of the building. For instance, based on the proposed approach, it takes about 391 days to repair occupancy-related components and re-occupy the SD-63 building after a significant earthquake (scenario 2) while it takes 153 days to restore the serviceability under the same earthquake.

Functionality and resilience can be studied in the context of community resilience considering the interdependency of the building facility and lifeline infrastructure systems (Bocchini et al. 2014; EERI 2019). Although the proposed framework can be applied to a small community consisted of a series of building facilities, it can be expanded to include the interdependence of the building on lifeline infrastructure such as water distribution systems.

# Chapter 7

## 7. Summary, Conclusions, and Future Work

### 7.1 Summary and Conclusions

A new risk-based multi-criteria decision framework is presented to integrate various resilience and sustainability measures involved in design and analysis of instrumented building environments. A novel multi-dimensional methodology is introduced for component-based functionality assessment, resilience quantification, and safety evaluation of steel and reinforced concrete (RC) building structures. In summary, the contributions of this dissertation are as follows:

1. A comprehensive investigation into the nonlinear performance of steel diagrid structures under static, time-history dynamic, and incremental dynamic analyses is presented. The impact of diagrid configuration, diagonal angles, and building height on seismic performance of diagrids are studied.
2. New quantitative and qualitative seismic performance criteria are proposed for steel diagrid frames. The performance criteria are used to study seismic loss of steel diagrid frames considering loss due to various structural and non-structural components.

3. A comprehensive yet practical multi-criteria decision-making (MCDM) model is introduced which integrates various resilience and sustainability indicators/measures to identify the optimal design alternative. The framework is consistent with FEMA P-58 method for loss analysis of building environments. The framework includes (1) three modules which are System Concept and Criteria module, Resilience and Sustainability Assessment module, and Multi-Criteria Decision-Making module, (2) four sets of criteria which are asset, time, life, and environmental losses, and (3) three decision models which are analytic hierarchy process (AHP), multi-attribute utility theory (MAUT), and technique for order preference by similarity to ideal solution (TOPSIS). Furthermore, risk in decision analysis in addition to risk in component-based vulnerability and loss analyses is included.
4. The proposed MCDM framework is used to combine resilience-based structural design and energy-based architectural design of building environments. Intensity-based and time-based seismic loss analyses are performed to quantify seismic repair cost and time and casualties. Economic input-output life-cycle analysis is performed to find greenhouse gas emissions due to construction, maintenance, and seismic repair. Also, whole-building energy simulation is performed to find the annual energy consumption and cost for heating, cooling, lighting, and equipment. The case studies are a group of RC archetype buildings.
5. A survey is conducted to find the weight factors for resilience and sustainability measures in design decision analysis of building environments. Various objectives

- including minimum asset loss, downtime, social loss, environmental loss, and annual energy consumption as well as maximum overall resilience are considered.
6. A new framework is introduced to incorporate component-based resilience quantification methods with structural health monitoring techniques. The proposed tri-lateral framework uses the data obtained from localized wireless sensor networks to detect and locate damage, develops component-based functionality curves to quantify the seismic resilience of the structure, and makes post-quake rapid decisions based on a multi-criteria safety evaluation method. Minor damages due to corrosion and major damages due to past extreme events are studied considering a life-cycle approach for functionality assessment. Using component-based functionality curves, resilience, robustness, and rapidity indices are calculated and their scenario-based recovery paths are studied.
  7. A novel multi-dimensional functionality analysis framework is introduced which produces functionality surfaces for asset, occupancy, and serviceability losses, quantifies occupancy and serviceability downtime and corresponding resilience indices for archetype steel and concrete structures.

Major conclusions and findings of this dissertation are summarized below:

1. The proposed framework integrates various sustainability and resilience criteria and presents a formal quantitative method to study the tradeoff between them. In an MCDM framework, various conflicting outputs can be taken into account, systematically. For instance, the 4-45 archetype which has the least asset and time losses received a smaller

- overall score (approximately 7% smaller) than 4-72A archetype with noticeably larger asset and time losses (24% and 44% larger, respectively). This conflicting outcome is mainly because the casualty is the highest for the 4-45 archetype and in the survey, most participants gave a high importance factor to life loss.
2. The benefits of sustainable design are more evident with an MCDM framework. Such that the environmental benefit may outweigh the shortcomings due to structural performance. For instance, the 4-63R20 archetype with only 20% recycled material achieved a higher score than 4-45 archetype which has the least asset and time losses among all archetypes for both MAUT and TOPSIS decision analysis methods (8-78% better scores with MAUT and 12-105% better scores with TOPSIS methods for various objectives). This is because reusing steel has a significant influence on environmental metrics and can be a cost-efficient construction strategy, though it has little impact on resilience measures.
  3. The steel diagrid buildings are found to have a substantial collapse capacity and lateral stiffness. Nonetheless, the non-structural loss due to large maximum absolute floor acceleration experienced by stiff diagrid frames may adversely impact the expected total loss.
  4. Diagrid seismic behavior is dictated by two key parameters: (1) the axial capacity of diagonals especially the corner ones and (2) the diagonal angle. Due to shear lag effect, the corner diagonal members are the key elements in diagrid behavior. Corner diagonals are where the initial yielding and/or local buckling occurs and failure or even partial yielding of them significantly decreases the lateral stiffness.

5. Having an incomplete module in diagrid frames adversely impacts the diagrid performance causing substantial structural and non-structural damage and loss such that the expected total loss may exceed the total replacement cost threshold. An alternate configuration is proposed where diagonal angle changes in the uppermost floors to avoid having an incomplete diagrid module. This alternate configuration found effective in reducing seismic loss, particularly life loss, achieving much better scores (total utility) than original archetype for various decision-making scenarios.
6. Compared to RC buildings with shear walls, RC framed buildings consumed noticeably more energy for cooling and heating (on average 12%). This is partly due to the shading effect provided by the wall and, to a lesser extent, due to the significant thermal mass of shear walls.
7. Archetype RC buildings with shear wall experience less monetary seismic loss and downtime and have high total utility scores in the decision analysis. As such, buildings with symmetric side shear walls ranked first in decision analysis even though they require a higher initial construction cost. Nonetheless, shear walls block the natural light resulting in slightly more energy use for lighting.
8. Glazing type in RC archetype buildings had little impact on resilience criteria but significant influence on heating and cooling energy use and cost. As such, using triple low-e glazing (HG) reduced the energy use, cost, and corresponding CO<sub>2</sub> eq emission as much as 48% compared to regular double glazing (BG). In general, archetypes with HG achieve a better score in decision analysis than archetypes with BG for most scenarios considering the conflicting factors of initial cost and energy consumed.

9. Localized nonlinear ARX system identification models are capable of detecting, locating, and measuring negligible damages such as corrosion in the structure. The ratio of variances of residual errors (DI), used as a damage-sensitive coefficient, was found to be an accurate indicator of damage in the structure for both stiff diagrid frame and ductile reinforced concrete frame. Using the ARX model, as few as one sensor at each floor can detect the damage and locate the damaged floor.
10. Maximum absolute floor acceleration is the most accurate demand parameter for locating damage whereas maximum floor displacement and interstory drift ratio can effectively detect and measure damages.
11. For steel diagrid buildings, the loss of occupancy is mostly due to minor damages to the diagonal members given the 0.25% interstory drift ratio minor damage limit state for them. While for special RC frames, minor damage to RC walls triggers evacuation, for which the minor damage IDR limit is 0.33%.
12. Most non-structural components of the building which contribute to serviceability are vulnerable to floor acceleration. Therefore, floors with large floor acceleration are likely to have significant serviceability loss and downtime. For instance, at the 4<sup>th</sup> floor of SD-63 archetype, large floor acceleration led to significant loss of serviceability compared to other floors while the occupancy loss and downtime of the 4<sup>th</sup> was less than the 1<sup>st</sup> to 3<sup>rd</sup> floors.
13. The greater part of total downtime is for restoring occupancy and the smaller part for restoring serviceability of the building. The downtime for occupancy and serviceability are particularly important for risk-informed functional recovery design of building facilities and the proposed framework identifies the tradeoffs and difference in

occupancy loss and serviceability loss in various floors. For example, based on the proposed approach, it takes about 391 days to repair occupancy-related components and re-occupy the SD-63 building after a an M7 earthquake with an epicentral distance of 15 km while it takes 153 days to restore the serviceability under the same earthquake.

## **7.2 Future Work**

This dissertation aims to provide a comprehensive study into diagrid seismic performance, integrated resilience, sustainability, and energy analyses, risk-informed multi-criteria decision analysis, localized structural damage identification, and multi-dimensional functionality assessment of building environments. Nonetheless, the following investigations are suggested for future studies aiming to extend the topics discussed here.

1. FEMA P-58 method for loss analysis does not include fragility specification for many structural systems such as steel plate shear walls or light-weight exterior concrete walls. Thus, the approach used here to develop performance criteria for steel diagrids can be applied to other novel structural systems and components to include them in FEMA P-58 fragility database.
2. FEMA casualty and fatality models used here are limited and are mostly suitable for comparison purposes. Building upon recent advances (Reinoso et al. 2018; Shapira et al. 2015), detailed and practical casualty estimation models need to be developed to achieve a more accurate estimation of casualties.
3. Multi-criteria decision models have advanced significantly over the past decade. Among recent studies, using fuzzy logic with TOPSIS method (Ervural et al. 2018) and

Bayesian adaptive decision models (Lee et al. 2018) can improve the flexibility and applicability of the proposed MCDM model.

4. The proposed quadrilateral MCDM framework can be extended and calibrated for the cost-benefit analysis of other structures such as bridges or infrastructure systems such as water distribution systems. These models can be the basis for a computer program which automatically makes decisions on structural and architectural design/retrofit projects.
5. Though the MCDM model described here may include various losses due to earthquakes, the required data can be obtained only through detailed case-based studies or through a community-oriented resilience assessment approach, which is out of the scope of this study and an important topic for future studies.
6. In addition to recycled steel, other sustainable design strategies such as using energy-efficient walls/roofs or walls/roofs with high thermal mass which affects energy consumption of the building can be explored as well.
7. Structural control models can minimize loss and improve the functionality of the system during earthquakes. Adding a semi-active or active structural control system to the proposed localized health monitoring and resilience quantification model will provide a more compatible and capable smart system for critical facilities (Saaed et al. 2015; Sattar et al. 2018).
8. Functionality and resilience can be studied in the context of community resilience considering the interdependency of the building facility and lifeline infrastructure systems (Bocchini et al. 2014; EERI 2019). Although the proposed framework can be applied to a small community consisted of a series of building facilities, it can be

expanded to include the interdependence of the building on lifeline infrastructure such as water distribution systems (WDS). WDS are critical during building normal operation for public health and after earthquakes for firefighting. Recent studies show WDS experience significant leakage and breakage damages due to strong ground motions (AWWA 2010; Eidinger and Avila 1999; Mazumder et al. 2019; O'Rourke et al. 2014) which indicates a clear need for integrated studies on seismic functionality of WDS and building facilities.

# Appendix I

## A I.1 Copyright Clearance for parts of Chapter 1

### JOHN WILEY AND SONS LICENSE TERMS AND CONDITIONS

Oct 15, 2019

This Agreement between Esmael Asadi ("You") and John Wiley and Sons ("John Wiley and Sons") consists of your license details and the terms and conditions provided by John Wiley and Sons and Copyright Clearance Center.

License Number	4690400667679
License date	Oct 15, 2019
Licensed Content Publisher	John Wiley and Sons
Licensed Content Publication	Structural Design of Tall and Special Buildings
Licensed Content Title	Diagrid: An Innovative, sustainable, and efficient structural system
Licensed Content Author	Esmael Asadi, Hojjat Adeli
Licensed Content Date	May 3, 2017
Licensed Content Volume	26
Licensed Content Issue	8
Licensed Content Pages	11
Type of use	Dissertation/Thesis
Requestor type	Author of this Wiley article
Format	Print and electronic
Portion	Text extract
Number of Pages	6
Will you be translating?	No
Title of your thesis / dissertation	Risk-informed Multi-criteria Decision Framework for Resilience and Sustainability Assessment of Instrumented Structures
Expected completion date	Nov 2019
Expected size (number of pages)	1
Requestor Location	Esmael Asadi 2672 Euclid Heights Blvd Apt 204  Cleveland, OH 44106 United States Attn:
Publisher Tax ID	EU826007151
Total	0.00 USD
Terms and Conditions	

#### TERMS AND CONDITIONS

This copyrighted material is owned by or exclusively licensed to John Wiley & Sons, Inc. or one of its group companies (each a "Wiley Company") or handed on behalf of a society with which a Wiley Company has exclusive publishing rights in relation to a particular work (collectively "WILEY"). By clicking "accept" in connection with completing this licensing transaction, you agree that the following terms and conditions apply to this transaction (along with the billing and payment terms and conditions established by the Copyright Clearance Center Inc., ("CCC's Billing and Payment terms and conditions"), at the time that you opened your RightsLink account (these are available at any time at <http://myaccount.copyright.com>).

#### Terms and Conditions

- The materials you have requested permission to reproduce or reuse (the "Wiley Materials") are protected by copyright.
- You are hereby granted a personal, non-exclusive, non-sub licensable (on a stand-alone basis), non-transferable, worldwide, limited license to reproduce the Wiley Materials for the purpose specified in the licensing process. This license, and any CONTENT (PDF or image file) purchased as part of your order, is for a one-time use only and limited to any maximum distribution number specified in the license. The first instance of republication or reuse granted by this license must be completed within two years of the date of the grant of this license (although copies prepared before the end date may be distributed thereafter). The Wiley Materials shall not be used in any other manner or for any other purpose, beyond what is granted in the license. Permission is granted subject to an appropriate acknowledgement given to the author, title of the material/book/journal and the publisher. You shall also duplicate the copyright notice that appears in the Wiley publication in your use of the Wiley Material. Permission is also granted on the understanding that nowhere in the text is a previously published source acknowledged for all or part of this Wiley Material. Any

third party content is expressly excluded from this permission.

- With respect to the Wiley Materials, all rights are reserved. Except as expressly granted by the terms of the license, no part of the Wiley Materials may be copied, modified, adapted (except for minor reformatting required by the new Publication), translated, reproduced, transferred or distributed, in any form or by any means, and no derivative works may be made based on the Wiley Materials without the prior permission of the respective copyright owner. **For STM Signatory Publishers clearing permission under the terms of the [STM Permissions Guidelines](#) only, the terms of the license are extended to include subsequent editions and for editions in other languages, provided such editions are for the work as a whole in situ and does not involve the separate exploitation of the permitted figures or extracts,** You may not alter, remove or suppress in any manner any copyright, trademark or other notices displayed by the Wiley Materials. You may not license, rent, sell, loan, lease, pledge, offer as security, transfer or assign the Wiley Materials on a stand-alone basis, or any of the rights granted to you hereunder to any other person.
- The Wiley Materials and all of the intellectual property rights therein shall at all times remain the exclusive property of John Wiley & Sons Inc, the Wiley Companies, or their respective licensors, and your interest therein is only that of having possession of and the right to reproduce the Wiley Materials pursuant to Section 2 herein during the continuance of this Agreement. You agree that you own no right, title or interest in or to the Wiley Materials or any of the intellectual property rights therein. You shall have no rights hereunder other than the license as provided for above in Section 2. No right, license or interest to any trademark, trade name, service mark or other branding ("Marks") of WILEY or its licensors is granted hereunder, and you agree that you shall not assert any such right, license or interest with respect thereto
- NEITHER WILEY NOR ITS LICENSORS MAKES ANY WARRANTY OR REPRESENTATION OF ANY KIND TO YOU OR ANY THIRD PARTY, EXPRESS, IMPLIED OR STATUTORY, WITH RESPECT TO THE MATERIALS OR THE ACCURACY OF ANY INFORMATION CONTAINED IN THE MATERIALS, INCLUDING, WITHOUT LIMITATION, ANY IMPLIED WARRANTY OF MERCHANTABILITY, ACCURACY, SATISFACTORY QUALITY, FITNESS FOR A PARTICULAR PURPOSE, USABILITY, INTEGRATION OR NON-INFRINGEMENT AND ALL SUCH WARRANTIES ARE HEREBY EXCLUDED BY WILEY AND ITS LICENSORS AND WAIVED BY YOU.
- WILEY shall have the right to terminate this Agreement immediately upon breach of this Agreement by you.
- You shall indemnify, defend and hold harmless WILEY, its Licensors and their respective directors, officers, agents and employees, from and against any actual or threatened claims, demands, causes of action or proceedings arising from any breach of this Agreement by you.
- IN NO EVENT SHALL WILEY OR ITS LICENSORS BE LIABLE TO YOU OR ANY OTHER PARTY OR ANY OTHER PERSON OR ENTITY FOR ANY SPECIAL, CONSEQUENTIAL, INCIDENTAL, INDIRECT, EXEMPLARY OR PUNITIVE DAMAGES, HOWEVER CAUSED, ARISING OUT OF OR IN CONNECTION WITH THE DOWNLOADING, PROVISIONING, VIEWING OR USE OF THE MATERIALS REGARDLESS OF THE FORM OF ACTION, WHETHER FOR BREACH OF CONTRACT, BREACH OF WARRANTY, TORT, NEGLIGENCE, INFRINGEMENT OR OTHERWISE (INCLUDING, WITHOUT LIMITATION, DAMAGES BASED ON LOSS OF PROFITS, DATA, FILES, USE, BUSINESS OPPORTUNITY OR CLAIMS OF THIRD PARTIES), AND WHETHER OR NOT THE PARTY HAS BEEN ADVISED OF THE POSSIBILITY OF SUCH DAMAGES. THIS LIMITATION SHALL APPLY NOTWITHSTANDING ANY FAILURE OF ESSENTIAL PURPOSE OF ANY LIMITED REMEDY PROVIDED HEREIN.
- Should any provision of this Agreement be held by a court of competent jurisdiction to be illegal, invalid, or unenforceable, that provision shall be deemed amended to achieve as nearly as possible the same economic effect as the original provision, and the legality, validity and enforceability of the remaining provisions of this Agreement shall not be affected or impaired thereby.
- The failure of either party to enforce any term or condition of this Agreement shall not constitute a waiver of either party's right to enforce each and every term and condition of this Agreement. No breach under this agreement shall be deemed waived or excused by either party unless such waiver or consent is in writing signed by the party granting such waiver or consent. The waiver by or consent of a party to a breach of any provision of this Agreement shall not operate or be construed as a waiver of or consent to any other or subsequent breach by such other party.
- This Agreement may not be assigned (including by operation of law or otherwise) by you without WILEY's prior written consent.

- Any fee required for this permission shall be non-refundable after thirty (30) days from receipt by the CCC.
- These terms and conditions together with CCC's Billing and Payment terms and conditions (which are incorporated herein) form the entire agreement between you and WILEY concerning this licensing transaction and (in the absence of fraud) supersedes all prior agreements and representations of the parties, oral or written. This Agreement may not be amended except in writing signed by both parties. This Agreement shall be binding upon and inure to the benefit of the parties' successors, legal representatives, and authorized assigns.
- In the event of any conflict between your obligations established by these terms and conditions and those established by CCC's Billing and Payment terms and conditions, these terms and conditions shall prevail.
- WILEY expressly reserves all rights not specifically granted in the combination of (i) the license details provided by you and accepted in the course of this licensing transaction, (ii) these terms and conditions and (iii) CCC's Billing and Payment terms and conditions.
- This Agreement will be void if the Type of Use, Format, Circulation, or Requestor Type was misrepresented during the licensing process.
- This Agreement shall be governed by and construed in accordance with the laws of the State of New York, USA, without regards to such state's conflict of law rules. Any legal action, suit or proceeding arising out of or relating to these Terms and Conditions or the breach thereof shall be instituted in a court of competent jurisdiction in New York County in the State of New York in the United States of America and each party hereby consents and submits to the personal jurisdiction of such court, waives any objection to venue in such court and consents to service of process by registered or certified mail, return receipt requested, at the last known address of such party.

#### **WILEY OPEN ACCESS TERMS AND CONDITIONS**

Wiley Publishes Open Access Articles in fully Open Access Journals and in Subscription journals offering Online Open. Although most of the fully Open Access journals publish open access articles under the terms of the Creative Commons Attribution (CC BY) License only, the subscription journals and a few of the Open Access Journals offer a choice of Creative Commons Licenses. The license type is clearly identified on the article.

##### **The Creative Commons Attribution License**

The [Creative Commons Attribution License \(CC-BY\)](#) allows users to copy, distribute and transmit an article, adapt the article and make commercial use of the article. The CC-BY license permits commercial and non-

##### **Creative Commons Attribution Non-Commercial License**

The [Creative Commons Attribution Non-Commercial \(CC-BY-NC\) License](#) permits use, distribution and reproduction in any medium, provided the original work is properly cited and is not used for commercial purposes.(see below)

##### **Creative Commons Attribution-Non-Commercial-NoDerivs License**

The [Creative Commons Attribution Non-Commercial-NoDerivs License \(CC-BY-NC-ND\)](#) permits use, distribution and reproduction in any medium, provided the original work is properly cited, is not used for commercial purposes and no modifications or adaptations are made. (see below)

##### **Use by commercial "for-profit" organizations**

Use of Wiley Open Access articles for commercial, promotional, or marketing purposes requires further explicit permission from Wiley and will be subject to a fee.

Further details can be found on Wiley Online Library

<http://olabout.wiley.com/WileyCDA/Section/id-410895.html>

#### **Other Terms and Conditions:**

**v1.10 Last updated September 2015**

**Questions? [customer@copyright.com](mailto:customer@copyright.com) or +1-855-239-3415 (toll free in the US) or +1-978-646-2777.**

## A I.2 Copyright Clearance for Chapter 2



Account Info

Help



**Title:** Journal of Structural Engineering  
**Article ID:** 0733-9445  
**Publication:** Publication1  
**Publisher:** CCC Republication  
**Date:** Jan 1, 1983  
 Copyright © 1983, CCC Republication

Logged in as:  
 Esmael Asadi  
 Account #:  
 3001535735

LOGOUT

### Order Completed

Thank you for your order.

This Agreement between Esmael Asadi ("You") and American Society of Civil Engineers ("American Society of Civil Engineers") consists of your order details and the terms and conditions provided by American Society of Civil Engineers and Copyright Clearance Center.

License number	Reference confirmation email for license number
License date	Oct, 16 2019
Licensed content publisher	American Society of Civil Engineers
Licensed content title	Journal of Structural Engineering
Licensed content date	Jan 1, 1983
Type of use	Thesis/Dissertation
Requestor type	Author of requested content
Format	Print, Electronic
Portion	page
Number of pages requested	15
The requesting person/organization	Esmael Asadi/Case Western Reserve University
Title or numeric reference of the portion(s)	Introduction - Conclusions
Title of the article or chapter the portion is from	Chapter 2 - Seismic Performance Assessment and Loss Estimation of Steel Diagrid Structures
Editor of portion(s)	N/A
Author of portion(s)	Esmael Asadi
Volume of serial or monograph	N/A
Page range of portion	1-15
Publication date of portion	Nov. 26th, 2019
Rights for	Main product
Duration of use	Life of current edition
Creation of copies for the disabled	no
With minor editing privileges	no
For distribution to	Worldwide
In the following language(s)	Original language of publication
With incidental promotional use	no
Lifetime unit quantity of new product	Up to 4,999
Title	Risk-Informed Multi-criteria Decision Framework for Resilience and Sustainability Assessment of Instrumented Structures
Institution name	Case Western Reserve University
Expected presentation date	Nov 2019
Requestor Location	Esmael Asadi 2672 Euclid Heights Blvd Apt 204  Cleveland, OH 44106 United States Attn:
Billing Type	Invoice
Billing address	Esmael Asadi 2672 Euclid Heights Blvd Apt 204  Cleveland, OH 44106 United States Attn: Esmael Asadi
Total (may include CCC user fee)	0.00 USD
Total	0.00 USD

CLOSE WINDOW

Copyright © 2019 Copyright Clearance Center, Inc. All Rights Reserved. [Privacy statement](#). [Terms and Conditions](#).  
 Comments? We would like to hear from you. E-mail us at [customercare@copyright.com](mailto:customercare@copyright.com)

## A I.3 Copyright Clearance for Chapter 3

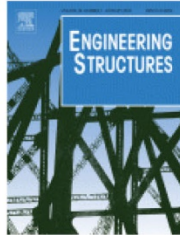


RightsLink®

Home

Create Account

Help



**Title:** Multi-criteria decision-making for seismic resilience and sustainability assessment of diagrid buildings

**Author:** Esmaeel Asadi, Abdullahi M. Salman, Yue Li

**Publication:** Engineering Structures

**Publisher:** Elsevier

**Date:** 15 July 2019

© 2019 Elsevier Ltd. All rights reserved.

LOGIN

If you're a [copyright.com user](#), you can login to RightsLink using your copyright.com credentials. Already a [RightsLink user](#) or want to [learn more?](#)

Please note that, as the author of this Elsevier article, you retain the right to include it in a thesis or dissertation, provided it is not published commercially. Permission is not required, but please ensure that you reference the journal as the original source. For more information on this and on your other retained rights, please visit: <https://www.elsevier.com/about/our-business/policies/copyright#Author-rights>

BACK

CLOSE WINDOW

Copyright © 2019 [Copyright Clearance Center, Inc.](#) All Rights Reserved. [Privacy statement](#). [Terms and Conditions](#). Comments? We would like to hear from you. E-mail us at [customer@copyright.com](mailto:customer@copyright.com)

# Bibliography

- Abate, D., Towers, M., Dotz, R., and Romani, L. (2009). "The Whitestone facility maintenance and repair cost reference 2009-2010." *Whitestone Research, California*.
- Abreu, D. P., Velasquez, K., Curado, M., and Monteiro, E. (2017). "A resilient Internet of Things architecture for smart cities." *Annals of Telecommunications*, 72(1), 19–30.
- ACI. (2014). *Building Code Requirements for Structural Concrete (ACI Standard 318-14)*. American Concrete Institute, Farmington Hills, MI.
- ACI 318-14. (2014). *Building Code Requirements for Structural Concrete (ACI 318-14) and Commentary*. (Reported by ACI Committee 318, ed.), American Concrete Institute, MI.
- AISC. (2010). *ANSI/AISC 360-10: An American National Standard – Specification for Structural Steel Building*. AMERICAN INSTITUTE OF STEEL CONSTRUCTION, Chicago, Illinois.
- AISC. (2011). *Steel Construction Manual 14th ed. American Institute of Steel Construction*. American Institute of Steel Construction, Chicago, IL.
- AISC. (2016a). *ANSI/AISC 341-16 Seismic provision for structural steel buildings*. AMERICAN INSTITUTE OF STEEL CONSTRUCTION, Chicago, Illinois.
- AISC. (2016b). *ANSI / AISC 360-16, Specification for Structural Steel Buildings*. AMERICAN INSTITUTE OF STEEL CONSTRUCTION, Chicago, Illinois.
- AISC. (2016c). "Environmental Product Declaration, Fabricated Hot-Rolled Structural Sections." American Institute of Steel Construction.
- AISC. (2017). *More than Recycled Content: The Sustainable Characteristics of Structural Steel*. American Institute of Steel Construction (AISC), Chicago, IL.
- Akgül, F., and Frangopol, D. M. (2004). "Lifetime performance analysis of existing steel girder bridge superstructures." *Journal of Structural Engineering*, 130(12), 1875–1888.
- AlHamaydeh, M., Aly, N., and Galal, K. (2017a). "Impact of Seismicity on Performance and Cost of RC Shear Wall Buildings in Dubai, United Arab Emirates." *Journal of Performance of Constructed Facilities*, 31(5), 04017083.
- AlHamaydeh, M., Aly, N., and Galal, K. (2017b). "Impact of seismicity on performance and cost of RC shear wall buildings in Dubai, United Arab Emirates." *Journal of Performance of Constructed Facilities*, 31(5), 04017083.
- Ali, M. M., and Moon, K. S. (2007). "Structural Developments in Tall Buildings: Current Trends and Future Prospects." *Architectural Science Review*.
- Alipour, A., and Shafei, B. (2016). "Seismic resilience of transportation networks with deteriorating components." *Journal of Structural Engineering*, 142(8), C4015015.
- Allen, R. M., Brown, H., Hellweg, M., Khainovski, O., Lombard, P., and Neuhauser, D. (2009). "Real-time earthquake detection and hazard assessment by Elarms across California." *Geophysical Research Letters*, 36(5).
- Alshamrani, O. S., Galal, K., and Alkass, S. (2014). "Integrated LCA–LEED sustainability assessment model for structure and envelope systems of school buildings." *Building and Environment*, 80, 61–70.
- Amezquita-Sanchez, J. P., and Adeli, H. (2016). "Signal processing techniques for vibration-based health monitoring of smart structures." *Archives of Computational Methods in Engineering*, 23(1), 1–15.
- Ang, A. H.-S., and Tang, W. H. (2007). "Probability concepts in engineering planning and design, vol. 2: Decision, risk, and reliability." *JOHN WILEY & SONS, INC., Hoboken, NJ*.

- Ang, A.-S., and De Leon, D. (2005). "Modeling and analysis of uncertainties for risk-informed decisions in infrastructures engineering." *Structure and Infrastructure Engineering*, 1(1), 19–31.
- Ansari, F. (2005). *Sensing issues in civil structural health monitoring*. Springer.
- ArchDaily. (2012). "Flashback: Hearst tower / Foster + partners." <<https://www.archdaily.com/204701/flashback-hearst-tower-foster-and-partners/>> (Jun. 20, 2017).
- Asadi, E., and Adeli, H. (2017). "Diagrid: An innovative, sustainable, and efficient structural system." *The Structural Design of Tall and Special Buildings*, 26(8), e1358.
- Asadi, E., and Adeli, H. (2018a). "Seismic performance factors for low- to mid-rise steel diagrid structural systems." *The Structural Design of Tall and Special Buildings*, e1505.
- Asadi, E., and Adeli, H. (2018b). "Nonlinear behavior and design of mid-to-highrise diagrid structures in seismic regions." *Eng. J. Am. Inst. Steel Constr.*, 55(3).
- Asadi, E., Li, Y., and YeongAe, H. (2018). "Seismic Performance Assessment and Loss Estimation of Steel Diagrid Structures." *ASCE Journal of Structural Engineering*.
- Asadi, E., Salman, A. M., and Li, Y. (2019a). "Localized Health Monitoring System for Seismic Resilience Quantification and Safety Evaluation of Smart Structures." *Structural Safety*, Under Review.
- Asadi, E., Salman, A. M., and Li, Y. (2019b). "Multi-criteria decision-making for seismic resilience and sustainability assessment of diagrid buildings." *Engineering Structures*, 191, 229–246.
- Asadi, E., Shen, Z., Zhou, H., Salman, A. M., and Li, Y. (2020). "Risk-informed Multi-criteria Decision Framework for Resilience, Sustainability, and Energy Analysis of Reinforced Concrete Buildings." *Journal of Building Performance Simulation*.
- ASCE. (2010). *Minimum design loads for buildings and other structures. ASCE/SEI Standard No. 7–10*. American Society of Civil Engineers, Reston, Virginia.
- ASCE. (2013). *Report card for America's infrastructure*. American Society of Civil Engineers, Reston, VA.
- ASCE. (2014). *Seismic Evaluation and Retrofit of Existing Buildings: ASCE Standard ASCE/SEI 41-13*. American Society of Civil Engineers, Reston, Virginia.
- ASCE. (2017a). *Minimum Design Loads and Associated Criteria for Buildings and Other Structures. ASCE/SEI Standard No. 7-16*, American Society of Civil Engineers, Reston, Virginia.
- ASCE. (2017b). *Minimum Design Loads and Associated Criteria for Buildings and Other Structures. ASCE/SEI Standard 7–16*. American Society of Civil Engineers, Reston, Virginia.
- ASHRAE. (2016a). "Energy standard for buildings except low-rise residential buildings." *ANSI/ASHRAE/IES Standard 90.1-2016*, 90.
- ASHRAE. (2016b). "Weather Data for Building Design Standards." *ANSI/ASHRAE Standard 169*, 169.
- ATC. (2009). "Quantification of building seismic performance factors." *Fema P695*, (June), 421.
- AWWA. (2010). *Risk and Resilience Management of Water and Wastewater Systems*. Denver, Colorado.
- Azarbakht, A., and Dolšek, M. (2010). "Progressive incremental dynamic analysis for first-mode dominated structures." *Journal of Structural Engineering*, 137(3), 445–455.
- Baglivo, C., Congedo, P. M., and Fazio, A. (2014). "Multi-criteria optimization analysis of external walls according to ITACA protocol for zero energy buildings in the mediterranean climate." *Building and Environment*, 82, 467–480.
- Baker, J. W. (2015). "Efficient analytical fragility function fitting using dynamic structural analysis." *Earthquake Spectra*, 31(1), 579–599.

- Basbagill, J., Flager, F., Lepech, M., and Fischer, M. (2013). "Application of life-cycle assessment to early stage building design for reduced embodied environmental impacts." *Building and Environment*, 60, 81–92.
- Beck, J. L., Kiremidjian, A., Wilkie, S., Mason, A., Salmon, T., Goltz, J., Olson, R., Workman, J., Irfanoglu, A., and Porter, K. (1999). "Decision support tools for earthquake recovery of businesses." *Final Report, CUREe-Kajima Joint Research Program Phase III, Consortium of Universities for Earthquake Engineering Research, Richmond, CA.*
- Belleri, A., and Marini, A. (2016). "Does seismic risk affect the environmental impact of existing buildings?" *Energy and Buildings*, 110, 149–158.
- Bertero, R. D., and Bertero, V. V. (1999). "Redundancy in earthquake-resistant design." *Journal of Structural Engineering*, 125(1), 81–88.
- Bhuiyan, M. T., and Leon, R. (2016). "Probabilistic Models for Critical Building Responses of High-rise Building." *Proceedings of 2016 IAJC-ISAM International Conference, Kissimmee, FL, USA.*
- Biondini, F., and Frangopol, D. M. (2014). *Time-variant robustness of aging structures*. CRC Boca Raton, FL.
- Biondini, F., and Frangopol, D. M. (2016). "Life-cycle performance of deteriorating structural systems under uncertainty." *Journal of Structural Engineering*, 142(9), F4016001.
- Black, G., Wenger, W. A. B., and Popov, E. P. (1980). "Inelastic Buckling of Steel Struts Under Cyclic Load Reversals." (October), 1–163.
- Boake, T. (2014). *Boake: Diagrid structures: systems, connections, details*. Birkhäuser: Switzerland.
- Bocchini, P., Asce, M., Frangopol, D. M., Asce, D. M., Ummenhofer, T., and Zinke, T. (2014). "Resilience and Sustainability of Civil Infrastructure : Toward a Unified Approach." *Journal of Infrastructure Systems*.
- Boore, D. M., and Atkinson, G. M. (2008). "Ground-motion prediction equations for the average horizontal component of PGA, PGV, and 5%-damped PSA at spectral periods between 0.01 s and 10.0 s." *Earthquake Spectra*, 24(1), 99–138.
- Bornn, L., Farrar, C. R., and Park, G. (2010). "Damage detection in initially nonlinear systems." *International Journal of Engineering Science, Structural Health Monitoring in the Light of Inverse Problems of Mechanics*, 48(10), 909–920.
- Bruneau, M., Barbato, M., Padgett, J. E., Zaghi, A. E., Mitrani-Reiser, J., and Li, Y. (2017). "State of the Art of Multihazard Design." *Journal of Structural Engineering*, 143(10), 03117002.
- Bruneau, M., Chang, S. E., Eguchi, R. T., Lee, G. C., O'Rourke, T. D., Reinhorn, A. M., Shinozuka, M., Tierney, K., Wallace, W. A., and Von Winterfeldt, D. (2003). "A framework to quantitatively assess and enhance the seismic resilience of communities." *Earthquake spectra*, 19(4), 733–752.
- Burton, H. V., Deierlein, G., Lallemand, D., and Lin, T. (2016). "Framework for Incorporating Probabilistic Building Performance in the Assessment of Community Seismic Resilience." *Journal of Structural Engineering*, 142(8), C4015007.
- Burton, H. V., Sreekumar, S., Sharma, M., and Sun, H. (2017). "Estimating aftershock collapse vulnerability using mainshock intensity, structural response and physical damage indicators." *Structural Safety*, 68, 85–96.
- Carmody, J., and Haglund, K. (2012). *Measure guideline: energy-efficient window performance and selection*. National Renewable Energy Lab.(NREL), Golden, CO (United States).
- Caterino, N., Iervolino, I., Manfredi, G., and Cosenza, E. (2009). "Comparative analysis of multi-criteria decision-making methods for seismic structural retrofitting." *Computer-Aided Civil and Infrastructure Engineering*.

- Celebi, M., Sanli, A., Sinclair, M., Gallant, S., and Radulescu, D. (2004). “Real-Time Seismic Monitoring Needs of a Building Owner—and the Solution: A Cooperative Effort.” *Earthquake Spectra*, 20(2), 333–346.
- Celik, O. C., and Ellingwood, B. R. (2010). “Seismic fragilities for non-ductile reinforced concrete frames—Role of aleatoric and epistemic uncertainties.” *Structural Safety*, 32(1), 1–12.
- Chang, J.-R., Chen, D.-H., and Hung, C.-T. (2005). “Selecting preventive maintenance treatments in Texas: using the technique for order preference by similarity to the ideal solution for specific pavement study-3 sites.” *Transportation Research Record: Journal of the Transportation Research Board*, (1933), 62–71.
- Charnish, B., and McDonnell, T. (2008). “The bow: Unique diagrid structural system for a sustainable tall building.” *CTBUH 2008, 8th World Congress - Tall and Green: Typology for a Sustainable Urban Future*, Dubai, 380–384.
- Chau, C. K., Leung, T. M., and Ng, W. Y. (2015). “A review on Life Cycle Assessment, Life Cycle Energy Assessment and Life Cycle Carbon Emissions Assessment on buildings.” *Applied Energy*, 143, 395–413.
- Chen, C.-H., Lai, J.-W., and Mahin, S. (2008). “Seismic performance assessment of concentrically braced steel frame buildings.” *Proceedings of the 14th World Conference on Earthquake Engineering*, Beijing, China.
- Cheng, M. H., Wu, S., Heaton, T. H., and Beck, J. L. (2014). “Earthquake early warning application to buildings.” *Engineering Structures*, 60, 155–164.
- Cheng, S., Chan, C. W., and Huang, G. H. (2003). “An integrated multi-criteria decision analysis and inexact mixed integer linear programming approach for solid waste management.” *Engineering Applications of Artificial Intelligence*, 16(5–6), 543–554.
- Chhabra, J. P. S., Hasik, V., Bilec, M. M., and Warn, G. P. (2018). “Probabilistic Assessment of the Life-Cycle Environmental Performance and Functional Life of Buildings due to Seismic Events.” *Journal of Architectural Engineering*, 24(1), 04017035.
- Chock, G. (2007). *ATC-20 post-earthquake building safety evaluations performed after the October 15, 2006 Hawai’i Earthquakes summary and recommendations for improvements (updated)*. STRUCTURAL ENGINEERS ASSOCIATION OF HAWAII.
- Christensen, C., Anderson, R., Horowitz, S., Courtney, A., and Spencer, J. (2006). *BEopt(TM) Software for Building Energy Optimization: Features and Capabilities*. National Renewable Energy Lab. (NREL), Golden, CO (United States).
- Cimellaro, G. P. (2016). “Urban resilience for emergency response and recovery.” *Fundamental Concepts and Applications*.
- Cimellaro, G. P., Reinhorn, A. M., and Bruneau, M. (2006). “Quantification of seismic resilience.” *Proceedings of the 8th US National conference on Earthquake Engineering*, 18–22.
- Cimellaro, G. P., Reinhorn, A. M., and Bruneau, M. (2010). “Framework for analytical quantification of disaster resilience.” *Engineering structures*, 32(11), 3639–3649.
- Cimellaro, G. P., Tinebra A., Renschler C., and Fragiadakis M. (2016). “New Resilience Index for Urban Water Distribution Networks.” *Journal of Structural Engineering*, 142(8), C4015014.
- CMU GDI. (2018). *Economic Input-Output Life Cycle Assessment (EIO-LCA), US 2002 Economic Benchmark model last update 2010*.
- Coburn, A. W., Spence, R. J., and Pomonis, A. (1992). “Factors determining human casualty levels in earthquakes: mortality prediction in building collapse.” *Proceedings of the First International Forum on Earthquake related Casualties. Madrid, Spain, July 1992*.
- Crawley, D. B., Lawrie, L. K., Winkelmann, F. C., Buhl, W. F., Huang, Y. J., Pedersen, C. O., Strand, R. K., Liesen, R. J., Fisher, D. E., and Witte, M. J. (2001). “EnergyPlus: creating

- a new-generation building energy simulation program.” *Energy and buildings*, 33(4), 319–331.
- Cremon, G., and Baker, J. W. (2018). “Quantifying the benefits of building instruments to FEMA P-58 rapid post-earthquake damage and loss predictions.” *Engineering Structures*, 176, 243–253.
- CSI. (2011). “CSI Analysis Reference Manual for SAP2000, ETABS, SAFE, and CSiBridge.” Computers and Structures, Inc., Berkeley, California, USA.
- De Iuliis, M., Kammouh, O., Cimellaro, G. P., and Tesfamariam, S. (2019). “Downtime estimation of building structures using fuzzy logic.” *International Journal of Disaster Risk Reduction*, 34, 196–208.
- Deco, A., Bocchini, P., and Frangopol, D. M. (2013). “A probabilistic approach for the prediction of seismic resilience of bridges.” *Earthquake Engineering & Structural Dynamics*, 42(10), 1469–1487.
- DesignBuilder. (2016). “DesignBuilder Documentation, DesignBuilder User Manual Version 5.” *DesignBuilder Software Ltd, UK*.
- Dezfuli, H., Stamatelatos, M., Maggio, G., Everett, C., Youngblood, R., Rutledge, P., Benjamin, A., Williams, R., Smith, C., and Guarro, S. (2010). “NASA Risk-Informed Decision Making Handbook.”
- DHS. (2003). “HAZUS-MH MRI technical manual.” Dept. of Homeland Security Emergency Preparedness and Response Directorate.” DHS (Department of Homeland Security), FEMA Mitigation Division, Washington, DC.
- Dong, Y., and Frangopol, D. M. (2015). “Risk, Resilience, and Sustainability Assessment of Infrastructure Systems in a Life-Cycle Context Considering Uncertainties.” *Proceedings of the 12th International Conference on Applications of Statistics and Probability in Civil Engineering (ICASP12)*, Vancouver, Canada.
- Dong, Y., and Frangopol, D. M. (2016). “Performance-based seismic assessment of conventional and base-isolated steel buildings including environmental impact and resilience.” *Earthquake Engineering & Structural Dynamics*, 45(5), 739–756.
- Dong, Y., Frangopol, D. M., and Saydam, D. (2013). “Time-variant sustainability assessment of seismically vulnerable bridges subjected to multiple hazards.” *Earthquake Engineering & Structural Dynamics*, 42(10), 1451–1467.
- Dong, Y., and Li, Y. (2017). “Evaluation of Hurricane Resilience of Residential Community Considering a Changing Climate, Social Disruption Cost, and Environmental Impact.” *Journal of Architectural Engineering*, 23(3), 04017008.
- Dyanati, M., Huang, Q., and Roke, D. (2015). “Life cycle cost-benefit evaluation of self-centering and conventional concentrically braced frames.” *12th International Conference on Applications of Statistics and Probability in Civil Engineering, Vancouver*.
- Dyer, J. S., Fishburn, P. C., Steuer, R. E., Wallenius, J., and Zionts, S. (1992). “Multiple criteria decision making, multiattribute utility theory: the next ten years.” *Management science*, 38(5), 645–654.
- EERI. (2019). “Functional Recovery: A Conceptual Framework-A white paper of the Earthquake Engineering Research Institute.” Earthquake Engineering Research Institute.
- Eidinger, J. M., and Avila, E. A. (1999). *Guidelines for the seismic evaluation and upgrade of water transmission facilities*. ASCE Publications, Reston, Virginia.
- Ekici, B., Cubukcuoglu, C., Turrin, M., and Sariyildiz, I. S. (2019). “Performative computational architecture using swarm and evolutionary optimisation: A review.” *Building and Environment*, 147, 356–371.
- Ellingwood, B. R. (2000). “LRFD: implementing structural reliability in professional practice.” *Engineering Structures*, 22(2), 106–115.

- Ellingwood, B. R. (2005). "Risk-informed condition assessment of civil infrastructure: state of practice and research issues." *Structure and infrastructure engineering*, 1(1), 7–18.
- Ellingwood, B. R. (2006). "Mitigating risk from abnormal loads and progressive collapse." *Journal of Performance of Constructed Facilities*, 20(4), 315–323.
- Ellingwood, B. R., and Kinali, K. (2009). "Quantifying and communicating uncertainty in seismic risk assessment." *Structural Safety, Risk Acceptance and Risk Communication*, 31(2), 179–187.
- Ellingwood, B. R., and Lee, J. Y. (2016). "Life cycle performance goals for civil infrastructure: intergenerational risk-informed decisions." *Structure and Infrastructure Engineering*, 12(7), 822–829.
- Ellingwood, B. R., and Leyendecker, E. V. (1978). "Approaches for design against progressive collapse." *Journal of the Structural Division*, 104(3), 413–423.
- Ellingwood, B. R., and Tekie, P. B. (1999). "Wind load statistics for probability-based structural design." *Journal of Structural Engineering*, 125(4), 453–463.
- Ellingwood, B. R., and Wen, Y.-K. (2005). "Risk-benefit-based design decisions for low-probability/high consequence earthquake events in Mid-America." *Progress in Structural Engineering and Materials*, 7(2), 56–70.
- Ervural, B. C., Zaim, S., Demirel, O. F., Aydin, Z., and Delen, D. (2018). "An ANP and fuzzy TOPSIS-based SWOT analysis for Turkey's energy planning." *Renewable and Sustainable Energy Reviews*, 82, 1538–1550.
- Faber, M. H., and Stewart, M. G. (2003). "Risk assessment for civil engineering facilities: critical overview and discussion." *Reliability engineering & system safety*, 80(2), 173–184.
- Fan, W., and Qiao, P. (2011). "Vibration-based damage identification methods: a review and comparative study." *Structural health monitoring*, 10(1), 83–111.
- Farrar, C. R., and Worden, K. (2007). "An introduction to structural health monitoring." *Philosophical Transactions of the Royal Society A: Mathematical, Physical and Engineering Sciences*, 365(1851), 303–315.
- Feese, C. A. (2013). "Assessment of seismic damage of buildings and related environmental impacts."
- FEMA. (1997). *NEHRP guidelines for the seismic rehabilitation of buildings*, FEMA 273. Federal Emergency Management Agency Washington, DC.
- FEMA. (2000). *FEMA-356: Prestandard and commentary for the seismic rehabilitation of buildings*. Building Seismic Safety Council for The Federal Emergency Management Agency.
- FEMA. (2005). *FEMA-440: Improvement of nonlinear static seismic analysis procedures*. Building Seismic Safety Council for The Federal Emergency Management Agency, Washington, D.C.
- FEMA. (2012). *FEMA P-58: Seismic performance assessment of buildings*. Building Seismic Safety Council for The Federal Emergency Management Agency, Washington, D.C.
- FEMA, Pacific Disaster Center, and USGS. (2017). *Hazus® Estimated Annualized Earthquake Losses for the United States*. Hazus Estimated Annualized Earthquake Losses for the United States, The Federal Emergency Management Agency, Washington, D.C.
- Ferreira, R. J., de Almeida, A. T., and Cavalcante, C. A. (2009). "A multi-criteria decision model to determine inspection intervals of condition monitoring based on delay time analysis." *Reliability Engineering & System Safety*, 94(5), 905–912.
- FHWA. (1994). *Technical Advisory: Motor Vehicle Accident Costs*. Federal Highway Administration, U.S. Dept. of Transportation, Washington, DC.
- Fisher, J. W., Kulak, G. L., and Smith, I. F. (1998). *A fatigue primer for structural engineers*. National Steel Bridge Alliance, American Institute of Steel Construction.

- Frangopol, D. M., and Liu, M. (2005). "Multiobjective optimization for risk-based maintenance and life-cycle cost of civil infrastructure systems." *IFIP Conference on System Modeling and Optimization*, Springer, 123–137.
- Gallivan, F., Ang-Olson, J., Papon, A., and Venner, M. (2010). "GREENHOUSE GAS MITIGATION MEASURES FOR TRANSPORTATION CONSTRUCTION, MAINTENANCE, AND OPERATIONS ACTIVITIES."
- Ghafory-Ashtiany, M., Mousavi, M., and Azarbakht, A. (2011). "Strong ground motion record selection for the reliable prediction of the mean seismic collapse capacity of a structure group." *Earthquake Engineering & Structural Dynamics*, 40(6), 691–708.
- Gholipour, M., Asadi, E., and Alinia, M. M. (2015). "The use of outrigger system in steel plate shear wall structures." *Advances in Structural Engineering*, 18(6), 853–872.
- Ghosh, J., and Padgett, J. E. (2010). "Aging considerations in the development of time-dependent seismic fragility curves." *Journal of Structural Engineering*, 136(12), 1497–1511.
- Ghosn, M., Dueñas-Osorio, L., Frangopol, D. M., McAllister, T. P., Bocchini, P., Manuel, L., Ellingwood, B. R., Arangio, S., Bontempi, F., and Shah, M. (2016). "Performance indicators for structural systems and infrastructure networks." *Journal of Structural Engineering*, 142(9), F4016003.
- Glaser, S. D., Li, H., Wang, M. L., Ou, J., and Lynch, J. (2007). "Sensor technology innovation for the advancement of structural health monitoring: a strategic program of US-China research for the next decade." *Smart Structures and Systems*, 3(2), 221–244.
- Govindan, K., and Jepsen, M. B. (2016). "ELECTRE: A comprehensive literature review on methodologies and applications." *European Journal of Operational Research*, 250(1), 1–29.
- Goyal, D., and Pabla, B. S. (2016). "The vibration monitoring methods and signal processing techniques for structural health monitoring: a review." *Archives of Computational Methods in Engineering*, 23(4), 585–594.
- Gsa, U. (2003). "Progressive collapse analysis and design guidelines for new federal office buildings and major modernization projects." *Washington, DC*.
- Guéguen, P., and Tiganescu, A. (2018). "Consideration of the Effects of Air Temperature on Structural Health Monitoring through Traffic Light-Based Decision-Making Tools." *Shock and Vibration*, 2018.
- Guggemos, A. A., and Horvath, A. (2003). "Framework for environmental analysis of commercial building structures." *Construction Research Congress: Wind of Change: Integration and Innovation*, 1–8.
- Guo, X., and Chen, Z. (2015). "Lifecycle multihazard framework for assessing flood scour and earthquake effects on bridge failure." *ASCE-ASME Journal of Risk and Uncertainty in Engineering Systems, Part A: Civil Engineering*, 2(2), C4015004.
- Han, R., Li, Y., and van de Lindt, J. (2014). "Assessment of seismic performance of buildings with incorporation of aftershocks." *Journal of Performance of Constructed Facilities*, 29(3), 04014088.
- Han, R., Li, Y., and van de Lindt, J. (2015). "Impact of aftershocks and uncertainties on the seismic evaluation of non-ductile reinforced concrete frame buildings." *Engineering Structures*, 100, 149–163.
- Han, R., Li, Y., and van de Lindt, J. (2016). "Seismic loss estimation with consideration of aftershock hazard and post-quake decisions." *ASCE-ASME Journal of Risk and Uncertainty in Engineering Systems, Part A: Civil Engineering*, 2(4), 04016005.
- Han, R., Li, Y., and van de Lindt, J. (2017). "Probabilistic Assessment and Cost-Benefit Analysis of Nonductile Reinforced Concrete Buildings Retrofitted with Base Isolation: Considering Mainshock–Aftershock Hazards." *ASCE-ASME Journal of Risk and Uncertainty in Engineering Systems, Part A: Civil Engineering*, 3(4), 04017023.

- Hendrickson, C., Horvath, A., Joshi, S., and Lave, L. (1998). "Peer reviewed: economic input–output models for environmental life-cycle assessment." *Environmental science & technology*, 32(7), 184A-191A.
- Heo, Y. (2009). "Framework for damage-based probabilistic seismic performance evaluation of reinforced concrete frames." University of California, Davis, CA.
- Heshmati, M., and Aghakouchak, A. A. (2019). "Quantification of seismic performance factors of steel diagrid system." *The Structural Design of Tall and Special Buildings*, 28(3), e1572.
- Holling, C. S. (1973). "Resilience and stability of ecological systems." *Annual review of ecology and systematics*, 4(1), 1–23.
- Hopfe, C. J., Augenbroe, G. L. M., and Hensen, J. L. M. (2013). "Multi-criteria decision making under uncertainty in building performance assessment." *Building and Environment*, 69, 81–90.
- Horvath, A. (2004). "Construction materials and the environment." *Annu. Rev. Environ. Resour.*, 29, 181–204.
- Horvath, A. (2006). "Environmental Assessment of Freight Transportation in the US." *The International Journal of Life Cycle Assessment*, 11(4), 229–239.
- Huang, C., Han, X., Ji, J., and Tang, J. (2010). "Behavior of concrete-filled steel tubular planar intersecting connections under axial compression, Part 1: Experimental study." *Engineering Structures*, 32(1), 60–68.
- Hwang, C.-L., and Yoon, K. (1981). "Methods for multiple attribute decision making." *Multiple attribute decision making*, Springer, 58–191.
- Hwang, S., and Lignos, D. G. (2017a). "Proposed Methodology for Earthquake-induced Loss Assessment of Instrumented Steel Frame Buildings: Building-Specific and City-Scale Approaches."
- Hwang, S.-H., and Lignos, D. G. (2017b). "Effect of modeling assumptions on the earthquake-induced losses and collapse risk of steel-frame buildings with special concentrically braced frames." *Journal of Structural Engineering*, 143(9), 04017116.
- Hwang, S.-H., and Lignos, D. G. (2018). "Nonmodel-based framework for rapid seismic risk and loss assessment of instrumented steel buildings." *Engineering Structures*, 156, 417–432.
- Ibn-Mohammed, T., Greenough, R., Taylor, S., Ozawa-Meida, L., and Acquaye, A. (2013). "Operational vs. embodied emissions in buildings—A review of current trends." *Energy and Buildings*, 66, 232–245.
- Invidiata, A., Lavagna, M., and Ghisi, E. (2018). "Selecting design strategies using multi-criteria decision making to improve the sustainability of buildings." *Building and Environment*, 139, 58–68.
- Islam, M. S. (1996). "Analysis of the Northridge earthquake response of a damaged non-ductile concrete frame building." *The structural design of tall buildings*, 5(3), 151–182.
- ISO. (1998). *Environmental management—Life cycle assessment—Goal and scope definition and inventory analysis*. ISO 14041, International Organization for Standardization, Geneva, Switzerland.
- ISO. (2007). *Sustainability in Building Construction: Environmental Declaration of Building Products*. ISO 21930-2007(E), International Organization for Standardization, Geneva, Switzerland.
- Izzuddin, B. A., Vlassis, A. G., Elghazouli, A. Y., and Nethercot, D. A. (2008). "Progressive collapse of multi-storey buildings due to sudden column loss—Part I: Simplified assessment framework." *Engineering structures*, 30(5), 1308–1318.
- Jafari, A., and Valentin, V. (2018). "Selection of optimization objectives for decision-making in building energy retrofits." *Building and Environment*, 130, 94–103.
- Jaquess, T. K., and Frank, K. H. (2002). *Characterization of the material properties of rolled sections*. SAC Joint Venture.

- Junnila, S., Horvath, A., and Guggemos, A. A. (2006). "Life-cycle assessment of office buildings in Europe and the United States." *Journal of Infrastructure Systems*, 12(1), 10–17.
- Kaatz, E., Root, D. S., Bowen, P. A., and Hill, R. C. (2006). "Advancing key outcomes of sustainability building assessment." *Building Research & Information*, 34(4), 308–320.
- Kamali, M., Hewage, K., and Milani, A. S. (2018). "Life cycle sustainability performance assessment framework for residential modular buildings: Aggregated sustainability indices." *Building and Environment*, 138, 21–41.
- Kanamori, H. (2005). "Real-Time Seismology and Earthquake Damage Mitigation." *Annual Review of Earth and Planetary Sciences*, 33(1), 195–214.
- Kappos, A. J., Chryssanthopoulos, M. K., and Dymiotis, C. (1999). "Uncertainty analysis of strength and ductility of confined reinforced concrete members." *Engineering Structures*, 21(3), 195–208.
- Keeble, B. R. (1988). "The Brundtland report: 'Our common future.'" *Medicine and War*, 4(1), 17–25.
- Keeney, R. L., and Wood, E. F. (1977). "An illustrative example of the use of multiattribute utility theory for water resource planning." *Water Resources Research*, 13(4), 705–712.
- Kim, J., and Kong, J. (2013). "Progressive collapse behavior of rotor-type diagrid buildings." *The Structural Design of Tall and Special Buildings*, 22(16), 1199–1214.
- Kim, J., and Lee, Y.-H. (2010). "Progressive collapse resisting capacity of tube-type structures." *The Structural Design of Tall and Special Buildings*, 19(7), 761–777.
- Kim, J., and Lee, Y.-H. (2012). "Seismic performance evaluation of diagrid system buildings." *The Structural design of tall and special buildings*, 21(10), 736–749.
- Kim, Y.-J., Jung In-Yong, Ju Young-Kyu, Park Soon-Jeon, and Kim Sang-Dae. (2010). "Cyclic Behavior of Diagrid Nodes with H -Section Braces." *Journal of Structural Engineering*, 136(9), 1111–1122.
- Kim, Y.-J., Kim, M.-H., Jung, I.-Y., Ju, Y. K., and Kim, S.-D. (2011). "Experimental investigation of the cyclic behavior of nodes in diagrid structures." *Engineering Structures*, 33(7), 2134–2144.
- Kinali, K., and Ellingwood, B. R. (2007). "Seismic fragility assessment of steel frames for consequence-based engineering: A case study for Memphis, TN." *Engineering Structures*, 29(6), 1115–1127.
- Kolozvari, K., Orakcal, K., and Wallace, J. W. (2014). "Modeling of cyclic shear-flexure interaction in reinforced concrete structural walls. I: Theory." *Journal of Structural Engineering*, 141(5), 04014135.
- Krawinkler, H. (2005). *Van Nuys hotel building testbed report: exercising seismic performance assessment*. Pacific Earthquake Engineering Research Center, College of Engineering ....
- Kumar, A., Sah, B., Singh, A. R., Deng, Y., He, X., Kumar, P., and Bansal, R. C. (2017). "A review of multi criteria decision making (MCDM) towards sustainable renewable energy development." *Renewable and Sustainable Energy Reviews*, 69, 596–609.
- Kwon, K., and Kim, J. (2014). "Progressive collapse and seismic performance of twisted diagrid buildings." *International Journal of High-Rise Buildings*, 3(3), 223–230.
- Lavappa, P. D., and Kneifel, J. D. (2018). *NISTIR 85-3273-33: Energy Price Indices and Discount Factors for Life-Cycle Cost Analysis – 2018, Annual Supplement to NIST Handbook 135*. US Department of Commerce, National Institute of Standards and Technology.
- Lee, J. Y., Burton, H. V., and Lallemand, D. (2018). "Adaptive decision-making for civil infrastructure systems and communities exposed to evolving risks." *Structural Safety*, 75, 1–12.

- Lee, J. Y., and Ellingwood, B. R. (2017). "A decision model for intergenerational life-cycle risk assessment of civil infrastructure exposed to hurricanes under climate change." *Reliability Engineering & System Safety*, 159, 100–107.
- Li, Y., Song, R., and Van De Lindt, J. W. (2014). "Collapse fragility of steel structures subjected to earthquake mainshock-aftershock sequences." *Journal of Structural Engineering*, 140(12), 04014095.
- Li, Y., Yin, Y., Ellingwood, B. R., and Bulleit, W. M. (2010). "Uniform hazard versus uniform risk bases for performance-based earthquake engineering of light-frame wood construction." *Earthquake Engineering & Structural Dynamics*, 39(11), 1199–1217.
- Limongelli, M. P. (2003). "Optimal location of sensors for reconstruction of seismic responses through spline function interpolation." *Earthquake Engineering and Structural Dynamics*, 32(7), 1055–1074.
- Ling, Q., Tian, Z., Yin, Y., and Li, Y. (2009). "Localized structural health monitoring using energy-efficient wireless sensor networks." *IEEE Sensors Journal*, 9(11), 1596–1604.
- Liu, C., Li, Q., Lu, Z., and Wu, H. (2018). "A review of the diagrid structural system for tall buildings." *The Structural Design of Tall and Special Buildings*, 27(4), e1445.
- Ljung, L. (2007). "System identification toolbox for use with MATLAB."
- Lloyd, S. M., and Ries, R. (2007). "Characterizing, Propagating, and Analyzing Uncertainty in Life-Cycle Assessment: A Survey of Quantitative Approaches." *Journal of Industrial Ecology*, 11(1), 161–179.
- Lounis, Z., and McAllister, T. P. (2016). "Risk-based decision making for sustainable and resilient infrastructure systems." *Journal of Structural Engineering*, 142(9), F4016005.
- Lozano-Minguez, E., Kolios, A. J., and Brennan, F. P. (2011). "Multi-criteria assessment of offshore wind turbine support structures." *Renewable Energy*, 36(11), 2831–2837.
- Lu, R., Luo, Y., and Conte, J. P. (1994). "Reliability evaluation of reinforced concrete beams." *Structural Safety*, 14(4), 277–298.
- Lu, Z., Wang, Z., Zhou, Y., and Lu, X. (2018). "Nonlinear dissipative devices in structural vibration control: A review." *Journal of Sound and Vibration*, 423, 18–49.
- Lynch, J. P., and Loh, K. J. (2006). "A summary review of wireless sensors and sensor networks for structural health monitoring." *Shock and Vibration Digest*, 38(2), 91–130.
- Mahapatro, A., and Mohan Khilar, P. (2013). "Detection and diagnosis of node failure in wireless sensor networks: A multiobjective optimization approach." *Swarm and Evolutionary Computation*, 13, 74–84.
- Martínez-Rocamora, A., Solís-Guzmán, J., and Marrero, M. (2017). "Ecological footprint of the use and maintenance phase of buildings: Maintenance tasks and final results." *Energy and Buildings*, 155, 339–351.
- Mateo, J. R. S. C. (2012). *Multi criteria analysis in the renewable energy industry*. Springer Science & Business Media.
- Matthews, J. C. (2015). "Disaster resilience of critical water infrastructure systems." *Journal of Structural Engineering*, 142(8), C6015001.
- Mazumder, R. K., Salman, A., Li, Y., and Yu, X. (2019). "Seismic Functionality and Resilience Analysis of Water Distribution Systems." *Journal of Pipeline Systems Engineering and Practice*.
- Mazumder, R. K., Salman, A. M., Li, Y., and Yu, X. (2018). "Reliability Analysis of Water Distribution Systems Using Physical Probabilistic Pipe Failure Method." *Journal of Water Resources Planning and Management*, 145(2), 04018097.
- Mazzoni, S., McKenna, F., Scott, M. H., and Fenves, G. L. (2006). "The open system for earthquake engineering simulation (OpenSEES) user command-language manual."
- McAllister Therese. (2016). "Research Needs for Developing a Risk-Informed Methodology for Community Resilience." *Journal of Structural Engineering*, 142(8), C4015008.

- Melchers, R. E. (1999). "Corrosion uncertainty modelling for steel structures." *Journal of Constructional Steel Research*, 52(1), 3–19.
- Melchers, R. E. (2003). "Probabilistic model for marine corrosion of steel for structural reliability assessment." *Journal of Structural Engineering*, 129(11), 1484–1493.
- Mele, E., Toreno, M., Brandonisio, G., and De Luca, A. (2014). "Diagrid structures for tall buildings: case studies and design considerations." *The Structural Design of Tall and Special Buildings*, 23(2), 124–145.
- Melillo, J. M., Richmond, T. (T. C. ), and W. Yohe, G. (2014). *Climate change impacts in the United States, highlights: US national climate assessment*. Government Printing Office.
- Menna, C., Asprone, D., Jalayer, F., Prota, A., and Manfredi, G. (2013). "Assessment of ecological sustainability of a building subjected to potential seismic events during its lifetime." *The International Journal of Life Cycle Assessment*, 18(2), 504–515.
- Milana, G., Olmati, P., Gkoumas, K., and Bontempi, F. (2015). "Ultimate capacity of diagrid systems for tall buildings in nominal configuration and damaged state." *Periodica Polytechnica. Civil Engineering*, 59(3), 381.
- Mitrani-Reiser, J. (2007). "An ounce of prevention: probabilistic loss estimation for performance-based earthquake engineering." California Institute of Technology.
- Moghaddasi B, N. S., and Zhang, Y. (2013). "Seismic analysis of diagrid structural frames with shear-link fuse devices." *Earthquake Engineering and Engineering Vibration*, 12(3), 463–472.
- Molina Hutt, C., Almufti, I., Willford, M., and Deierlein, G. (2015). "Seismic loss and downtime assessment of existing tall steel-framed buildings and strategies for increased resilience." *Journal of Structural Engineering*, 142(8), C4015005.
- Montuori, G. M., Mele, E., Brandonisio, G., and Luca, A. D. (2014). "Design criteria for diagrid tall buildings: Stiffness versus strength." *The Structural Design of Tall and Special Buildings*, 23(17), 1294–1314.
- Moon, K. S. (2008). "Sustainable structural engineering strategies for tall buildings." *The Structural Design of Tall and Special Buildings*, 17(5), 895–914.
- Moon, K. S. (2011). "Diagrid structures for complex-shaped tall buildings." *Procedia Engineering*, 14, 1343–1350.
- Moon, K.-S., Connor, J. J., and Fernandez, J. E. (2007). "Diagrid structural systems for tall buildings: characteristics and methodology for preliminary design." *The Structural Design of Tall and Special Buildings*, 16(2), 205–230.
- Moussavi Nadoushani, Z. S., Akbarnezhad, A., Ferre Jornet, J., and Xiao, J. (2017). "Multi-criteria selection of façade systems based on sustainability criteria." *Building and Environment*, 121, 67–78.
- Naeim, F., Hagie, S., Alimordi, A., and Miranda, E. (2006). "AUTOMATED POST-EARTHQUAKE DAMAGE ASSESSMENT OF INSTRUMENTED BUILDINGS." *Advances in Earthquake Engineering for Urban Risk Reduction*, Nato Science Series: IV: Earth and Environmental Sciences, S. T. Wasti and G. Ozcebe, eds., Springer Netherlands, 117–134.
- NGDC/WDS. (2019). "Global Significant Earthquake Database." National Geophysical Data Center (NOAA)/World Data Service (NGDC/WDS), DOI: 10.7289/V5TD9V7K.
- NOAA. (2019). "Billion-Dollar Weather and Climate Disasters, NOAA National Centers for Environmental Information (NCEI) U.S." <<https://www.ncdc.noaa.gov/billions/>> (Mar. 13, 2019).
- Nocera, F., and Gardoni, P. (2019). "A ground-up approach to estimate the likelihood of business interruption." *International Journal of Disaster Risk Reduction*, 101314.

- Ochoa, L., Hendrickson, C., and Matthews, H. S. (2002). "Economic input-output life-cycle assessment of US residential buildings." *Journal of Infrastructure Systems*, 8(4), 132–138.
- Ohata, A., Furuta, K., and Nita, H. (2006). "Identification of nonlinear ARX model with input and output dependent coefficients." *2006 IEEE Conference on Computer Aided Control System Design, 2006 IEEE International Conference on Control Applications, 2006 IEEE International Symposium on Intelligent Control*, IEEE, 2577–2582.
- O'Rourke, T. D., Jeon, S.-S., Toprak, S., Cubrinovski, M., Hughes, M., van Ballegooy, S., and Bouziou, D. (2014). "Earthquake Response of Underground Pipeline Networks in Christchurch, NZ." *Earthquake Spectra*, 30(1), 183–204.
- Padgett, J. E., and DesRoches, R. (2007). "Bridge functionality relationships for improved seismic risk assessment of transportation networks." *Earthquake Spectra*, 23(1), 115–130.
- Padgett, J. E., and Li, Y. (2016). "Risk-based assessment of sustainability and hazard resistance of structural design." *Journal of Performance of Constructed Facilities*, 30(2).
- Park, H. S., Hwang, J. W., and Oh, B. K. (2018). "Integrated analysis model for assessing CO2 emissions, seismic performance, and costs of buildings through performance-based optimal seismic design with sustainability." *Energy and Buildings*, 158, 761–775.
- Paspuleti, C. (2002). "Seismic analysis of an older reinforced concrete frame Structure." PhD Thesis, Citeseer.
- PCA. (2002). "Concrete information: Types and causes of concrete deterioration." Portland Cement Association.
- Pham, A. T., Tan, K. H., and Yu, J. (2017). "Numerical investigations on static and dynamic responses of reinforced concrete sub-assemblages under progressive collapse." *Engineering Structures*, 149, 2–20.
- Phillips, R., Troup, L., Fannon, D., and Eckelman, M. J. (2017). "Do resilient and sustainable design strategies conflict in commercial buildings? A critical analysis of existing resilient building frameworks and their sustainability implications." *Energy and Buildings*, 146, 295–311.
- Porter, K., Mitrani-Reiser, J., and Beck, J. L. (2006). "Near-real-time loss estimation for instrumented buildings." *The Structural Design of Tall and Special Buildings*, 15(1), 3–20.
- Ramirez, C. M., Liel, A. B., Mitrani-Reiser, J., Haselton, C. B., Spear, A. D., Steiner, J., Deierlein, G. G., and Miranda, E. (2012). "Expected earthquake damage and repair costs in reinforced concrete frame buildings." *Earthquake Engineering & Structural Dynamics*, 41(11), 1455–1475.
- Ramirez, C. M., and Miranda, E. (2012a). "Significance of residual drifts in building earthquake loss estimation." *Earthquake Engineering & Structural Dynamics*, 41(11), 1477–1493.
- Ramirez, C. M., and Miranda, E. (2012b). "Significance of residual drifts in building earthquake loss estimation." *Earthquake Engineering & Structural Dynamics*, 41, 1477–1493.
- Reinhorn, A. M., and Cimellaro, G. P. (2014). "Consideration of resilience of communities in structural design." *Performance-Based Seismic Engineering: Vision for an Earthquake Resilient Society*, Springer, 401–421.
- Reinoso, E., Jaimes, M. A., and Esteva, L. (2018). "Estimation of life vulnerability inside buildings during earthquakes." *Structure and Infrastructure Engineering*, 14(8), 1140–1152.
- Robati, M., Kokogiannakis, G., and McCarthy, T. J. (2017). "Impact of structural design solutions on the energy and thermal performance of an Australian office building." *Building and Environment*, 124, 258–282.

- Rojah, C. (2005). "ATC-20-1 Field Manual: Postearthquake Safety Evaluation of Buildings." *Applied Technology Council: Redwood City, CA, USA*.
- Roostaie, S., Nawari, N., and Kibert, C. J. (2019). "Sustainability and resilience: A review of definitions, relationships, and their integration into a combined building assessment framework." *Building and Environment*.
- RSMeans. (2018). *RSMeans Data Online*. Gordian, Rockland, MA.
- Saaed, T. E., Nikolakopoulos, G., Jonasson, J.-E., and Hedlund, H. (2015). "A state-of-the-art review of structural control systems." *Journal of Vibration and Control*, 21(5), 919–937.
- Saaty, T. L. (1990). "How to make a decision: the analytic hierarchy process." *European journal of operational research*, 48(1), 9–26.
- Sadeghi, S., and Rofooei, F. R. (2018). "Quantification of the seismic performance factors for steel diagrid structures." *Journal of Constructional Steel Research*, 146, 155–168.
- Saini, A., and Tien, I. (2018). "Methodology for real-time prediction of structural seismic risk based on sensor measurements." *Structural Safety*, 73, 54–63.
- Sakurai, S., Ellingwood, B. R., and Kushiya, S. (2001). "Probabilistic study of the behavior of steel frames with partially restrained connections." *Engineering structures*, 23(11), 1410–1417.
- Sanchez-Silva, M., Klutke, G.-A., and Rosowsky, D. V. (2011). "Life-cycle performance of structures subject to multiple deterioration mechanisms." *Structural Safety*, 33(3), 206–217.
- Sattar, S., McAllister, T. P., McCabe, S. L., Johnson, K. J., Segura, C. L., Clavin, C., Fung, J. F., Levitan, M. L., and Harrison, K. W. (2018). *Research Needs to Support Immediate Occupancy Building Performance Following Natural Hazard Events*. National Institute of Standards and Technology Special Publication (NIST SP) - 1224.
- Schmidt, B. J., and Bartlett, F. M. (2002). "Review of resistance factor for steel: data collection." *Canadian Journal of Civil Engineering*, 29(1), 98–108.
- Shankaranarayanan, G., and Cai, Y. (2006). "Supporting data quality management in decision-making." *Decision Support Systems*, 42(1), 302–317.
- Shapira, S., Aharonson-Daniel, L., Shohet, I. M., Peek-Asa, C., and Bar-Dayyan, Y. (2015). "Integrating epidemiological and engineering approaches in the assessment of human casualties in earthquakes." *Natural Hazards*, 78(2), 1447–1462.
- Sharrard, A. L., Matthews, H. S., and Ries, R. J. (2008). "Estimating construction project environmental effects using an input-output-based hybrid life-cycle assessment model." *Journal of Infrastructure Systems*, 14(4), 327–336.
- Simonen, K., Huang, M., Aicher, C., and Morris, P. (2018). "Embodied carbon as a proxy for the environmental impact of earthquake damage repair." *Energy and Buildings*, 164, 131–139.
- Singh, S. (2017). "Smart Building Market worth 31.74 Billion USD by 2022." *MarketsandMarkets Research Private Ltd. Northbrook, IL*, <<http://www.marketsandmarkets.com/PressReleases/smart-building.asp>> (Oct. 5, 2017).
- Sohanghpurwala, A. A. (2006). *Manual on service life of corrosion-damaged reinforced concrete bridge superstructure elements*. NCHRP (National Cooperative Highway Research Program), Transportation Research Board.
- Sohn, H., and Farrar, C. R. (2001). "Damage diagnosis using time series analysis of vibration signals." *Smart materials and structures*, 10(3), 446.
- Stewart, M. G. (2001). "Reliability-based assessment of ageing bridges using risk ranking and life cycle cost decision analyses." *Reliability Engineering & System Safety*, 74(3), 263–273.
- Stewart, M. G., Wang, X., and Nguyen, M. N. (2011). "Climate change impact and risks of concrete infrastructure deterioration." *Engineering Structures*, 33(4), 1326–1337.

- Stewart, M. G., Wang, X., and Nguyen, M. N. (2012). "Climate change adaptation for corrosion control of concrete infrastructure." *Structural Safety*, 35, 29–39.
- Suo, Q., and Stewart, M. G. (2009). "Corrosion cracking prediction updating of deteriorating RC structures using inspection information." *Reliability engineering & system safety*, 94(8), 1340–1348.
- Sutley, E. J., van de Lindt, J. W., and Peek, L. (2016a). "Community-Level Framework for Seismic Resilience. II: Multiobjective Optimization and Illustrative Examples." *Natural Hazards Review*, 18(3), 04016015.
- Sutley, E. J., van de Lindt, J. W., and Peek, L. (2016b). "Community-level framework for seismic resilience. i: coupling socioeconomic characteristics and engineering building systems." *Natural Hazards Review*, 18(3), 04016014.
- Takewaki, I., Nakamura, M., Nakamura, M., and Yoshitomi, S. (2012). *System Identification for Structural Health Monitoring*. WIT Press.
- Tesfamariam, S., and Goda, K. (2015). "Loss estimation for non-ductile reinforced concrete building in Victoria, British Columbia, Canada: effects of mega-thrust Mw9-class subduction earthquakes and aftershocks." *Earthquake Engineering & Structural Dynamics*, 44(13), 2303–2320.
- Tomei, V., Imbimbo, M., and Mele, E. (2018). "Optimization of structural patterns for tall buildings: The case of diagrid." *Engineering Structures*, 171, 280–297.
- Tran, T. A., and Wallace, J. W. (2015). "Cyclic testing of moderate-aspect-ratio reinforced concrete structural walls." *ACI Structural Journal*, 112(6), 653.
- Trifunac, M. D., Ivanovic, S. S., and Todorovska, M. I. (1999). "Instrumented 7-storey reinforced concrete building in Van Nuys, California: description of the damage from the 1994 Northridge Earthquake and strong motion data." *Report CE 99*, 2.
- Uriz, P. (2005). "Towards earthquake resistant design of concentrically braced steel structures." Department of Civil and Environmental Engineering, University of California, Berkeley, CA.
- Uriz, P., Filippou, F. C., and Mahin, S. A. (2008). "Model for cyclic inelastic buckling of steel braces." *Journal of structural engineering*, 134(4), 619–628.
- Uriz, P., and Mahin, S. A. (2004). "Seismic vulnerability assessment of concentrically braced steel frames." *International Journal of Steel Structures*, 4(4), 239–248.
- US BLS. (2018). "Average Energy Prices In Boston-Cambridge-Newton – December 2018 : New England Information Office : U.S. Bureau of Labor Statistics." <[https://www.bls.gov/regions/new-england/news-release/averageenergyprices\\_boston.htm](https://www.bls.gov/regions/new-england/news-release/averageenergyprices_boston.htm)> (Aug. 4, 2019).
- USGS. (2017). *Earthquake Hazard Program - Unified Hazard Tool*. United States Geological Survey.
- Ustinovichius, L., Zavadkas, E. K., and Podvezko, V. (2007). "Application of a quantitative multiple criteria decision making (MCDM-1) approach to the analysis of investments in construction." *Control and cybernetics*, 36(1), 251.
- Vamvatsikos, D., and Cornell, C. A. (2002). "Incremental dynamic analysis." *Earthquake Engineering & Structural Dynamics*, 31(3), 491–514.
- Venkittaraman, A., and Banerjee, S. (2014). "Enhancing resilience of highway bridges through seismic retrofit." *Earthquake Engineering & Structural Dynamics*, 43(8), 1173–1191.
- Vidal, F., Navarro, M., Aranda, C., and Enomoto, T. (2014). "Changes in dynamic characteristics of Lorca RC buildings from pre-and post-earthquake ambient vibration data." *Bulletin of Earthquake Engineering*, 12(5), 2095–2110.
- Vlassis, A. G., Izzuddin, B. A., Elghazouli, A. Y., and Nethercot, D. A. (2008). "Progressive collapse of multi-storey buildings due to sudden column loss—Part II: Application." *Engineering Structures*, 30(5), 1424–1438.

- Voropai, N. I., and Ivanova, E. Y. (2002). "Multi-criteria decision analysis techniques in electric power system expansion planning." *International journal of electrical power & energy systems*, 24(1), 71–78.
- Wallenius, J., Dyer, J. S., Fishburn, P. C., Steuer, R. E., Zionts, S., and Deb, K. (2008). "Multiple criteria decision making, multiattribute utility theory: Recent accomplishments and what lies ahead." *Management science*, 54(7), 1336–1349.
- Wang, J., Chen, H., Yuan, Y., and Huang, Y. (2019). "A novel efficient optimization algorithm for parameter estimation of building thermal dynamic models." *Building and Environment*, 153, 233–240.
- Wang, Y.-M., and Elhag, T. M. (2006). "Fuzzy TOPSIS method based on alpha level sets with an application to bridge risk assessment." *Expert systems with applications*, 31(2), 309–319.
- Wei, H.-H., Shohet, I. M., Skibniewski, M. J., Shapira, S., and Yao, X. (2015). "Assessing the lifecycle sustainability costs and benefits of seismic mitigation designs for buildings." *Journal of Architectural Engineering*, 22(1), 04015011.
- Wood, D. A., and Khosravianian, R. (2015). "Exponential utility functions aid upstream decision making." *Journal of Natural Gas Science and Engineering*, 27, 1482–1494.
- Wu, Y.-M., and Kanamori, H. (2008). "Development of an Earthquake Early Warning System Using Real-Time Strong Motion Signals." *Sensors*, 8(1), 1–9.
- Xing, Z., and Mita, A. (2012). "A substructure approach to local damage detection of shear structure." *Structural Control and Health Monitoring*, 19(2), 309–318.
- Yamin, L. E., Hurtado, A., Rincon, R., Dorado, J. F., and Reyes, J. C. (2017). "Probabilistic seismic vulnerability assessment of buildings in terms of economic losses." *Engineering Structures*, 138, 308–323.
- Yin, Y.-J., and Li, Y. (2010). "Loss estimation of light-frame wood construction subjected to mainshock-aftershock sequences." *Journal of Performance of Constructed Facilities*, 25(6), 504–513.
- Zavadskas, E. K., Kaklauskas, A., Peldschus, F., and Turskis, Z. (2007). "Multi-attribute assessment of road design solutions by using the COPRAS method." *Baltic Journal of Road & Bridge Engineering*, 2(4).
- Zhang, C., Zhao, F., and Liu, Y. (2012). "Diagrid tube structures composed of straight diagonals with gradually varying angles." *The structural design of tall and special buildings*, 21(4), 283–295.
- Zhao, F., and Zhang, C. (2015). "Diagonal arrangements of diagrid tube structures for preliminary design." *The Structural Design of Tall and Special Buildings*, 24(3), 159–175.
- Zheng, L., and Lai, J. (2018). "Environmental and economic evaluations of building energy retrofits: Case study of a commercial building." *Building and Environment*, 145, 14–23.
- Zhou, W., Zhang, J., and Cao, Z. (2013). "Experiment and analysis on X-shaped reinforced concrete joint in diagrid structures." *ACI Structural Journal*, 110(2), 171.
- Zhu, B., and Frangopol, D. M. (2016). "Time-variant risk assessment of bridges with partially and fully closed lanes due to traffic loading and scour." *Journal of Bridge Engineering*, 21(6), 04016021.
- Zhu, Z., German, S., and Brilakis, I. (2011). "Visual retrieval of concrete crack properties for automated post-earthquake structural safety evaluation." *Automation in Construction*, 20(7), 874–883.